Fisheries New Zealand
Tini a Tangaroa

Spatial and temporal distribution of seven deepwater sharks in New Zealand waters

New Zealand Aquatic Environment and Biodiversity Report No. 271

B. Finucci, E.G. Jones, C. Marsh, M. Pinkerton,
N. Sibanda, P. Sutton, M.P. Francis

ISSN 1179-6480 (online)
ISBN 978-1-99-101905-9 (online)

September 2021

New Zealand Government

Requests for further copies should be directed to:

Publications Logistics Officer
Ministry for Primary Industries
PO Box 2526
WELLINGTON 6140

Email: brand@mpi.govt.nz
Telephone: 0800 00 83 33
Facsimile: 04-894 0300

This publication is also available on the Ministry for Primary Industries websites at:
http://www.mpi.govt.nz/news-and-resources/publications
http://fs.fish.govt.nz go to Document library/Research reports

TABLE OF CONTENTS

EXECUTIVE SUMMARY

Finucci, B.[1]; Jones, E.G.[1]; Marsh, C. [1]; Pinkerton, M.[1]; Sibanda, N.[2]; Sutton, P.[1]; Francis, M.P.[1] (2021). Spatial and temporal distribution of seven deepwater sharks in New Zealand waters.

New Zealand Aquatic Environment and Biodiversity Report No. 271. **167 p.**

At least 112 cartilaginous fishes (sharks, rays, and chimaeras) occur in New Zealand waters, and many of them are predominantly found in the deep sea. Cartilaginous fishes generally have low productivity because of their low to moderate growth rates, and low fecundity, resulting in small litter sizes and long (frequently multi-year) reproductive cycles. This low productivity has been found to be more pronounced in deepwater species, increasing their vulnerability to fishing activities. The most recent Fisheries New Zealand qualitative risk assessment for chondrichthyans found that some species of deepwater sharks had relatively high risk of adverse impacts from fishing. The highest-risk non-QMS shark species from this process included Plunket's shark *Scymnodon plunketi*, Baxter's dogfish *Etmopterus granulosus*, Seal shark *Dalatias licha*, Shovelnose dogfish *Deania calcea*, Longnose velvet dogfish *Centroselachus crepidater*, Leafscale gulper shark *Centrophorus squamosus*, and Owston's dogfish *Centroscymnus owstonii*. It was noted that abundance indices for these species were mostly unreliable, making it difficult to assess risk of fishing to these species with confidence.

Spatial distribution models (SDMs) are used for interpreting spatial distribution knowledge, stock structure, and gaps in distribution and aggregations. One promising modelling technique is the Vector Autoregressive Spatio-Temporal (VAST) model, which differs from other SDMs in that it was developed to simultaneously estimate spatio-temporal variation in population density for multiple species. Here, VAST models were applied to research trawl survey data and environmental predictors (depth, seabed rugosity, sea surface temperature, bottom temperature, and chlorophyll-a) to provide updated scientific information on stock status for seven deepwater shark species. By moving from qualitative to quantitative data, improved distributional knowledge would allow 1) an evaluation of species distribution and potential stock boundaries; 2) comparisons to be made with similar populations elsewhere; 3) better informed qualitative risk assessment through better understanding the nature of spatial overlaps between species and fisheries; and 4) provision of quantitative species distribution maps that could be used to inform management. To validate the distribution patterns determined from the research trawl survey data, VAST models were also run with commercial fishery catch and effort data from the Fisheries New Zealand Observer programme.

Deepwater sharks were found to be ubiquitous around New Zealand waters, with each species shown to have a unique distributional pattern. Some species were widespread across the New Zealand Exclusive Economic Zone and showed continuous distributions along the continental shelf and slope, whereas others exhibited more disjointed distributions. Three areas were identified as deepwater shark "hotspots" in New Zealand waters, where species were found to have relatively high densities and probability of encounter: 1) Puysegur (for six of the seven species); 2) southeast portion of Chatham Rise (seven species); and 3) southern Campbell Plateau (for six of the seven species). These areas warrant further investigation to understand the environmental drivers for these hotspots, their importance to deepwater sharks (e.g., breeding grounds, pupping grounds), as well as to quantify the abundances and class compositions of these species in these regions. Puysegur and parts of the southeast Chatham Rise are also areas of high fishing activity, thus increasing the risk posed by fisheries to the shark species, and interactions should be monitored closely.

[1] National Institute of Water and Atmospheric Research (NIWA), New Zealand.
[2] Victoria University of Wellington, New Zealand.

All species assessed here were found to spatially segregate by sex, size, and maturity stage. There was very little evidence to suggest any temporal or spatial changes in the distributions and abundance of the species examined here. The lack of trends may be indicative of relatively stable population abundance since the start of the time series (mid 1980s), although any effects from the introduction of deepwater fishing remain unknown because deepwater fisheries began in the late 1970s/early 1980s. Any suggestion of seasonal movement patterns was not evident here, given that most research trawl sampling of these species occurs at the same time of year (December-January).

VAST is a potentially powerful tool to incorporate into species distributional modelling, although the understanding of population structure or movement patterns of these species was not improved with this work. A combination of comparative population genomics and long-term tagging is recommended to fully understand population structure and movement patterns of these species around New Zealand. The observer data provided similar patterns of density and probability of encounter for all species, suggesting these data could be used as validation for assessing the species distributions around New Zealand. Fisheries observer data are also useful in providing information on these species in areas and across time periods that are not sampled by the trawl survey; however, very little biological data were available and improved fisheries observer sampling (e.g., length and sex) of deepwater sharks is recommended.

1. INTRODUCTION

Cartilaginous fishes (sharks, rays, and chimaeras) generally have low productivity because of their low to moderate growth rates, and low fecundity, resulting in small litter sizes and long (frequently multi-year) reproductive cycles. This low productivity has been found to be more pronounced in deepwater species, increasing their vulnerability to fishing activities (Simpfendorfer & Kyne 2009). At least 112 cartilaginous species occur in New Zealand waters (Ford et al. 2018), and many of them are predominantly found in the deep sea (Finucci et al. 2019). Eleven chondrichthyans are managed under the Quota Management System (QMS) as 27 management units or "stocks". The status of these stocks is poorly understood, with no current quantitative stock assessment available for any New Zealand chondrichthyan stock. For most deepwater species found in New Zealand waters catches are not restricted, with no species-specific management available.

The most recent Fisheries New Zealand risk assessment for chondrichthyans found that some species of deepwater sharks had relatively high risk of adverse impacts from fishing (Ford et al. 2018). The highest-risk non-QMS shark species from this qualitative assessment included Plunket's shark *Scymnodon plunketi*, Baxter's dogfish *Etmopterus granulosus*, Seal shark *Dalatias licha*, Shovelnose dogfish *Deania calcea*, Longnose velvet dogfish *Centroselachus crepidater*, Leafscale gulper shark *Centrophorus squamosus*, and Owston's dogfish *Centroscymnus owstonii*. The panel assessing risk noted that abundance indices for these species were mostly unreliable (Francis et al. 2016), making it difficult to assess risk of fishing to these species with confidence.

Improved knowledge of spatial distributions can increase certainty of the risk to, and status of, deepwater sharks. Many sharks are known to segregate by sex and/or size spatially and temporally, including deepwater species (Finucci et al. 2018). As a result, a fishery might capture only juveniles, or only mature females, resulting in differential exploitation by sex or size class. Some information is available on the spatial distributions of these deepwater shark species in New Zealand waters; however, most data are qualitative rather than quantitative. For example, Wetherbee (2000) reported the distribution and abundance patterns of deepwater sharks across the Chatham Rise, and Tracey et al. (2004, 2012) described variation in the distribution of deepwater sharks between different seamount complexes and slope habitats from this area. Clark & King (1989) described the distribution of deepwater sharks around the North Island of New Zealand, with a particular focus on *Deania calcea*. Parker & Francis (2012) reported the distribution, depth ranges, population length frequency distributions, and sex ratios from the Chatham Rise and Sub-Antarctic surveys for *Deania calcea* and *Centrophorus squamosus*. In 2010, an extensive literature review of existing data and spatial distributions around New Zealand was conducted for six of the seven species (excluding *S. plunketi*) (Blackwell 2010); this analysis, however, did not include any modelling of distributional data and size and sex were only considered for a few species where data were available. Most recently, stock status indicators based on distribution data, as the proportion of space where a species was present (detected), and a spatial concentration statistic, for six of the seven species (excluding *Centroscymnus owstonii*) was reported by Francis et al. (2016).

By moving from qualitative to quantitative data, improved distributional knowledge would allow 1) an evaluation of species distribution and potential stock boundaries; 2) comparisons to be made with similar populations elsewhere; 3) better informed qualitative risk assessment (e.g., Ford et al. 2018), through better understanding of the nature of spatial overlaps between species and fisheries; and 4) provision of quantitative species distribution maps that could be used for a quantitative spatial-overlap based assessment approach (e.g., Zhou et al. 2011, Griffiths et al. 2018), similar to that used for pelagic sharks by Hoyle et al. (2017) and Fu et al. (2016).

A number of tools exist for modelling species occurrence. For example, Boosted Regression Trees (BRTs) have been found to be useful for describing New Zealand marine species distributions, and the covariates that influence them, allowing a prediction of full species distribution (Leathwick et al. 2006). More recently, the Vector Autoregressive Spatio-Temporal (VAST) model was developed to

simultaneously estimate spatio-temporal variation in population density for multiple species (Thorson & Barnett 2017). In this study, research trawl survey data were used to assess the best method for modeling species distributions and providing updated scientific information on stock status for seven deepwater shark species.

1.1 Objectives

This report was prepared as an output from the Fisheries New Zealand project ENV2018-06 "Improved distribution information for higher risk non-QMS shark species" which has the following objectives.

Overall objective:

To improve our understanding of the spatial distribution of high-risk non-QMS sharks.

Specific objectives:

- Update, using new analytical techniques where applicable, predictive layers of distribution from Leathwick et al. (2006) for the seven demersal shark species.
- Analyse and discuss any patterns in distribution in regard to depth, sex and stage (where possible) for the seven shark species.
- Compare the patterns from specific objectives 1 and 2 above with observer records and patterns observed from overseas in order to better understand the reliability of these predictions.

2. METHODS

2.1 Species of interest

The following seven non-targeted deepwater sharks were selected for this analysis. These species were identified as being at high risk from commercial fisheries by a recent qualitative risk assessment analysis for New Zealand cartilaginous fishes (Ford et al. 2018).

- Plunket's shark *Scymnodon plunketi*
- Baxter's dogfish *Etmopterus granulosus*
- Seal shark *Dalatias licha*
- Shovelnose dogfish *Deania calcea*
- Longnose velvet dogfish *Centroselachus crepidater*
- Leafscale gulper shark *Centrophorus squamosus*
- Owston's dogfish *Centroscymnus owstonii*

2.2. Data preparation and grooming

2.2.1 Research trawl surveys

Research trawl surveys have been used for decades worldwide to estimate the relative abundance of demersal fish species. In New Zealand, trawl survey abundance estimates are routinely generated for QMS fish species from series of surveys carried out at the same time of year in specific regions, and then used in stock assessments for those species (Fisheries New Zealand 2019). Here, catch data from the Fisheries New Zealand research trawl database *trawl* that is managed by NIWA were used to model the distribution of seven shark species in the 200 nm Economic Exclusive Zone (EEZ). A number of previous studies have used subsets of the *trawl* database to assess species richness, and identify and classify fish assemblages and their relationships with a range of environmental variables, in part or all of the EEZ (Anderson et al. 1998, Beentjes et al. 2002, Bull et al. 2001, Francis et al. 2002, Leathwick

et al. 2006, Stephenson et al. 2018, Stephenson et al. 2020), and further details of the database can be found in those reports.

Data were extracted from the *trawl* database and groomed for spatial outliers (obvious errors in location data). Tows were selected where gear type was bottom trawl, gear performance was 1 or 2 (excellent or satisfactory), tow speed was between 1.0 and 5.4 knots, and distance towed was less than 5 nautical miles (nm). Tows beyond the New Zealand EEZ were also removed. The start position of the trawl was used as the tow position. Depth (m) was defined as mean of the minimum and maximum depths recorded per tow. Tows at depths shallower than 200 m were removed (n = 7, all from Chatham Rise). Distribution maps and depth plots revealed occasional outliers for which location or depth had obviously been mis-recorded. These errors were corrected where possible, or the record was omitted if not. All analyses were completed using R (R Core Team 2018).

Surveys were predominantly carried out by research vessels RV *Tangaroa* and RV *Kaharoa* through much of the EEZ, and by the chartered commercial fishing vessel FV *Wanaka* around the North Island (Figure 1). This data set was similar to that described by Dunn et al. (2009), with deepwater bottom trawl survey series available: for Chatham Rise, the Sub-Antarctic (including Campbell Plateau), and west coast South Island using a full-wing bottom trawl towed on flat seabed; for Chatham Rise, east coast North Island, Challenger Plateau, and south coast South Island, using a "rough bottom" trawl, towed on both flat and rough ground; and for Challenger Plateau, Chatham Rise, and around the North Island, by chartered commercial vessels. Details regarding the surveys by *Wanaka* were reported by Clark & King (1989). There have been no bottom trawl surveys off the south-west South Island.

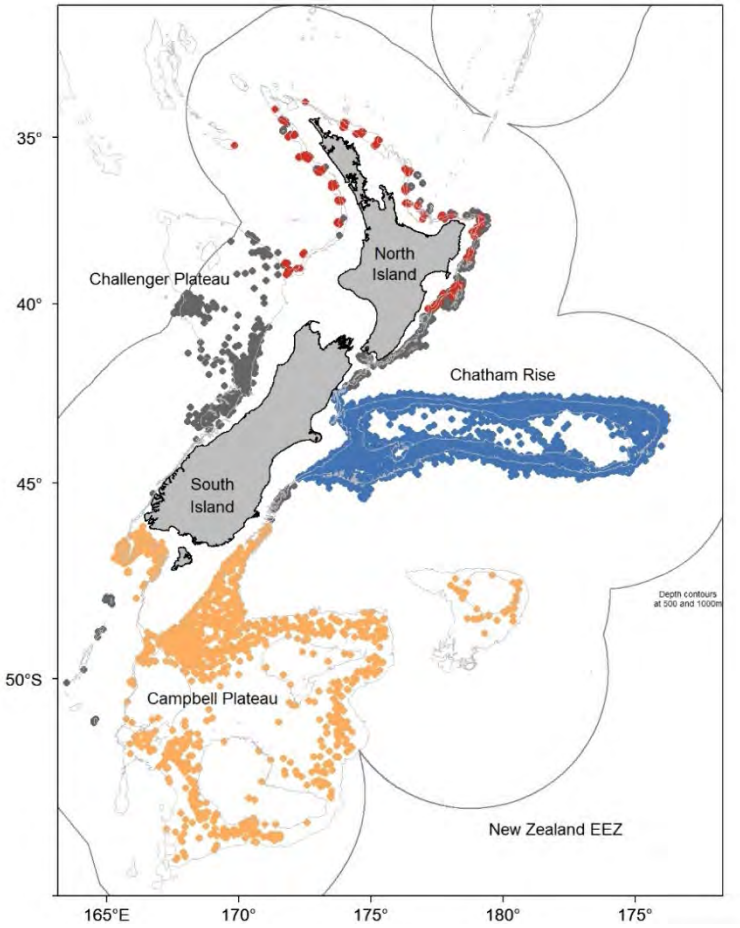

Figure 1: Location of all research trawl tows and division of tows by region (blue, Chatham Rise; orange, Sub-Antarctic; red, *Wanaka* surveys). Grey points represent additional tows included in the overall Economic Exclusive Zone (EEZ) analysis.

2.2.2 Biological data

The accuracy of deepwater shark identification is suspected to have improved through time. In addition, some species codes changed their meaning over time. For example, BSH, which now applies to *Dalatias licha*, was historically applied to any deepwater "black shark" in commercial fishing returns and may have also been used in this way on trawl surveys. Species identification improved after the introduction of specific field identification guides (Tracey & Shearer 2002, McMillan et al. 2019). These field identification guides were not available pre-1981 and thus, catch data prior to this date were excluded.

As part of a large project assessing marine species distributions across New Zealand (Anderson et al. 1998, Francis et al. 2002, Leathwick et al. 2006), research trawl data were extensively groomed to assess the accuracy of species identification. Identification was indexed as 1 (high confidence in species identification), 2 (identification may include two species), or 3 (confidence in identification only to the genus). For the present study, catches pre-2005 were only used where the ID index was rated as 1, with the exception of *Dalatias licha* where indices 1 and 2 were both included to increase the number of observations pre-1990. For all catches post-2005, species identification was assumed to be correct and all catch records were included.

In recent years, there has been an increased collection of biological data for these species during research trawl surveys (e.g., maturity staging of deepwater sharks since 2009). Maturity staging of individuals followed NIWA's standard protocols (Appendix 1 Macroscopic Staging Key). Some issues relating to distinguishing immature females (stage 2) from resting mature females (stage 6) have been raised (E. Jones, NIWA, pers. comm., Dutilloy & Dunn 2020). In this study, some large females assessed as stage 2 were reassigned as stage 6 (and vice versa) based on additional measurements (e.g., uterus width) reported from sample collections. From these maturity staging data, mean size-at-maturity (L_{50}) was calculated for males and females separately by fitting logistic models to the proportion of mature individuals at length using non-linear least squares. Maturity data (immature 0, mature 1) were aggregated by 1-cm length class intervals for each sex. The logistic function had the form:

$$Y_a = [1 + e^{-b\,(a-c)}]^{-1}$$

where Y_a is the proportion of mature individuals in size class a, b is the slope, and c is the length at which 50% of the individuals were mature. Mean lengths at maturity for each species are reported in Table 1. Estimates produced here were similar (under 10% difference) to those reported from previous studies (see Finucci et al. 2018). Based on the mean maturity estimates, individuals were classified as either immature or mature. When only a subset of each catch was measured (when catches were large), the length-frequency distribution of measured sharks was scaled up (by weight) to the total catch.

Table 1: Male and female mean length at maturity (cm) for each species used to define immature and mature individuals.

	This study		Estimates from Finucci et al. (2018)	
Species	Male	Female	Male	Female
Dalatias licha	108.5	123.9	95	120
Centrophorus squamosus	99.3	120.4	99	119
Centroscymnus owstonii	70.1	102.4	71	98
Centroselachus crepidater	65.5	86.5	62	81
Etmopterus granulosus	56.0	70.2	55	64
Scymnodon plunketi	109.1	134.2	100	129
Deania calcea	78.6	102.4	78	106

2.2.3 Observer data

To validate the distribution patterns determined from the research trawl survey data, commercial fishery catch and effort data from the Fisheries New Zealand Observer programme were extracted from the Fisheries New Zealand *cod* database for all bottom trawl events over the same (1982–2018) time period. Very few observer records included biological measurements (overall, between 20 observations for *S. plunketi* and 84 for *Centrophorus squamosus*) and so species were not classified by sex or maturity stage.

2.3 Spatial analyses

2.3.1 Summaries of occurrence

Spatial distribution models (SDMs) are conducted for interpreting spatial distribution knowledge, stock structure, and gaps in distribution and aggregations. There are many modelling techniques that can be used for SDMs; prior assessment of species spatial distributions around New Zealand used Boosted Regression Trees (BRT) (Leathwick et al. 2006). Here, alternative model frameworks were also considered and included Generalised Additive Models (GAMs) (Hastie and Tibshirani 1990) and Vector-Autoregressive Spatio-temporal (VAST) models (Thorson & Barnett 2017).

All three methods can model presence/absence data with both biotic and abiotic covariates but differ in model structure and assumptions. However, only the VAST method incorporates both presence/absence and abundance estimation in a single unified model structure (Thorson & Barnett 2017). A preliminary investigation was conducted and presented to the New Zealand Aquatic Environment Working Group (AEWG) to help provide insight on which method would be best suited for this project.

2.3.2 Estimates of Abundance

2.3.2.1 Preliminary investigation

A preliminary investigation to guide model selection for the abundance analyses was conducted by configuring BRT, GAM, and VAST models on training data (presence/absence data of *Deania calcea* on the Chatham Rise (Figure 2), and assessing their fit with a cross validation method (area under curve and receiver operating characteristic curve), described below (Leathwick et al. 2006).

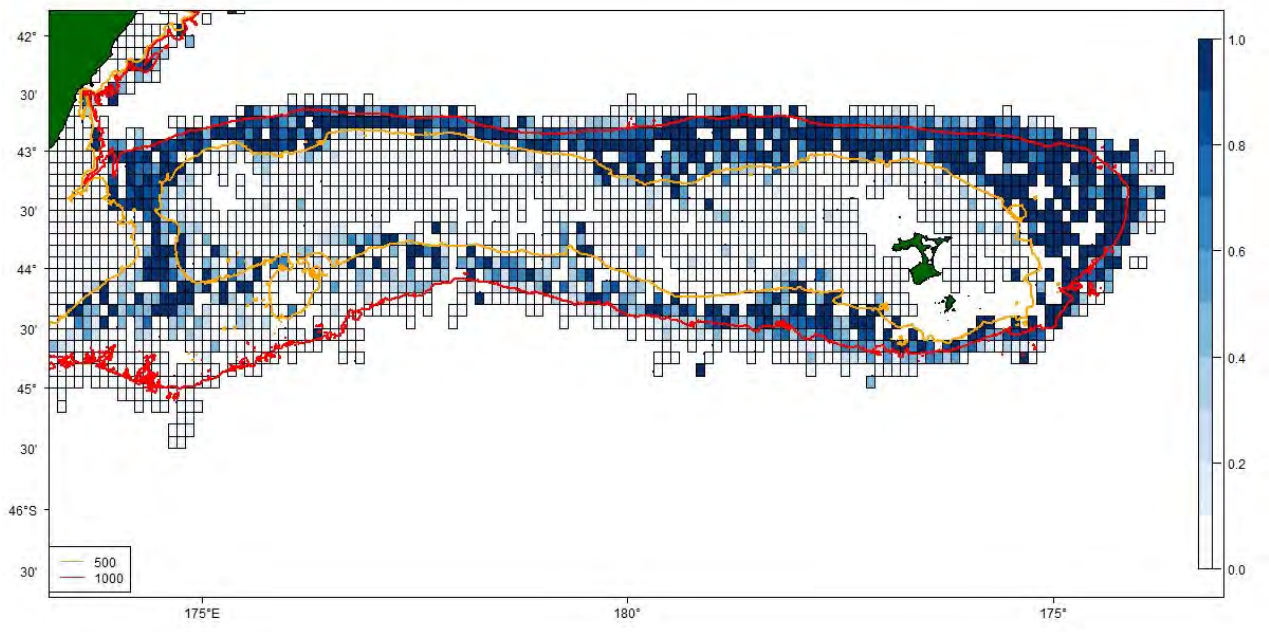

Figure 2: Average occurrence of *Deania calcea* from all trawl surveys on the Chatham Rise between 2005 and 2013 defined by a 0.1 by 0.1 latitude and longitude spatial resolution. Yellow and red lines represent the 500 and 1000 m isobaths, respectively.

Following Leathwick et al. (2006), relevant operational and environmental predictors available were collated; including vessel, gear method, latitude, longitude, average depth of trawl tow, bottom temperature, sea surface temperature, time (day/month/year), and stratum (based on a reference survey). Predictors were checked for collinearity and were not found to be strongly correlated. Predictors explaining at least 1% of relative influence were retained. GAM models were fitted using the *mgcv* R library (version 1.8.23) (Wood 2006), the BRT models were fitted with the *gbm* R library (version 2.1.4) and a VAST model was also established following Thorson (2019). For all methods, the binomial distribution was assumed with logistic link function. Residuals were checked for model violations before prediction accuracy was assessed. All three models used the same training dataset which consisted of 70% of the Chatham Rise data, and a testing dataset for the remaining 30%.

Prediction accuracy was assessed using area under curve (AUC) (Fielding & Bell, 1997) and deviance explained by the models. AUC is a measure between 0.5 and 1.0, where a value of 0.5 means scores for two groups do not differ (i.e., the model is not capable distinguishing between true positive and true negative outcomes), while a score of 1.0 indicates no overlap in the distributions of the group scores (i.e. the model is able to distinguish between true positive and true negative outcomes. A receiver operating characteristic curve (ROC) curve, a graphical diagnostic curve that describes how well a model can classify a binary outcome (presence/absence), was used to visualise model performance and AUC metric was calculated to quantify how well each method preformed (Figure 3).

From this analysis, it was determined that the BRT model was the worst performing model and VAST and GAM models performed in a similar manner. GAMs, however, cannot be extrapolated, or interpreted for covariates, and VAST models allow for spatial-temporal interactions and the incorporation of multiple categories as described in the next section. Based on VAST's ability to outperform BRT models and its additional features that GAMs do not have, it was determined by the AEWG that the VAST method would be used for the main analysis.

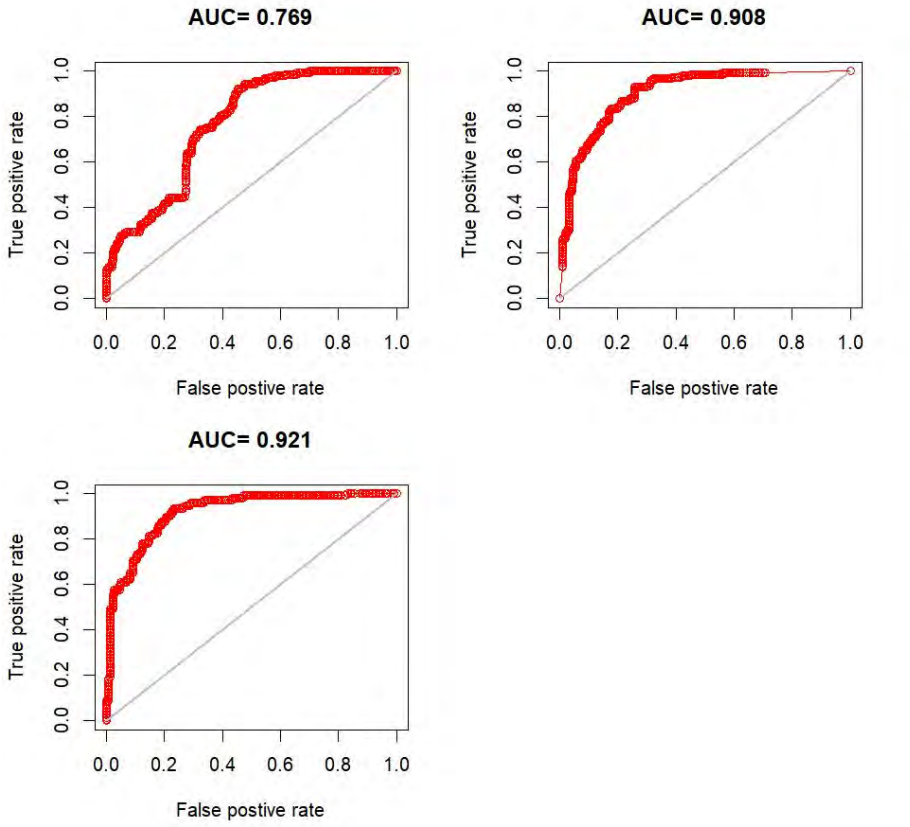

Figure 3: Area Under Curve (AUC) for each model, Boosted Regression Tree model (BRT, left panel), Generalised Additive model (GAM, centre panel), and Vector Autoregressive Spatio-Temporal model (VAST, right panel).

2.3.2.2 VAST model

The Vector-Autoregressive Spatio-temporal (VAST) model was introduced to simultaneously estimate spatio-temporal variation in population density for single or multiple species over one or many years. It has been found to be more parsimonious and have better predictive performance compared to fitting separate single species models (Thorson & Barnett 2017). VAST combines and builds upon a number of techniques and *R* packages developed over several peer-reviewed articles, namely:

- fitting mixed effects models using automatic differentiation and Laplace approximation in the *TMB* software;
- estimation of spatio-temporal processes using stochastic partial differential equations (SPDE) in *R-INLA*;
- using SPDE approximations within *TMB* for single species data implemented in *SpatialDeltaGLMM*;
- use of spatial factor analysis (SFA) to estimate spatial covariation for multiple species in a single time interval implemented in package *Spatial FA*;
- extension of the SFA method to spatial factor dynamic analysis that could account for both spatial and spatio-temporal covariation for multiple species — implemented in package *SpatialDFA*

The design principles of VAST include:

- Area weighting: VAST predicts population density for all locations within a spatial domain (e.g., spatial boundaries for a given stock). Derived quantities (e.g., total abundance) are then predicted by aggregating population density across the spatial domain while weighting density estimates by the area associated with each estimate. The estimate of total abundance can be treated as an abundance index that is directly comparable with other data sources and model estimates of population biomass.
- Distinct catchability and habitat covariates: explicit distinction is made between habitat and catchability covariates.
- Condition on missing covariates through spatially correlated random effects.
- Bridge between univariate and multivariate applications which can be used for single and multiple species analyses. The latter has an advantage over performing multiple single species analyses and then combining the results, and thus ignoring correlations among species.

Model description

Because VAST is a relatively new technique in fisheries data analyses it is described in some detail here. The VAST model inputs specified for this work are described in Appendix 2. VAST predicts variation in density across multiple locations $s = 1, 2, \ldots, S$, time intervals $t = 1, 2, \ldots, T$ for multiple categories $c = 1, \ldots, C$. Categories could be multiple species or multiple size/age/sex classes for an individual species. The spatial resolution of the model is also user-defined, presented as 'knots' (described below).

For each iteration in VAST, the minimum number of observations required in one year for a species or class (sex and maturity stage) was set at 10, and the minimum number of events (tows per year) required by a vessel was set at five. Area swept (square kilometres) was used for the spatial resolution and was defined in the model as the distance towed multiplied by the doorspread. If area swept could not be calculated, then an average tow length of 3 nm (5.6 km) was given and converted to square kilometres (km^{-2}) using average doorspread, which was used to define a given area.

Given catch data y_i for observation i, the probability distribution for y_i is decomposed into two components representing

- the probability $\gamma(s_i, t_i, c_i)$ of encounter
- the catch rates $\lambda(s_i, t_i, c_i,)$, given that species c_i is encountered at location s_i in year t_i.

Data types

Catch data can be counts, abundance (catch weight), or presence/absence. The type of data used determines the type of model, distributions, and link functions to be used.

The data types used in the research surveys and fisheries observer data were:

Abundance data. VAST uses a delta model for biomass data. The first component of a delta model estimates the probability of encountering a species at a given location and time, and the second component of the model estimates positive catch rates on condition that the species is encountered.

Presence/absence (binary) data. For binary data the VAST model is reduced to just a single component. In such cases, the first component estimates the encounter probability, and the second component is 'turned off'.

Link functions and observation error distributions

Each of the two components has an associated linear predictor that represents the effect of annual intercepts, density covariates, catchability covariates, vessel effects, spatial random effects, and spatio-temporal random effects on the component. The linear predictor, $p_1(i)$, associated with the probability of encounter component for observations i is calculated as:

$$p_1(i) = \overbrace{\beta_1(c_i, t_i)}^{\text{Annual intercept}} + \overbrace{\sum_{f=1}^{n_{\omega_1}} L_{\omega_1}(c_i, f)\omega_1(s_i, f)}^{\text{Spatial effect}} + \overbrace{\sum_{f=1}^{n_{\epsilon_1}} L_{\epsilon_1}(c_i, f)\epsilon_1(s_i, f, t_i)}^{\text{Spatio-temporal effect}}$$
$$+ \overbrace{\sum_{f=1}^{n_{\eta_1}} L_{\eta_1}(c_i, f)\eta_1(v_i, f)}^{\text{Vessel effect}} + \overbrace{\sum_{d=1}^{n_d} \gamma_1(c_i, t_i, d)X(s_i, t_i, d)}^{\text{Density covariate}}$$
$$+ \overbrace{\sum_{k=1}^{n_k} \lambda_1(k)Q(i, k)}^{\text{Catchability covariate}} ,$$

where c_i is the category for observation i, t_i is the year, and s_i is the knot corresponding to the spatial location. Knots are created as part of a triangulated mesh used to approximate the spatial domain. The mesh is used in the stochastic partial differential equation (SPDE) approach in the estimation of spatial and spatio-temporal random effects. The linear predictor $p_2(i)$ for the catch rate component is similarly defined.

The linear predictors each include fixed effects for n_d density covariates $X(s, t, d)$ defined at every location and year, and n_k catchability covariates $Q(i,k)$ defined at every observation. A factor model representing random effects for spatial, spatio-temporal, and vessel effects is also included. Using an appropriate link function for $p_1(i)$ and a transformation function for $p_2(i)$ determined by the distribution assumed for the positive catch rates, the linear predictors are then transformed to predict sample data.

Delta log-normal model

In a conventional delta model with a lognormal distribution used for the positive catch rates, the linear predictors are transformed using

- $r_1(i) = \text{logit}^{-1}(p_1(i))$
- $r_2(i) = a_i \times \exp(p_2(i))$,

where a_i represents effort. The statistical distribution that gives probabilities for the biomass catch values is calculated as:

$$f_Y(y_i) = \begin{cases} 1 - r_1(i), & \text{if } Y = 0 \\ r_1(i) \times f_{LN}\left(y_i | r_2(i), \sigma_m^2(c_i)\right) & \text{if } Y > 0, \end{cases}$$

where y is the observed abundance, σ^2_m (c_i) is the residual variance on the log scale for the positive catch rates, and f_{LN} ($y_i|r_2(i)$, σ^2_m (c_i)) is the density function for the log-normal distribution with parameters $r_2(i)$ and σ^2_m (c_i).

VAST then predicts population density $d(s, c, t)$ for each location, category, and time from the two transformed linear predictors, but excluding terms related to catchability (vessel effects and catchability covariates). For the conventional delta log-normal model, density is predicted as:

$$\begin{aligned} d(s,c,t) = \text{logit}^{-1} \Bigg(& \beta_1(c_i,t_i) + \sum_{f=1}^{n_{\omega_1}} L_{\omega_1}(c_i,f)\omega_1(s_i,f) + \sum_{f=1}^{n_{\epsilon_1}} L_{\epsilon_1}(c_i,f)\epsilon_1(s_i,f,t_i) \\ & + \sum_{d=1}^{n_d} \gamma_1(c_i,t_i,d)X(s_i,t_i,d) \Bigg) \\ & \times \exp\Bigg(\beta_2(c_i,t_i) + \sum_{f=1}^{n_{\omega_2}} L_{\omega_2}(c_i,f)\omega_2(s_i,f) + \sum_{f=1}^{n_{\epsilon_2}} L_{\epsilon_2}(c_i,f)\epsilon_2(s_i,f,t_i) \\ & + \sum_{d=1}^{n_d} \gamma_2(c_i,t_i,d)X(s_i,t_i,d) \Bigg) \end{aligned}$$

VAST then calculates derived quantities from its predictions of local density $d(s,c,t)$. For example, an abundance index $I(c,t,l)$ for category c in time t for spatial stratum l is calculated as:

$$I(c,t,l) = \sum_{s=1}^{n_s} a(s,l) \times d(s,c,t),$$

where $a(s,l)$ is the area associated with knot s that is within stratum l. The area $a(s, l)$ is used to determine the relative weighting of density estimates at different knots when calculating derived quantities.

2.3.2.3 Environmental predictors

Potential environmental predictors for the predictive distribution models were collated for analysis with the VAST models following Leathwick et al. (2006). These included:

- Bathymetry (m): depth at seafloor complied from multi-beam and single-beam echo sounders, satellite gravimetric inversion, and others; subsampled (5-km resolution) version of the NIWA 250-m regional bathymetry (Mitchell et al. 2012).

- Seabed rugosity: roughness of the seafloor calculated as the standard deviation of depths in a surrounding 3 x 3 km neighbourhood (Leathwick et al. 2012).

- Salinity at depth (psu): annual average water salinity concentration at the seafloor (using New Zealand bathymetry layer) based on methods from Ridgway et al. (2002), with oceanographic data from CARS2009 (2009).

- Chlorophyll-a concentration (mgChl-a m^{-3}, monthly composite): near surface concentration of chlorophyll-a 1997–2018 estimated from MODIS-Aqua (version R2018.0; NASA 2018a) and SeaWiFS (version R2018.0, NASA 2018a) satellite sensors, blended using the overlap period 2002–2010 (Pinkerton et al. 2019).

- Sea surface temperature (°C km^{-1}, monthly average): the Optimum Interpolation Sea Surface Temperature (OISST) version 2 data were used based on satellite measurements by the Advanced Very High Resolution Radiometer series for the period 1981–2018 (Reynolds et al. 2002).

- Dissolved organic matter (detrital absorption coefficient at 443 nm): based on SeaWiFS ocean colour remote sensing data, modified Case 2 atmospheric correction, and modified Case 2 inherent optical property algorithm (Pinkerton 2016).

- Bottom temperature (°C km^{-1}, monthly average): annual average water temperature at the seafloor (using New Zealand bathymetry layer) based on methods from Ridgway et al. (2002), with oceanographic data from CARS2009 (2009).

Several of the predictors were found to be highly correlated with several other predictors, and salinity and dissolved organic matter were removed from the analysis (highly correlated with chlorophyll-a concentration and sea surface temperature). In addition, chlorophyll-a concentration was only available from 1997 onwards. Thus, two time series were produced for each species, with and without the addition of chlorophyll-a concentration: (1) 1997–2018 (short time series) and (2) 1982–2018 (long time series). The time series and predictors included are reported in Table 2.

Table 2: Environmental predictors included in each model time series.

Data source	Time series	Bathymetry	Seabed rugosity	Sea surface temperature	Bottom temperature	Chlorophyll-a
Research Trawl	1982–2018	√	√	√	√	
Research Trawl	1997–2018	√	√	√	√	√
Observer	2008–2018	√	√	√	√	√

2.3.2.4 Areas of interest

The occurrence and abundance of the seven deepwater shark species was examined across the entire New Zealand EEZ. To investigate any distributional patterns based on sex and/or life history stage, the data were divided into three regions: (1) Chatham Rise, (2) Sub-Antarctic, and (3) North Island (Figure 1). Using the North Island dataset, seasonal patterns were also investigated for the most commonly reported species, *Deania calcea*, as these were consistently surveyed throughout an entire year. Seasonal patterns were not trialled elsewhere as most surveying on Chatham Rise and the Sub-Antarctic occurred only in in December-January.

3. RESULTS

3.1 Research trawl data

Approximately 8700 observations of the seven species combined were used in this analysis (Table 3). Most (56%) observations were reported by surveys conducted by RV *Tangaroa*. On Chatham Rise, a number of observations were reported by chartered fishing vessels *Amaltal Explorer* (AEX), *Otago Buccaneer* (BUC), *Cordella* (COR), *James Cook* (JCO), and *San Waitaki* (SWA) in early years (pre-1997), and in the Sub-Antarctic, AEX and *Will Watch* (WIL) also contributed to observations. All data from around the North Island were provided by the *Wanaka* series in 1985–86. By year, throughout the EEZ, most observations (~60%) were recorded between 1989 and 1999, with little information available pre-1989 (Table 4). Since 2012, data for these species have only been available every other year, because of the change from annual to biennial surveys by RV *Tangaroa*.

Throughout the EEZ and the entire time series, *Deania calcea* (293 t) was the most caught species by weight, followed by *E. granulosus* (245 t) and *Centroselachus crepidater* (106 t) (Table 5). *Dalatias licha* was the least caught species, with just under 20 t reported. *Deania calcea* was the most caught species on Chatham Rise with 137 t (Table 6) and in the Sub-Antarctic, *E. granulosus* was the most caught species by weight with 50 t (Table 7). From the North Island (*Wanaka*) surveys, *Deania calcea* was the most caught of the seven species with nearly 16 t; under 2 t caught of each of the other species were caught and only 36 kg of *S. plunketi* were caught (Table 8).

On Chatham Rise, the catches of most species comprised largely immature individuals (Table 9). Only *Centroscymnus owstonii* comprised mostly mature individuals and *E. granulosus* comprised roughly equal amounts of immature and mature individuals. *Centroscymnus owstonii* was the only species whose catches were dominated by males; catches of all other species were dominated by females.

In the Sub-Antarctic, *Deania calcea* and *Centrophorus squamosus* were evenly split between immature and mature individuals, *Centroselachus crepidater* were mostly mature, and the remaining species were primarily immature (Table 9). *Centrophorus squamosus*, *Centroscymnus owstonii*, and *E. granulosus* had approximately even sex ratios, whereas the remaining species were mostly females.

Table 3: Total number of observations (tows) by vessels in the research trawl database and the number of observations included in the VAST model where the minimum number of events required (*n* = 5 tows per year) was met. All tows from the *Wanaka* (WNK) series were included in the model.

			Chatham Rise			Sub-Antarctic		
		EEZ	1982 series		1997 series	1982 series		1997 series
Vessel	All	Included	All	Included	Included	All	Included	Included
TAN	6 405	4 960	3 970	3 230	1 920	1 449	1 261	823
COR	1 048	804	900	656	0	0	0	0
AEX	1 004	620	501	142	72	182	182	0
SWA	622	370	616	364	266	5	0	0
BUC	532	130	532	130	0	0	0	0
THH	528	512	0	0	0	0	0	0
WIL	397	397	25	25	0	118	118	0
JCO	388	224	169	108	0	1	0	0
ARR	360	66	186	0	0	0	0	0
WNK	249	248	0	0	0	0	0	0
GIL	197	197	8	8	0	82	82	0
ORA	117	0	95	0	0	0	0	0
SMT	88	70	0	0	0	0	0	0
SHI	69	50	50	50	0	19	0	0
GAL	64	0	0	0	0	0	0	0
KAH	58	32	10	6	0	0	0	0
TVI	46	27	26	25	25	0	0	0
AMA	32	6	32	6	6	0	0	0
SEX	28	20	0	0	0	0	0	0
CCY	23	23	0	0	0	0	0	0
AKS	4	0	0	0	0	4	0	0
SRA	4	0	4	0	0	0	0	0
KAT	3	0	3	0	0	0	0	0
KTN	3	0	3	0	0	0	0	0
OFR	3	0	0	0	0	0	0	0
REH	2	0	2	0	0	0	0	0
Total	12 274	8 756	7 132	4 750	2 289	1 860	1 643	823

Table 4: Total number of observations (tows) annually in the research trawl database and the number of observations included in the VAST model where the minimum number of observations per year (n = 10) and the minimum number of events per vessel (n = 5) was met.

	EEZ		Chatham Rise		Sub-Antarctic		*Wanaka* series	
Year	All	Included	All	Included	All	Included	All	Included
1982	41	0	37	0	1	0	0	0
1983	105	0	8	0	17	0	0	0
1984	222	117	153	71	0	0	0	0
1985	357	167	137	25	0	0	142	142
1986	565	291	360	172	6	0	107	107
1987	614	198	411	0	0	0	0	0
1988	387	112	259	15	0	0	0	0
1989	577	575	286	286	47	47	0	0
1990	898	898	468	468	135	135	0	0
1991	370	362	163	158	174	174	0	0
1992	978	591	446	238	318	209	0	0
1993	650	309	299	215	139	81	0	0
1994	738	464	432	281	109	85	0	0
1995	645	448	537	421	11	11	0	0
1996	215	189	134	108	78	78	0	0
1997	129	112	118	102	0	0	0	0
1998	280	250	204	174	51	51	0	0
1999	180	121	153	111	1	0	0	0
2000	289	275	157	144	52	51	0	0
2001	303	163	177	58	57	57	0	0
2002	336	176	279	119	53	53	0	0
2003	117	94	54	54	35	35	0	0
2004	212	183	166	137	46	46	0	0
2005	375	277	261	171	59	59	0	0
2006	197	186	75	71	61	61	0	0
2007	185	183	130	128	54	54	0	0
2008	123	118	69	66	52	52	0	0
2009	249	192	130	73	56	56	0	0
2010	390	293	177	158	0	0	0	0
2011	278	216	126	64	65	65	0	0
2012	342	328	205	194	53	53	0	0
2013	197	196	76	76	0	0	0	0
2014	247	220	179	157	55	55	0	0
2015	50	50	47	47	0	0	0	0
2016	214	185	145	116	23	23	0	0
2017	22	20	2	0	0	0	0	0
2018	197	197	72	72	52	52	0	0
Total	12 274	8 756	7 132	4 750	1 860	1 643	249	249

Table 5: Catch weight (kg) for each species reported from trawl surveys across the New Zealand EEZ annually

Year	*Dalatias licha*	*Centrophorus squamosus*	*Centroscymnus owstonii*	*Centroselachus crepidater*	*Etmopterus granulosus*	*Scymnodon plunketi*	*Deania calcea*
1982	16	7	14	48	1 007	40	205
1983	182	195	626	184	551	32	394
1984	190	125	1 245	836	7 335	208	3 272
1985	980	1 782	2 020	1 221	2 326	62	10 631
1986	678	1 364	2 837	3 069	7 377	553	22 178
1987	2 154	1 093	3 330	3 477	10 983	448	14 629
1988	1 510	733	2 661	6 514	3 994	235	11 808
1989	998	1 511	2 339	4 445	7 015	610	14 526
1990	2 056	2 211	6 697	10 363	9 579	1 196	20 488
1991	649	1 204	803	2 225	25 676	1 807	4 254
1992	1 272	3 195	4 337	11 684	31 810	2 272	23 583
1993	727	1 736	1 548	3 618	8 084	316	18 555
1994	1 038	2 194	3 943	8 088	35 499	2 266	22 998
1995	298	777	951	4 692	6 592	241	11 831
1996	415	328	683	2 761	4 280	596	3 752
1997	81	287	145	746	2 985	163	1 830
1998	272	1 479	625	3 383	4 636	154	7 091
1999	178	763	1 402	1 679	13 207	969	4 517
2000	223	1 599	453	1 553	13 656	1 967	2 790
2001	380	1 264	377	1 283	8 499	1 137	5 502
2002	201	1 044	1 215	2 457	4 941	485	4 544
2003	166	311	97	1 943	764	172	2 356
2004	289	687	823	2 056	6 892	366	6 673
2005	634	2 245	2 199	3 277	5 631	376	5 225
2006	360	1 858	912	1 999	1 465	244	3 358
2007	222	956	609	2 539	1 633	129	7 132
2008	268	1 369	572	1 710	737	88	3 801
2009	362	2 025	665	2 382	3 135	601	5 357
2010	656	2 296	2 142	2 952	2 326	176	12 702
2011	407	3 189	1 056	2 160	2 143	413	6 412
2012	566	2 970	1 481	2 995	3 861	306	7 474
2013	384	2 486	1 003	1 495	576	278	5 908
2014	345	1 524	750	2 348	3 784	494	6 975
2015	32	67	73	133	267	59	248
2016	176	1 239	1 411	2 059	2 426	443	5 750
2017	63	21	43	11	11	211	255
2018	134	1 687	1 285	1 883	767	332	4 059
Total	19 563	49 816	53 371	106 265	246 450	20 443	293 064

Table 6: Catch weight (kg) for each species reported from trawl surveys on Chatham Rise annually. '–' denotes no catch.

Year	*Dalatias licha*	*Centrophorus squamosus*	*Centroscymnus owstonii*	*Centroselachus crepidater*	*Etmopterus granulosus*	*Scymnodon plunketi*	*Deania calcea*
1982	–	–	–	–	–	–	–
1983	–	–	–	–	–	–	–
1984	3	–	18	112	5 370	14	155
1985	7	15	75	83	347	6	170
1986	315	173	1 660	2 460	2 123	324	9 081
1987	–	–	–	–	–	–	–
1988	76	–	66	122	135	12	513
1989	261	154	1 636	3 727	4 986	352	8 165
1990	337	246	3 985	7 583	6 511	240	10 990
1991	373	57	51	383	1 969	39	3 101
1992	634	838	1 441	6 205	2 944	37	11 620
1993	153	156	256	606	3 250	66	5 564
1994	258	261	1 568	3 541	15 459	895	6 723
1995	206	400	615	3 667	4 599	226	9 284
1996	58	126	441	1 351	2 725	73	2 428
1997	75	141	133	701	2 612	102	1 635
1998	112	232	313	1 929	3 202	94	4 519
1999	166	334	990	1 467	8 064	274	3 490
2000	110	300	190	856	12 355	1 859	1 716
2001	140	250	184	326	333	39	2 009
2002	88	232	583	872	2 301	314	3 327
2003	65	92	10	320	347	61	1 633
2004	254	228	574	1 013	3 985	205	5 028
2005	127	491	1 290	1 073	1 604	115	3 001
2006	32	98	200	561	668	90	1 507
2007	91	610	518	1 556	1 189	92	6 705
2008	133	416	517	620	182	60	1 959
2009	104	166	63	217	679	150	1 713
2010	308	865	951	2 335	1 598	89	5 028
2011	151	288	510	1 122	224	73	2 873
2012	142	557	845	2 472	3 094	130	5 548
2013	175	275	362	1 262	416	38	5 054
2014	279	362	635	1 561	2 452	410	4 716
2015	28	31	73	123	267	59	227
2016	135	532	404	1 799	1 507	77	4 941
2017	–	–	–	–	–	–	–
2018	100	210	523	1 101	441	81	2 444
Total	5 493	9 134	21 674	53 122	97 935	6 695	136 867

Table 7: Catch weight (kg) for each species reported from trawl surveys on Sub-Antarctic annually. '–' denotes no catch.

Year	*Dalatias licha*	*Centrophorus squamosus*	*Centroscymnus owstonii*	*Centroselachus crepidater*	*Etmopterus granulosus*	*Scymnodon plunketi*	*Deania calcea*
1982	–	–	–	–	–	–	–
1983	–	–	–	–	–	–	–
1984	–	–	–	–	–	–	–
1985	–	–	–	–	–	–	–
1986	–	–	–	–	–	–	–
1987	–	–	–	–	–	–	–
1988	–	–	–	–	–	–	–
1989	25	588	11	306	688	43	381
1990	172	867	29	1 915	2 042	171	1 273
1991	275	1 090	696	1 799	23 511	1 767	1 069
1992	114	1 042	1 181	1 372	10 029	1 388	1 557
1993	95	711	76	1 134	519	50	1 343
1994	177	1 514	529	692	4 056	494	473
1995	4	278	–	–	28	–	143
1996	85	97	224	1 309	1 142	446	1 005
1997	–	–	–	–	–	–	–
1998	107	1 233	244	1 114	534	35	2 092
1999	–	–	–	–	–	–	–
2000	51	620	143	633	628	1	231
2001	190	712	85	452	552	16	1 082
2002	81	434	284	864	539	57	1 006
2003	43	175	47	1 590	378	35	429
2004	32	385	51	966	339	18	1 262
2005	53	647	244	1 816	430	31	1 107
2006	245	380	125	1 310	705	64	1 502
2007	131	346	81	983	441	37	408
2008	133	949	55	1 089	555	27	1 839
2009	70	874	100	1 710	708	68	1 641
2010	–	–	–	–	–	–	–
2011	70	446	72	755	819	168	2 076
2012	74	906	109	397	473	58	976
2013	–	–	–	–	–	–	–
2014	8	417	21	495	529	26	1 723
2015	–	–	–	–	–	–	–
2016	0	155	7	65	93	25	13
2017	–	–	–	–	–	–	–
2018	13	362	32	622	292	71	983
Total	2 248	15 228	4 443	23 390	50 030	5 095	25 613

Table 8: Catch weight (kg) for each species reported from *Wanaka* surveys annually. '–' denotes no catch.

Year	*Dalatias licha*	*Centrophorus squamosus*	*Centroscymnus owstonii*	*Centroselachus crepidater*	*Etmopterus granulosus*	*Scymnodon plunketi*	*Deania calcea*
1985	405	441	923	165	170	–	7 445
1986	223	833	815	190	87	36	8 351
Total	628	1 274	1 738	355	256	36	15 796

Table 9: Estimated catch weight (kg) for each species where sex and maturity stage (immature female, IF; immature male, IM; mature female, MF; mature male, MM) were recorded from research trawl data. For the Wanaka series, sufficient information was available only *for Deania calcea.*

Sex/ maturity	*Dalatias licha*	*Centrophorus squamosus*	*Centroscymnus owstonii*	*Centroselachus crepidater*	*Etmopterus granulosus*	*Scymnodon plunketi*	*Deania calcea*
Chatham Rise							
IF	476	533	583	5 383	9 222	177	12 889
IM	337	239	172	2 847	2 591	78	3 951
MF	40	197	300	1 844	3 963	26	1 984
MM	32	83	1 147	2 885	6 284	54	8 636
Sub-Antarctic							
IF	136	322	205	1 287	2 229	90	2 051
IM	95	223	157	553	874	52	306
MF	31	255	29	1 676	613	4	712
MM	1	277	136	1 110	1 657	15	1 890
Wanaka							
IF	–	–	–	–	–	–	1 148
IM	–	–	–	–	–	–	530
MF	–	–	–	–	–	–	529
MM	–	–	–	–	–	–	1 083

3.2 Observer data

Observer data were available from 2008, and more were available from Chatham Rise than Sub-Antarctic (Table 10). *Deania calcea* was the most reported species by weight on Chatham Rise, whereas *Centrophorus squamosus* was the most reported species by weight in the Sub-Antarctic. Models for *Centroscymnus owstonii* and *Centrophorus squamosus* on Chatham Rise and for all species on Sub-Antarctic did not converge, so a smaller time series from 2012 onwards was modelled for both areas. In the Sub-Antarctic, this allowed models to converge for *Centrophorus squamosus*, *E. granulosus*, and *Deania calcea*.

Table 10: Total number of observations reported annually from fisheries included in the VAST model where the minimum number of observations per year (*n* = 10) and the minimum number of events per vessel (*n* = 5) was met, and catch weight (kg) for each species reported from Chatham Rise and Sub-Antarctic.

Year	n	*Dalatias licha*	*Centrophorus squamosus*	*Centroscymnus owstonii*	*Centroselachus crepidater*	*Etmopterus granulosus*	*Scymnodon plunketi*	*Deania calcea*
Chatham Rise								
2008	661	10 356	591	271	7 159	11 216	50	60 545
2009	1 204	6 152	1 598	1 137	14 754	58 322	5 379	58 369
2010	84	1 077	10	0	466	2 980	558	1 795
2011	497	6 539	112	206	299	16 482	77	26 501
2012	515	599	3 037	432	918	22 583	191	6 573
2013	527	878	2 309	158	2 407	20 847	595	13 596
2014	366	1 339	1 578	17	585	4 238	170	11 527
2015	449	815	1 528	220	2 556	7 254	652	7 223
2016	672	573	5 887	4 132	3 474	16 037	764	16 476
2017	463	3 310	6 194	89	112	29 982	476	10 201
2018	1 041	7 081	3 778	2 805	4 856	20 970	2 544	65 597
Total	6 479	38 719	26 622	9 467	37 586	210 911	11 456	278 403
Sub-Antarctic								
2008	246	11	0	43	115	14 320	0	3
2009	72	0	56	0	14	2 118	0	5
2010	1	0	200	0	0	0	0	150
2011	18	3	0	0	0	322	0	23
2012	74	376	5 774	457	12	1 270	470	1 708
2013	215	2 049	12 343	0	1 375	2 867	1 591	13 898
2014	36	59	411	21	0	445	17	6
2015	103	435	3 765	0	515	1 148	259	649
2016	59	332	6 237	0	80	2 074	69	694
2017	160	718	6 779	0	161	2 420	241	1 771
2018	251	993	42 926	0	2 155	3 758	386	16 228
Total	1 235	4 976	78 491	521	4 427	30 742	3 033	35 135

3.3 Multi-species

A multi-species analysis for the New Zealand EEZ combined all species across all years. Overall density and probability of encounter across all years (from 1997) for each species are shown in Figure 4 and Figure 5. Time series from 2010–2018 for each species and residual plots are available in Appendix 4.

Dalatias licha

Dalatias licha was most frequently predicted off the east coast of the North Island, on the northern and southeast Chatham Rise, off the west coast of the South Island, and at Puysegur (Figure 4, Appendix 3 for GAM outputs). High densities of this species were predicted off Puysegur, the west coast of the South Island, Challenger Plateau, the east coast between Banks Peninsula and East Cape, and the northern Chatham Rise (Figure 4). The probability of encounter was highest in waters west of the Chatham Islands, on the Challenger Plateau, and off Puysegur (Figure 5). *Dalatias licha* was absent from the Bounty Plateau but occurred over Campbell Plateau.

Centrophorus squamosus

Centrophorus squamosus was predicted on the northern and southeast Chatham Rise, at Puysegur, on the western Campbell Plateau, and off the west coast South Island (Figure 4, Appendix 3 for GAM outputs). Highest densities were predicted around the northwest North Island, on the Challenger Plateau, at Puysegur, and on the southwest of Campbell Plateau (Figure 4). Probability of encounter was highest off Puysegur (Figure 5). On Chatham Rise, the species abundance was greatest at the eastern end, and occurrence was greatest on the northern and eastern Chatham Rise (Figure 4, Figure 5). In the Sub-Antarctic, *Centrophorus squamosus* density and probability of encounter were highest off Puysegur and southward on the continental shelf on the western Campbell Plateau (Figure 4, Figure 5).

Centroscymnus owstonii

Centroscymnus owstonii was predicted predominantly off the east coast of the North Island, on the northern Chatham Rise, at Puysegur, and off the west coast South Island (Figure 4, Appendix 3 for GAM outputs). Highest densities occurred around the North Island, on the northern Chatham Rise, at Puysegur, and off the west coast of the South Island (Figure 4). Probability of encounter was highest in the central area of the northern slope and northeast of Chatham Rise (Figure 5). The waters off the Otago region were highlighted as an area of relatively high probability of encounter (Figure 5).

Centroselachus crepidater

Centroselachus crepidater was predicted along the northern and eastern slopes of Chatham Rise, off Puysegur, on the northern slope of Campbell Plateau, and off the west coast of the South Island (Figure 4, Appendix 3 for GAM outputs). Highest densities occurred on the northern and eastern slopes of Chatham Rise, at Puysegur, and on the northern slope of Campbell Plateau, whereas probability of encounter was highest on the Chatham Rise and at Puysegur; however, there was large variation in the species availability throughout these areas (Figure 4). On the Chatham Rise, the highest density occurred on the eastern portion of Chatham Rise (Figure 4). Probability of encounter was also high here, as well as off the east coast of the South Island and parts of the central northern Chatham Rise. Density and probability of encounter was highest off Puysegur and on the northern Campbell Plateau in the Sub-Antarctic (Figure 4, Figure 5). The waters off the Otago region were highlighted as an area of relatively high probability of encounter (Figure 5).

Etmopterus granulosus

Etmopterus granulosus was predicted to be along the east coast of the North Island, on the slope of Chatham Rise, across most of Campbell Plateau, and off Puysegur (Figure 4, Appendix 3 for GAM outputs). Density was particularly high for this species, with highest densities occurring off Puysegur and off Otago on the east coast of the South Island (Figure 4). Probability of encounter was highest

from the southern Chatham Rise to the northern half of the Campbell Plateau, on the Bounty Plateau, and off Puysegur. On the Chatham Rise, density and probability of encounter were highest on the southern slope. In the Sub-Antarctic, these modelled outputs were strongest around the outer edge of Campbell Plateau, as well as off the Bounty Plateau (Figure 4, Figure 5). The highest density was at Puysegur and in waters off the Otago region (Figure 4).

Scymnodon plunketi

Scymnodon plunketi was sparsely predicted in parts of the Chatham Rise, off Puysegur, and off the west coast of the South Island (Figure 4, Appendix 3 for GAM outputs). Highest densities occurred off the south-eastern slope of Chatham Rise and off Puysegur (Figure 4). Probability of encounter was highest off Puysegur and on the southern Campbell Plateau (Figure 5). The waters off the Otago region were highlighted as the highest area of density and probability of encounter for this species (Figure 4, Figure 5).

Deania calcea

Deania calcea was predicted along the west and east coasts of the North Island, the slope of Chatham Rise, off Puysegur, on the southern slope of Campbell Plateau, and off the west coast of the South Island (Figure 4, Appendix 3 for GAM outputs). Highest densities occurred around the North Island, on the northern and eastern slopes of Chatham Rise, at Puysegur, and off the west coast South Island. The probability of encounter was highest off the east coast North Island, on the eastern Chatham Rise, and at Puysegur (Figure 4, Figure 5). On the Chatham Rise, density was high along the northern slope, and the highest density was on the southeast slope (Figure 4). Probability of encounter was highest along the northern Chatham Rise. Density and probability of encounter in the Sub-Antarctic were concentrated at Puysegur and a small region of the southern slope of Campbell Plateau (Figure 5). Around the North Island, density was highest off the southeast and northwest coasts, and probability of encounter was high and evenly distributed around the region (Figure 4, Figure 5). The waters off the Otago region were highlighted as an area of relatively high density and probability of encounter (Figure 4, Figure 5).

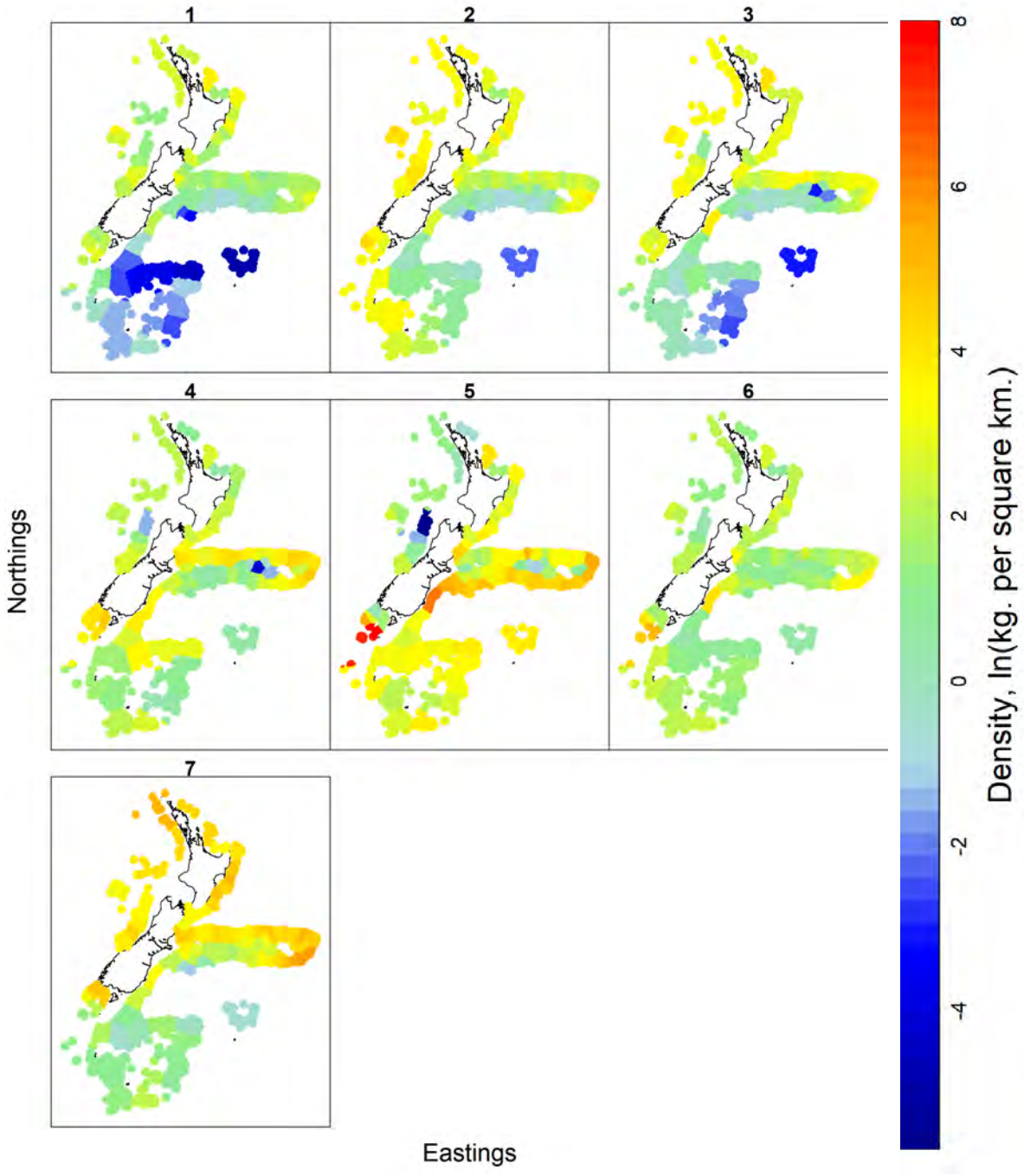

Figure 4: **VAST outputs for relative density (kg km^{-2}) of (from top left) *Dalatias licha*, *Centrophorus squamosus*, *Centroscymnus owstonii*, *Centroselachus crepidater*, *Etmopterus granulosus*, *Scymnodon plunketi*, and *Deania calcea* throughout New Zealand waters, all years combined. Time series for each species from 2010 are shown in Appendix 5 to Appendix 11.**

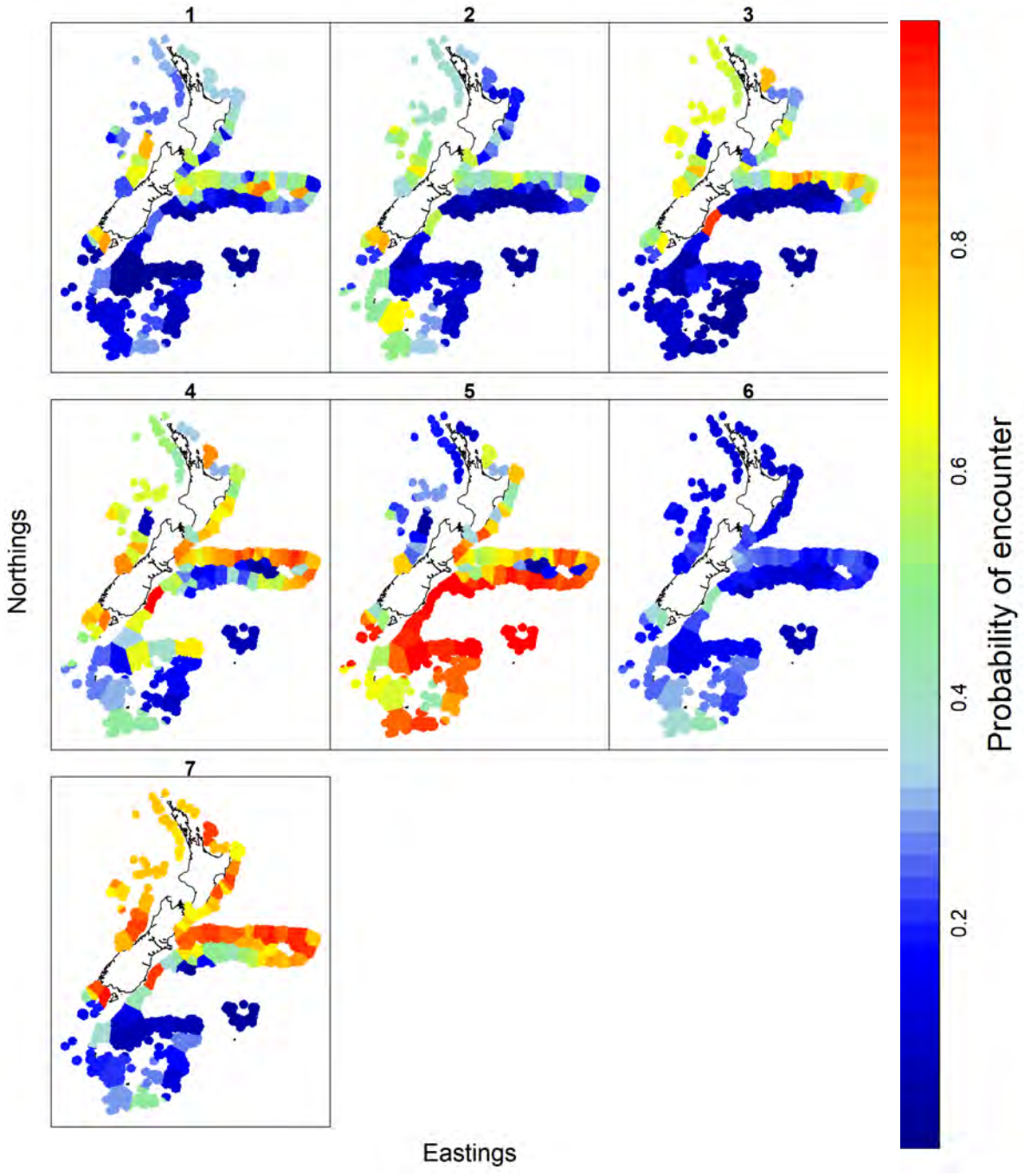

Figure 5: VAST outputs for probability of encounter of (from top left) *Dalatias licha*, *Centrophorus squamosus*, *Centroscymnus owstonii*, *Centroselachus crepidater*, *Etmopterus granulosus*, *Scymnodon plunketi*, and *Deania calcea* across the New Zealand waters, all years combined. Time series for each species from 2010 are shown in Appendix 5 to Appendix 11.

3.4 *Dalatias licha*

The *Dalatias licha* single species model predicted less density of the species around the North Island and overall more probability of encounter than the multi-species analysis (Figure 6, Figure 7). The VAST models for the Sub-Antarctic-only data did not converge and are not shown here. From the *Wanaka* surveys, *Dalatias licha* density was highest around the south-east coast of the North Island, but probability of encounter was low (Figure 8).

Model outputs are presented for Chatham Rise data separated by sex and maturation stage; both density and probability of encounter were low (Figure 9, Figure 10). Given the small sample sizes, particularly for mature individuals (< 50 observations for each sex), trends observed here are probably not reflective of true population structure. No trends in density or probability of encounter were observed in any region over the entire time series; this suggests spatial structure had remained constant over the time period studied (see Appendix 5 *Dalatias licha*, Figure 63 to Figure 71 for the full time series and residual plots).

Model outputs from observer data provided a different pattern of density and probability of encounter of *Dalatias licha* on the Chatham Rise, with highest densities occurring close to the east coast South Island and the southeast corner of Chatham Rise, whereas the highest probability of encounter was predicted for shallower waters west of Chatham Islands (Figure 11).

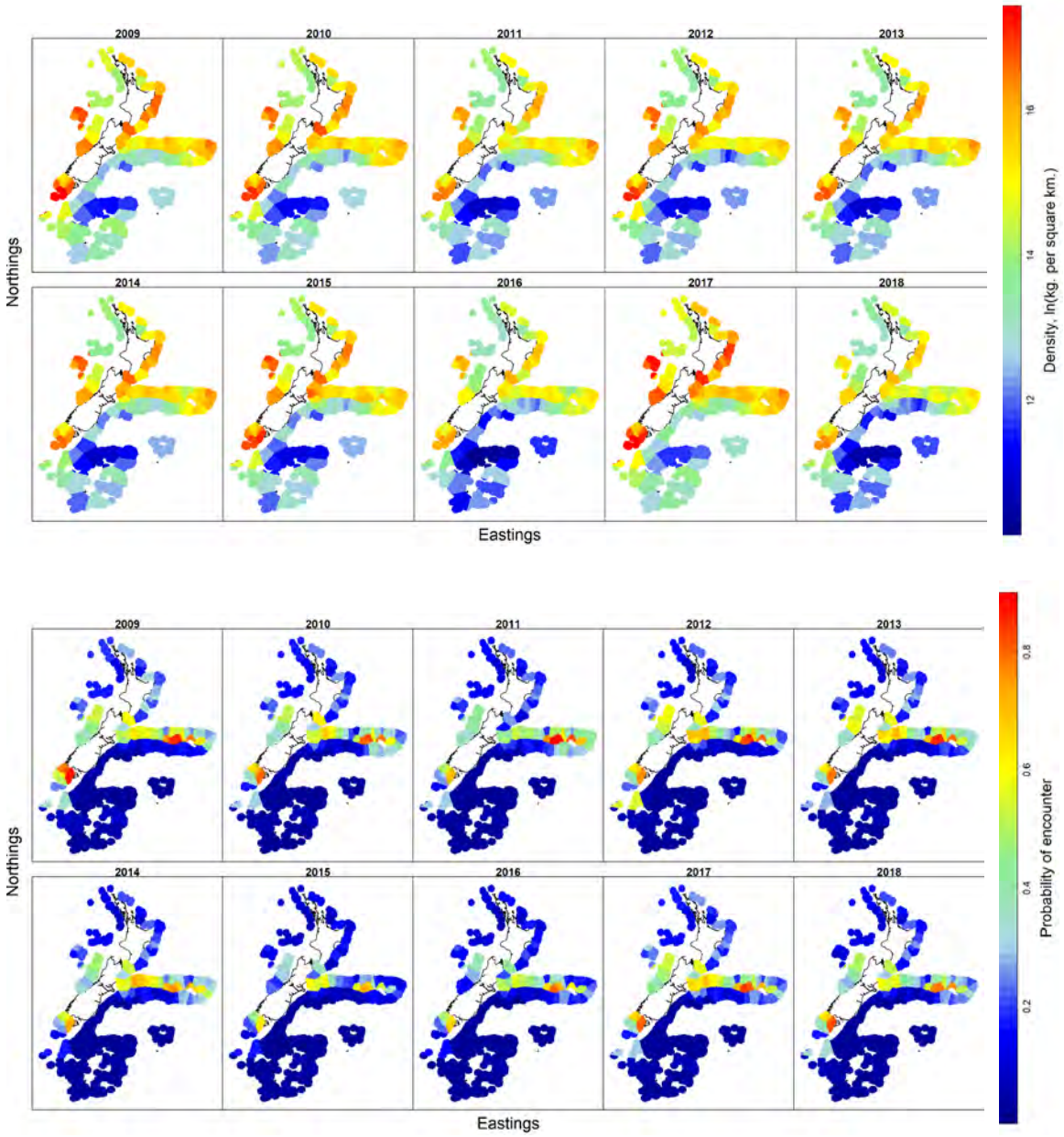

Figure 6: VAST outputs for relative density (kg km^{-2}, top panel) and probability of encounter (bottom panel) of *Dalatias licha* throughout New Zealand waters in the past decade (2009–2018, from left to right for each panel). The full time series is shown in Appendix 5. Note that scales for density plots vary from plot to plot.

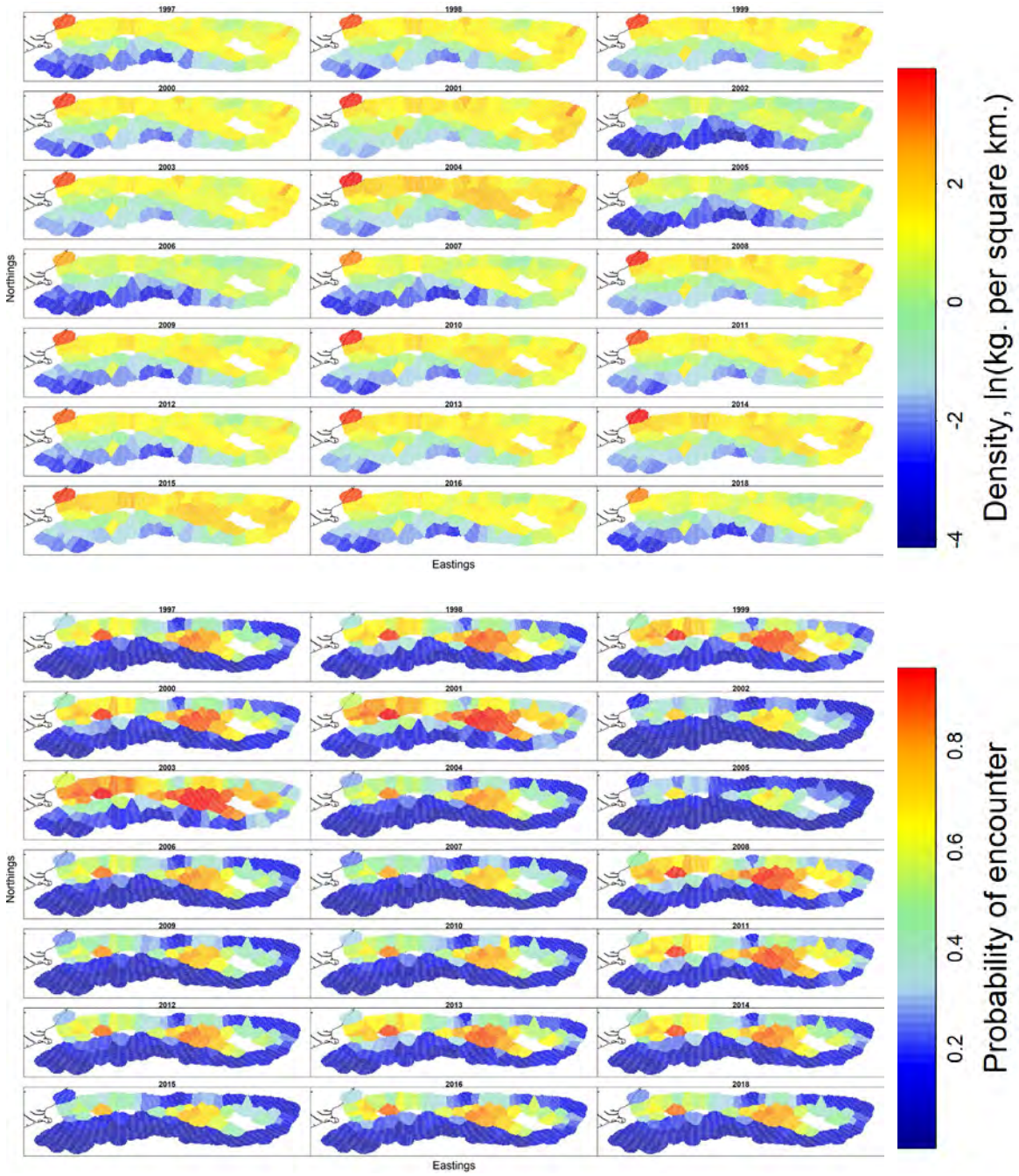

Figure 7: **VAST outputs for relative density (kg km^{-2}, top panel) and probability of encounter (bottom panel) of *Dalatias licha* across Chatham Rise (1997–2018, from left to right for each panel). The full time series is shown in Appendix 5.**

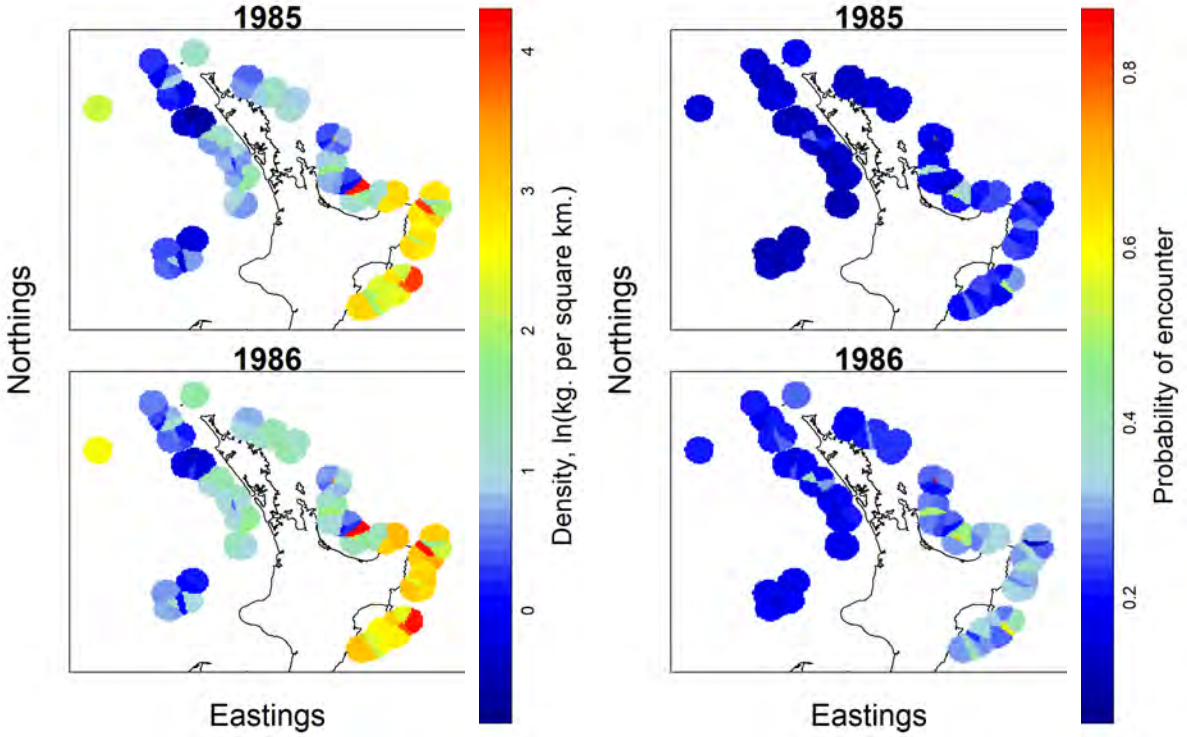

Figure 8: VAST outputs for relative density (kg km^{-2}, left panel) and probability of encounter (right panel) of *Dalatias licha* around the North Island of New Zealand in 1985–1986.

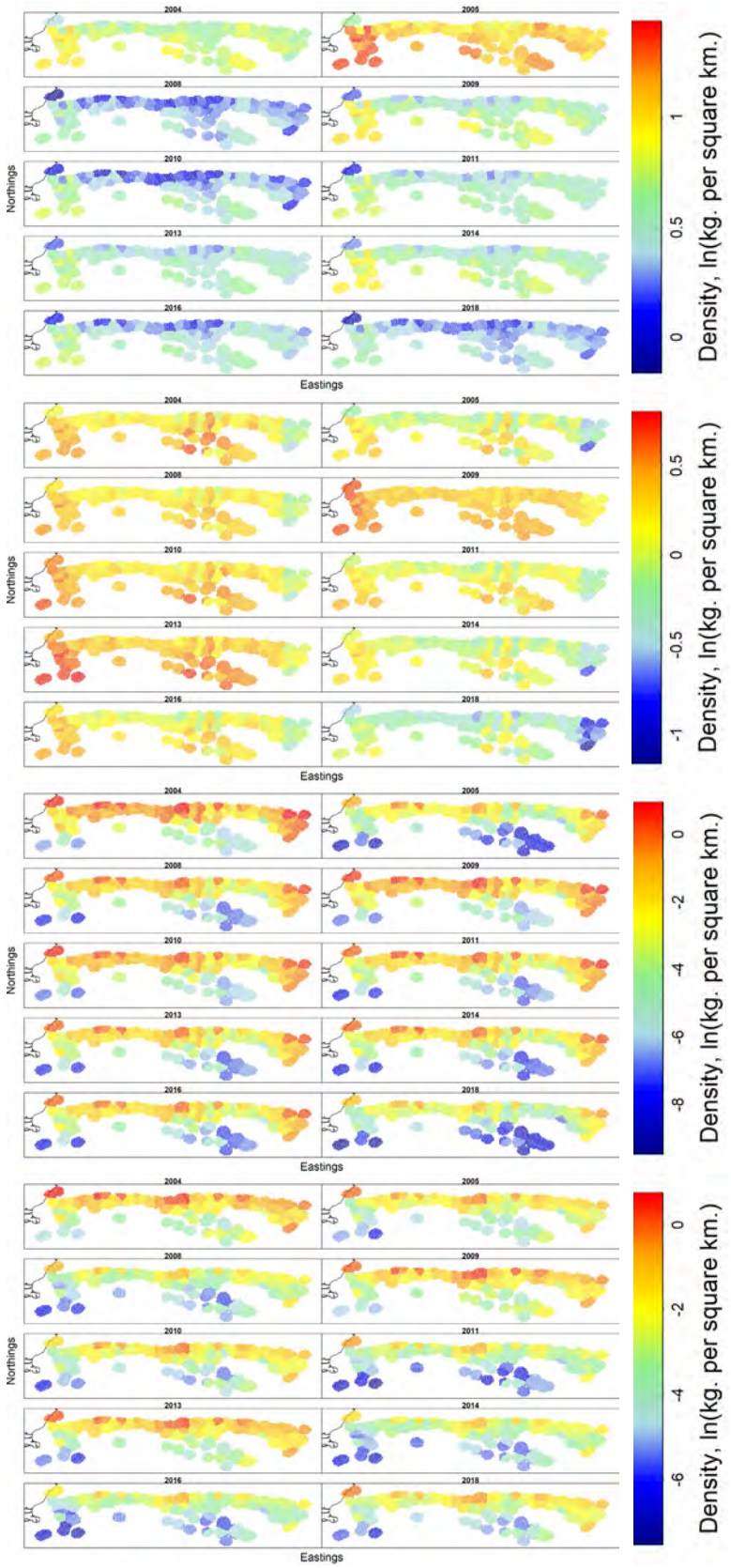

Figure 9: **VAST outputs for relative density (kg km^{-2}) of *Dalatias licha* by class (from top panel: immature female, immature male, mature female, mature male) across Chatham Rise (2004–2018, from left to right for each panel). Note that scales for density plots vary from plot to plot.**

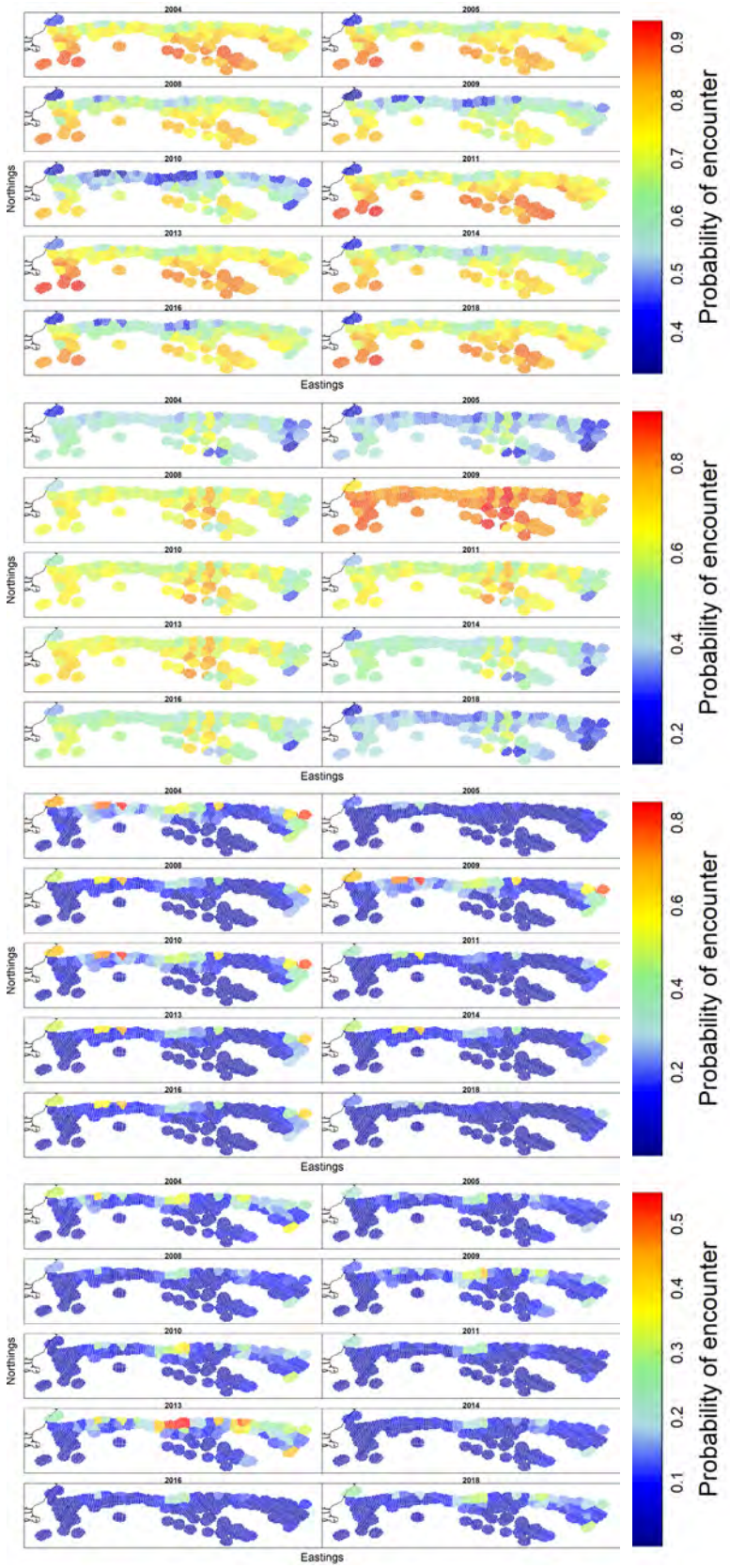

Figure 10: VAST outputs for probability of encounter of *Dalatias licha* by class (from top panel: immature female, immature male, mature female, mature male) across Chatham Rise (2004–2018, from left to right for each panel).

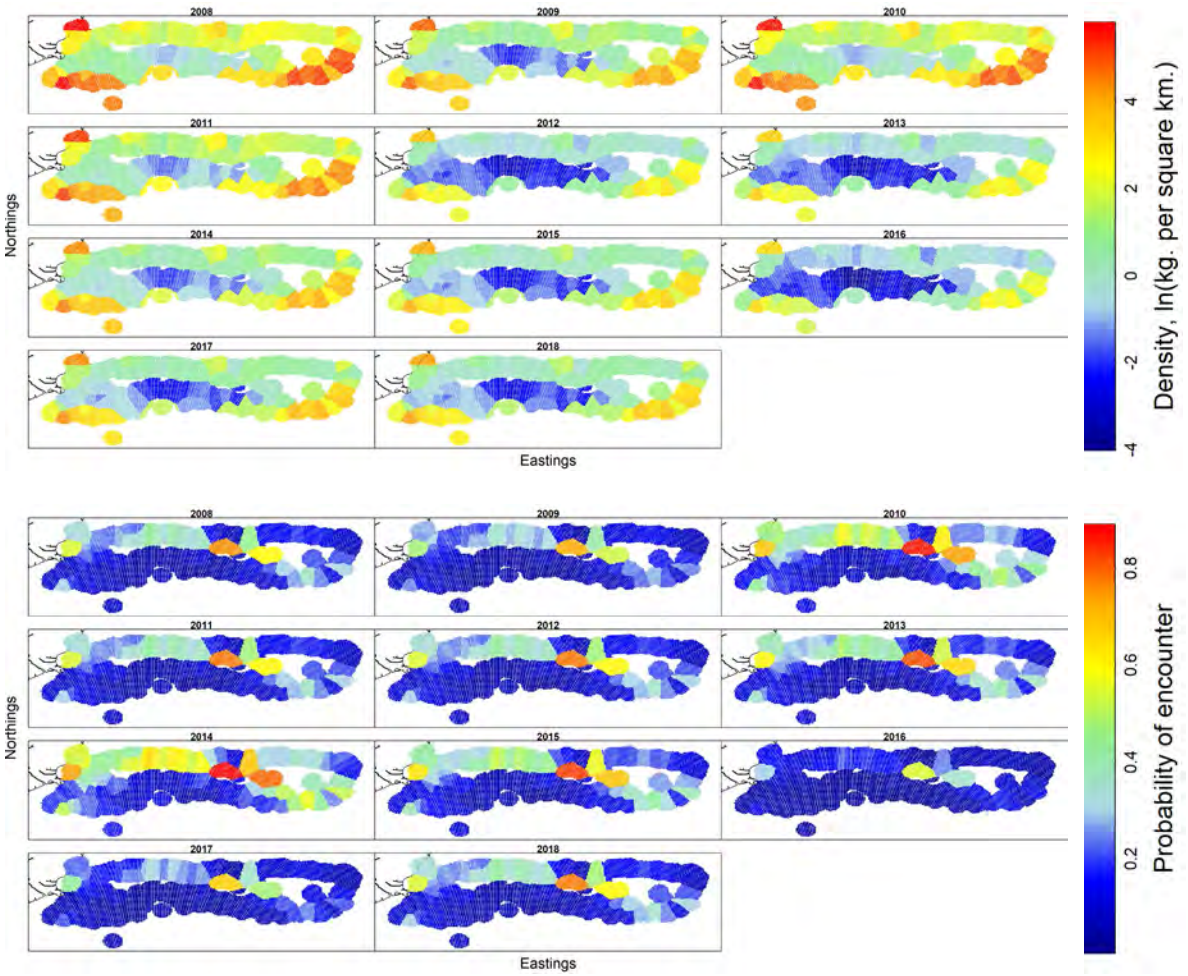

Figure 11: VAST outputs for relative density (kg km^{-2}, top panel) and probability of encounter (bottom panel) of *Dalatias licha* across Chatham Rise using observer records (2008–2018, from left to right for each panel).

3.5 *Centrophorus squamosus*

The single-species analysis was similar to the multi-species analysis for *Centrophorus squamosus* (Figure 12–Figure 14). Here, predicted density was highest off the west coast South Island, on southeast Chatham Rise, and at Puysegur, and probability of encounter was highest at Puysegur. For Chatham Rise, the models did not converge for the long time series, or by sex and maturity stage, likely due to few data. From the *Wanaka* surveys, *Centrophorus squamosus* was most abundant along the north west coast of the North Island, with a stronger spatial pattern in 1986 than in 1985 (Figure 15).

For the Sub-Antarctic, the models predicted that immature individuals were very rare in abundance and mainly restricted to the area at Puysegur and to a lesser extent on the western margin of the Campbell Plateau, whereas the distribution of mature females was strongest along the southwest Campbell Plateau (Figure 16 and Figure 17). Mature males were rare, being predicted mostly on the northeast Campbell Plateau and at Puysegur, the area where the density of immature females and immature males was predicted to be high.

The model using observer data for Chatham Rise initially failed to converge for this species. Given the small sample sizes before 2012, these years were removed, and this allowed model convergence. Highest density was concentrated in the central northern and southeast parts of Chatham Rise (although density was relatively low throughout the area); probability of encounter was low, and restricted to the central northern part of Chatham Rise (Figure 18). In the Sub-Antarctic, the observer data model showed

a similar pattern of density and probability of encounter to the research trawl data, with highest densities and probability of encounter predicted at Puysegur and the southwest part of the Campbell Plateau.

There appears to be an increasing trend in probability of encounter, but not relative density, at Puysegur throughout the entire time series (see Appendix 6 *Centrophorus squamosus*, Figure 72 to Figure 81 for the full time series and residual plots). This may be attributed to the data containing a large number of small individuals, because this region was a hotspot for immature individuals.

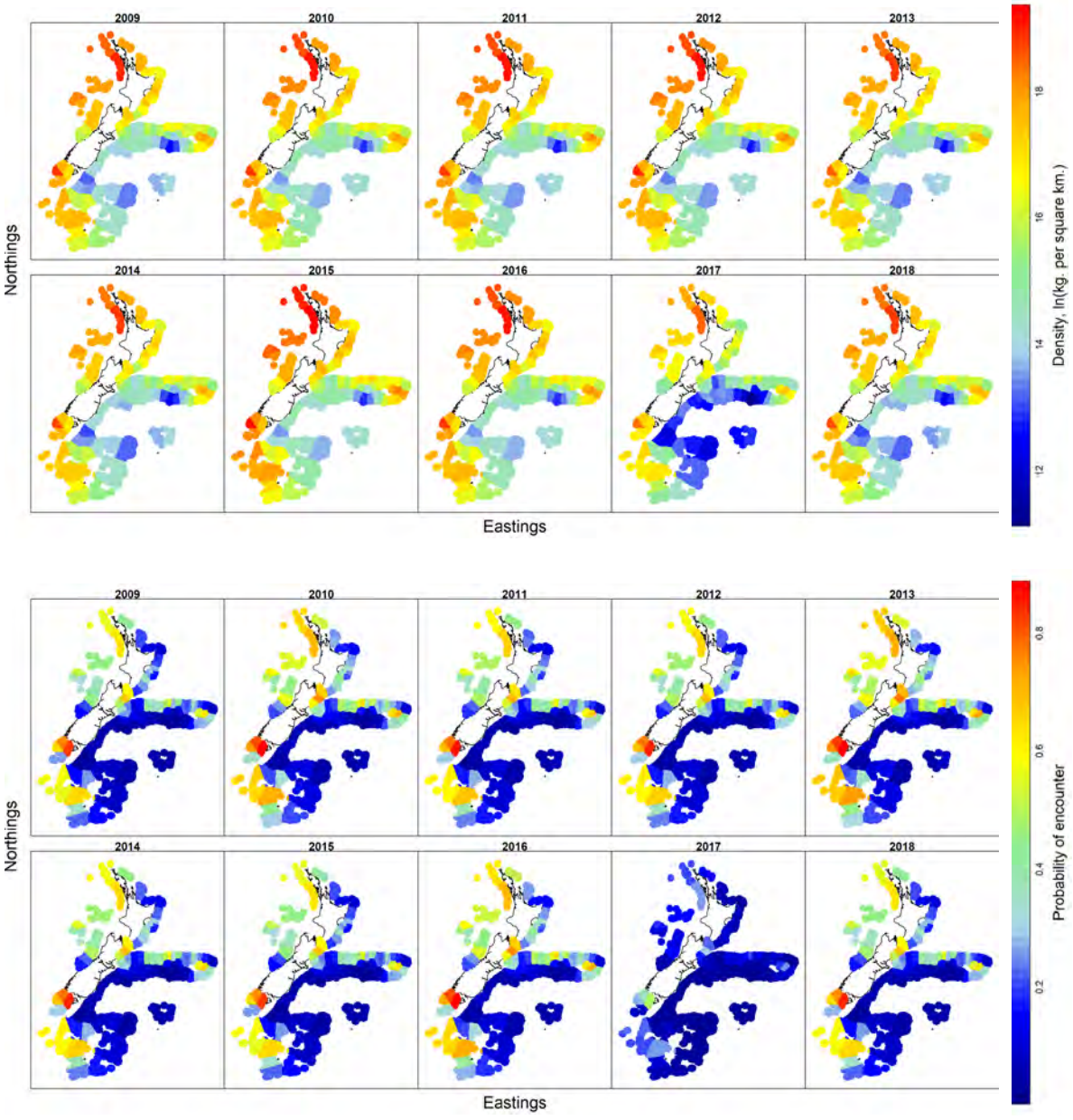

Figure 12: VAST outputs for relative density (kg km^{-2}, top panel) and probability of encounter (bottom panel) of *Centrophorus squamosus* throughout the New Zealand waters in the past decade (2009–2018, from left to right for each panel). The full time series is shown in Appendix 6. Note that scales for density plots vary from figure to figure.

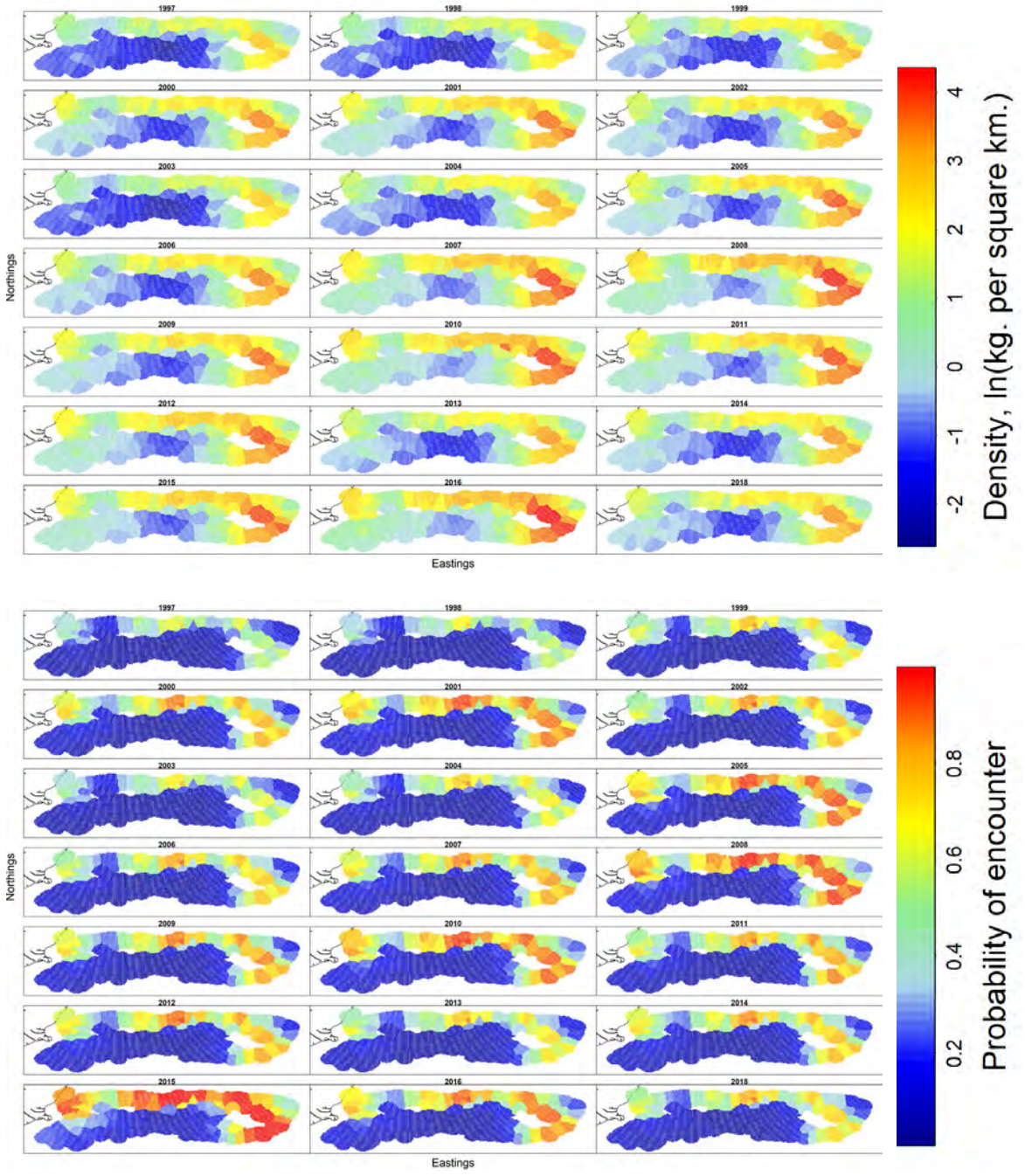

Figure 13: VAST outputs for relative density (kg km^{-2}, top panel) and probability of encounter (bottom panel) of *Centrophorus squamosus* across Chatham Rise (1997–2018, from left to right for each panel). The full time series is not available for *C. squamosus* (the model did not converge).

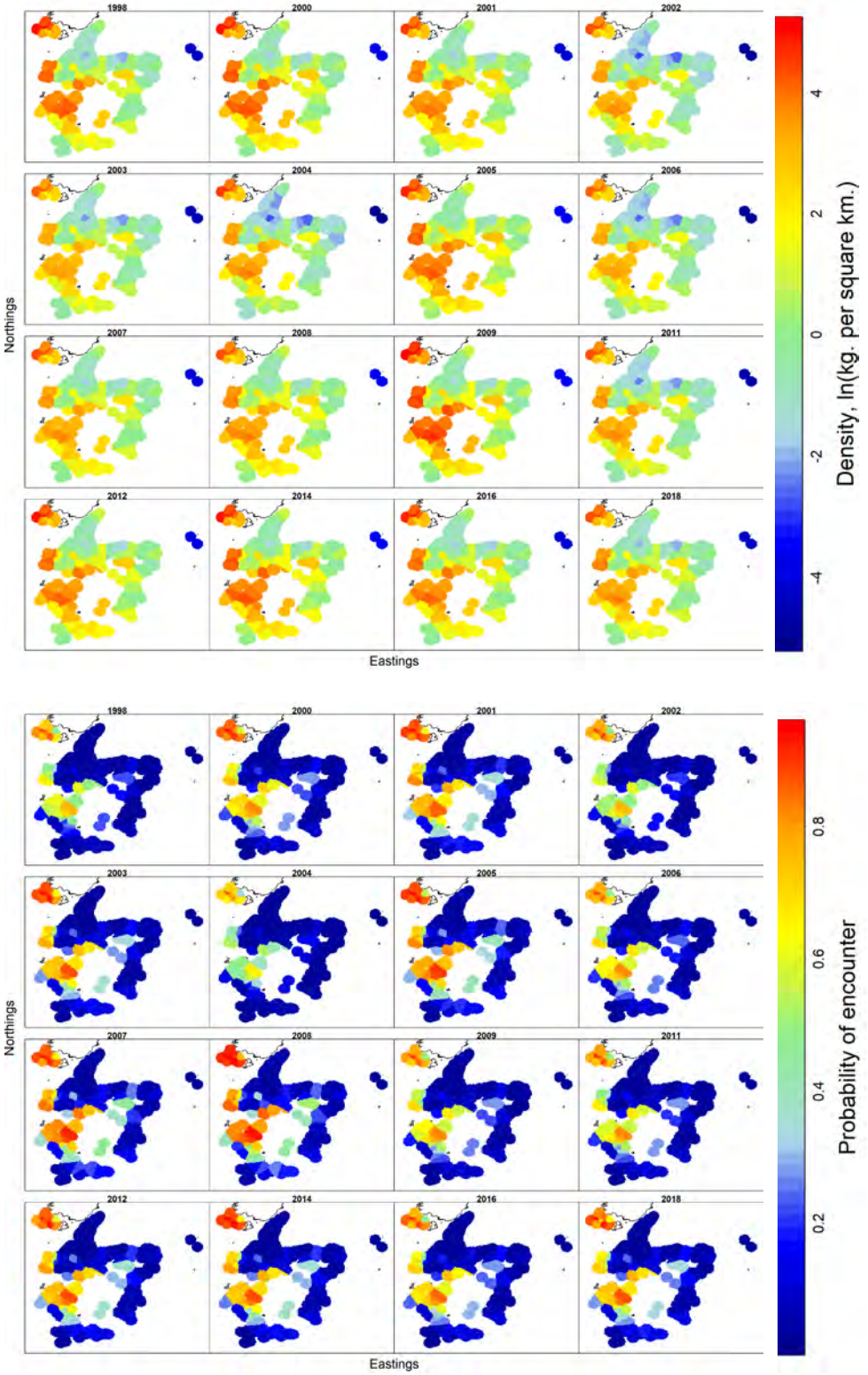

Figure 14: VAST outputs for relative density (kg km^{-2}, top panel) and probability of encounter (bottom panel) of *Centrophorus squamosus* across the Sub-Antarctic (1998–2018, from left to right for each panel). The full time series is shown in Appendix 6.

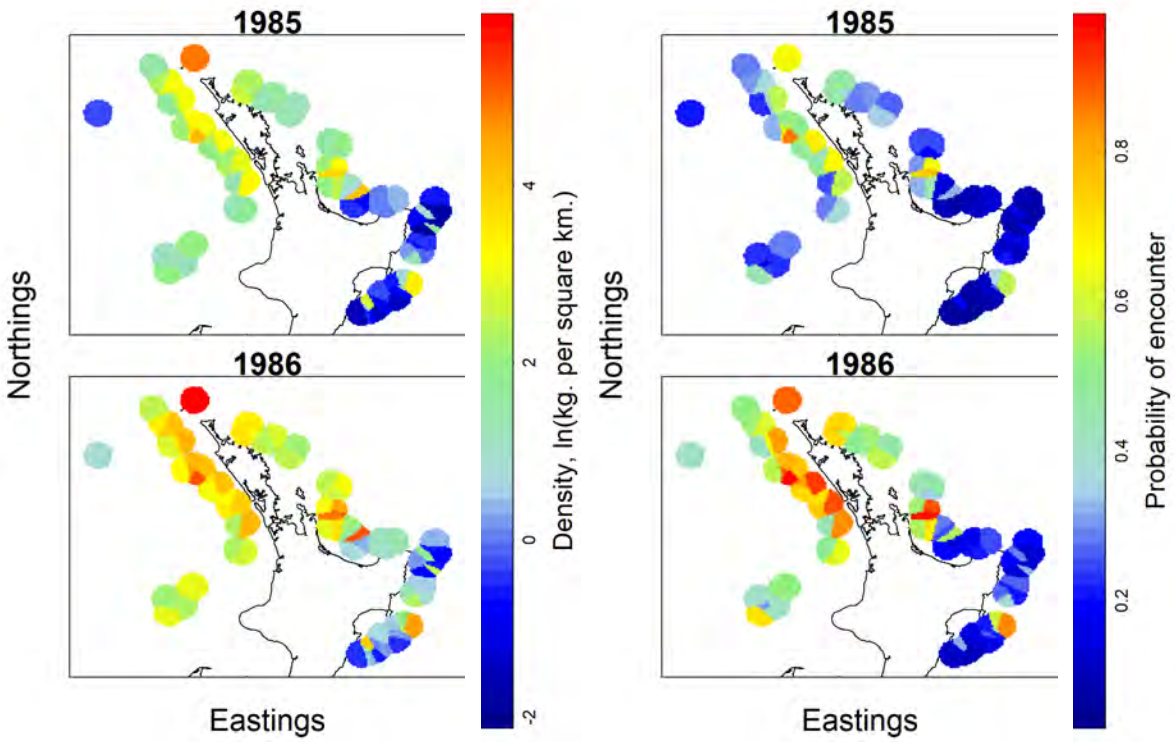

Figure 15: VAST outputs for relative density (kg km^{-2}, left panel) and probability of encounter (right panel) of *Centrophorus squamosus* around the North Island of New Zealand in 1985–1986.

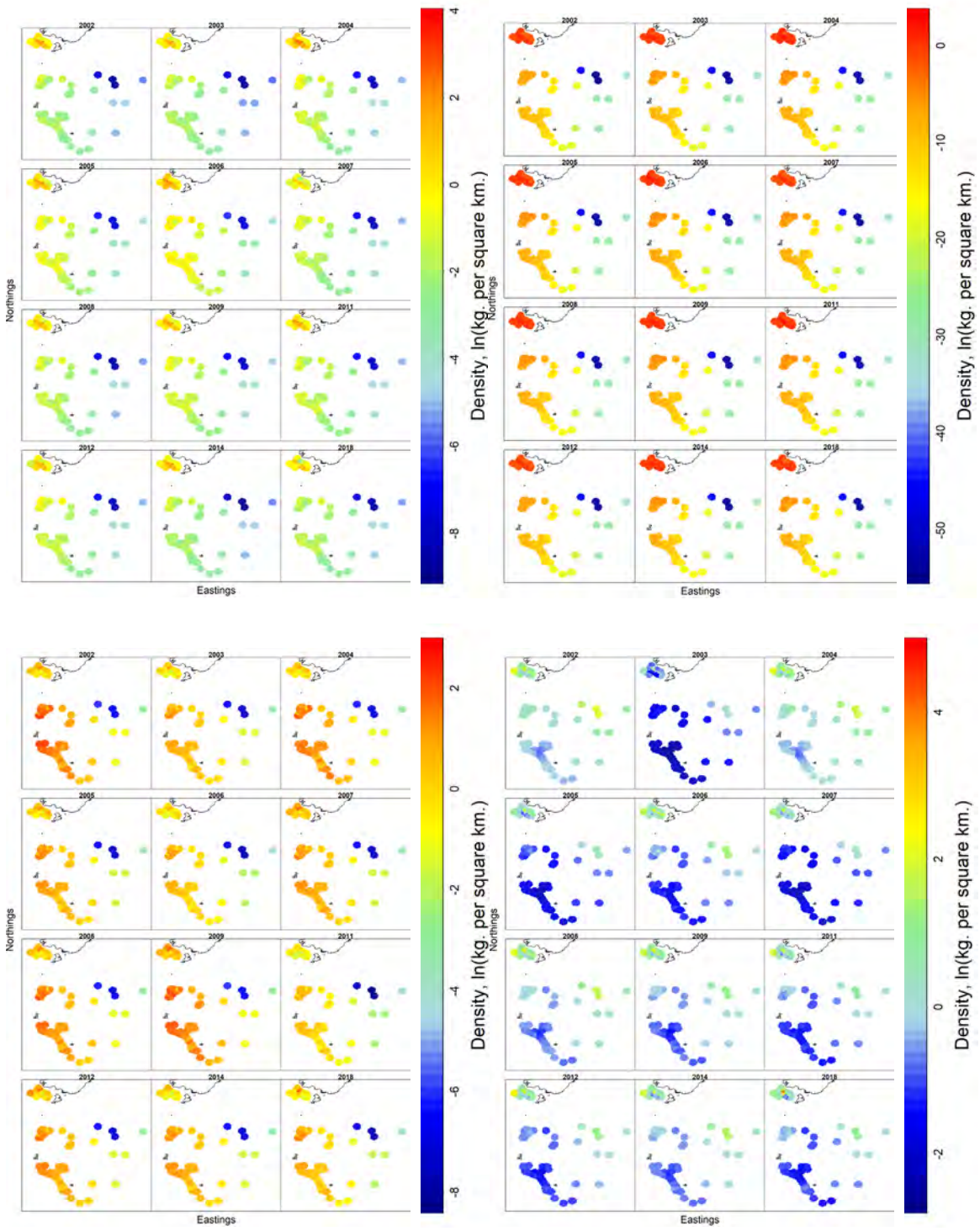

Figure 16: VAST outputs for relative density (kg km^{-2}) of *Centrophorus squamosus* by class (clockwise from top left: immature female, immature male, mature female, mature male) across the Sub-Antarctic (2002–2018, from left to right for each panel). Note that scales for density plots vary from plot to plot.

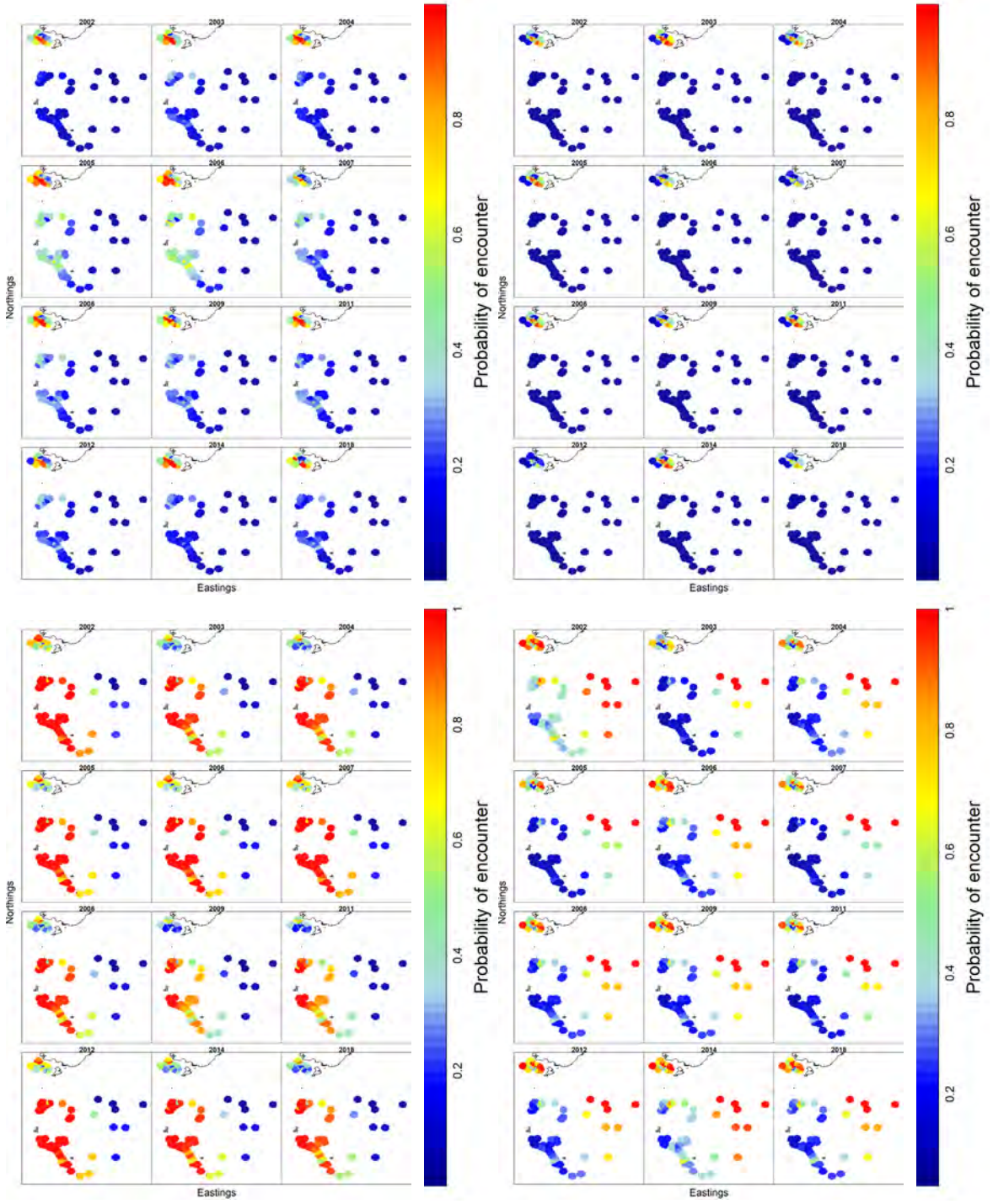

Figure 17: VAST outputs for probability of occurrence of *Centrophorus squamosus* by class (clockwise from top left: immature female, immature male, mature female, mature male) across the Sub-Antarctic (2002–2018, from left to right for each panel).

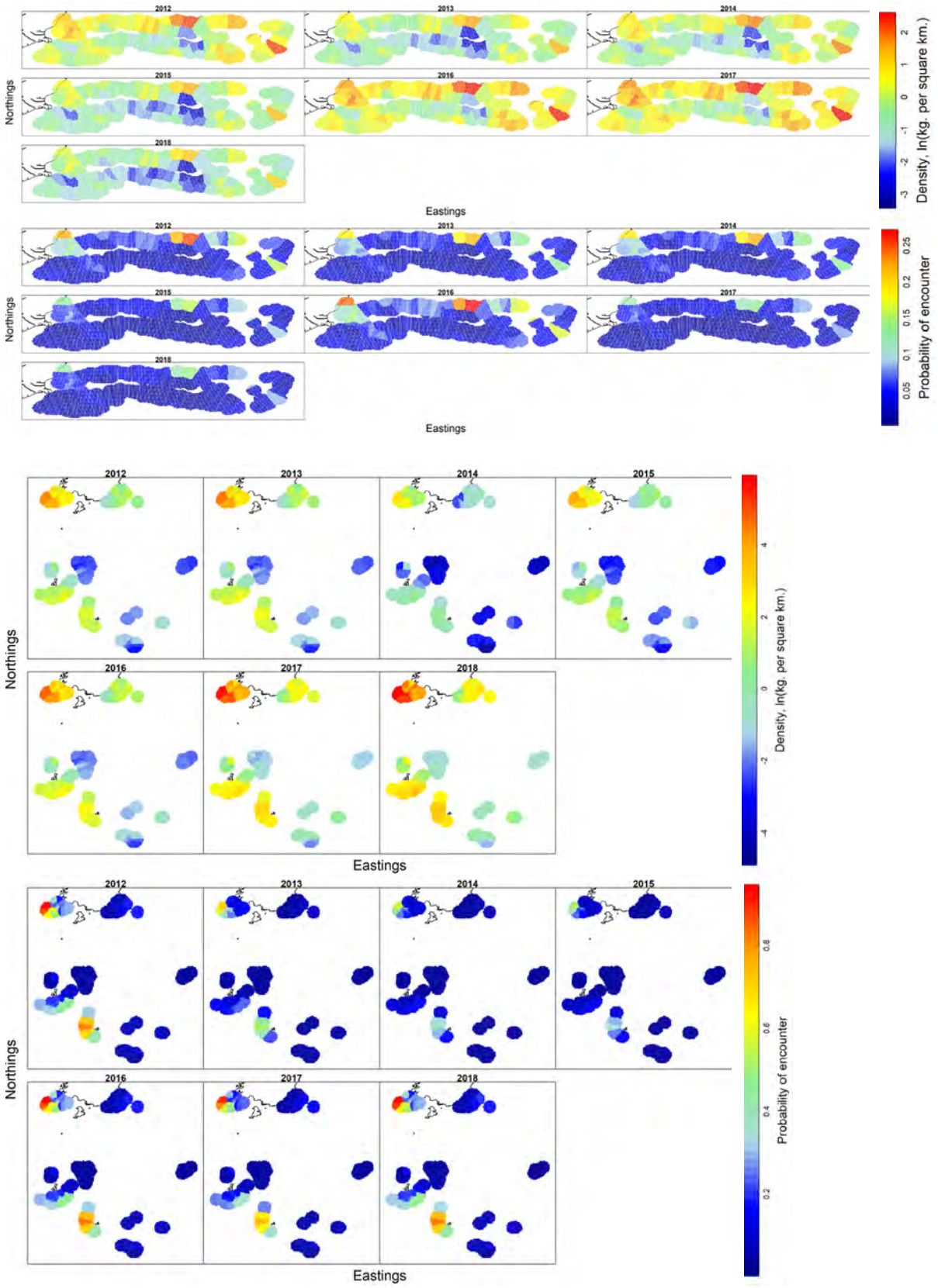

Figure 18: VAST outputs for relative density (kg km^{-2}) and probability of encounter of *Centrophorus squamosus* across Chatham Rise (top panels) and the Sub-Antarctic (bottom panels) using observer records (2012–2018, from left to right for each panel). Note that scales for density plots vary from plot to plot.

3.6 *Centroscymnus owstonii*

The single-species analysis was very similar to the multi-species analysis for *Centroscymnus owstonii* (Figure 19, Figure 20). The models for the Sub-Antarctic-only data did not converge and are not shown here. Predicted densities and probability of encounter were highest in waters north of Auckland (Figure 21).

Densities on the Chatham Rise were relatively evenly distributed for the sex and maturity stages, although probability of encounter was highest for immature female and mature male (Figure 22, Figure 23). There was little overlap in predicted distributions of immature and mature males.

The model using observer data for Chatham Rise initially failed to converge for this species. Given the small sample sizes before 2012, these years were removed, and this allowed model convergence. Highest density, albeit very low, was concentrated to the northeast Chatham Rise; probability of encounter was low, and mainly restricted to one area of northeast Chatham Rise (Figure 24).

No trends in density or probability of encounter were observed in any region across the entire time series (see Appendix 7 *Centroscymnus owstonii*, Figure 82 to Figure 90 for the full time series and residual plots).

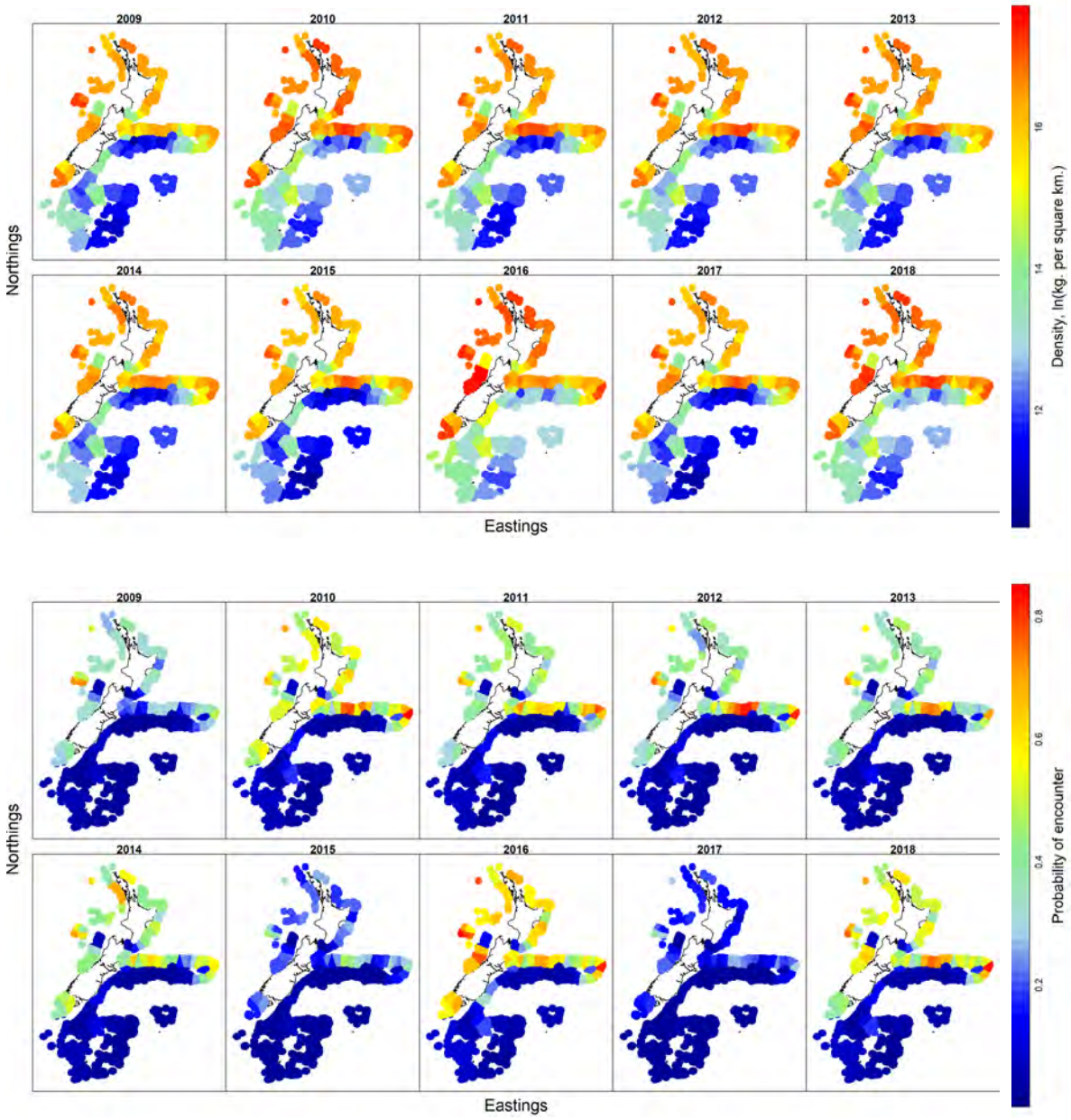

Figure 19: VAST outputs for relative density (kg km^{-2}, top panel) and probability of encounter (bottom panel) of *Centroscymnus owstonii* across the New Zealand waters in the past decade (2009–2018, from left to right for each panel). The full time series is shown in Appendix 7. Note that scales for density plots vary from figure to figure.

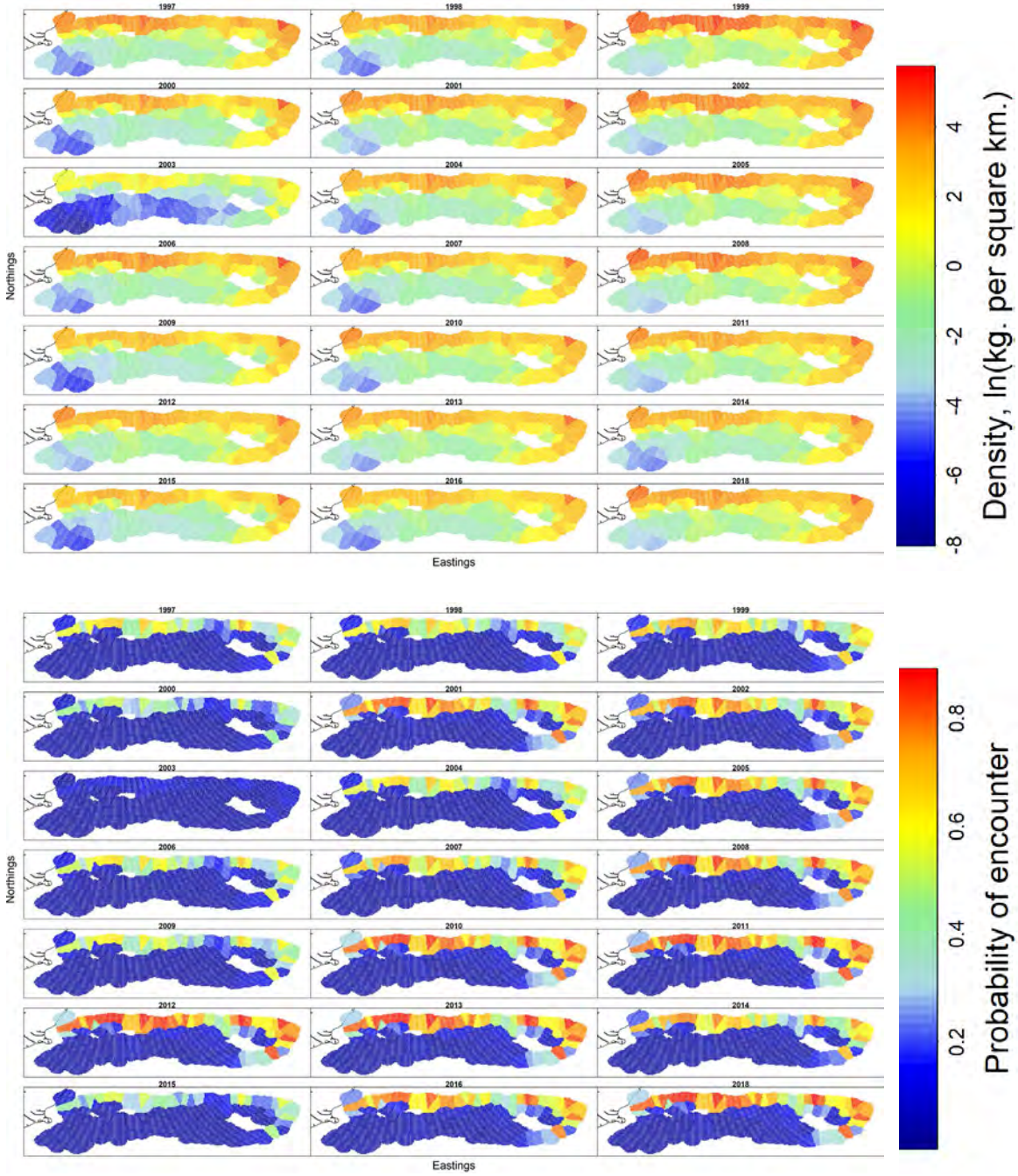

Figure 20: VAST outputs for relative density (kg km^{-2}, top panel) and probability of encounter (bottom panel) of *Centroscymnus owstonii* across Chatham Rise (1997–2018, from left to right for each panel). The full time series is shown in Appendix 7.

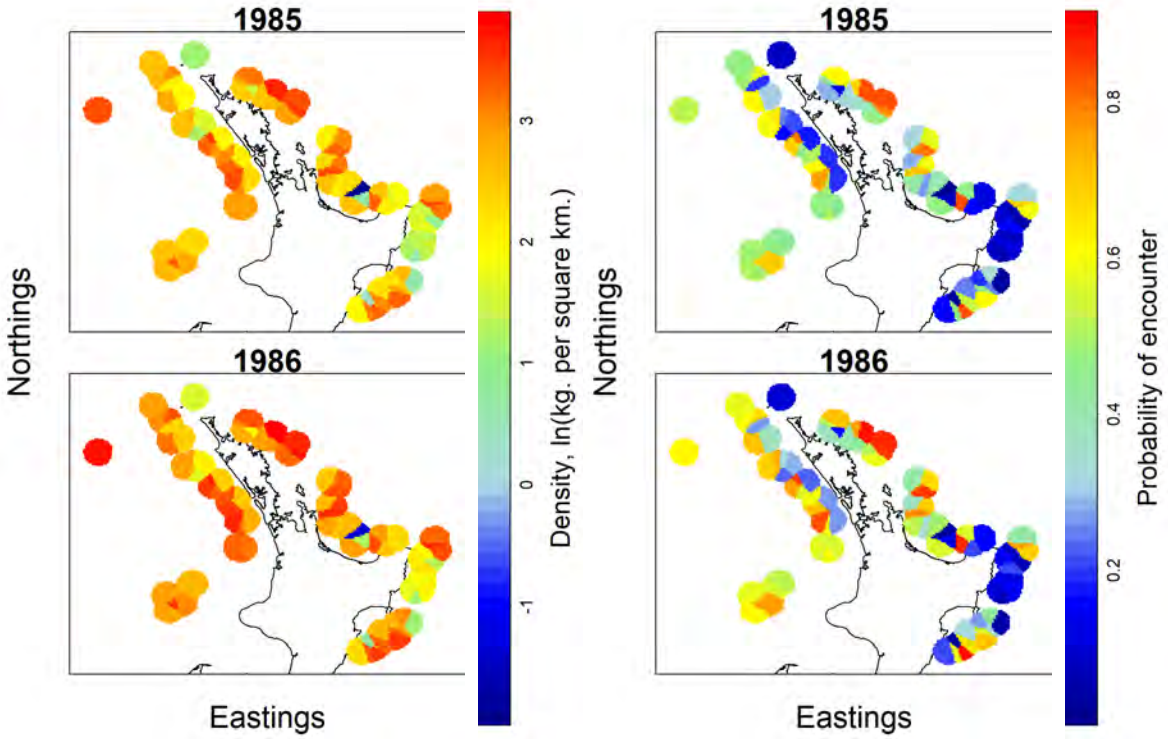

Figure 21: VAST outputs for relative density (kg km^{-2}, left panel) and probability of encounter (right panel) of *Centroscymnus owstonii* around the North Island of New Zealand in 1985–1986.

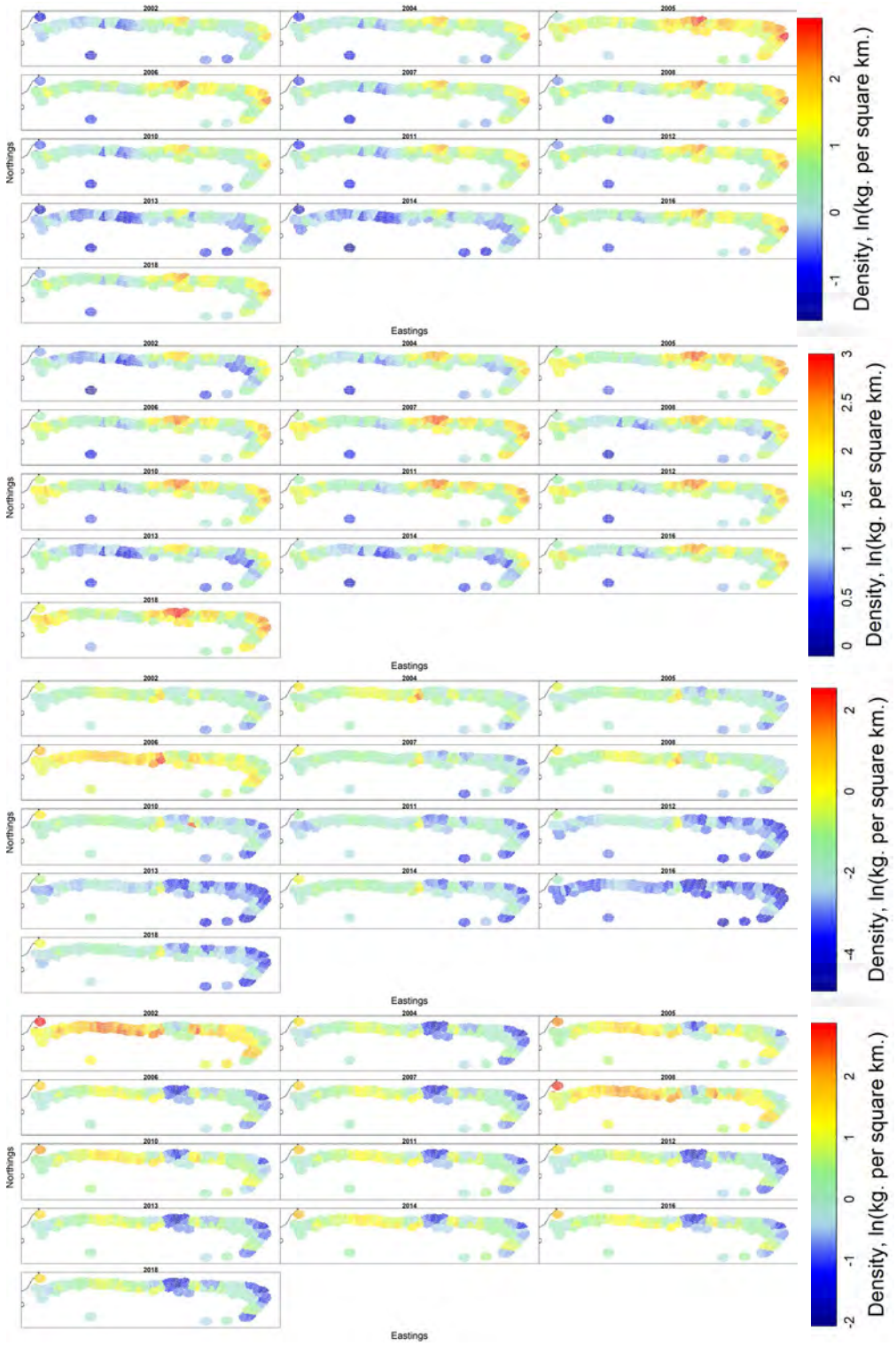

Figure 22: VAST outputs for relative density (kg km^{-2}) of *Centroscymnus owstonii* by class (from top: immature female, immature male, mature female, mature male) across Chatham Rise (2002–-2018, from left to right for each panel). Note that scales for density plots vary from plot to plot.

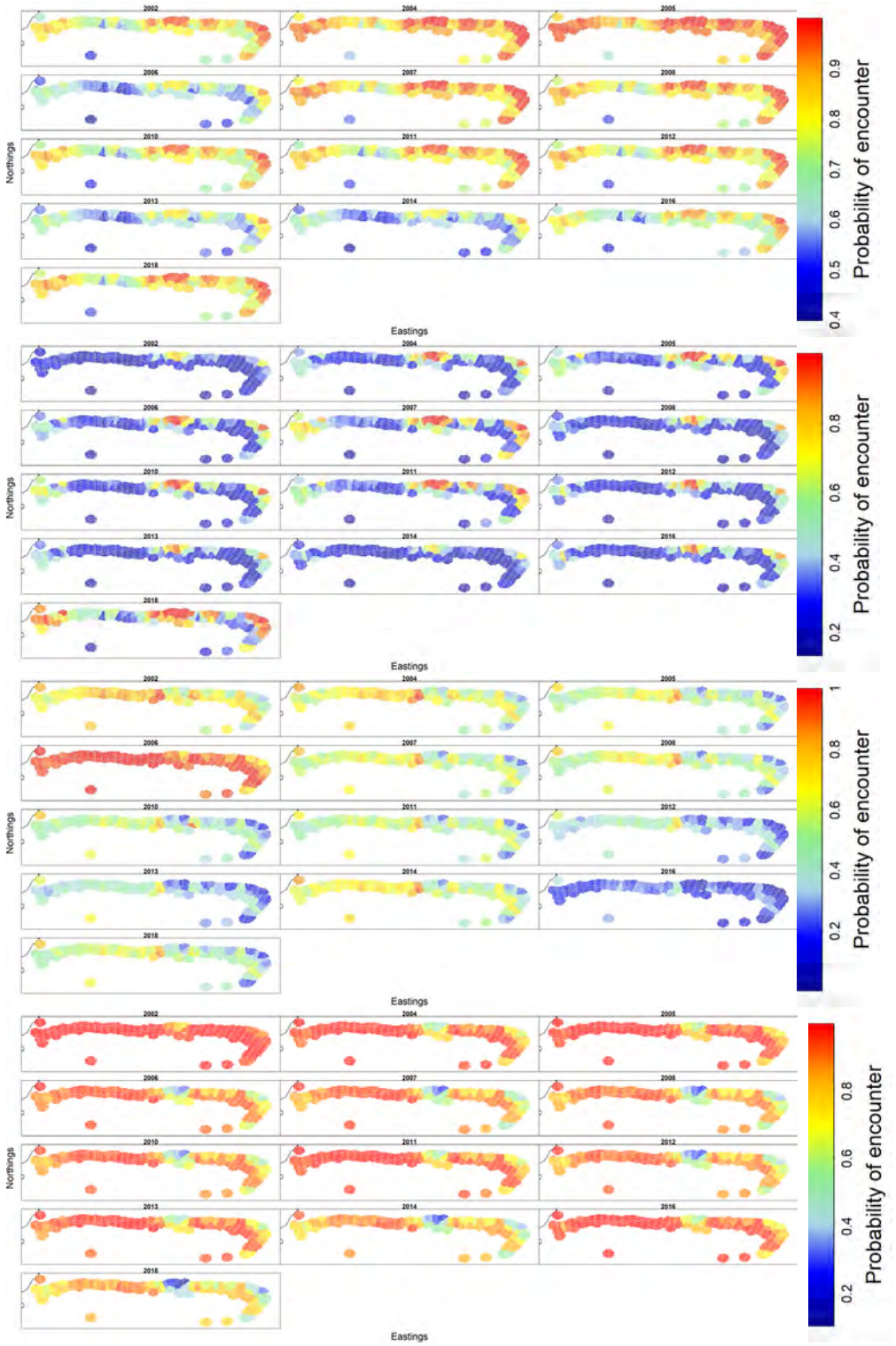

Figure 23: VAST outputs for probability of encounter of *Centroscymnus owstonii* by class (from top: immature female, immature male, mature female, mature male) across Chatham Rise (2002–-2018, from left to right for each panel).

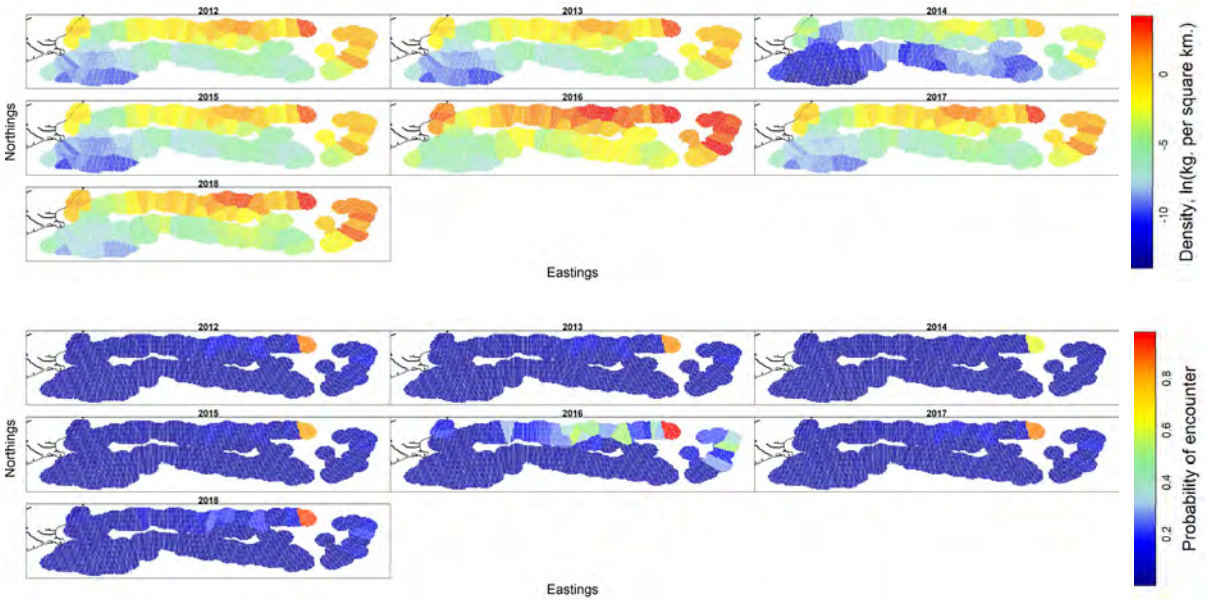

Figure 24: VAST outputs for relative density (kg km^{-2}, top panel) and probability of encounter (bottom panel) of *Centroscymnus owstonii* across Chatham Rise using observer records (2012–2018, from left to right for each panel).

3.7 *Centroselachus crepidater*

The single-species analysis was similar to the multi-species analysis for *Centroselachus crepidater*, with more distribution around the North Island and less off the west coast of the South Island (Figure 25–Figure 27). The models for the long time series of Sub-Antarctic-only data did not converge and plots are not shown here. Around the North Island, density was highest off the southeast and west coasts, and probability of encounter was highest off the southeast coast (Figure 28).

On the Chatham Rise, densities were similar across sex and maturity stage, with highest densities of immature individuals predicted closer inshore off the western end of the Chatham Rise (Figure 29). Highest densities for mature females occurred on the eastern-most area of the Chatham Rise, while mature male density was highest on central northern slope of Chatham Rise (Figure 29). Probability of encounter was very high for most of Chatham Rise for immature females, but was more variable for immature males, which were predicted mainly on the northwest and southeast Chatham Rise (Figure 30). Mature females were most likely to be encountered on the central northern slope and eastern end of the Chatham Rise, whereas mature males were more likely on the northern and southeast Chatham Rise (Figure 30).

In the short Sub-Antarctic time series, densities were similar across sex and maturity stages, with the highest densities at Puysegur and the northern Campbell Plateau (Figure 31). Probability of encounter was similarly distributed for females, with highest probabilities of occurrence at Puysegur and the northern slope of the Campbell Plateau (Figure 32). Mature females had a more widespread distribution in this area, including high probability of occurrence at the southern-most area of the Campbell Plateau.

Model outputs from the observer data for *Centroselachus crepidater* showed similarities to trawl survey data, with the highest density reported from north eastern Chatham Rise and highest probability of encounter from south east Chatham Rise (Figure 33).

No trends in density or probability of encounter were observed in any region across the entire time series (see Appendix 8 *Centroselachus crepidater*, Figure 91 to Figure 100 for the full time series and residual plots).

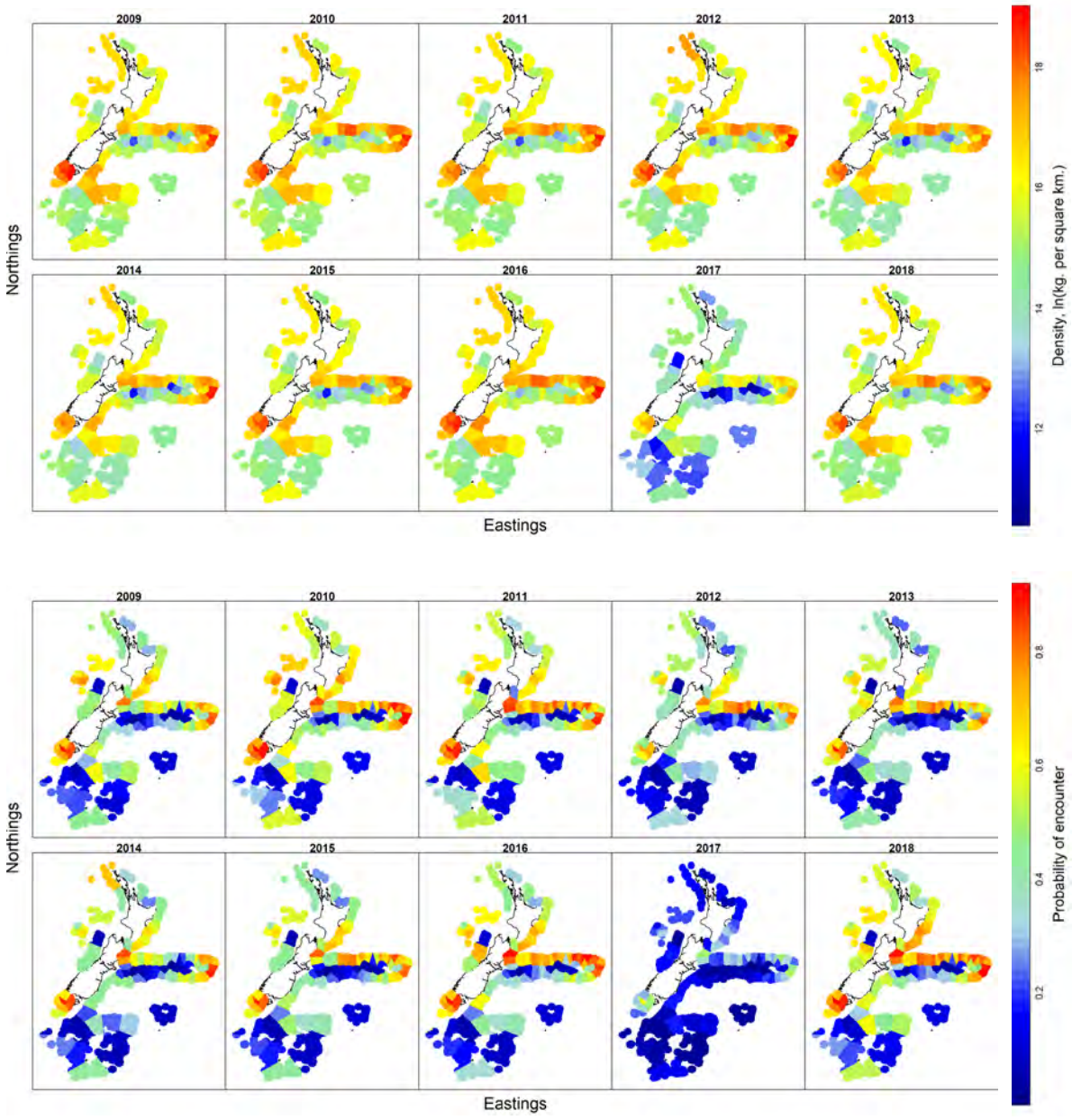

Figure 25: VAST outputs for relative density (kg km^{-2}, top panel) and probability of encounter (bottom panel) of *Centroselachus crepidater* across the New Zealand waters in the past decade (2009–-2018, from left to right for each panel). The full time series is shown in Appendix 8. Note that scales for density plots vary from figure to figure.

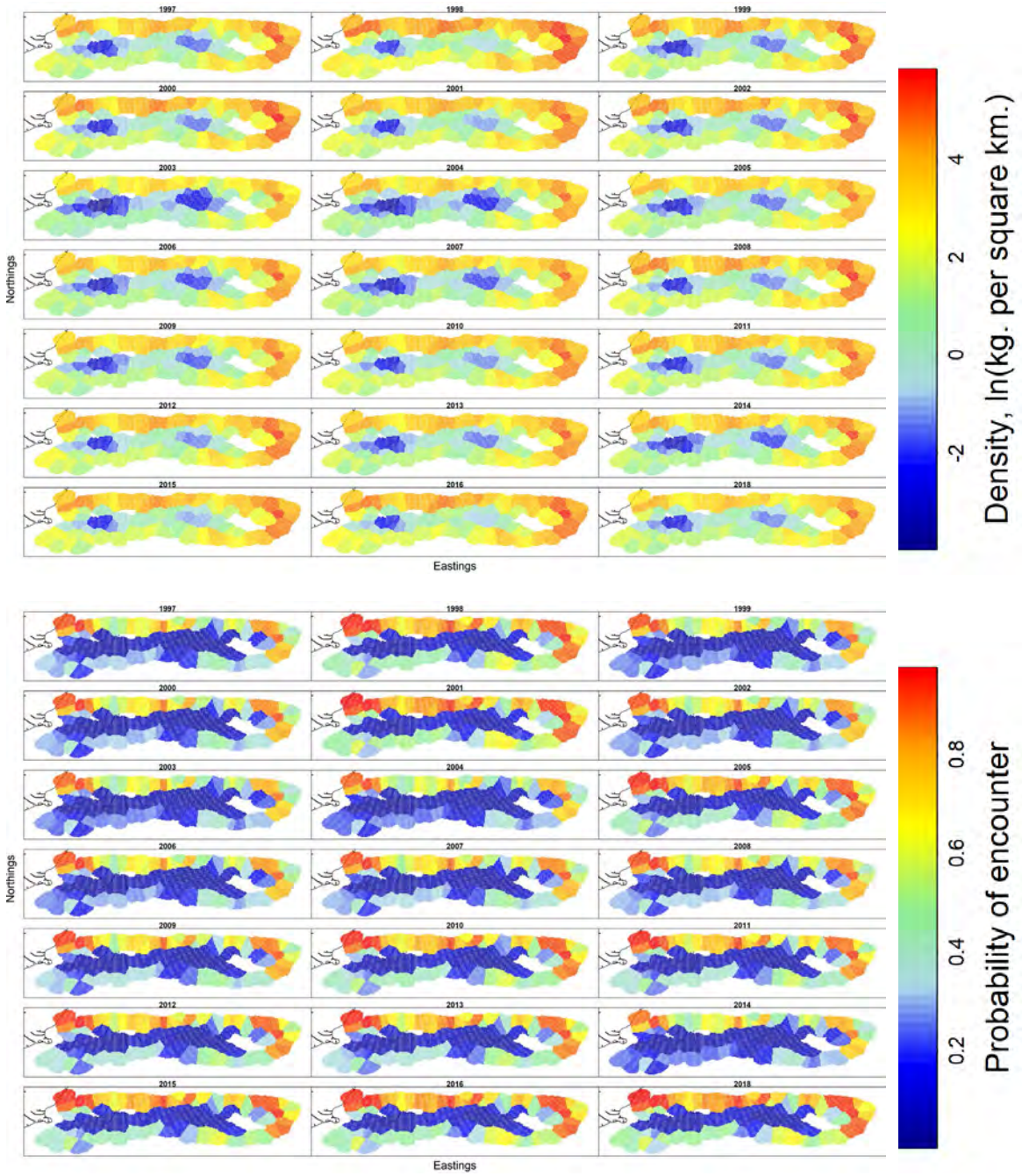

Figure 26: VAST outputs for density (kg km^{-2}, top panel) and probability of encounter (bottom panel) of *Centroselachus crepidater* across Chatham Rise (1997–2018, from left to right for each panel). The full time series is shown in Appendix 8.

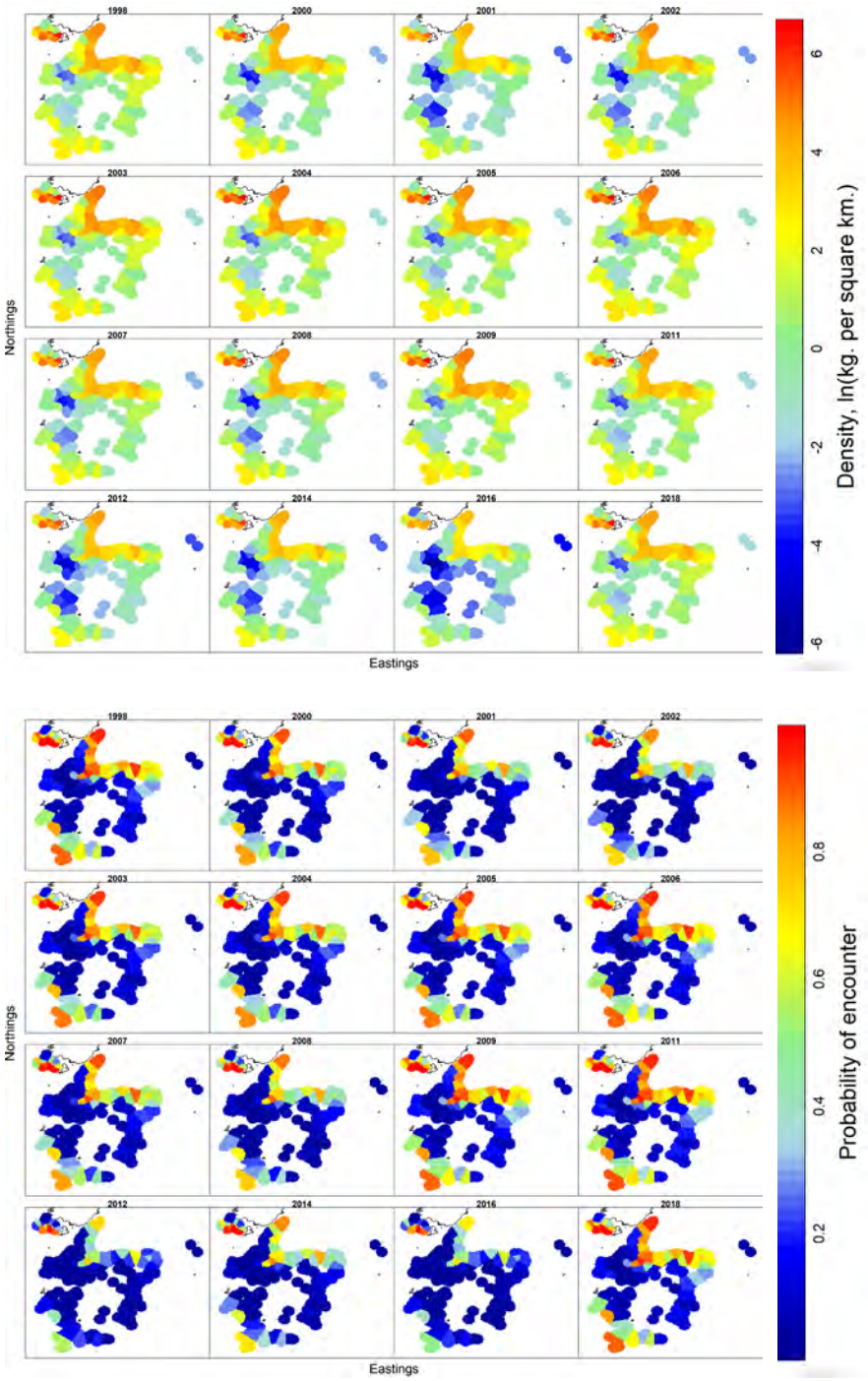

Figure 27: VAST outputs for relative density (kg km^{-2}, top panel) and probability of encounter (bottom panel) of *Centroselachus crepidater* across the Sub-Antarctic (1998–2018, from left to right for each panel). The 1982 time series for *C. crepidater* did not converge.

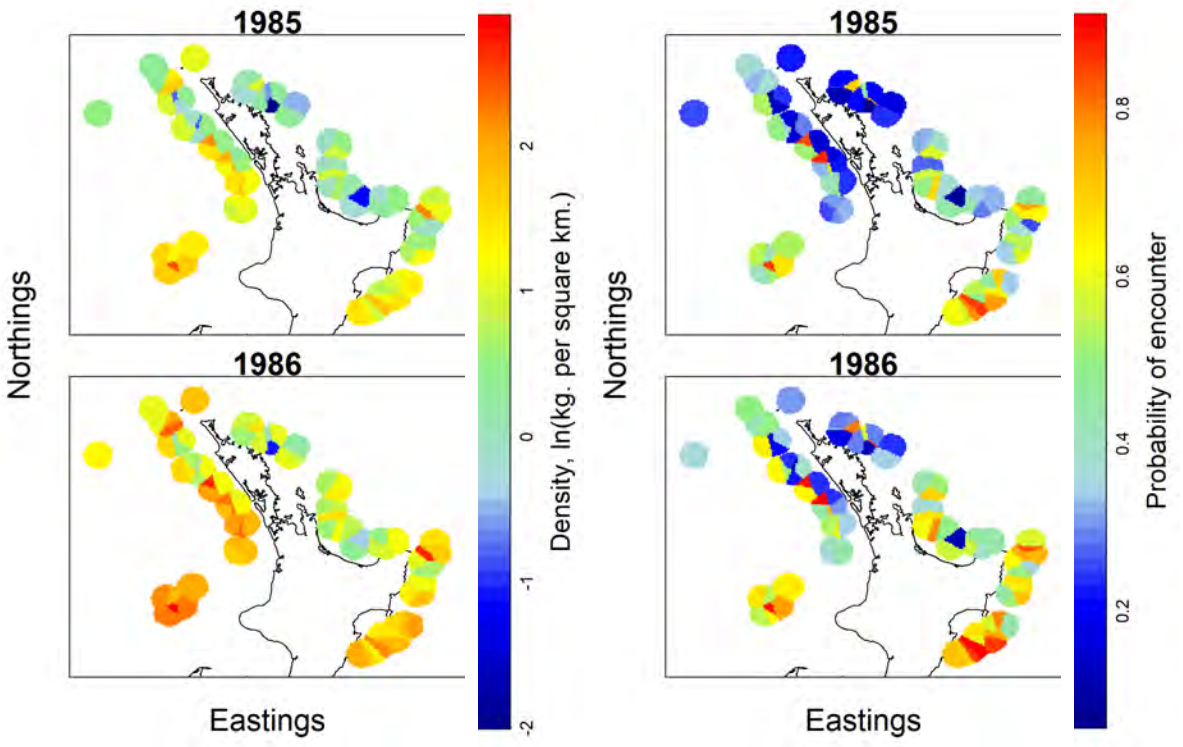

Figure 28: VAST outputs for relative density (kg km^{-2}, left panel) and probability of encounter (right panel) of *Centroselachus crepidater* around the North Island of New Zealand in 1985-86.

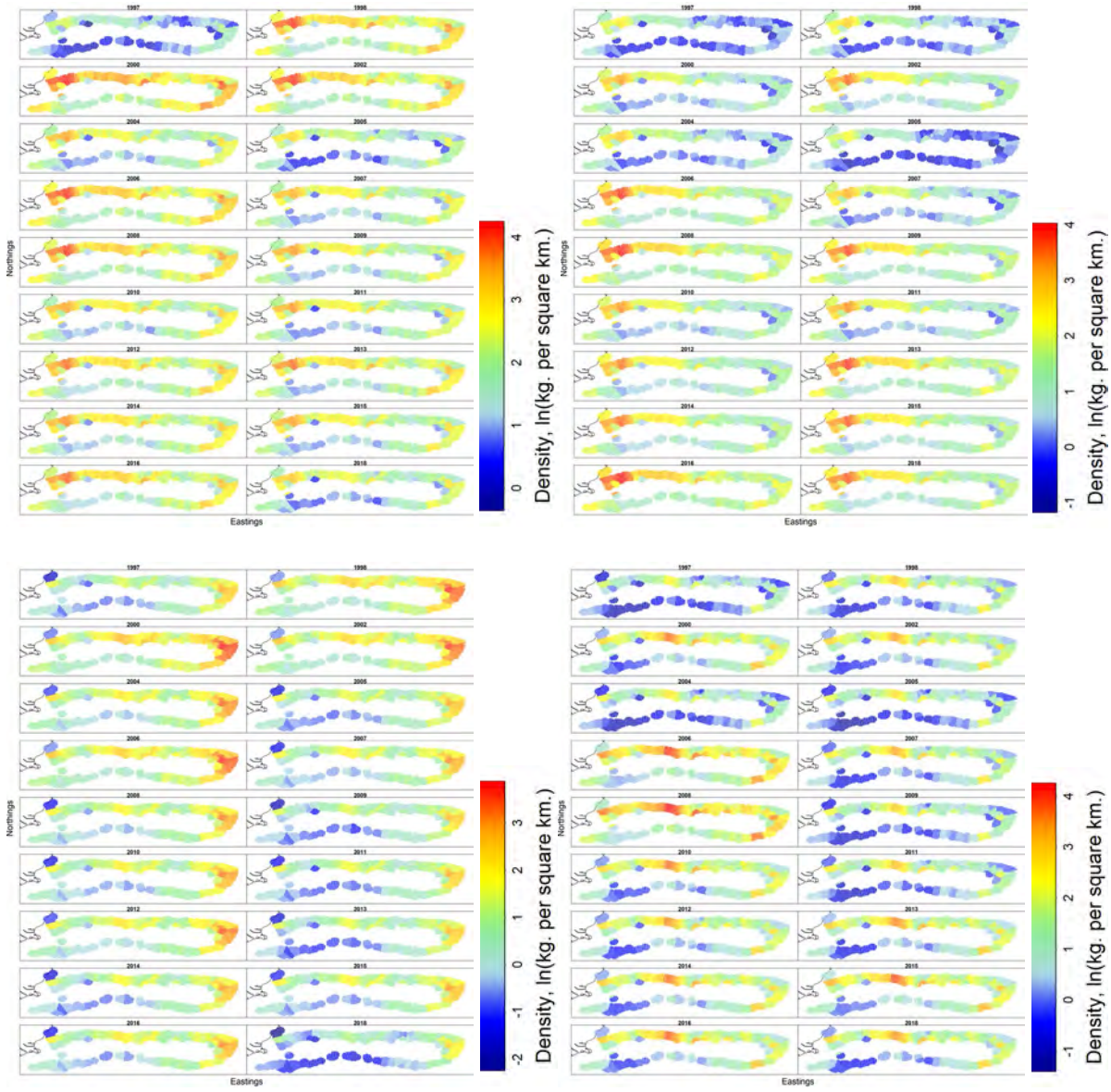

Figure 29: VAST outputs for relative density (kg km^{-2}) of *Centroselachus crepidater* by class (clockwise from top left: immature female, immature male, mature female, mature male) across Chatham Rise (1997–2018, from left to right for each panel). Note that scales for density plots vary from plot to plot.

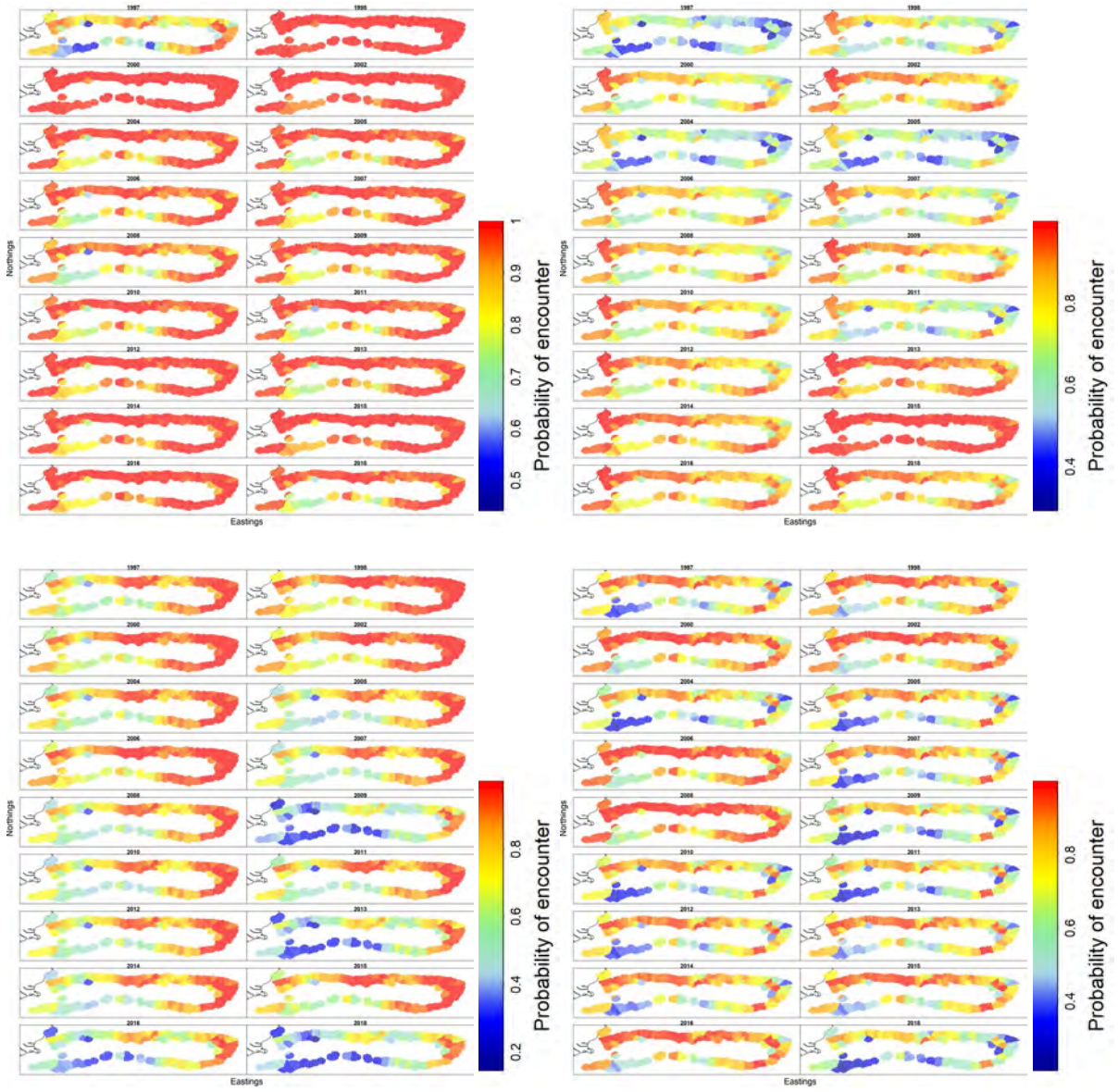

Figure 30: VAST outputs for probability of encounter of *Centroselachus crepidater* by class (clockwise from top left: immature female, immature male, mature female, mature male) across Chatham Rise (1997–2018, from left to right for each panel).

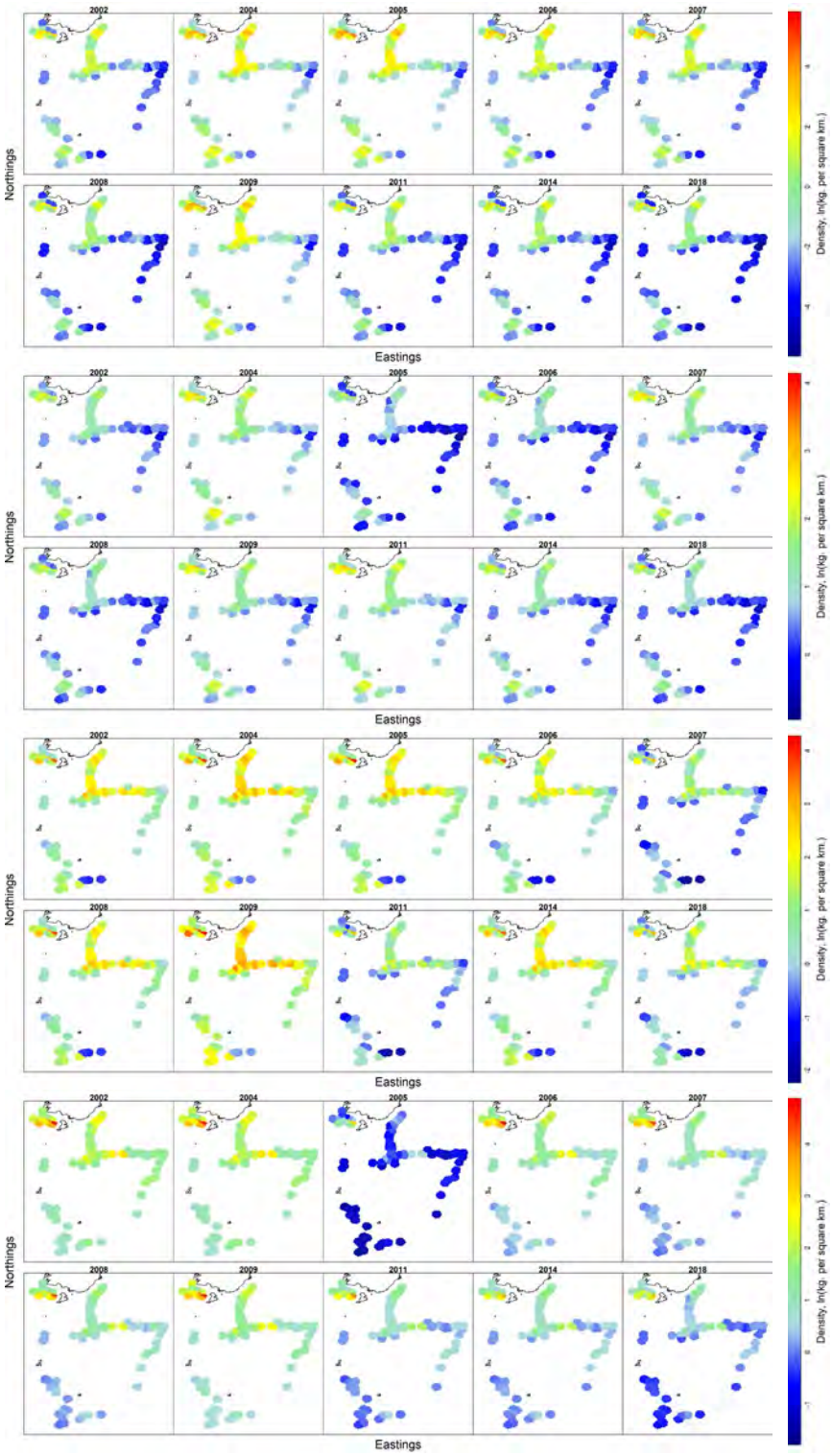

Figure 31: VAST outputs for relative density (kg km^{-2}) of *Centroselachus crepidater* by class (from top: immature female, immature male, mature female, mature male) across the Sub-Antarctic (2002–2018, from left to right for each panel). Note that scales for density plots vary from plot to plot.

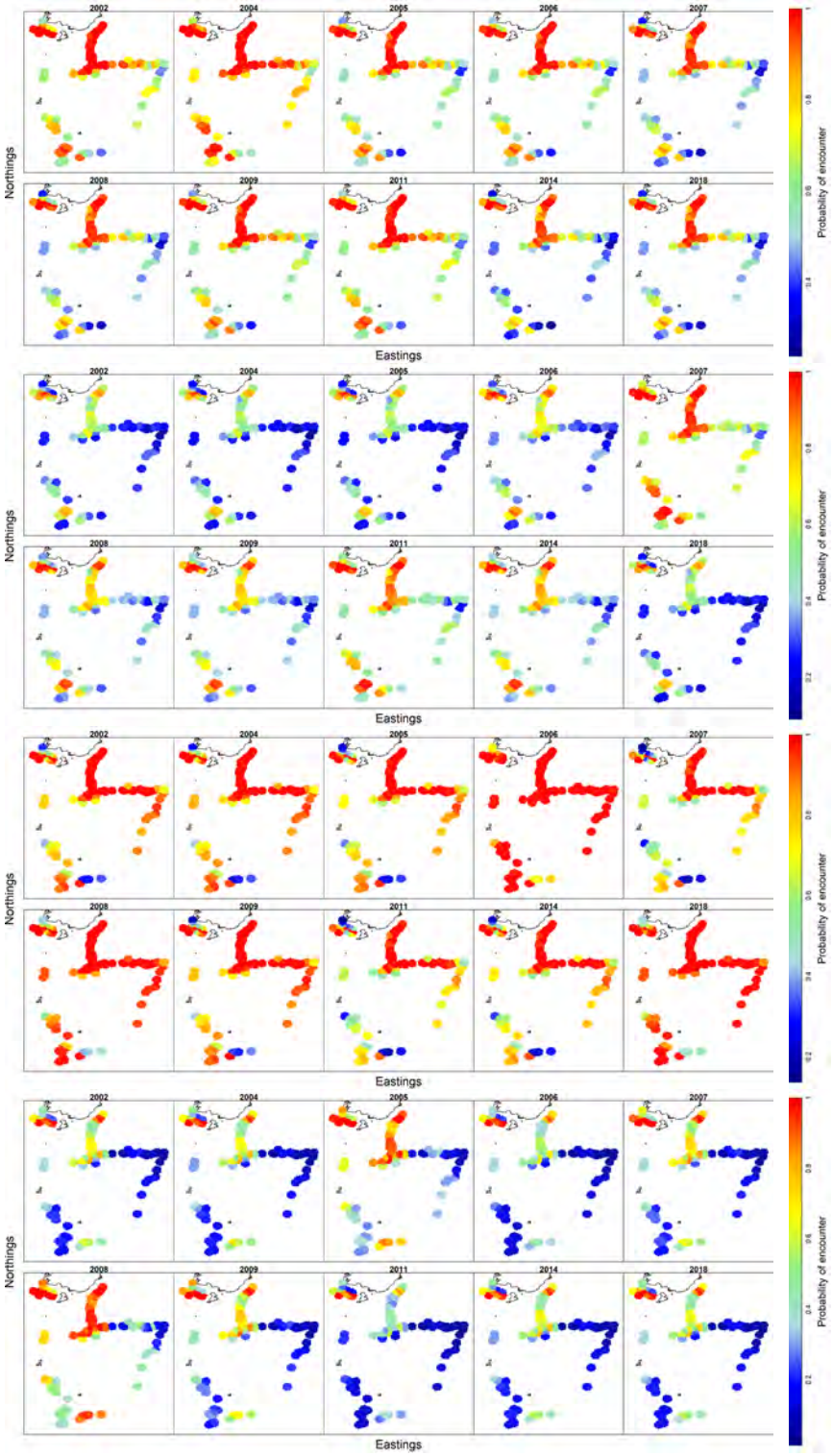

Figure 32: VAST outputs for probability of encounter of *Centroselachus crepidater* by class (from top: immature female, immature male, mature female, mature male) across the Sub-Antarctic (2002–2018, from left to right for each panel).

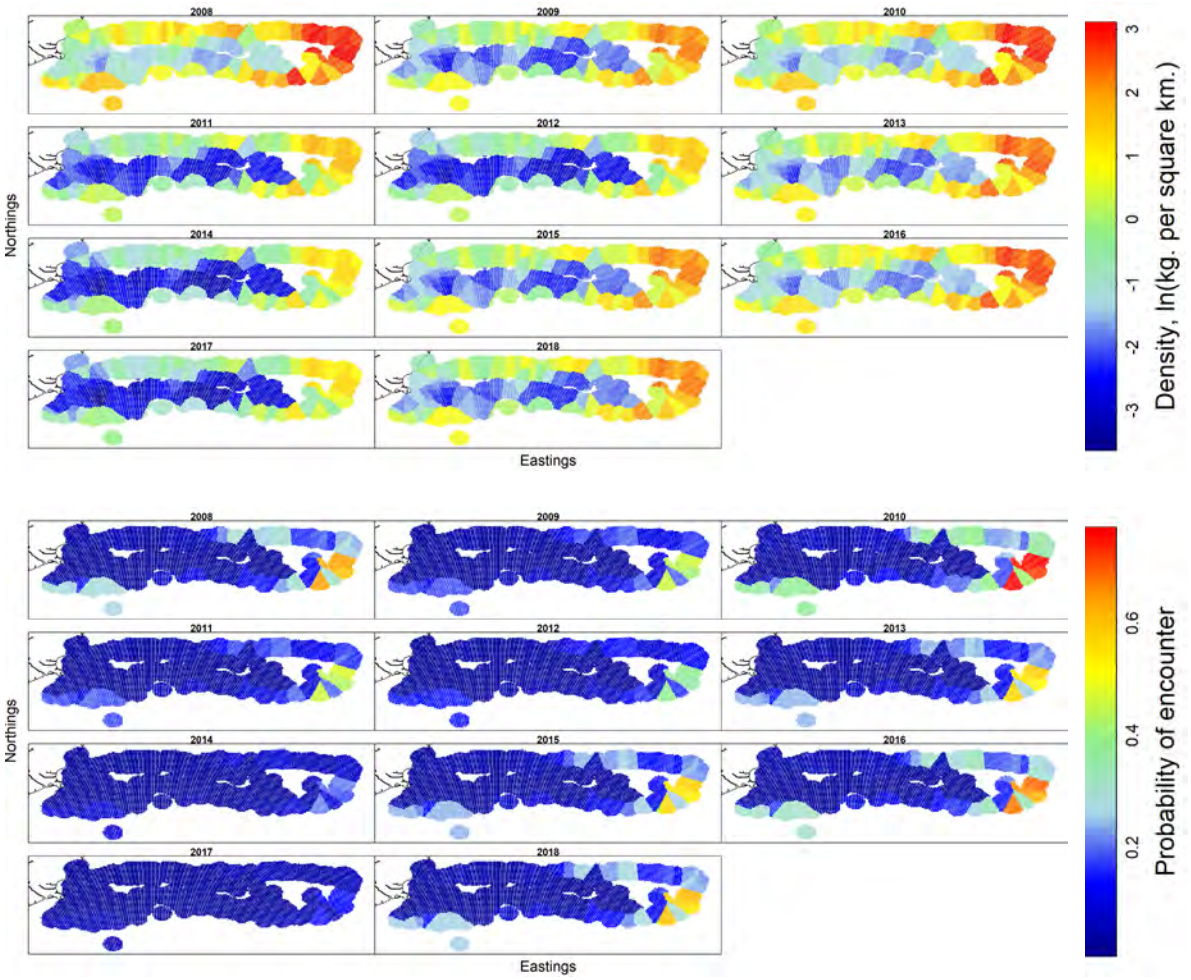

Figure 33: VAST outputs for relative density (kg km^{-2}, top panel) and probability of encounter (bottom panel) of *Centroselachus crepidater* across Chatham Rise using observer records (2008–2018, from left to right for each panel).

3.8 *Etmopterus granulosus*

The single-species analysis was very similar to the multi-species analysis for *E. granulosus* (Figure 34–Figure 36). The models for the North Island data did not converge and are not shown here.

On the Chatham Rise, predicted densities were similar across sex and maturity stages, with highest densities located on the southwestern Chatham Rise and for mature males, on the eastern-most area of the Chatham Rise (Figure 37). Probability of encounter was very high around most of Chatham Rise for immature females, but was more restricted to the southern Chatham Rise, particularly the southwestern corner, for immature males (Figure 38). Mature females and males were frequently encountered around most of the Chatham Rise (Figure 38).

In the Sub-Antarctic, highest densities of immature individuals occurred on the northern Campbell Plateau, whereas mature individuals were more abundant on the central and northeastern parts of the Campbell Plateau (Figure 39). Probability of encounter was highest for immature females at Puysegur and on the northern area of Campbell Plateau (Figure 40). Immature males had a lower overall probability of occurrence than immature females, but their predicted distribution was similar. Mature females were also most frequently encountered on the northern Campbell Plateau but mature males were more widespread around most of the slope of the Campbell Plateau (Figure 40).

Model outputs from the observer data for *E. granulosus* showed similarities to trawl survey data, with highest density and probability of encounter reported from southern Chatham Rise (Figure 41). In the Sub-Antarctic, the highest density and probability of encounter occurred in discrete areas on the north, east, and west areas of the Campbell Plateau.

No trends in density or probability of encounter were observed in any region across the entire time series (see Appendix 9 *Etmopterus granulosus*, Figure 101 to Figure 113 for the full time series and residual plots).

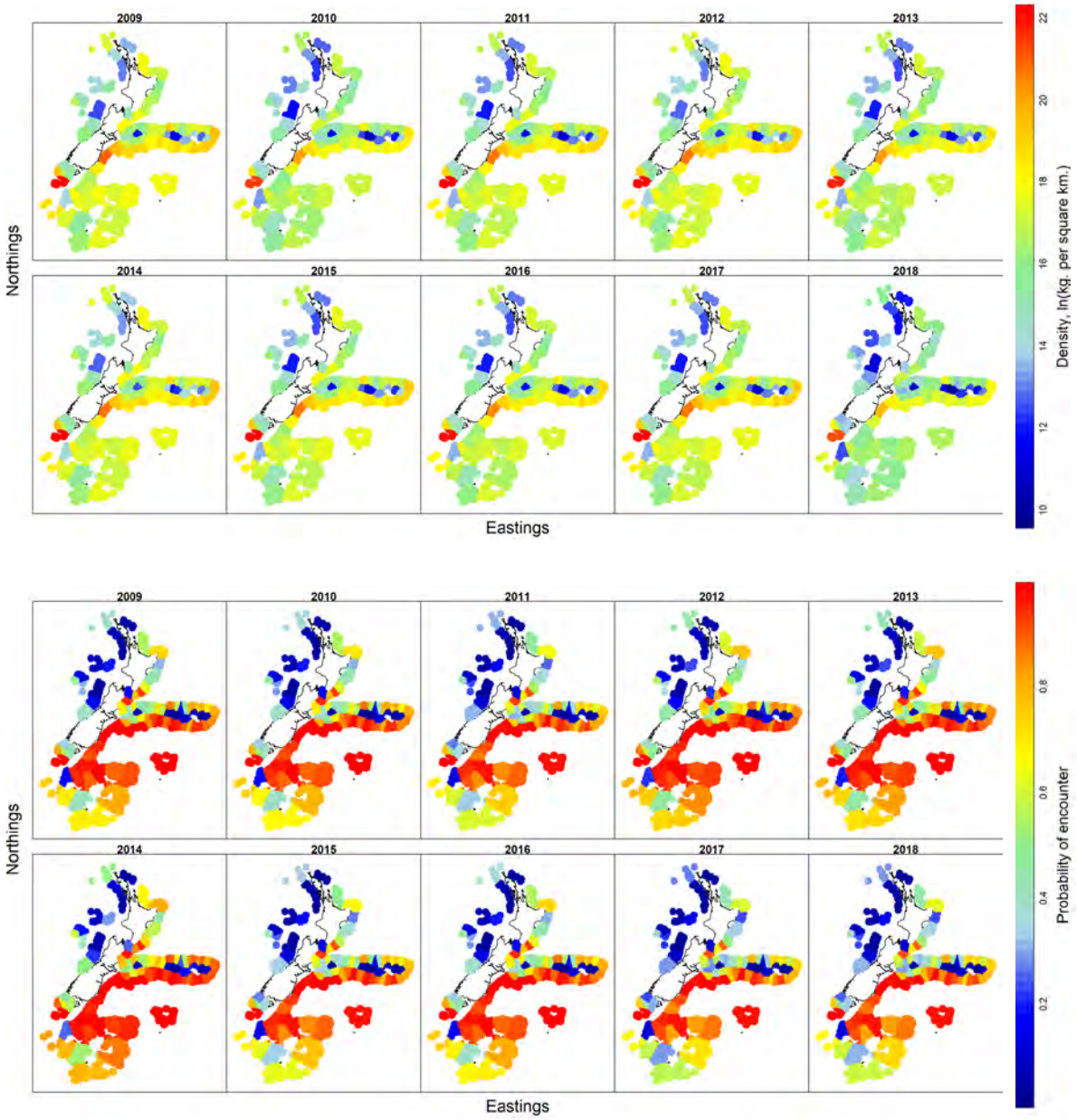

Figure 34: VAST outputs for relative density (kg km^{-2}, top panel) and probability of encounter (bottom panel) of *Etmopterus granulosus* across the New Zealand waters in the past decade (2009–2018, from left to right for each panel). The full time series is shown in Appendix 9. Note that scales for density plots vary from figure to figure.

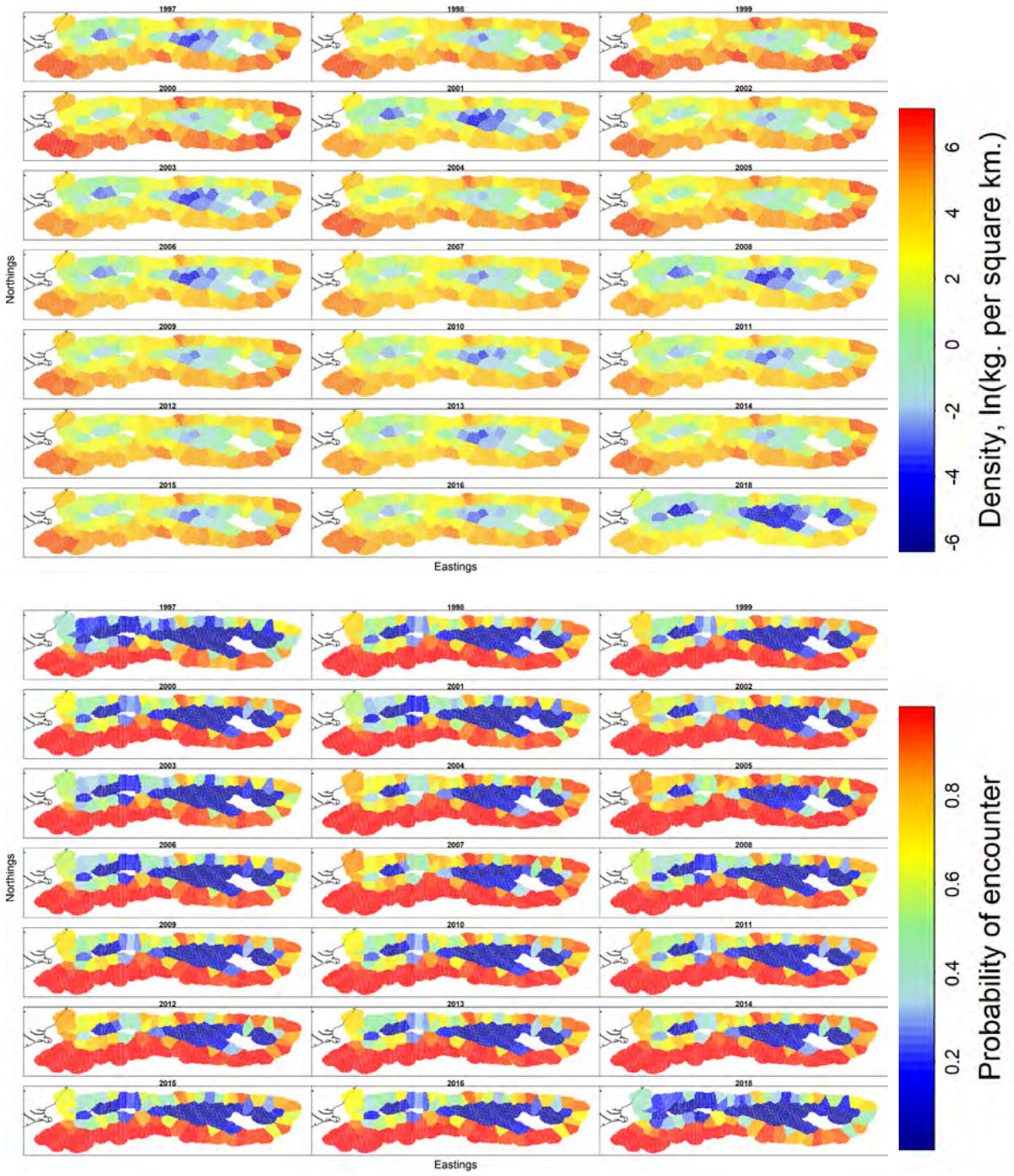

Figure 35: VAST outputs for relative density (kg km^{-2}, top panel) and probability of encounter (bottom panel) of *Etmopterus granulosus* across Chatham Rise (1997–2018, from left to right for each panel). The full time series is shown in Appendix 9.

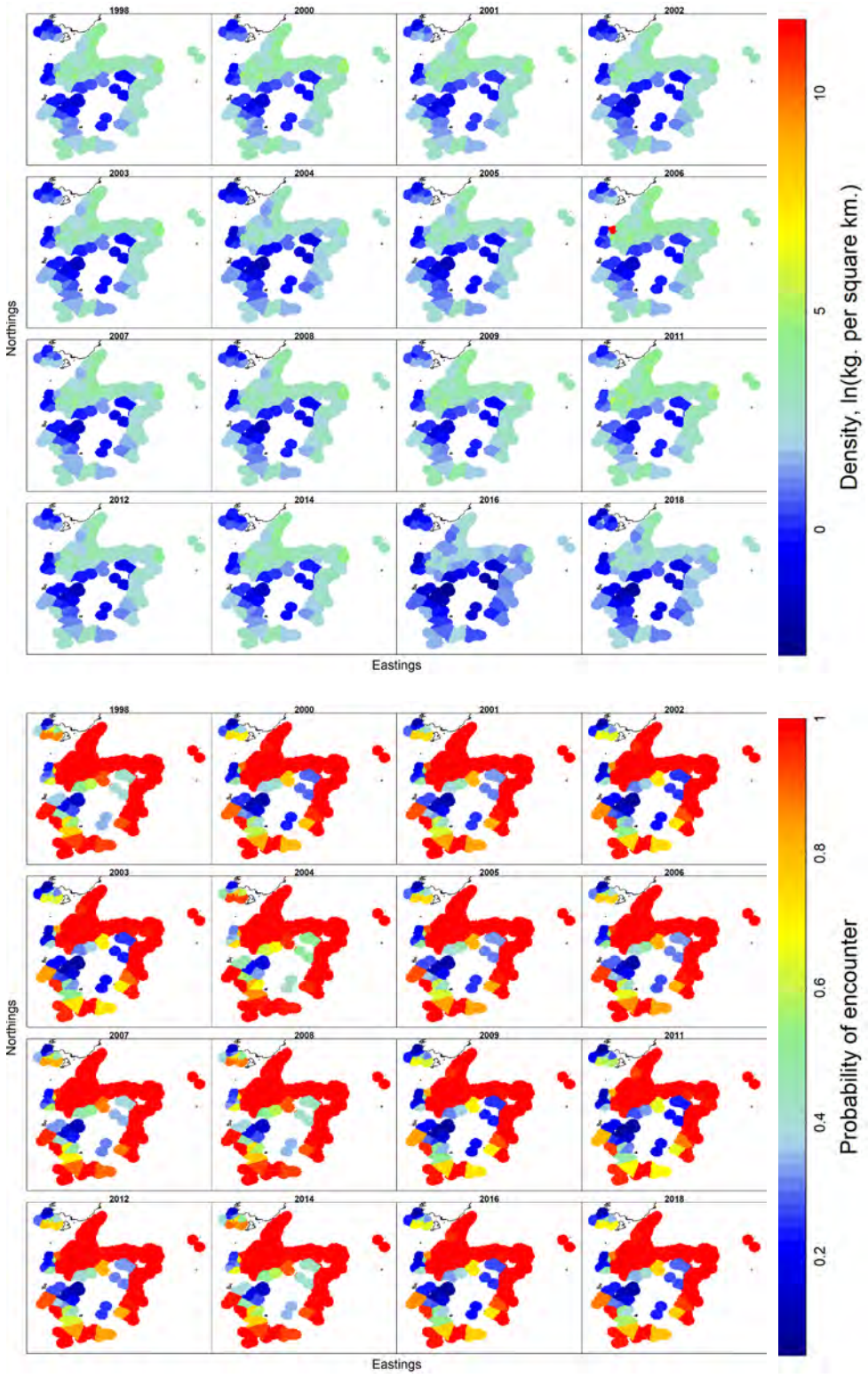

Figure 36: VAST outputs for relative density (kg km^{-2}, top panel) and probability of encounter (bottom panel) of *Etmopterus granulosus* across the Sub-Antarctic (1998–2018, from left to right for each panel). The full time series is shown in Appendix 9.

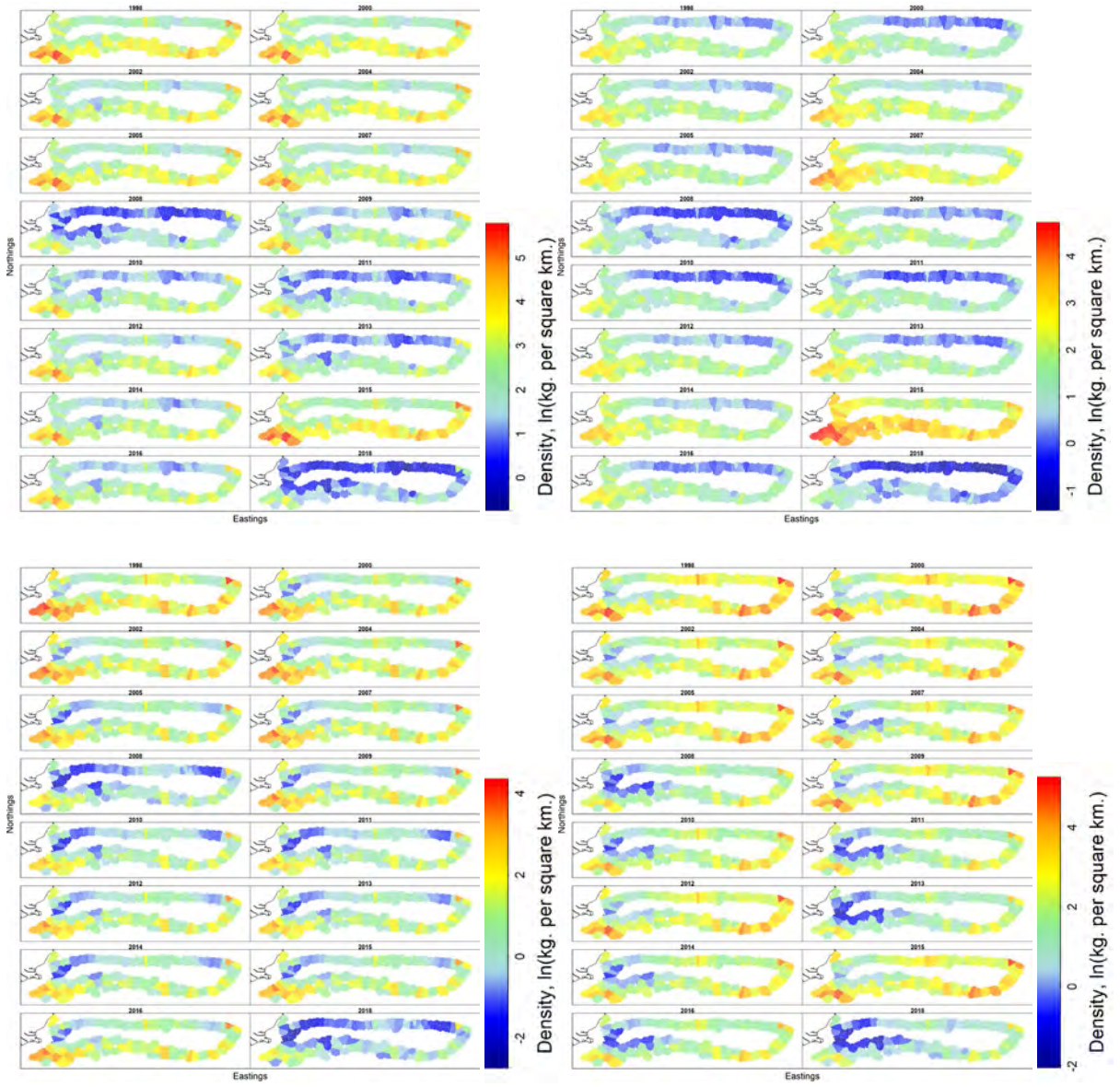

Figure 37: VAST outputs for relative density (kg km^{-2}) of *Etmopterus granulosus* by class (from top left: immature female, immature male, mature female, mature male) across Chatham Rise (1998–-2018, from left to right for each panel). Note that scales for density plots vary from plot to plot.

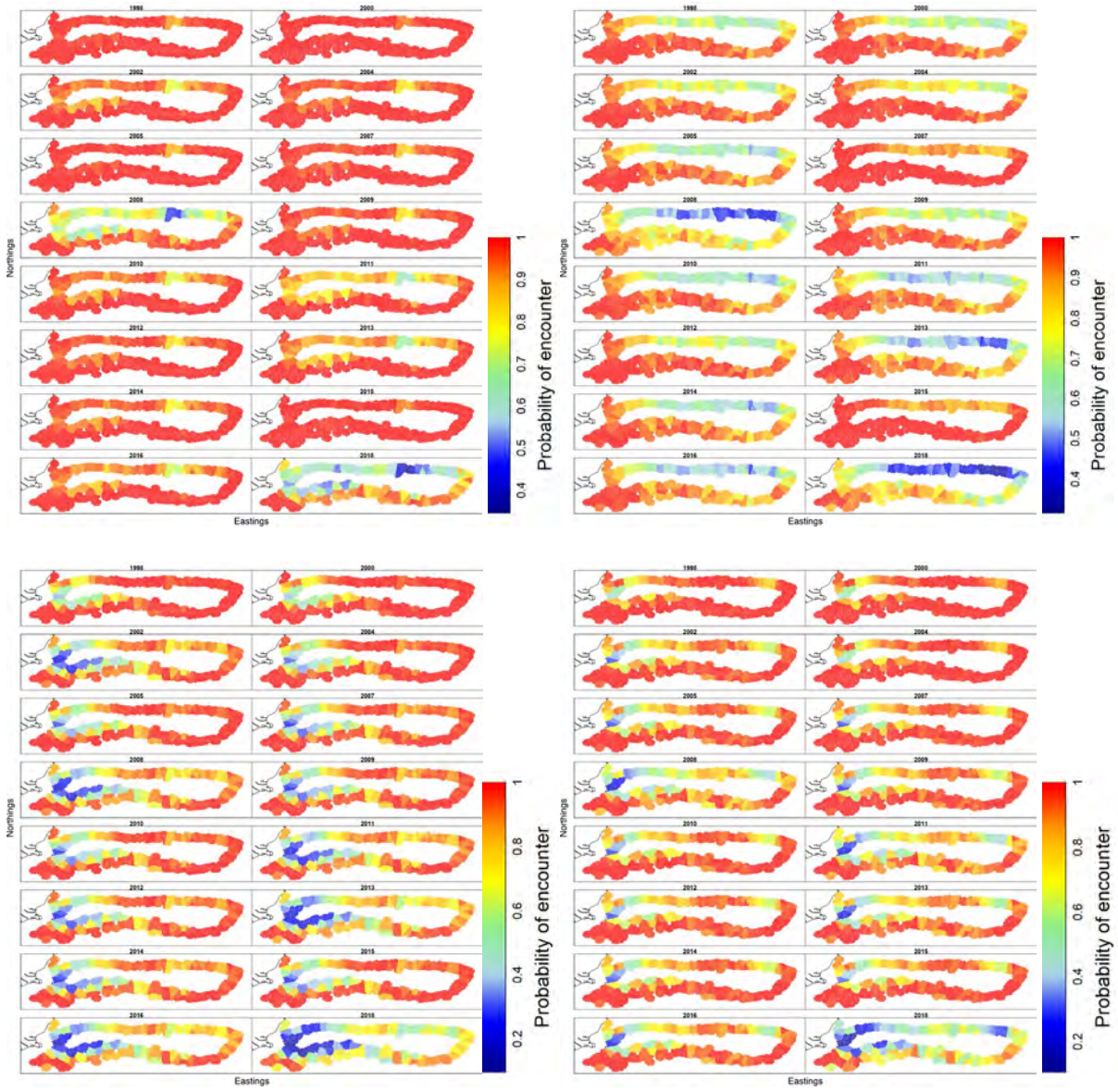

Figure 38: VAST outputs for probability of encounter of *Etmopterus granulosus* by class (clockwise from top left: immature female, immature male, mature female, mature male) across Chatham Rise (1998–2018, from left to right for each panel).

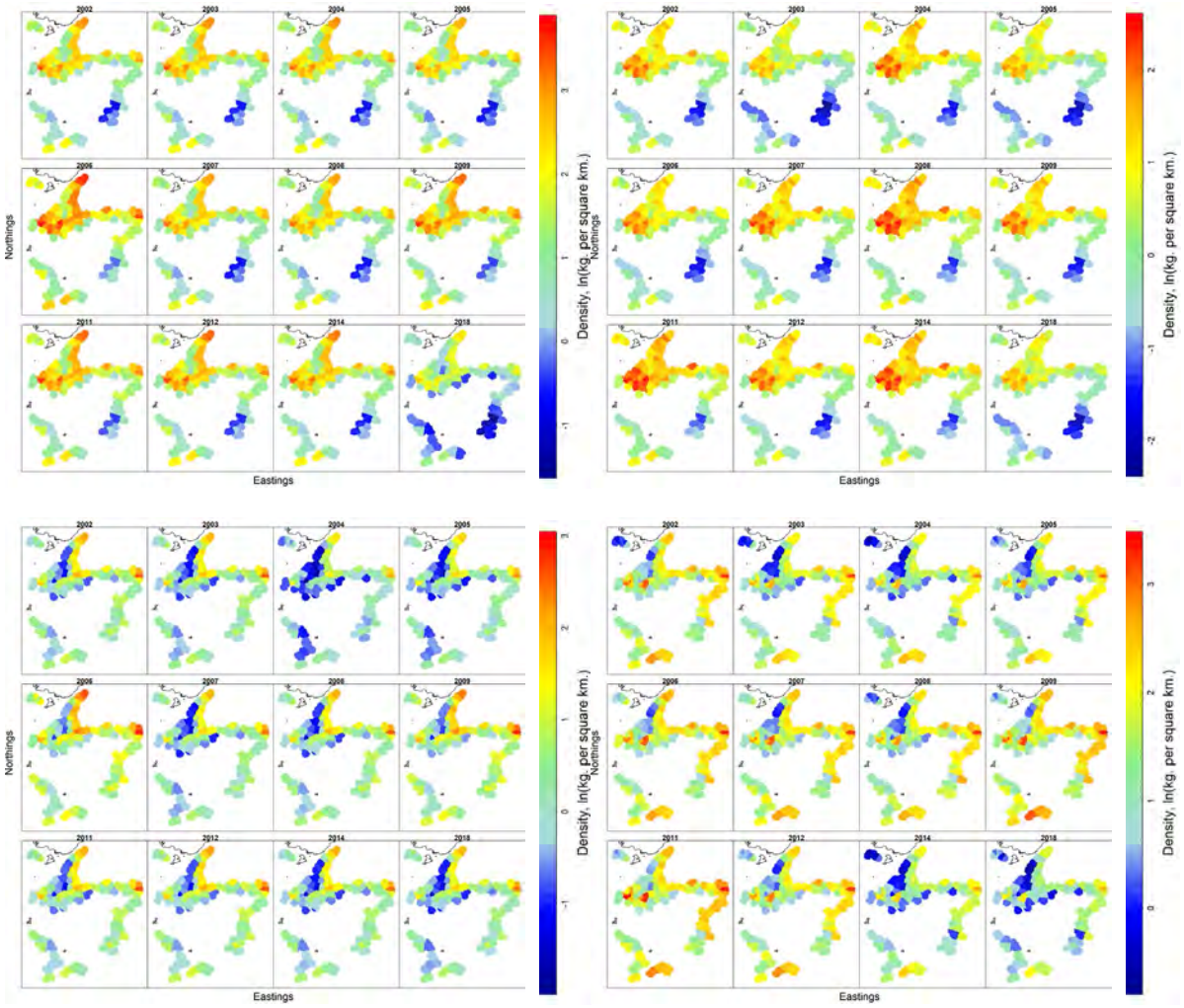

Figure 39: VAST outputs for relative density (kg km^{-2}) of *Etmopterus granulosus* by class (clockwise from top left: immature female, immature male, mature female, mature male) across the Sub-Antarctic (2002–2018, from left to right for each panel). Note that scales for density plots vary from plot to plot.

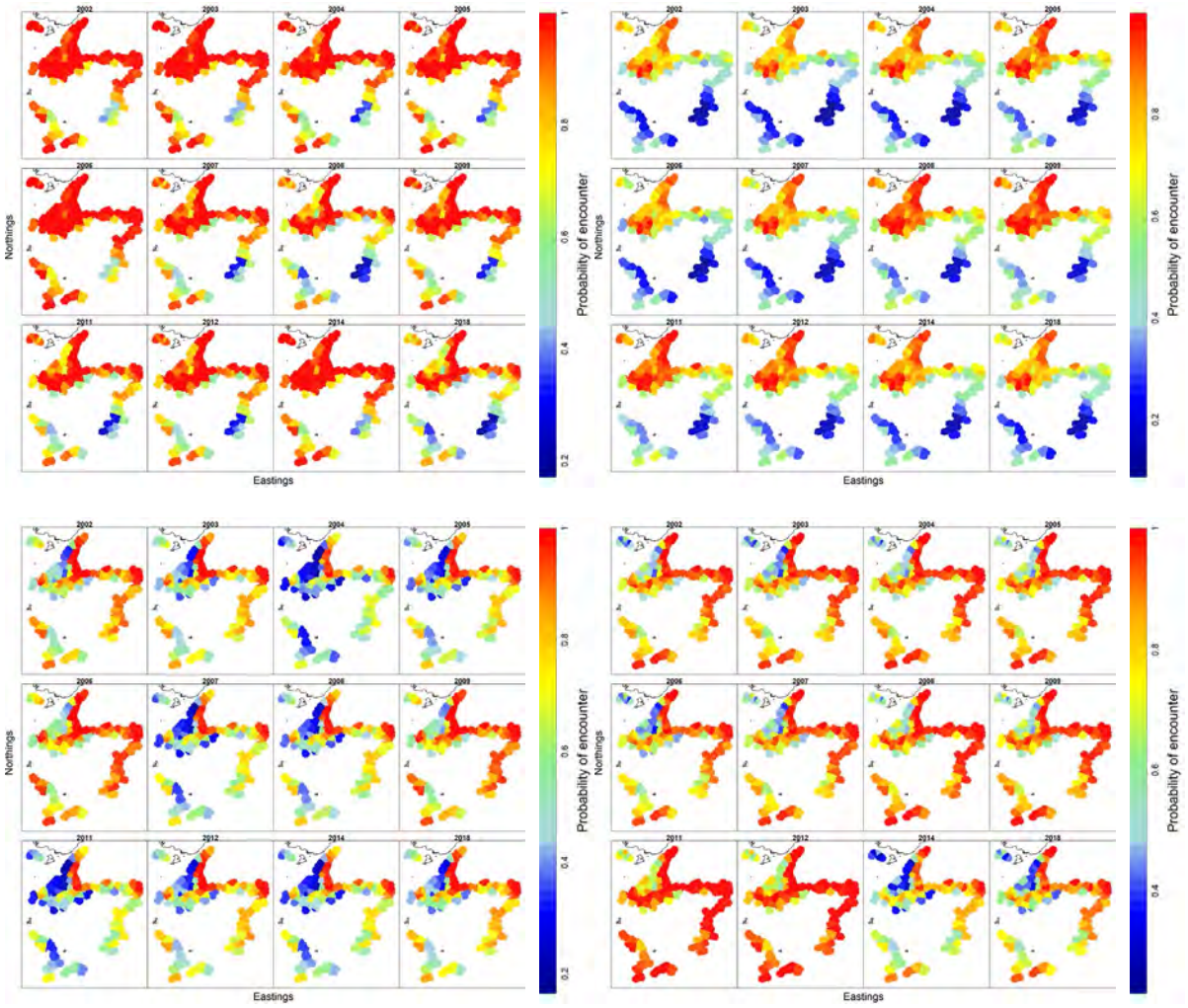

Figure 40: VAST outputs for relative density probability of encounter of *Etmopterus granulosus* by class (clockwise from top left: immature female, immature male, mature female, mature male) across the Sub-Antarctic (2002–2018, from left to right for each panel).

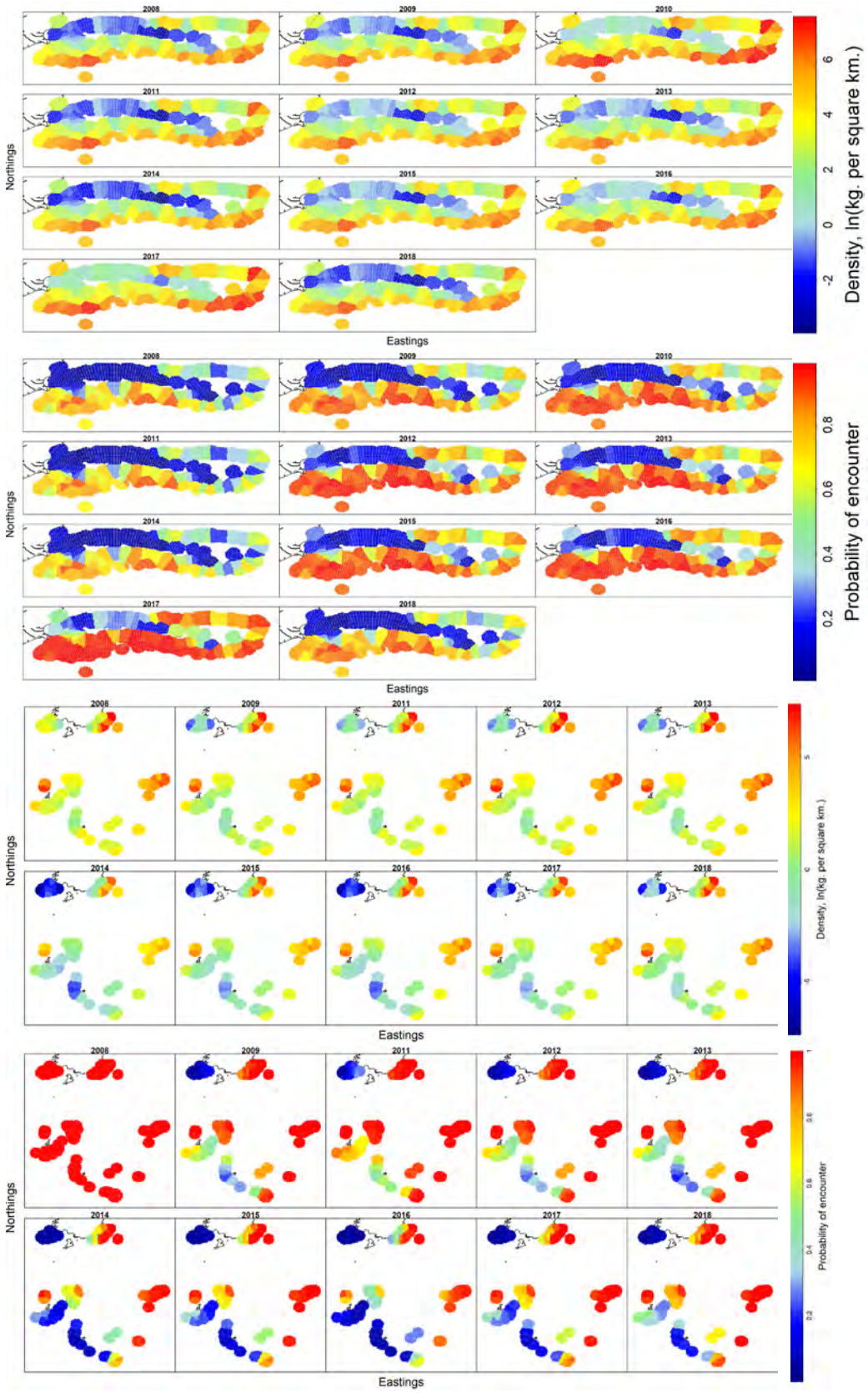

Figure 41: VAST outputs for relative density (kg km^{-2}) and probability of encounter of *Etmopterus granulosus* across Chatham Rise (top panels) and the Sub-Antarctic (bottom panels) using observer records (2008–2018, from left to right for each panel). Note that scales for density plots vary from plot to plot.

3.9 *Scymnodon plunketi*

The single-species analysis predicted lower density of *S. plunketi* off Puseygur and lower probability of encounter in the Sub-Antarctic than the predicted density in the multi-species analysis (Figure 42, Figure 43). The 1997 time series model for *S. plunketi* did not converge, and the full time series model provided some indication of higher density on the south eastern part of Chatham Rise, but overall low probability of encounter (Figure 114 and Figure 115). In the Sub-Antarctic, density and probability were also low, with some higher density predicted at Puysegur, southeast of Otago, and on the northern Campbell Plateau (Figure 43). The species appears to be nearly absent in the area in 2000. Given the small sample sizes, patterns observed here are probably not reflective of true population structure. The 1982 time series models for the Sub-Antarctic data, and the North Island data, did not converge and are not shown here. Because of the lack of convergence, *S. plunketi* data were not further divided into sex and maturity stage.

Model outputs from the observer data for *S. plunketi* showed a similar pattern to the trawl survey data, with highest density and probability of encounter restricted to the eastern part of Chatham Rise (Figure 44).

No trends in density or probability of encounter were observed in any region across the entire time series (see Appendix 10 *Scymnodon plunketi*, Figure 114 to Figure 120 for full time series and residual plots).

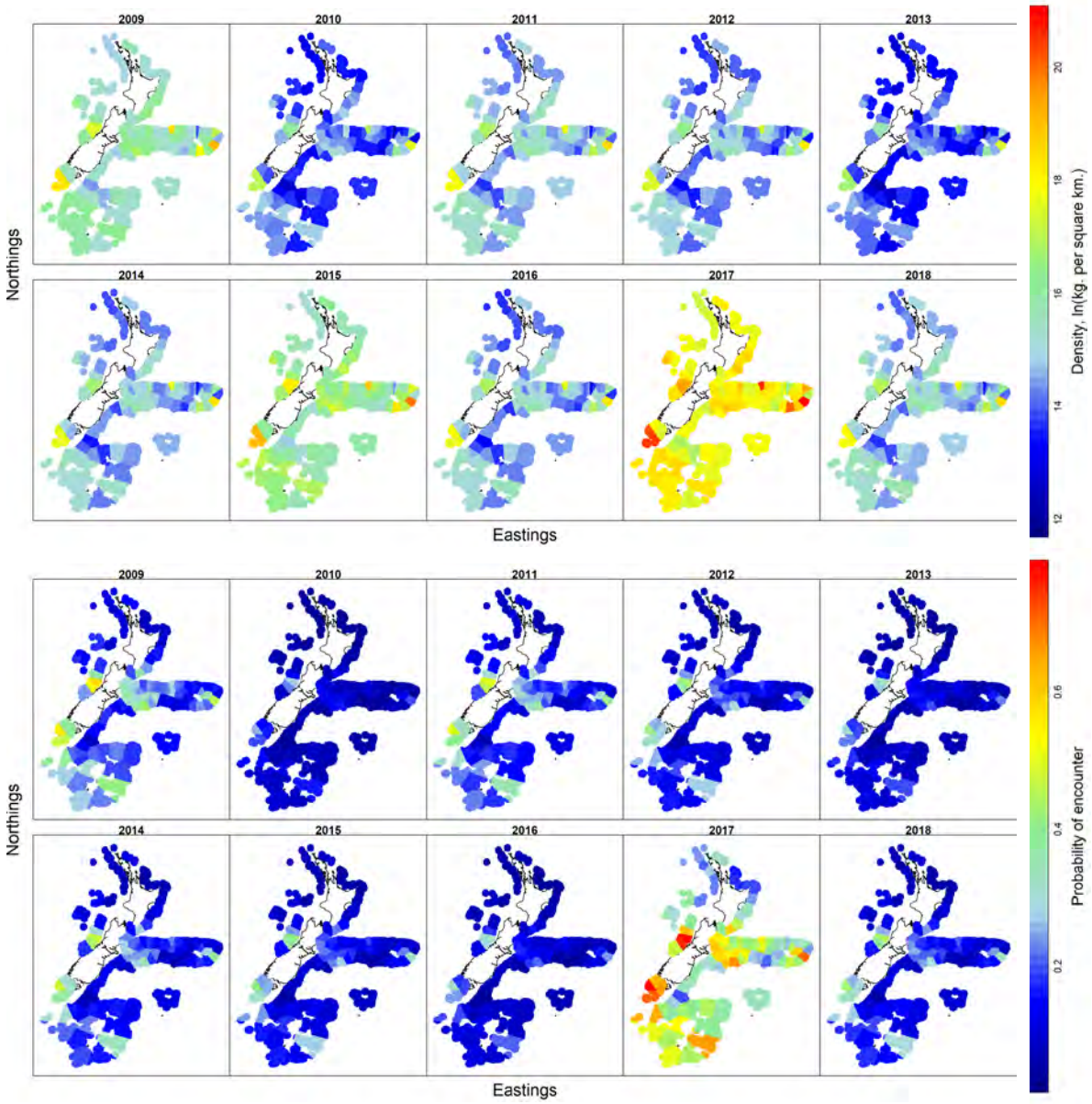

Figure 42: VAST outputs for relative density (kg km^{-2}, top panel) and probability of encounter (bottom panel) of *Scymnodon plunketi* across the New Zealand waters in the past decade (2009–2018, from left to right for each panel). The full time series is shown in Appendix 10. Note that scales for density plots vary from figure to figure.

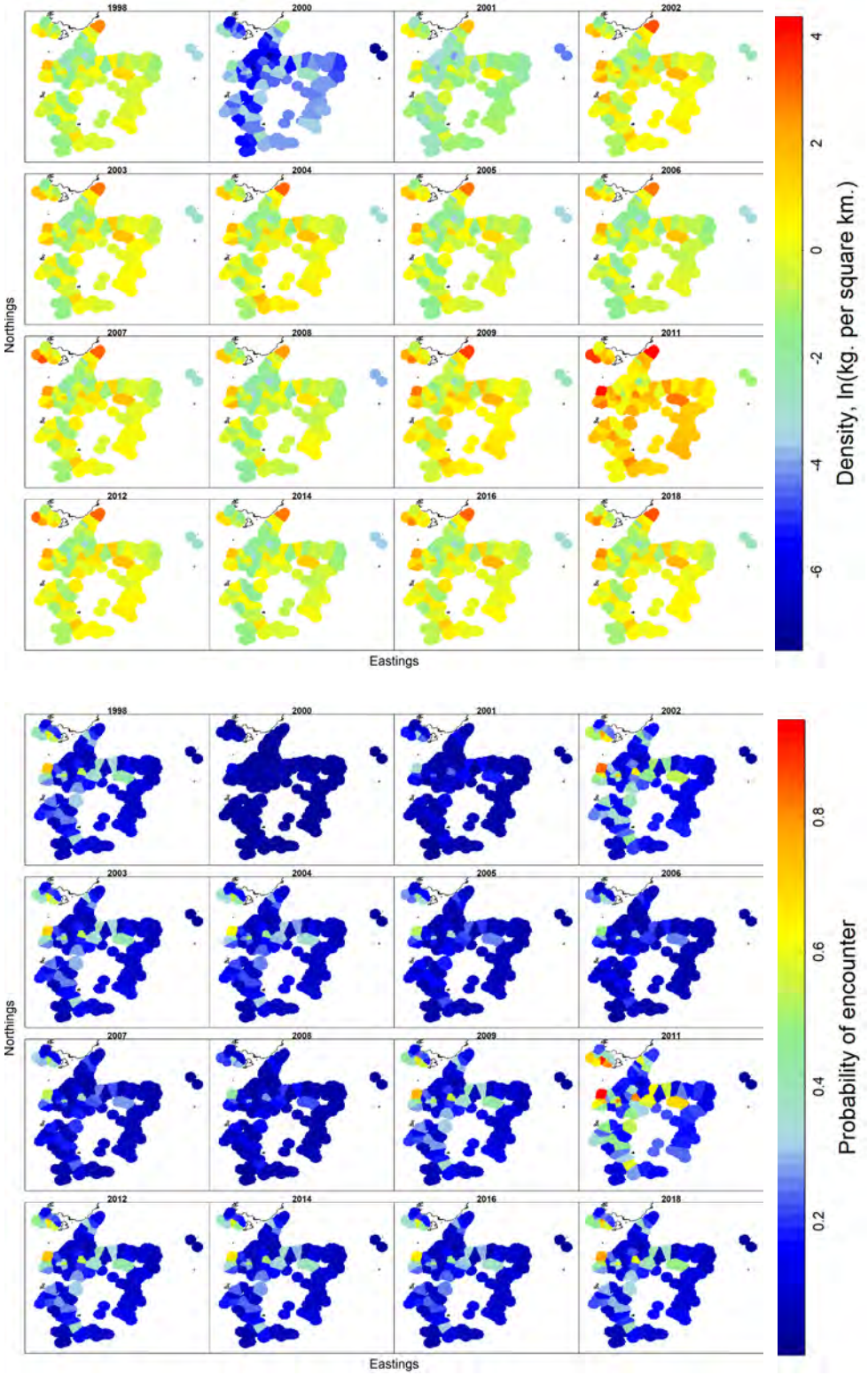

Figure 43: VAST outputs for relative density (kg km^{-2}, top panel) and probability of encounter (bottom panel) of *Scymnodon plunketi* across the Sub-Antarctic (1998–2018, from left to right for each panel). The full time series is not available for *S. plunketi* (the model did not converge).

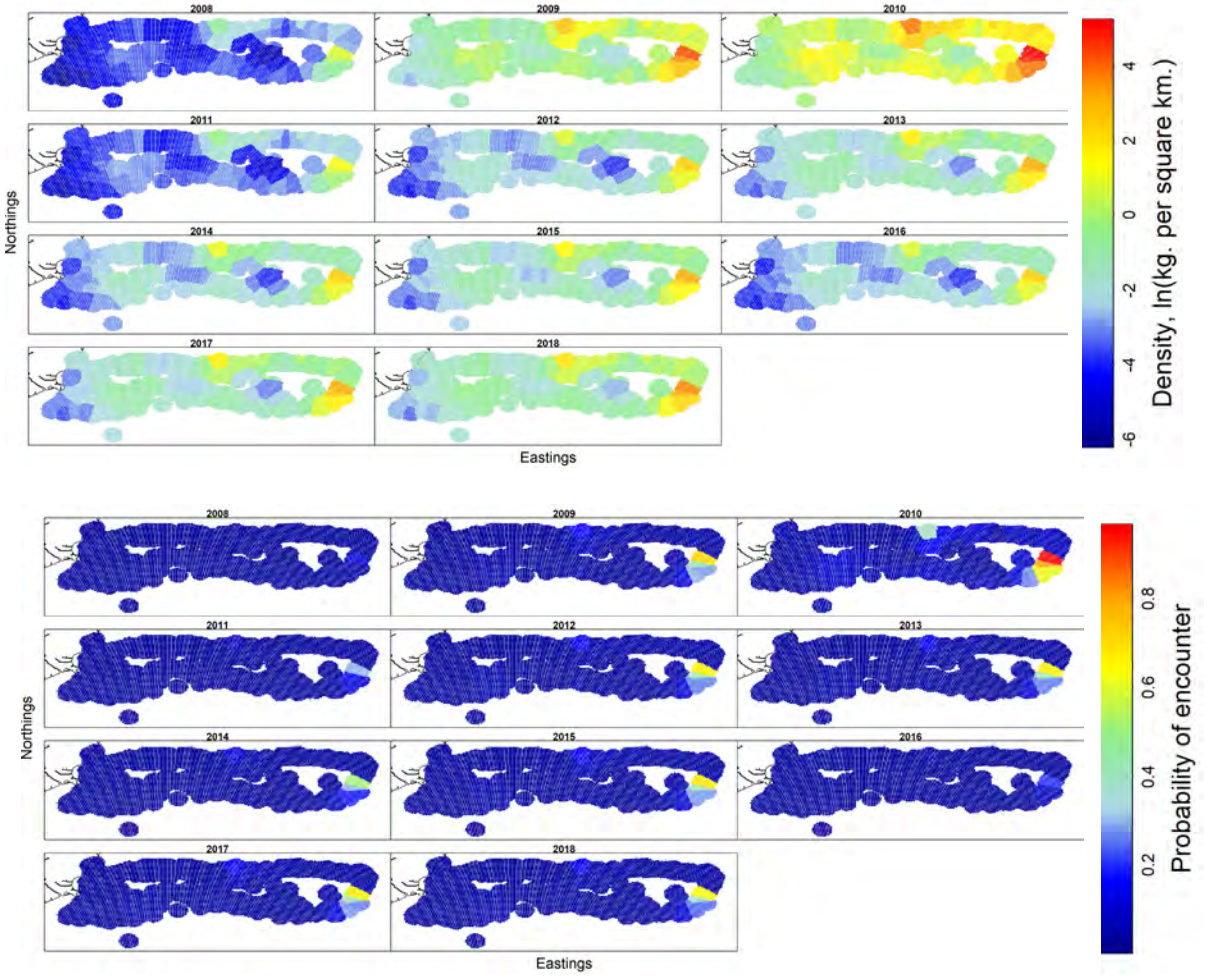

Figure 44: VAST outputs for relative density (kg km^{-2}, top panel) and probability of encounter (bottom panel) of *Scymnodon plunketi* across Chatham Rise using observer records (2008–2018, from left to right for each panel).

3.10 *Deania calcea*

The single-species analysis was similar to the multi-species analysis for *Deania calcea*, with greater probability of encounter around the North Island, off the west coast South Island, and Chatham Rise (Figure 45–Figure 47). On Chatham Rise, predicted densities of females, both immature and mature, were highest to the southeast of Chatham Rise (Figure 49). Males were distributed more evenly along the northern and south-eastern slopes, although some years showed higher predicted densities of mature males concentrated along the northeast area. Probability of encounter was high for most of Chatham Rise for immature females, although in some years they were concentrated in the east; immature males were more likely to be encountered along the northwest and eastern parts of Chatham Rise (Figure 50). Mature female frequency was highest in the southeast and the highest occurrence for mature males was along the northern and eastern slope.

In the Sub-Antarctic, densities were low and similar for sex and maturity stages, with the highest densities at Puysegur (Figure 51). Probability of encounter for all classes was also highest at Puysegur (Figure 52). Immature and mature females were also encountered along the southwest slope of Campbell Plateau.

Model outputs from the observer data for *Deania calcea* showed similarities to trawl survey data, with the highest density reported from northern Chatham Rise, particularly in the east, and highest

probability of encounter concentrated in areas along the eastern slope (Figure 53). In the Sub-Antarctic, density and probability of encounter were highest at Puysegur and the southern portion of the Campbell Plateau (Figure 53).

No trends in density or probability of encounter were observed in any region across the entire time series (see Appendix 11 *Deania calcea*, Figure 121 to Figure 135 for full time series and residual plots).

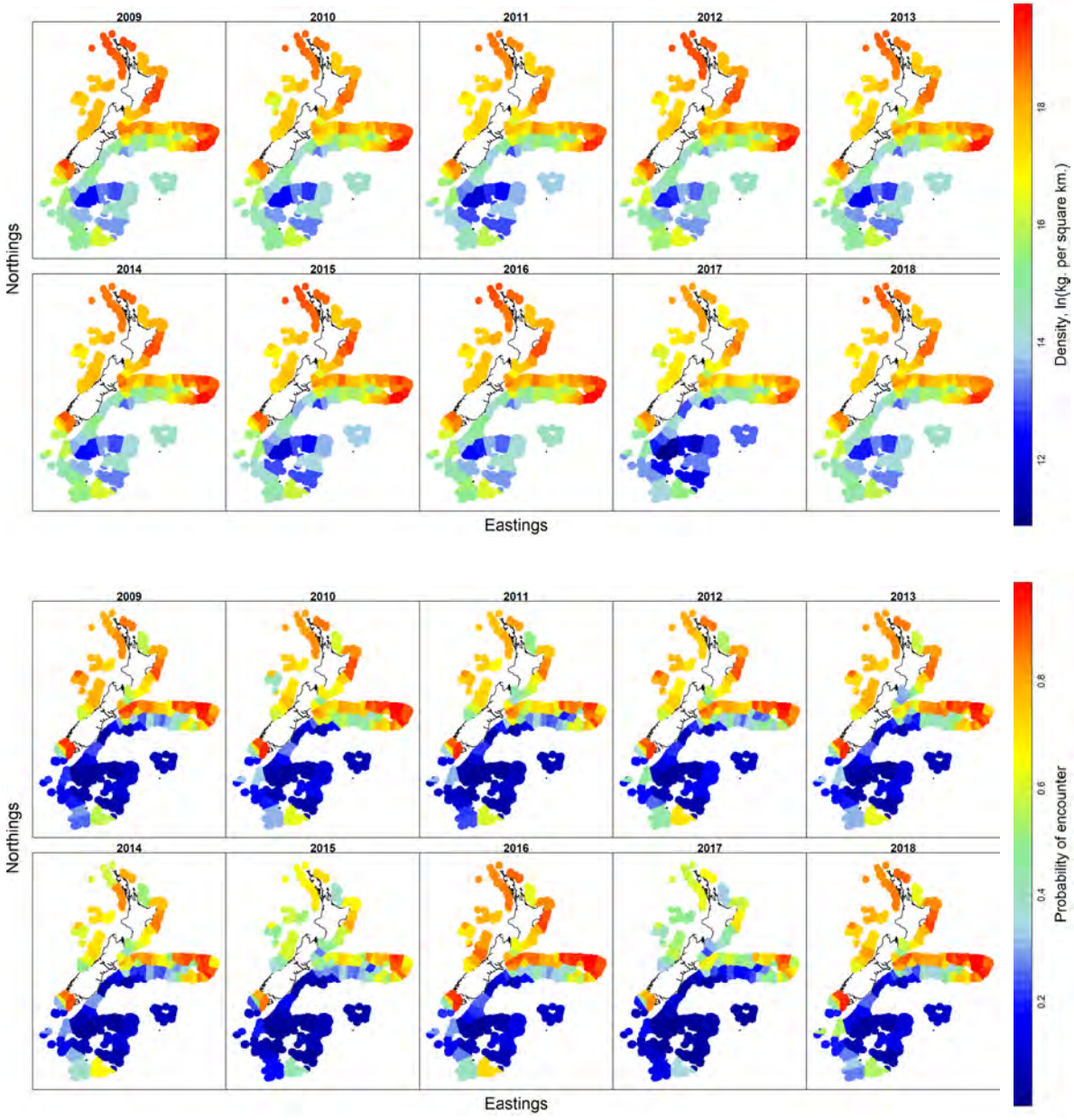

Figure 45: VAST outputs for relative density (kg km^{-2}, top panel) and probability of encounter (bottom panel) of *Deania calcea* across the New Zealand waters in the past decade (2009–2018, from left to right for each panel). The full time series is shown in Appendix 11. Note that scales for density plots vary from figure to figure.

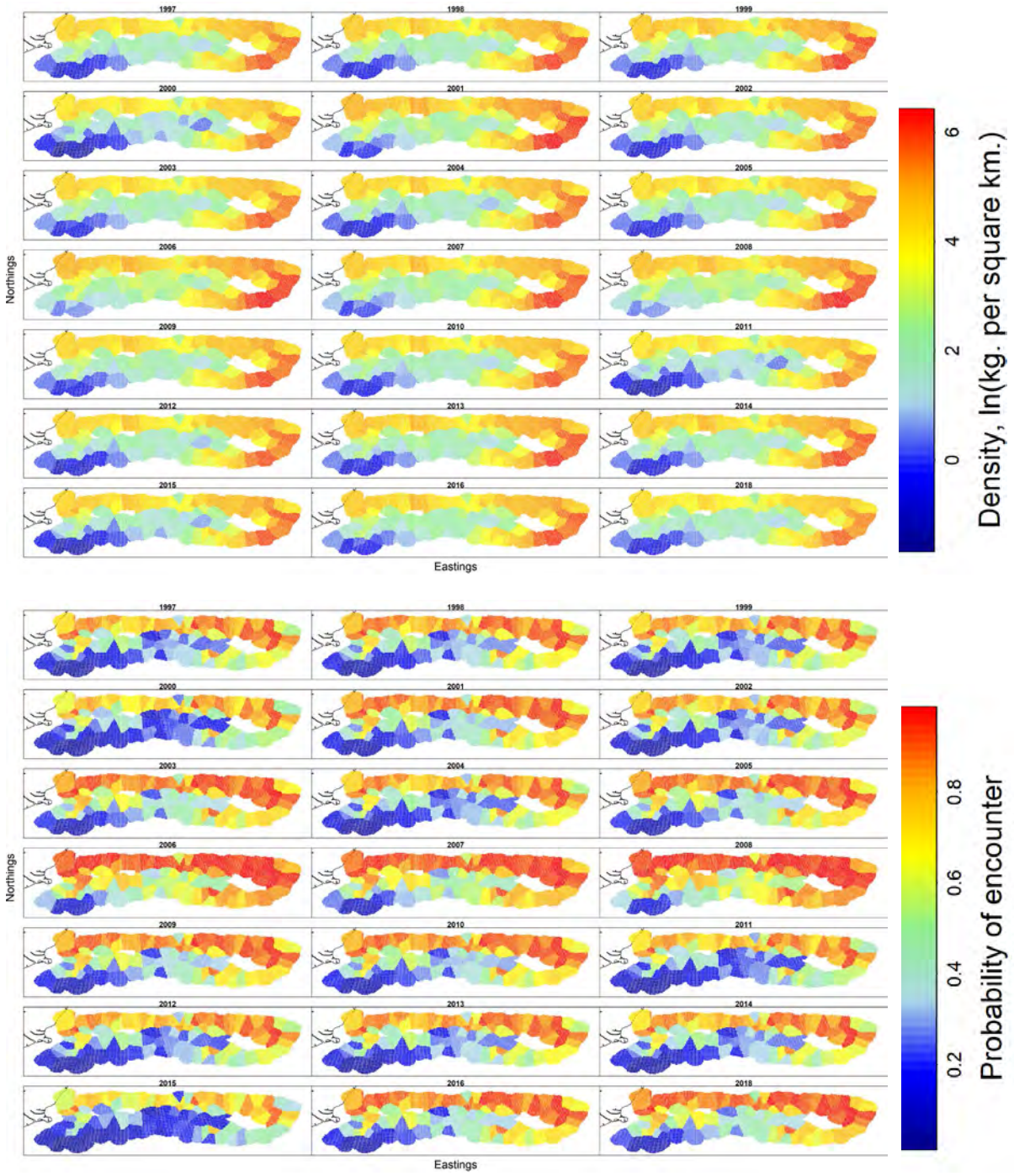

Figure 46: VAST outputs for relative density (kg km^{-2}, top panel) and probability of encounter (bottom panel) of *Deania calcea* across Chatham Rise (1997–2018, from left to right for each panel). The full time series is shown in Appendix 11.

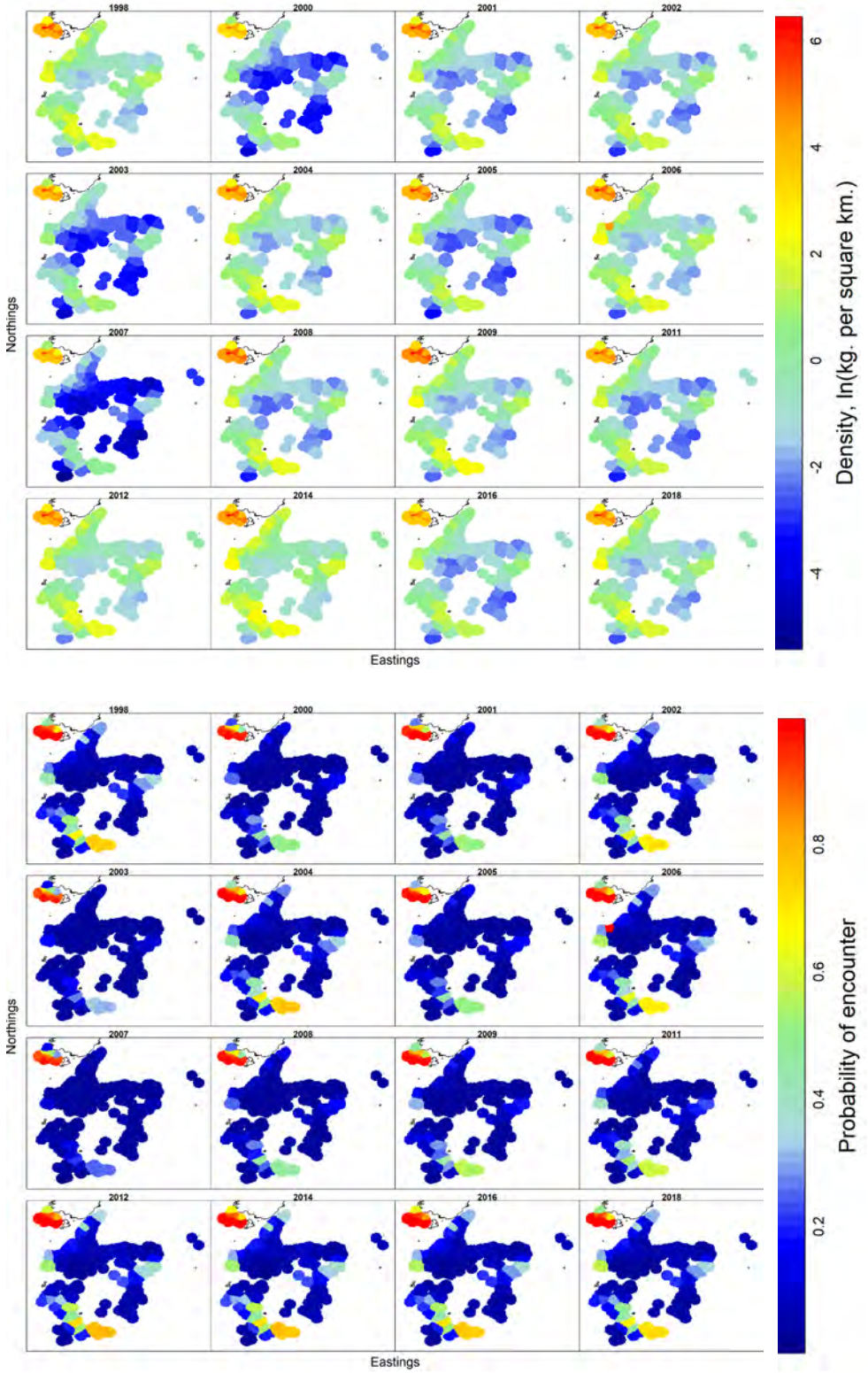

Figure 47: VAST outputs for relative density (kg km^{-2}, top panel) and probability of encounter (bottom panel) of *Deania calcea* across the Sub-Antarctic (1998–2018, from left to right for each panel). The full time series is shown in Appendix 11.

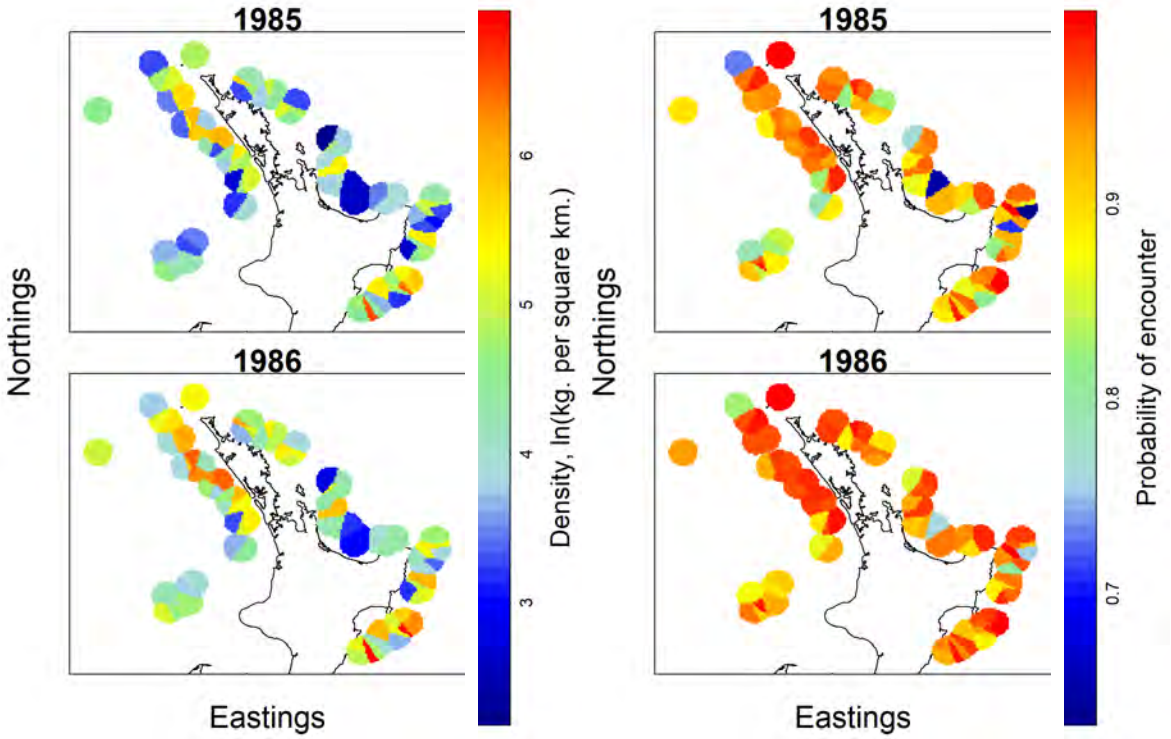

Figure 48: VAST outputs for relative density (kg km^{-2}, left panel) and probability of encounter (right panel) of *Deania calcea* around the North Island of New Zealand in 1985-1986.

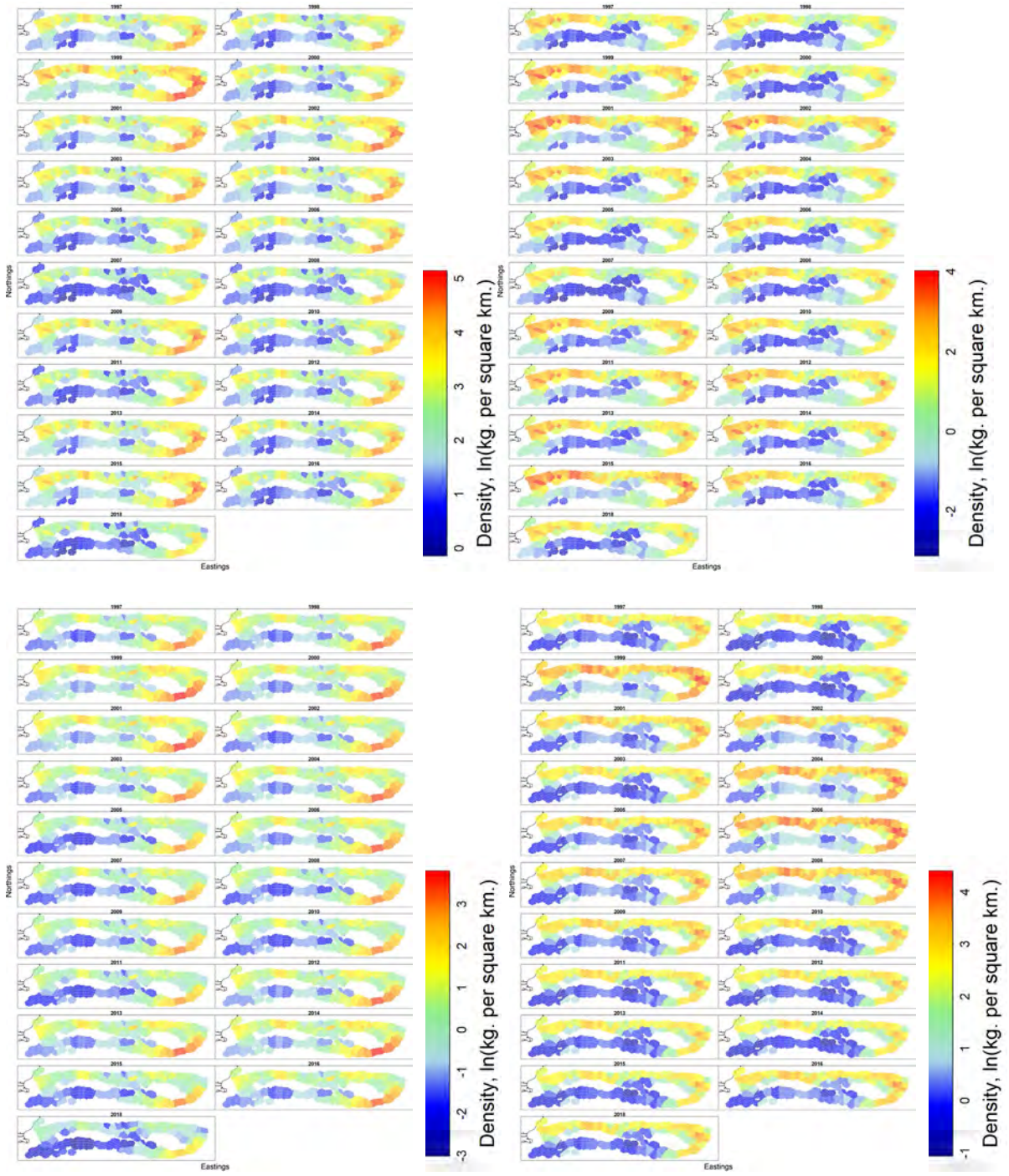

Figure 49: VAST outputs for relative density (kg km^{-2}) of *Deania calcea* by class (from top left: immature female, immature male, mature female, mature male) across Chatham Rise (1997–2018, from left to right for each panel). Note that scales for density plots vary from plot to plot.

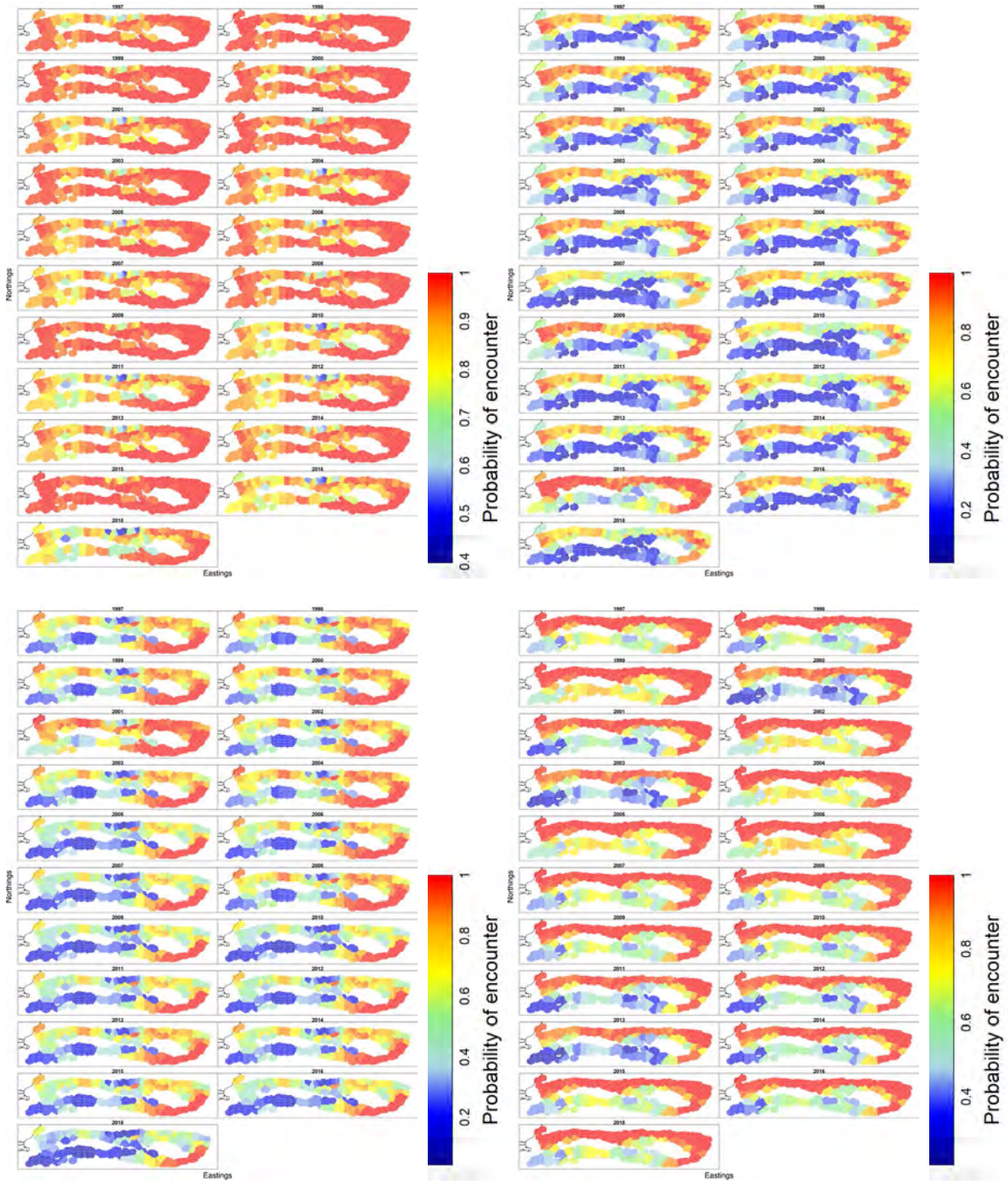

Figure 50: VAST outputs for probability of encounter of *Deania calcea* by class (from top left: immature female, immature male, mature female, mature male) across Chatham Rise (1997–2018, from left to right for each panel).

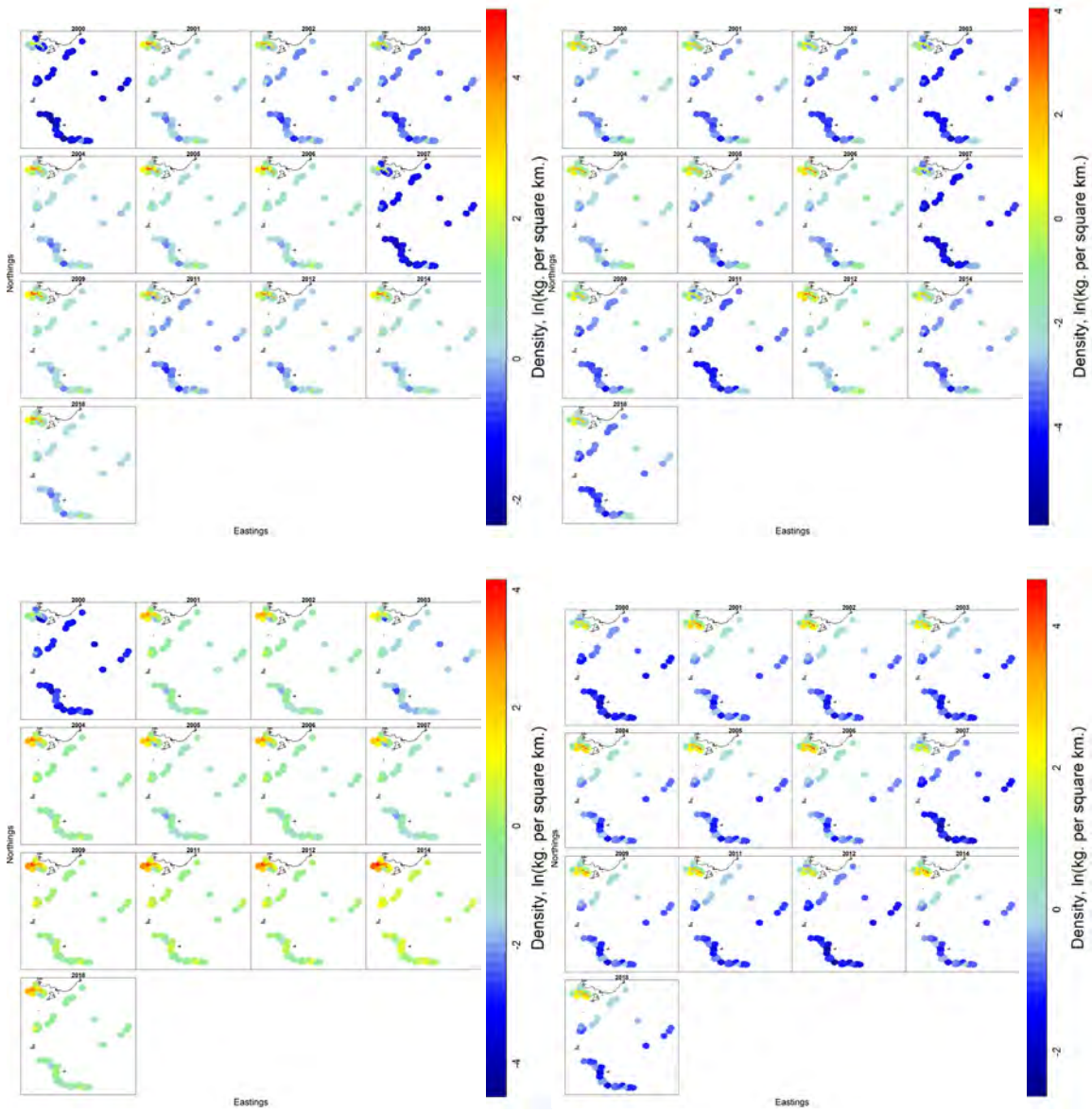

Figure 51: VAST outputs for relative density (kg km^{-2}) of *Deania calcea* by class (from top left: immature female, immature male, mature female, mature male) across the Sub-Antarctic (2000–2018, from left to right for each panel). Note that scales for density plots vary from plot to plot.

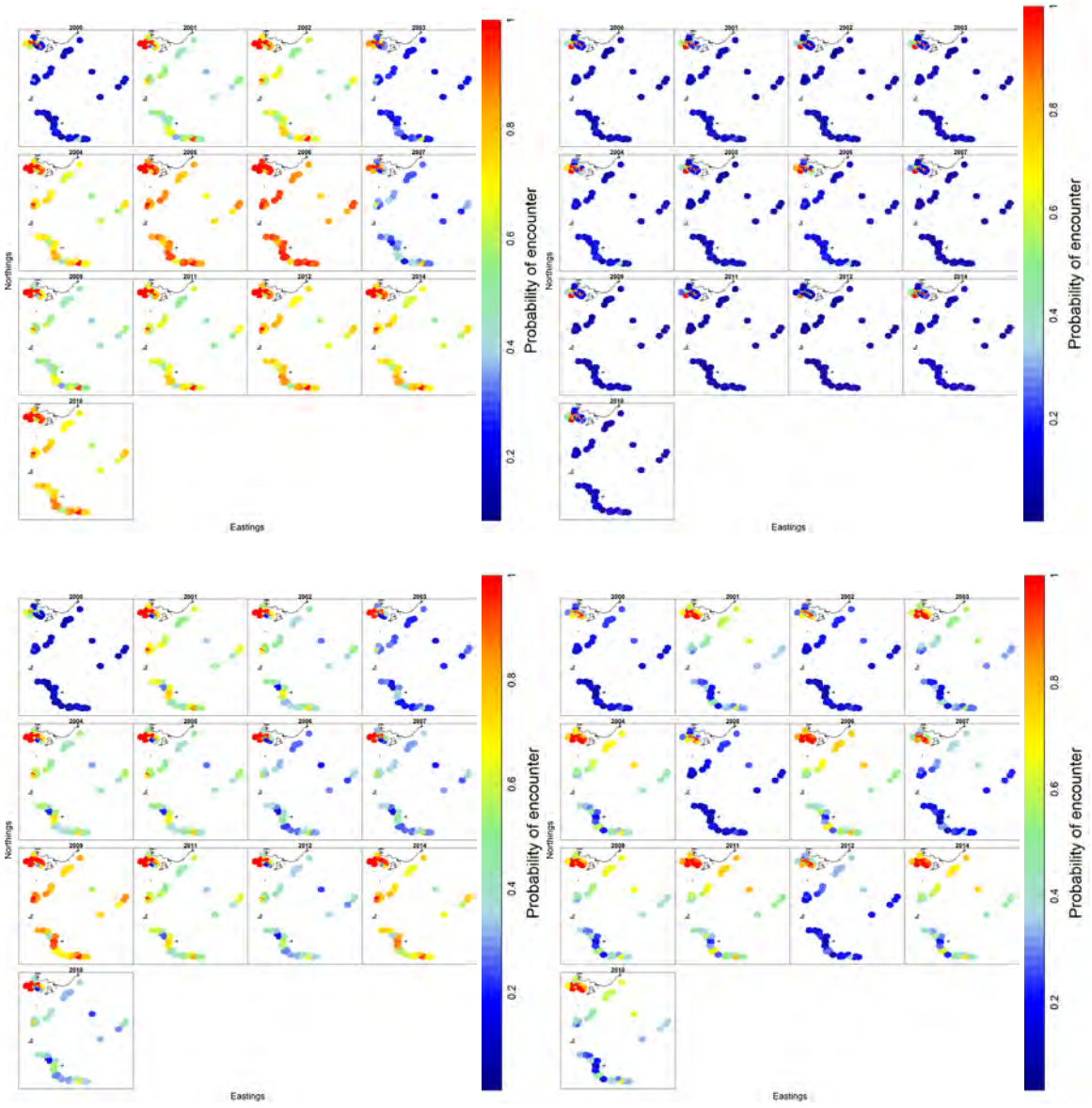

Figure 52: VAST outputs for probability of encounter of *Deania calcea* by class (from top left: immature female, immature male, mature female, mature male) across Sub-Antarctic (2000–2018, from left to right for each panel).

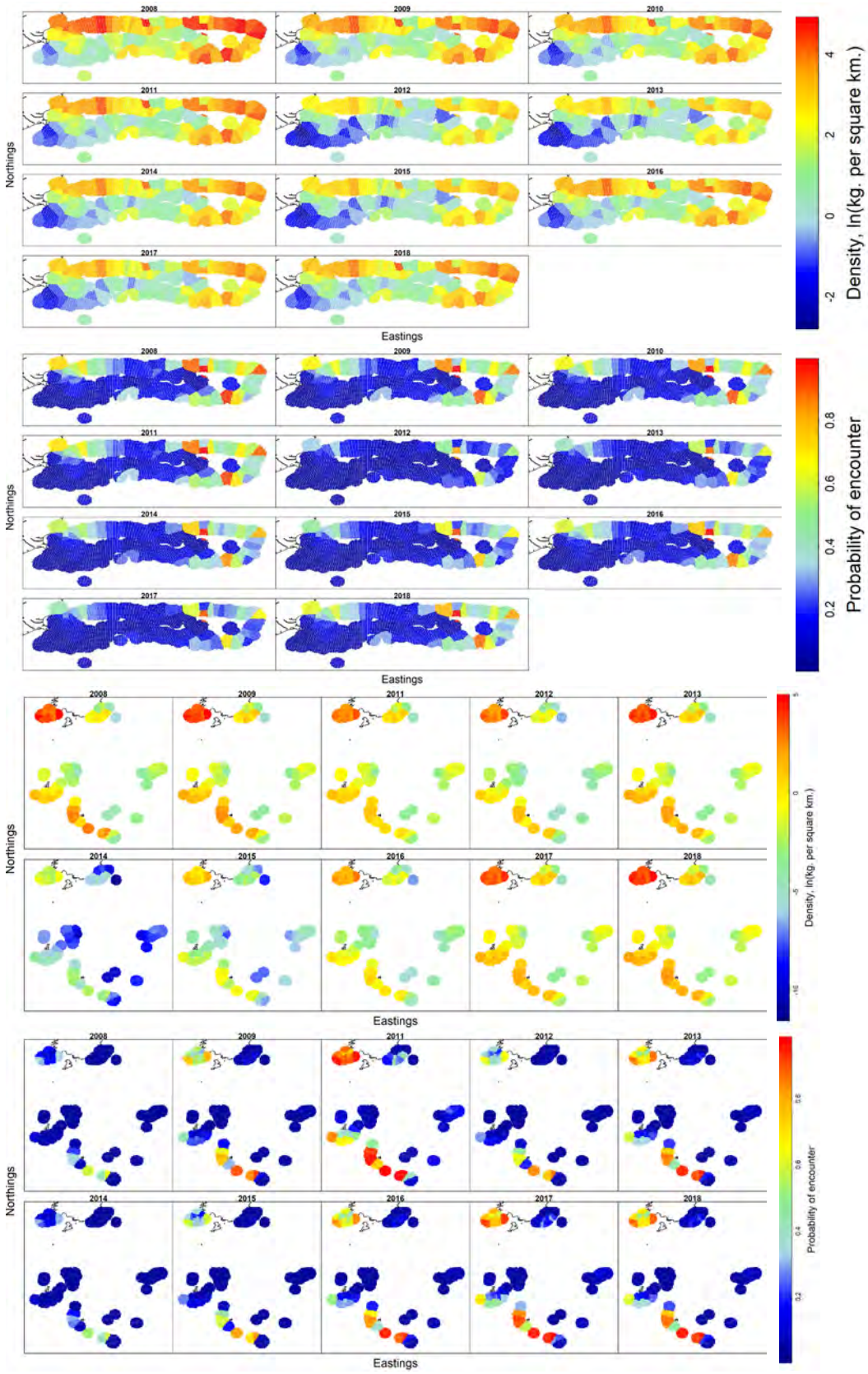

Figure 53: VAST outputs for relative density (kg km^{-2}) and probability of encounter of *Deania calcea* across Chatham Rise (top panels) and Sub-Antarctic (bottom panels) using observer records (2008–2018, from left to right for each panel). Note that scales for density plots vary from plot to plot.

3.10.1 Seasonal patterns of *Deania calcea* around the North Island

Seasonal changes in the distribution of *Deania calcea* around the North Island were also modelled by sex and maturity class, with density and probability of encounter shown in Figure 54 and Figure 55. Data were divided into four seasons: spring (Sep-Nov), summer (Dec-Feb), autumn (Mar-May), and winter (Jun-Aug).

Immature female

Immature female density was highest off the east coast and around the northern North Island. Probability of encounter did not change with season and was high around most of the North Island with the exception of the southwest coast.

Immature male

Immature male density was similar to immature female density, with higher densities off the southeast coast. Density was highest in autumn. Probability of encounter did not change with season and was high around most of the North Island with the exception of the southwest coast.

Mature female

Mature female density did not change with season and was highest off the southeast coast North Island. Probability of encounter was variable but higher in spring and summer seasons.

Mature male

Mature male density was highest off the west coast North Island and did not change with season. Probability of encounter was high, particularly off the west coast. There was some indication of seasonal trends, with higher probability of encounter around the northern North Island in spring and summer and higher probability of encounter off the southeast coast in summer.

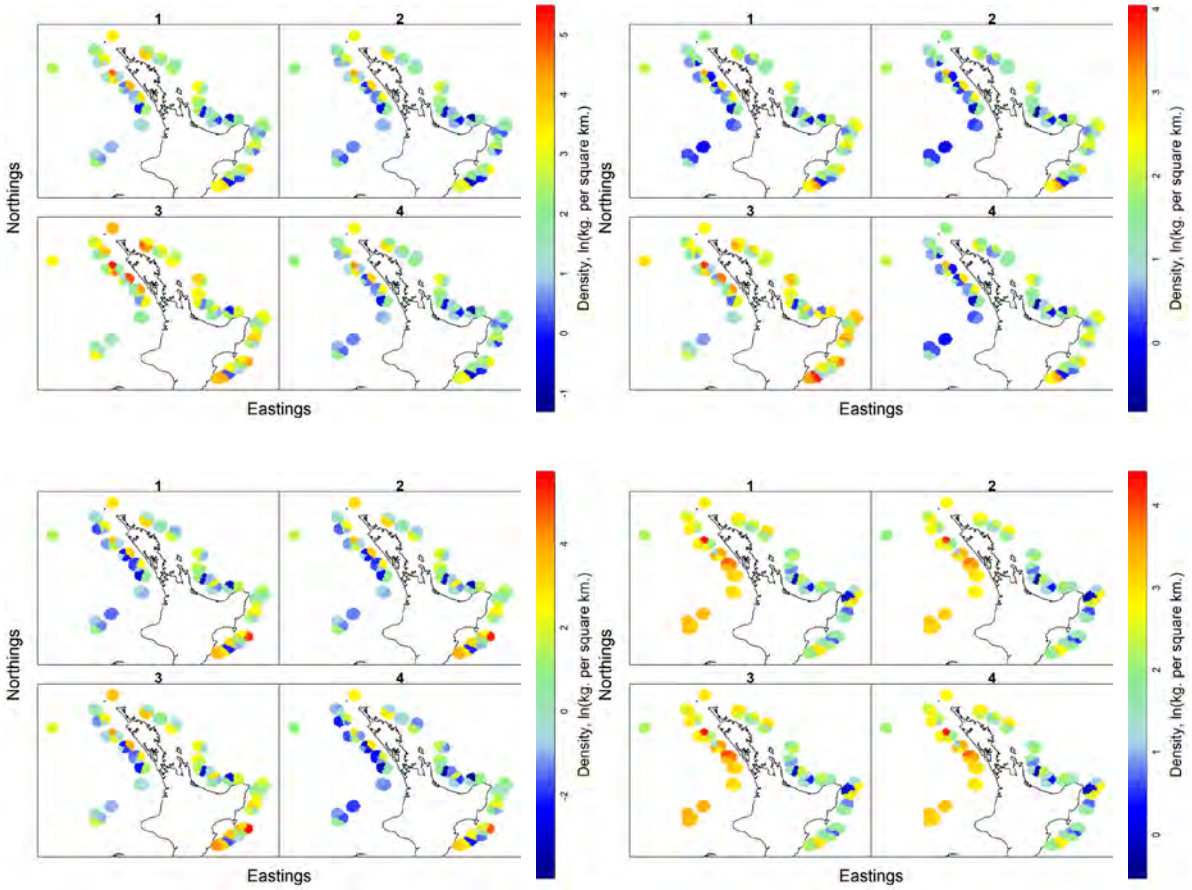

Figure 54: VAST outputs for seasonal relative density (kg km^{-2}) of *Deania calcea* by class (clockwise from top left immature female, immature male, mature female, mature male) around the North Island of New Zealand in 1985–1986 (spring, 1; summer, 2; autumn, 3; winter, 4). Note that scales for density plots vary from plot to plot.

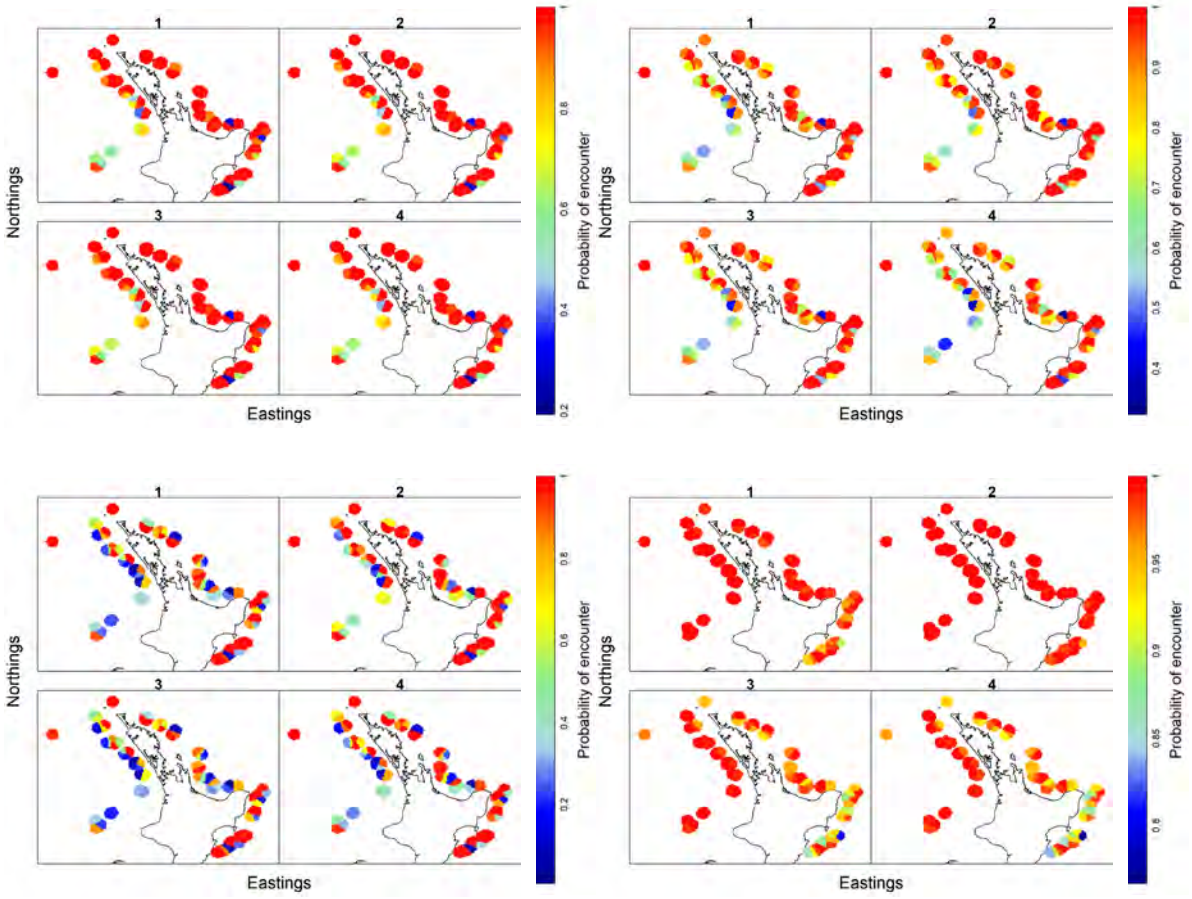

Figure 55: VAST outputs for seasonal probability of encounter of *Deania calcea* by class (clockwise from top left immature female, immature male, mature female, mature male) around the North Island of New Zealand in 1985–1986 (spring, 1; summer, 2; autumn, 3; winter, 4).

4. DISCUSSION

4.1 Distributional knowledge of deepwater sharks

Deepwater sharks are ubiquitous around New Zealand, with each species shown to have a different distributional pattern. Some species, such as *Deania calcea*, *Centroselachus crepidater*, and *Etmopterus granulosus*, were widespread across the New Zealand EEZ and showed continuous distributions along the continental shelf and slope. Others, like *Centrophorus squamosus* and *Scymnodon plunketi* had more disjointed distributions, with areas of high relative density scattered across the EEZ. *Dalatias licha* and *Centroscymnus owstonii* were found to have more northern distributions, whereas *Centrophorus squamosus* and *E. granulosus* were most prevalent in the Sub-Antarctic.

The models identified three areas as deepwater shark 'hotspots' in New Zealand waters, where species were found to have relatively high densities and probability of encounter: 1) Puysegur (for six of the seven species, except *Centroscymnus owstonii*); 2) the southeast portion of Chatham Rise (seven species); and 3) the southern Campbell Plateau (for six of the seven species, not *Centroscymnus owstonii*). These areas warrant further investigation to understand the environmental drivers for these hotspots, their importance to deepwater sharks (e.g., breeding grounds, pupping grounds), as well as to quantify the abundances and class compositions of these species in these regions. Puysegur and parts of the southeast Chatham Rise are also areas of high fishing activity, thus potentially increasing the risk to the species from fishing activity, and interactions should be monitored closely.

All species assessed here were spatially segregated by sex, size, and maturity stage. This is likely characteristic of most, if not all, chondrichthyans, and is well documented in the literature (e.g., Mucientes et al. 2009, Holt et al. 2013, Finucci et al. 2018). This behaviour has been shown to be advantageous for a number of reasons; females often segregate from males to reduce costs associated with mating events which can negatively impact female fitness through body inflictions and harassment (Pratt & Carrier 2001), and segregation by size can reduce intra-specific predation of juveniles (Guttridge et al. 2012). Such behaviours, however, can also negatively impact species or populations: spatially focused fishing could result in high and differential mortality of the sexes (Mucientes et al. 2009), and species such as *Squalus acanthias* have undergone extensive population reduction outside New Zealand due to targeted fishing of mature females (García de la Rosa et al. 2004). In this analysis, it was shown that juvenile individuals and mature males of *Centrophorus squamosus* in the Sub-Antarctic are distributed in areas where fishing effort is high (e.g., Puysegur, northern Campbell Plateau); mature females, however, were predicted to be distributed on the southern portion of the Campbell Plateau, where there is limited fishing.

There was very little evidence to suggest any temporal or spatial changes in the populations of the species examined here. The lack of trends may be indicative of relatively stable population abundance since the start of the time series (mid-1980s). Any effects that took place immediately after the introduction of deepwater fishing remain unknown, however, as deepwater fisheries emerged in the late 1970s/early 1980s (Clark 2009). There was also no strong evidence of seasonal trends, although data for such an analysis are limited and were restricted to *Deania calcea* around the North Island over the course of one year. Repeating the *Wanaka* survey around the North Island would provide contemporary data that could offer comparable results to those reported in 1985–86 and offer better insight into the distributions and abundances of a number of deepwater species where sampling is very limited.

For *Centrophorus squamosus*, the modelling of EEZ data suggested that probability of encounter at Puysegur has increased since the late 1990s/early 2000s. This may, however, be reflective of more accurate identification of immature individuals during recent times. Puysegur was highlighted as an area of relative high abundance for immature *Centrophorus squamosus,* and this species has historically been difficult to identify, particularly at small sizes. Misidentification may also be influencing patterns of distributions or abundances of some species where morphologically-similar looking species are known to occur in New Zealand waters but are rarely reported due to a lack of easily distinguishable characteristics. For example, it is known there are three species from the genus *Deania* in New Zealand waters, but only one of these, *Deania calcea*, has been reported in research trawl surveys.

The species included in this work are all known from distributions outside of New Zealand. The following sections describes work on these species outside New Zealand waters and compares this information to the distributional patterns predicted here.

4.2 Global knowledge of deepwater shark distributions

4.2.1 *Dalatias licha*

Dalatias licha has a widespread yet patchy distribution in the Atlantic and Indo-West Central Pacific Oceans (Roberts et al. 2015). In New Zealand, it is found at depths 50–1000 m, and generally below 300 m. In the Northeast Atlantic Ocean, it has been reported from Norway to Northwest Africa; it is considered relatively rare although has found to be particularly abundant on the southern Mid-Atlantic Ridge, with a historic targeted fishery around the Azores indicating higher densities in this area (ICES-WGEF 2018). Despite documented declines of the species in the North Atlantic Ocean (ICES-WGEF 2018), fisheries operating around the Azores continue to report large catches of *Dalatias licha*; approximately 38 t of annual catch was reported from bottom longline and handline fisheries between 2004 and 2011 (Fauconnet et al. 2019).

Commercial fishery catches from the Azores reported minimum fish sizes of about 100 cm total length, with no known small individuals caught (da Silva 1988). Sex ratio varied with depth, with mature

females more abundant at shallower depths and males more abundant deeper. However, catch was found to be highly selective by fishing gear type, with handlines catching larger individuals than trawl and capable of fishing at deeper depths (da Silva 1988).

Although only mature species were recorded from the Azores demersal longlines, a wider length range including immature individuals was recorded more broadly in the North Atlantic Ocean from trawl fisheries off Ireland and Scotland (Henderson et al. 2003, Neat et al. 2015), to the south off the coast of West and South Africa (Bass et al. 1976, Pascual-Alayon et al. 2017), and in the Mediterranean Sea (e.g., Capapé et al. 2008). In these areas, the sex ratio was varied with more females than males reported off Scotland, but males were more commonly caught in the south-western Mediterranean, giving some indication of segregation, at least by sex.

Data on population structure of this species from the South Pacific Ocean were sparse; historically high catches in trawl fisheries and a sharp decline in population was reported in the Southern and Eastern Scalefish and Shark Fishery (SESSF) (Walker & Gason 2007). Length ranges and maturity information from New South Wales (NSW) and Tasmania were dominated by immature fish, and females were more numerous than males (Daley et al. 2002).

Similar to the Atlantic Ocean, the species is caught in relatively low numbers in New Zealand trawl fisheries, generally as single individuals (Finucci et al 2018), despite it having a relatively large population in New Zealand waters (Ford et al. 2015). Highest relative abundance for the species in this study was along the west coast South Island and Puysegur. There are anecdotal reports of historic high catch rates of at least some mature specimens from Cook Strait and the Kaikoura Canyon (Garrick 1960). This area was also identified as an area of relatively high relative abundance and high probability of encounter. If the species was to aggregate in New Zealand in a similar location to the Azores archipelago, we may expect to find it at a latitude about 37.7° S (with the geographical coordinates of the Azores at 37.74° N, 25.67° W). This could equate to the east coast North Island, where relative abundance, but not probability of encounter, was highlighted as moderately high. The species is regularly reported from commercial longline fisheries overseas (e.g., Fauconnet et al. 2019) and within New Zealand (Finucci et al. 2020), suggesting trawl surveys may not be appropriate to sample the species.

4.2.2 *Centrophorus squamosus*

Centrophorus squamosus is a wide-ranging benthopelagic shark reported from a patchy distribution across the Indo-Pacific Ocean and Atlantic Ocean (Roberts et al. 2015). In New Zealand, it has been reported from depths of 260–1440 m and is thought to have a moderately sized population (Ford et al. 2015). It is one of the more well-studied species, with extensive fishery-dependent and independent data from the eastern Atlantic Ocean in particular. A constrained correspondence analysis (CCA) incorporating all available data showed different life stages were influenced by environmental variables including depth, water temperature, and salinity (Moura et al. 2014). In conjunction with distributional maps, the CCA analysis indicated species segregation by sex, size, and maturity stage. Moura et al. (2014) reported that mature females were less common than mature males or immature individuals and appeared to have a more restricted distribution. On the contrary, mature males were found to be widespread in the region; this contrasts the results reported here from the Sub-Antarctic; mature males were confined to Puysegur and the northeast Campbell Plateau.

Mature and post-natal females have been shown to be associated with shallower depths and warmer waters, with clear associations with submarine features such as the Mid Atlantic Ridge and Tore-Madeira Ridge, Rockall Trough and Rockall Bank (Girard & Du Buit 1999, Moura et al. 2014). Reports of gravid females from the region were rare and isolated events (e.g., Bañón et al. 2008, Severino et al. 2009) and have not been reported from United Kingdom and Irish waters despite extensive surveying over many years (e.g., Clarke 2001, Neat et al. 2015). The work presented here did not distinguish between maturity stages beyond immature or mature but suggested that areas along the Stewart-Snares shelf in the Sub-Antarctic host high densities of mature female *Centrophorus squamosus*.

Population genetics have indicated low genetic variability and migration of individuals between populations, although long-term genetic divergence between the Northeast Atlantic Ocean and New Zealand was reported (Veríssimo et al. 2012). This same study also showed that females were less dispersive than males and possibly philopatric. Recent tagging studies of *Centrophorus squamosus* (both sexes) observed movements over several months with individuals travelling several hundred kilometres; one individual was observed migrating from the Cantabrian Sea to the Porcupine Bank (Rodríguez-Cabello & Sánchez 2014, Rodríguez-Cabello et al. 2016). Such distances could be akin to movements between Puysegur and the west coast of the North Island, for example. However, population connectivity around New Zealand is currently unknown.

Here, highest relative densities of the species (combined stage and sex) were predicted along the western coasts, particularly off the North Island, as well as off Puysegur. Relative densities were lower across much of the Chatham Rise with the exception of the southeastern area. The models did not converge for the Chatham Rise, so patterns of segregation by sex and maturity size were not available. Scaled length frequencies for this species from the Chatham Rise and Sub-Antarctic trawl surveys, reported by Parker & Francis (2012), indicated immature individuals were present in both regions, and particularly abundant in the Sub-Antarctic. This appears to contrast with the VAST results, in which the relative density of immature females was restricted off Puysegur and the relative density for immature males was near zero.

4.2.3 *Centroscymnus owstonii*

Centroscymnus owstonii is known from a patchy distribution in the Atlantic Ocean and Indo-Pacific Ocean (Roberts et al. 2015). It is reported from New Zealand waters of depths of 320–1284 m and has a relatively large population (Ford et al. 2015). In Suruga Bay, central Japan, female *Centroscymnus owstonii* were noted to segregate by maturity stage, with gravid females at shallower depths than non-gravid females, and immature animals occurring at deeper depths (Yano & Tanaka 1988). Mature females were also captured at shallower (100–1000 m) depths than mature males (800–900 m). Elsewhere, the species has been infrequently recorded from the Northeast Atlantic Ocean (Moura et al. 2008).

Population data for *Centroscymnus owstonii* was only available from the Southwest Pacific Ocean. In Australia, this species is found from central New South Wales to Shark Bay in Western Australia and was classed as a relatively common species (Walker & Gason 2007). Full size ranges (from about 30 cm to over 100 cm) were present in samples from both NSW and Tasmania (Daley et al. 2002). Catches from NSW were dominated by immature individuals, whereas samples from Tasmania consisted of mature males and females with very few immature individuals.

In New Zealand waters, full size ranges and all maturity stages have been recorded. In previous work, adult individuals were found to be more common on Chatham Rise and off the west coast South Island than in the Sub-Antarctic area (Francis et al. 2018). This was evident in the VAST analysis as well, and Puysegur was also highlighted as an area where relative abundance of the species was high. *Centroscymnus owstonii* has been described as a species highly associated with seamounts (Tracey et al. 2012); such patterns could be observed for this species on the Chatham Rise, where probability of encounter was highest around the Graveyard Seamounts and Andes (north and southeast Chatham Rise, respectively). There were insufficient data available to compare any latitudinal differences in distributions among the maturity stages, as observed in Australia.

4.2.4 *Centroselachus crepidater*

Centroselachus crepidater has a similar distribution to *Centroscymnus owstonii* in the Atlantic Ocean and Indo-Pacific Ocean (Roberts et al. 2015). It has been reported at depths of 420–1350 m in New Zealand waters and has a large population size (Ford et al. 2015). In the Northeast Atlantic Ocean, it is commonly reported on the shelf to the west of Scotland and Ireland between 500 and 1600 m, as well as on seamounts, with a trend of increasing catch rates to the south (Neat et al. 2015). All life history

stages were recorded in both the Scottish and Irish trawl surveys with length ranges of 24 cm–91 cm (O'Hea et al. 2008, Neat et al. 2015), although immature individuals were much less numerous and noted as absent from trawl and longline catches further south on Porcupine Bank (Clarke et al. 2001). Sex ratios were reported as skewed, with females more numerous than males (Moore et al. 2013, Neat et al. 2015).

Centroselachus crepidater was also described as a common species (Walker & Gason 2007) around southern Australia (including southern NSW, Victoria, and Tasmania) and was caught in higher numbers in the western area of its known distribution (Daley et al. 2002). Size structure and sex ratios varied between regions; the catches off NSW had relatively balanced sex ratios and were dominated by immature individuals of 30–50 cm, with very few fish over 60 cm. Catches around Tasmania, however, were dominated by adults, particularly females.

As in the Northeast Atlantic Ocean, sex ratios have been found to be skewed towards females in New Zealand (Francis et al. 2018). In contrast to the Northeast Atlantic Ocean, immature individuals were found in abundance on the Chatham Rise alongside adult males and females (Francis et al. 2018). This pattern was predicted in the VAST outputs, with immature and mature individuals of both sexes reported at similar rates of relative abundance both on the Chatham Rise and in the Sub-Antarctic, although the spatial distribution of these sex and size classes varied. Unlike some of the other larger species presented here, mature females were just as common, if not more common, than the other life history classes from the VAST analysis.

4.2.5 *Etmopterus granulosus*

Etmopterus granulosus is thought to have a circumpolar distribution in the Southern Hemisphere in the Atlantic and Indo-Pacific Oceans (Roberts et al. 2015). In New Zealand waters, it is found at depths between 367 and 1638 m, and the population size is considered to be large based on commercial, observer, and research trawl data (Ford et al. 2015). In New Zealand waters *E. granulosus* is amongst the top 10 species associated with seamount trawl catches (Tracey et al. 2012). Segregation by size and sex has been reported from research trawl samples on Chatham Rise, with approximately twice as many females as males collected and most specimens caught were mature (Wetherbee 1996, Finucci et al. 2018).

Data on population structure from elsewhere are sparse. In Australia it is reported as the most commonly caught shark in the orange roughy fishery on seamounts off eastern and southern Tasmania, with fishery-independent trawl catch rates of this species up to five times higher than those of other dogfish (up to 32 tonnes) (Daley et al. 2002). Catch rates were much lower further north off the NSW coast (Daley et al. 2002). Latitude has been shown as an important predictor of distribution for other *Etmopterus* species (Neat et al. 2015). This was apparent in the VAST outputs for *E. granulosus*, which showed a more southern distribution of the species. Modelled distribution of immature and mature individuals, of both sexes, had similar rates of relative abundance both on Chatham Rise and in the Sub-Antarctic, although the spatial distribution of these sex and size classes varied. Unlike some of the other larger species presented here, mature females were just as common, if not more common, than the other life history classes from the VAST analysis.

4.2.6 *Scymnodon plunketi*

Scymnodon plunketi is known from southern Australia, New Zealand, parts of the western Indian Ocean, and possibly Chile (as *Centroscymnus macracanthus*) (Roberts et al. 2015). In New Zealand, it is reported from depths of 180–1500 m, and usually below 600 m. Data on the species across its distribution are sparse. *Scymnodon plunketi* was infrequently reported off Tasmania; some large catches (460 kg/h) were reported in some years, which may suggest the species aggregates in certain locations at certain times of year (Daley et al. 2002). Similar to other large bodied deepwater sharks, it is likely that *S. plunketi* engages in segregation by sex and size. For other somniosids, catches of *Centroscymnus coelolepis* from Rockall Trough were dominated by large mature individuals of both sexes (Neat et al.

2015), and, in Suruga Bay, females of the same species displayed well-defined patterns of depth segregation by maturity stage, with gravid females caught in shallower waters than non-gravid individuals (Yano & Tanaka 1988).

Scymnodon plunketi was the least abundant of the species observed here but was thought to have a relatively large population in New Zealand waters (Ford et al. 2015). There is some evidence of considerable local declines, where biomass estimates of *S. plunketi* were reported to decline in 1994 to 6% of that reported from the previous decade (Clark et al. 2000). The year 2017 stood out from the other years in the time series, with much higher relative abundance estimates provided by VAST. According to the model, probability of encounter was highest of the west coast South Island and Puysegur in this year. This was thought to be an outlier in the data, given the low number of tows available in the year (n=20). Alternatively, this may have been an unusual year where more individuals were reported than expected, similar to the phenomena observed off Tasmania (Daley et al. 2002). By catch weight alone, only 211 kg of the species were reported in 2017. However, unlike nearly every other year in the time series where *S. plunketi* was the least reported species (in terms of weight) among the deepwater sharks considered here, the species was the second highest reported species in 2017, coming second only to *Deania calcea*.

4.2.7 *Deania calcea*

Deania calcea has a patchy wide ranging distribution in the east Atlantic Ocean and Indo-Pacific Ocean (Roberts et al. 2015). It is reported from depths of 30–1340 m in New Zealand, but is generally between 600 and 900 m, and is thought to have a relatively large population in New Zealand waters (Ford et al. 2015). The species is relatively well studied in the eastern Atlantic Ocean. Studies at smaller scales off the west coast of Scotland and Ireland reported some latitudinal trends in abundance, with higher catch rates found along the southern slopes of the Rockall Trough, declining to the north and south of this region (Clarke et al. 2002, Neat et al. 2015). Incorporating all available data from the region, Moura et al. (2014) found all life history stages have been present in most regions, with spatial segregation by size, sex, and maturity stage. Immature females outnumbered mature females in almost all regions, and gravid females were found to geographically restricted. Immature individuals (under 55 cm) were found to be scarce in the Northeast Atlantic Ocean, making up under 1% of the catch. However, small immature individuals were reported to be abundant further south in the Central and South Atlantic Ocean (off Mauritania and Namibia). Similar to *Centrophorus squamosus*, mature female *Deania calcea* were associated with shallower depths than were immature individuals and mature males.

In south-eastern Australia, *Deania calcea* was one of the most abundant sharks species caught at mid-slope depths (Daley et al. 2002, Irvine et al. 2012). Some regional differences were reported, including differing sex ratios, with females dominating the waters of NSW, whereas males were more abundant in Tasmanian waters. Immature fish (under 55 cm) were present in both areas, comprising up to 70% of the catch in NSW, although differing mesh sizes used on different surveys preclude further comparisons.

The VAST outputs show similarities to patterns described elsewhere. The species is relatively widespread and abundant, with a preference for waters north of the Sub-Tropical Convergence. Spatial segregation of the sexes and maturity stages was evident, with strong patterns of relative density and probability of occurrence on Chatham Rise and, to a lesser degree, in the Sub-Antarctic. Unlike the Atlantic Ocean population, where segregation by size appears to occur over a vast area, segregation within New Zealand appears to occur over a much finer scale. Population genetics have indicated some genetic variability between populations on a global scale (Keggin 2017), and any regional variability in population structure should be investigated because population connectivity around New Zealand is currently unknown.

Despite previous work suggesting the species may exhibit seasonal migrations around the North Island (Clark & King 1989), no such patterns were found using VAST.

4.3 Observer data

The time series for the observer data did not extend back as far as the research trawl data; 2008 was the first year where sufficient observer data were available for all species except *Centrophorus squamosus* and *Centroscymnus owstonii*, for which data from 2012 onward were used. Although the data set was smaller in size than the trawl survey data set, the observer data provided similar patterns of density and probability of encounter for all species, suggesting these data could be used as validation for assessing the species' distributions around New Zealand. Observer data are also useful in providing information on these species in areas and for time periods that are not sampled by the trawl survey. However, very little biological data were available and, thus, it was not possible to assess any spatial trends by sex or maturity stage. It is recommended that biological data be collected by observers for future studies; at the very least, sex and length estimates could be useful to infer maturity of an animal (immature/mature).

4.4 VAST model suitability

VAST is a potentially powerful tool to incorporate into species distributional modelling, but given the large number of user defined features, sufficient time is required to setup and trial the model to achieve optimal outcomes. For some species, model convergence was not always achieved, particularly for species with limited data (e.g., *Scymnodon plunketi*). To maximise the sample sizes, all available trawl survey data were utilised. This incorporated trips from multiple vessels using different gear configurations, and, for the purposes of this work here, it was assumed that species catchability was equal (and may have influenced the multi-species analysis as described below); VAST also accounts for any differences in vessels with the 'OverdispersionConfig'. In some years, data availability was very low and, to achieve model convergence, some years were removed from the time series; for the research trawl series, 1982–1983 were not included in the models and for the observer data, years preceding 2012 were removed. Separating data by region offered higher resolution of patterns and possibly more consistent and comparable trends given routine sampling that has occurred on Chatham Rise and across the Sub-Antarctic since the 1990s. This type of analysis may be useful for the west coast South Island data in the future when a longer time series becomes available.

The multi-species analysis provided similar results to those of the single-species analysis and could be useful for data poor species. However, there is still a risk of overcompensating the distributions of well-known species on lesser known species. For example, for *E. granulosus* (one of the most represented species) the probability of encounter was found to be very high in waters off the Otago coast. In the multi-species analysis, this also became an area of high probability of encounter for most species, but such patterns were not highlighted in the single-species analysis, even for well-sampled species like *Deania calcea*.

When compared with other species distribution models (SDMs), VAST is not intended to identify environmental processes which best describe species distributions (Brodie et al. 2020). VAST is best used for examining trends of these processes over space and time. A number of studies have used SDMs to quantify the distributions of sharks; however, most of these studies have examined shallow water species (e.g., Sequeria et al. 2012, Klippel et al. 2016, Sguotti et al. 2016). In the central Mediterranean Sea, habitat suitability models were used to investigate the habitat preference of nine elasmobranch species including *Dalatias licha* in relation to five environmental predictors (depth, sea surface temperature, surface salinity, slope, and rugosity) (Lauria et al. 2015). This work found that depth, seafloor morphology (rugosity), and sea surface temperature were the primary drivers of elasmobranch habitat suitability; these variables were all included in the models here.

Depth was found to be the most important predictor of species distributions around New Zealand waters (Leathwick et al. 2006), and depth has been attributed to differences in deepwater shark assemblages in the Northeast Atlantic Ocean (O'Hea et al. 2020). Bottom temperature was also included in the models because it has been previously hypothesised that the Subtropical Front (STF), which runs along the

southern tip of the South Island, northward along the continental shelf break of the South Island and across the northern Chatham Rise, influences the distributions of some deepwater sharks (M.P. Francis, NIWA, unpublished data). Bottom temperature has been found to influence marine species found in deep, colder waters south of the STF where oxygen levels are low (Stephenson et al. 2020). Chlorophyll-a concentration was included as a proxy of productivity (Pinkerton et al. 2019) but appeared to have little effect on species distributions.

Although VAST presents insight into distribution and abundance trends, it does not increase our understanding of population structure or movement patterns of these species. At present, it is assumed that these species have one population within New Zealand waters. Population genetic studies have suggested both wide-scale intermixing of deepwater shark populations (*Centrophorus squamosus*, Veríssimo et al. 2012) and possible regionally structured populations (*Deania calcea*, Keggin 2017). The presence of all size and sex classes in one area, such as the Chatham Rise, may suggest that at least some of these species have regionally structured populations around New Zealand. In addition, any seasonal patterns of movement of these species is unlikely to be highlighted in such analyses, given that most research trawl sampling of these species occurs at the same time of year (December-January). A combination of comparative population genomics and long-term tagging is recommended to fully understand population structure and movement patterns of these species around New Zealand.

5. ACKNOWLEDGMENTS

We thank Fisheries New Zealand, Rich Ford (Fisheries New Zealand), and members of the Aquatic Environment Working Group for their reviews of the analyses and report. This report was reviewed by Matt Dunn (NIWA) and Marco Milardi (Fisheries New Zealand). This work was funded by Fisheries New Zealand project ENV2018-06.

6. REFERENCES

Anderson, O.F.: Bagley, N.W.; Hurst, R.J.; Francis, M.P.; Clark, M.R.; McMillan, P.J. (1998). Atlas of New Zealand fish and squid distributions from research bottom trawls. *NIWA Technical Report 42*. 303 p.

Bañón, R.; Piñeiro, C.; Casas, M. (2008). Biological observations on the gulper shark *Centrophorus granulosus* (Chondrichthyes: Centrophoridae) off the coast of Galicia (north-western Spain, eastern Atlantic). *Journal of the Marine Biological Association of the United Kingdom 88*: 411–414.

Bass, A.J.; D'Aubrey, J.D.; Kistnasamy, N. (1976). Sharks of the east coast of southern Africa VI. The family Oxynotidae, Squalidae, Dalatiidae and Echinorhinidae. *South African Association for Marine Biological Research Investigational Report of the Oceanographic Research Institute 45*: 1–103.

Beentjes, M.P.; Bull, B.; Hurst, R.J.; Bagley, N.W. (2002). Demersal fish assemblages along the continental shelf and upper slope of the east coast of the South Island, New Zealand. *New Zealand Journal of Marine and Freshwater Research 36*: 197–223.

Blackwell, R.G. (2010). Distribution and abundance of deepwater sharks in New Zealand waters, 2000–01 to 2005–06. *New Zealand Aquatic Environment and Biodiversity Report No. 57*. 51 p.

Brodie, S.J.; Thorson, J.T.; Carroll, G.; Hazen, E.L.; Bograd, S.; Haltuch, M.A.; Holsman, K.K.; Kotwicki, S.; Samhouri, J.F.; Willis-Norton, E.; Selden, R.L. (2020). Trade-offs in covariate selection for species distribution models: a methodological comparison. *Ecography 43*: 11–24.

Bull, B.; Livingston, M.E.; Hurst, R.; Bagley, N. (2001). Upper-slope fish communities on the Chatham Rise, New Zealand, 1992-1999. *New Zealand Journal of Marine and Freshwater Research 35*: 795–815.

Capapé, C.; Hemida, F.; Quignard, J-P.; Ben Amor, M.M.; Reynaud, C. (2008). Biological observations on a rare deep-sea shark, *Dalatias licha* (Chondrichthyes: Dalatiidae), off the Maghreb coast (south-western Mediterranean). *Pan-American Journal of Aquatic Sciences 3*: 355–360.

CARS2009. (2009). CSIRO Atlas of regional seas. www.cmar.csiro.au/cars.

Clark, M.R. (2009). Deep-sea seamount fisheries: A review of global status and future prospects. *Latin American Journal of Aquatic Research 37*: 501–512.

Clark, M.R.; Anderson, O.F.; Francis, R.I.C.C.; Tracey, D.M. (2000). The effects of commercial exploitation on orange roughy (*Hoplostethus atlanticus*) from the continental slope of the Chatham Rise, New Zealand, from 1979 to 1997. *Fisheries Research 45*: 217–238.

Clark, M.R.; King, K.J. (1989). Deepwater fish resources off the North Island, New Zealand: results of a trawl survey, May 1985 to June 1986. *New Zealand Fisheries Technical Report No. 11*. 56 p.

Clarke, M.W. (2001). Aspects of the biology of three exploited deepwater sharks *Centrophorus squamosus*, *Centroscymnus coelolepis* and *Deania calceus* (Elasmobranchii : Squalidae) from the continental slopes of the Rockall Trough and Porcupine Bank. *Cybium 25*: 395–396.

Clarke, M.W.; Connolly, P.L.; Bracken, J.J. (2001). Aspects of reproduction of the deep water sharks *Centroscymnus coelolepis* and *Centrophorus squamosus* from west of Ireland and Scotland. *Journal of the Marine Biological Association of the United Kingdom 81*: 1019–1029.

Clarke, M.W.; Connolly, P.L.; Bracken, J.J. (2002). Catch, discarding, age estimation, growth and maturity of the squalid shark *Deania calceus* west and north of Ireland. *Fisheries Research 56*: 139–153.

da Silva, H.M. (1988). Growth and reproduction of kitefin shark, *Dalatias licha* (Bonn, 1788) in Azorean waters. *ICES CM 1988/g:21, Copenhagen, No 15*. 16 p.

Daley, R.; Stevens, K.; Graham, K. (2002). Catch analysis and productivity of deepwater dogfish resource in southern Australia. *FRDC Project 1998/108*. 106 p.

Dunn, M.; Hurst, R.; Renwick, J.; Francis, C.; Devine, J.; McKenzie, A. (2009). Fish abundance and climate trends in New Zealand. *New Zealand Aquatic Environment and Biodiversity Report No. 31*. 75 p.

Dutilloy, A.; Dunn, M.R. (2020). Observations of sperm storage in some deep-sea elasmobranchs. *Deep Sea Research Part I: Oceanographic Research Papers 166*: 103405.

Fauconnet, L.; Pham, C.K.; Canha, A.; Afonso, P.; Diogo, H.; Machete, M.; Silva, H.M.; Vandeperre, F.; Morato, T. (2019). An overview of fisheries discards in the Azores. *Fisheries Research 209*: 230–241.

Fielding, A.H; Bell, J.F. (1997). A review of methods for the assessment of prediction errors in conservation presence/absence models. *Environmental Conservation 24*: 38–49.

Finucci, B.; Anderson, O.F.; Edwards, C.T.T. (2020). Non-target fish and invertebrate catch and discards in New Zealand ling longline fisheries from 2002–03 to 2017–18. *New Zealand Aquatic Environment and Biodiversity Report No. 241*. 83 p.

Finucci, B.; Duffy, C.A.; Francis, M.P.; Gibson, C.; Kyne, P.M. (2019). The extinction risk of New Zealand chondrichthyans. *Aquatic Conservation: Marine and Freshwater Ecosystems 29*: 783–797.

Finucci, B.; Dunn, M.R.; Jones, E.G. (2018). Aggregations and associations in deep-sea chondrichthyans. *ICES Journal of Marine Science 75*: 1613–1626.

Fisheries New Zealand (2019). Fisheries Assessment Plenary, May 2019: stock assessments and stock status. Compiled by the Fisheries Science and Information Group, Fisheries New Zealand, Wellington, New Zealand. 1641 p.

Ford, R.B.; Francis, M.P.; Holland, L.; Clark, M.R.; Duffy, C.A.J.; Dunn, M.R.; Jones, E.; Wells, R. (2018). Qualitative (Level 1) risk assessment of the impact of commercial fishing on New Zealand chondrichthyans: an update for 2017. *New Zealand Aquatic Environment and Biodiversity Report No. 201*. 103 p.

Ford, R.B.; Galland, A.; Clark, M.R.; Crozier, P.; Duffy, C.A.J.; Dunn, M.; Francis, M.P.; Wells, R. (2015). Qualitative (level 1) risk assessment of the impact of commercial fishing on New Zealand chondrichthyans. *New Zealand Aquatic Environment and Biodiversity Report No. 157*. 111 p.

Francis, M.P.; Hurst, R.J.; McArdle, B.H.; Bagley, N.W.; Anderson, O.F. (2002). New Zealand demersal fish assemblages. *Environmental Biology of Fishes 65*: 215–234.

Francis, M.P.; Jones, E.G.; Maolagáin, C.Ó.; Lyon, W.S. (2018). Growth and reproduction of four deepwater sharks in New Zealand waters. *New Zealand Aquatic Environment and Biodiversity Report No. 196*. 55 p.

Francis, M.P.; Roberts, J.; MacGibbon, D,J. (2016). Indicator based analysis on the status of eight shark and chimaera species in New Zealand waters. *New Zealand Fisheries Assessment Report 2016/65*. 87 p.

Fu, D.; Roux, M.-J.; Clarke, S.; Francis, M.; Dunn, A.; Hoyle, S.; Edwards, C. (2016). Pacific-wide sustainability risk assessment of bigeye thresher shark (*Alopias superciliosus*). Prepared for Western and Central Pacific Fisheries Commission. (Unpublished NIWA Client Report 2016089WN, for project WCP16301 NIWA, Wellington, April 2018.) 102 p.

García de la Rosa, S.B.; Sánchez, M.F.; Prenski, L.B.; Sánchez, R.P. (2004). Caracterización biológica y estado de explotación del tiburon espinoso (*Squalus acanthias*) biological characterization and exploitation state. *In*: Boschi, E.E. (ed.), *El Mar Argentino y sus Recursos Pesquero*. INIDEP No. 1294.

Garrick, J.A.F. (1960). Studies on New Zealand elasmobranchii. Part XI. Squaloids of the genera *Deania*, *Etmopterus*, *Oxynotus* and *Dalatias* in New Zealand waters. *Transactions of the Royal Society of New Zealand 88*: 489–517.

Girard, M.; Du Buit, M.H. (1999). Reproductive biology of two deep-water sharks from the British Isles, *Centroscymnus coelolepis* and *Centrophorus squamosus* (Chondrichthyes: Squalidae). *Journal of the Marine Biological Association of the United Kingdom 79*: 923–931.

Griffiths, S.P.; Kesner-Reyes; Garilao, K.; Duffy, C.V.; Roman, M. (2018). Development of a flexible ecological risk assessment (ERA) approach for quantifying the cumulative impacts of fisheries on bycatch species in the eastern Pacific Ocean. *IATTC Document SAC-09-12*.

Guttridge, T.L.; Gruber, S.H.; Franks, B.R.; Kessel, S.T.; Gledhill, K.S.; Uphill, J.; Krause, J.; Sims, D.W. (2012). Deep danger: intra-specific predation risk influences habitat use and aggregation formation of juvenile lemon sharks *Negaprion brevirostris*. *Marine Ecology Progress Series 445*: 279–291.

Hastie, T.; Tibshirani, R. (1990). *Generalized Additive Models*. London: Chapman and Hall.

Henderson, A.C.; Flannery, K.; Dunne, J, (2003). Biological observations on shark species taken in commercial fisheries to the west of Ireland. *Biology and Environment: proceedings of the Royal Irish Academy 103B*: 1–7.

Holt, R.E.; Foggo, A.; Neat, F.C.; Howell, K.L. (2013). Distribution patterns and sexual segregation in chimaeras: implications for conservation and management. *ICES Journal of Marine Science 70*: 1198–1205.

Hoyle, S.D.; Semba, Y.; Kai, M.; Okamoto, H. (2017). Development of Southern Hemisphere porbeagle shark stock abundance indicators using Japanese commercial and survey data. *New Zealand Fisheries Assessment Report 2017/07*. [WCPFC Scientific Committee 13th regular session WCPFC-SC13- SA-IP-15.] 64 p.

ICES-WGEF (2018). Report of the ICES Working Group on Elasmobranch Fishes (WGEF). *ICES CM 2018/ACOM:16*. International Council for the Exploration of the Seas, Copenhagen, Denmark.

Irvine, S.B.; Daley, R.K.; Graham, K.J.; Stevens, J.D. (2012). Biological vulnerability of two exploited sharks of the genus *Deania* (Centrophoridae). *Journal of Fish Biology 80*: 1181–1206.

Keggin, T. (2017). Population genomics of two deep sea sharks: *Centroselachus crepidater* and *Deania calcea*. (Doctoral dissertation, Durham University.)

Klippel, S.; Amaral, S.; Vinhas, L. (2016). Development and evaluation of species distribution models for five endangered elasmobranchs in southwestern Atlantic. *Hydrobiologia 779*: 11–33.

Lauria, V.; Gristina, M.; Attrill, M.J.; Fiorentino, F.; Garofalo, G. (2015). Predictive habitat suitability models to aid conservation of elasmobranch diversity in the central Mediterranean Sea. *Scientific Reports 5*: 13245.

Leathwick, J.R.; Elith, J.; Francis, M.P.; Hastie, T.; Taylor, P. (2006). Variation in demersal fish species richness in the oceans surrounding New Zealand: an analysis using boosted regression trees. *Marine Ecology Progress Series 321*: 267–281.

Leathwick J.R.; Rowden A.; Nodder S.; Gorman R.; Barsley S.; Pinkerton M.; Baird S.J.; Hadfield M.; Currie, K.; Goh, A. (2012). A Benthic-optimised Marine Environment Classification (BOMEC) for New Zealand waters. *New Zealand Aquatic Environment and Biodiversity Report No. 88.* 54 p.

McMillan, P.J.; Francis, M.P.; James, G.D.; Paul, L.J.; Marriott, P.; Mackay, E.; Wood, B.A.; Stevens, D.W.; Griggs, L.H.; Baird, S.J.; Roberts, C.D.; Stewart, A.L.; Struthers, C.D.; Robbins, J.E. (2019). New Zealand fishes. A field guide to common species caught by bottom, midwater, and surface fishing. *New Zealand Aquatic Environment and Biodiversity Report No. 208*. 295 p.

Mitchell, J.S.; Mackay, K.A.; Neil, H.L.; Mackay, E.J.; Pallentin, A.; Notman P. (2012). Undersea New Zealand, 1:5,000,000. *NIWA Chart, Miscellaneous Series No. 92*.

Moore, D.M.; Neat, F.C.; McCarthy, I.D. (2013). Population biology and ageing of the deep water sharks *Galeus melastomus*, *Centroselachus crepidater* and *Apristurus aphyodes* from the Rockall Trough, north-east Atlantic. *Journal of the Marine Biological Association of the United Kingdom 93*: 1941–1950.

Moura, T.; Figueiredo, I.; Neves, A.; Farias, I.; Serra-Pereira, B.; Gordo, L.S. (2008). First occurrence of the deepwater shark *Centroscymnus owstonii* on the Portuguese continental slope. *Cybium 32*: 271–272.

Moura, T.; Jones, E.; Clarke, W.W.; Cotton, C.F.; Crozier, P. et al. (2014). Large-scale distribution of three deep-water squaloid sharks: Integrating data on sex, maturity, and environment. *Fisheries Research 157*: 47–61.

Mucientes, G.R.; Queiroz, N.; Sousa, L.L.; Tarroso, P.; Sims, D.W. (2009). Sexual segregation of pelagic sharks and the potential threat from fisheries. *Biology Letters 5*: 156–159.

NASA Goddard Space Flight Center; Ocean Ecology Laboratory; Ocean Biology Processing Group (2018a). SeaWiFS Ocean Color Reprocessing 2018.0 https://oceancolor.gsfc.nasa.gov/reprocessing/r2018/seawifs/ (Accessed May 2018).

NASA Goddard Space Flight Center; Ocean Ecology Laboratory; Ocean Biology Processing Group (2018b). MODIS/Aqua Ocean Color Reprocessing 2018.0 https://oceancolor.gsfc.nasa.gov/reprocessing/r2018/aqua/ (Accessed May 2018).

Neat, F.C.; Burns, F.; Jones, E.; Blasdale, T. (2015). The diversity, distribution and status of deep-water elasmobranchs in the Rockall Trough, north-east Atlantic Ocean. *Journal of Fish Biology 87*: 1469–1488.

O'Hea, B.; Davie, S.; Johnston, G.; O'Dowd, L. (2020). Assemblages of deepwater shark species along the North East Atlantic Continental Slope. *Deep Sea Research Part I: Oceanographic Research Papers 157*: 103207.

O'Hea, B.; Johnston, G.; Gerritsen, H.D.; Leahy, Y.; Mohn, C.; Wall, D. (2008). Deepwater Survey 2008 Preliminary Report. Marine Institute, Fisheries Science Services.

Parker, S.J.; Francis, M. (2012). Productivity of two species of deepwater sharks, *Deania calcea* and *Centrophorus squamosus* in New Zealand. *New Zealand Aquatic Environment and Biodiversity Report No. 103.* 44 p.

Pascual-Alayon, P.J.; Hernandez, C.; Hidalgo, M.; Puerto, M.A. (2017). Deep Chondrichthyes in Mauritanian waters. *In*: Ramos, A.; Ramil, F.; Sanz, J.L. (eds), pp. 201–240, *Deep-Sea ecosystems off Mauritania: Research of marine Biodiversity and Habitats in the Northwest African Margin*. Netherlands, Springer.

Pinkerton, M. (2016). Ocean colour satellite observations of phytoplankton in the New Zealand EEZ, 1997–2016. (Unpublished NIWA Client Report WLG2016-19 prepared for the Ministry for the Environment, New Zealand.)

Pinkerton, M.H.; Sutton, P.J.H.; Wood, S. (2019). Satellite indicators of phytoplankton and ocean surface temperature for New Zealand. (Unpublished NIWA Client Report 2018180WNrev1 prepared for the Ministry for the Environment, New Zealand.)

Pratt, H.L. Jr; Carrier, J.C. (2001). A review of elasmobranch reproductive behavior with a case study on the nurse shark, *Ginglymostoma cirratum*. *Environmental Biology of Fishes 60*: 157–188.

R Core Team (2018). R: A language and environment for statistical computing. *R Foundation for Statistical Computing*, Vienna, Austria. https://www.R-project.org/.

Reynolds, R.W.; Rayner, N.A.; Smith, T.M.; Stokes, D.C.; Wang, W. (2002). An improved in situ and satellite SST analysis for climate. *Journal of Climate 15*: 1609–1625.

Ridgway K.R.; Dunn, J.R; Wilkin, J.L. (2002). Ocean interpolation by four-dimensional least squares -Application to the waters around Australia. *Journal of Atmospheric and Oceanic Technology 19*: 1357–1375.

Roberts, C.; Stewart, A.L.; Struthers, C.D. (eds.). (2015). *The Fishes of New Zealand*. Wellington: Te Papa Press.

Rodríguez-Cabello, C.; González-Pola, C.; Sánchez, F. (2016). Migration and diving behavior of *Centrophorus squamosus* in the NE Atlantic. Combining electronic tagging and Argo hydrography to infer deep ocean trajectories. *Deep Sea Research Part I: Oceanographic Research Papers 115*: 48–62.

Rodríguez-Cabello, C.; Sánchez, F. (2014). Is *Centrophorus squamosus* a highly migratory deep-water shark? *Deep Sea Research Part I Oceanographic Research Papers 92*: 1–10.

Sequeira, A.; Mellin, C.; Rowat, D.; Meekan, M.G.; Bradshaw, C.J. (2012). Ocean-scale prediction of whale shark distribution. *Diversity and Distributions 18*: 504–518.

Severino, R.B.; Afonso-Dias, I.; Delgado, J.; Afonso-Dias, M. (2009). Aspects of the biology of the leaf-scale gulper shark *Centrophorus squamosus* (Bonnaterre, 1788) off Madeira archipelago. *Life and Marine Sciences 26*: 57–61.

Sguotti, C.; Lynam, C.P.; García-Carreras, B.; Ellis, J.R.; Engelhard, G.H. (2016). Distribution of skates and sharks in the North Sea: 112 years of change. *Global Change Biology 22*: 2729–2743.

Simpfendorfer, C.A.; Kyne, P.M. (2009). Limited potential to recover from overfishing raises concerns for deep-sea sharks, rays and chimaeras. *Environmental Conservation 36*: 97–103.

Stephenson, F.; Leathwick, J.R.; Francis, M.P.; Lundquist, C.J. (2020). A New Zealand demersal fish classification using gradient forest models. *New Zealand Journal of Marine and Freshwater Research 54*: 60–85.

Stephenson, F.; Leathwick, J.R.; Geange, S.W.; Bulmer, R.H.; Hewitt, J.E.; Anderson, O.F.; Rowden, A.A.; Lundquist, C.J. (2018). Using gradient forests to summarize patterns in species turnover across large spatial scales and inform conservation planning. *Diversity and Distributions 24*: 1641–656.

Thorson, J.T.; Barnett, L.A.K. (2017). Comparing estimates of abundance trends and distribution shifts using single- and multispecies models of fishes and biogenic habitat. *ICES Journal of Marine Science 75*: 1311–1321.

Thorson, J.T. (2019). Guidance for decisions using the Vector Autoregressive Spatio-Temporal (VAST) package in stock, ecosystem, habitat and climate assessments. *Fisheries Research 210*: 143–161.

Tracey, D.; Shearer, P. (2002). An identification guide for deepwater shark species. 16 p. NIWA. (Unpublished report held by NIWA library, Wellington.)

Tracey, D.M.; Bull, B.; Clark, M.R.; Mackay, K. (2004). Fish species composition on seamounts and adjacent slope in New Zealand waters. *New Zealand Journal of Marine and Freshwater Research 38*: 163–182.

Tracey, D.M.; Clark, M.R.; Anderson, O.F.; Kim, S.W. (2012). Deep-sea fish distribution varies between seamounts: results from a seamount complex off New Zealand. *PLoS ONE* 7: 1–12.

Veríssimo, A.; McDowell, J.R.; Graves, J.E. (2012). Genetic population structure and connectivity in a commercially exploited and wide-ranging deepwater shark, the leafscale gulper (*Centrophorus squamosus*). *Marine and Freshwater Research 63*: 505–512.

Walker, T.I. Gason, A.S. 2007. Shark and other chondrichthyan byproduct and bycatch estimation in the Southern and Eastern Scalefish and Shark Fishery. *Final report to Fisheries and Research Development Corporation Project No. 2001/007*. 182 p.

Wetherbee, B.M. (1996). Distribution and reproduction of the southern lantern shark from New Zealand. *Journal of Fish Biology 49:* 1186–1196.

Wetherbee, B.M. (2000). Assemblage of deep-sea sharks on Chatham Rise, New Zealand. *Fishery Bulletin 98:* 189–198.

Wood, S.N. (2006). Low-rank scale-invariant tensor product smooths for generalized additive mixed models. *Biometrics 62*: 1025–1036.

Yano, K.; Tanaka, S. (1988). Size at maturity, reproductive cycle, fecundity and depth segregation of the deep sea squaloid sharks *Centroscymnus owstonii* and *C. coelolepis* in Surga Bay, Japan. *Nippon Suisan Gakkaishi 54*: 167–174.

Zhou, S.; Smith, A.D.M.; Fuller, M. (2011). Quantitative ecological risk assessment for fishing effects on diverse data-poor non-target species in a multi-sector and multi-gear fishery. *Fisheries Research 112*: 168–178.

Appendix 1: Macroscopic Staging Key

Current NIWA macroscopic staging key for sharks and rays

Stage	Stage method	Name	Males	Females
1	SS	Immature	Claspers shorter than pelvic fins, soft and uncalcified, unable or difficult to splay open	Ovaries small and undeveloped. Oocytes not visible, or small (pin-head sized) and translucent whitish
2	SS	Maturing	Claspers longer than pelvic fins, soft and uncalcified, unable or difficult to splay open or rotate forwards	Some oocytes enlarged, up to about pea-sized or larger, and white to cream.
3	SS	Mature	Claspers longer than pelvic fins, hard and calcified, able to splay open and rotate forwards to expose clasper spine	Some oocytes large (greater than pea-sized) and yolky (bright yellow)
4	SS	Gravid I	*Not applicable*	Uteri contain eggs or egg cases but no embryos are visible
5	SS	Gravid II	*Not applicable*	Uteri contain visible embryos. *Not applicable to egg laying sharks and skates.*
6	SS	Post-partum	*Not applicable*	Uteri flaccid and vascularised indicating recent birth

Appendix 2: VAST Model Inputs

Spatial domain

The number of knots used in the models was *n_x* = 100.

Number of spatial and spatio-temporal factors

The number of spatial and spatio-temporal factors used for each component were defined via input:

FieldConfig = c("Omega1"=0, "Epsilon1"=0, "Omega2"=0, "Epsilon2"=0)

where FieldConfig[1] controls $n_{\omega 1}$, FieldConfig[2] controls $n_{\varepsilon 1}$, FieldConfig[3] controls $n_{\omega 2}$, and FieldConfig[4] controls $n_{\varepsilon 2}$, and a value of zero "turns off" that component of spatial or spatio-temporal covariation.

The following configurations were used:

- Single species occurrence (both time series): FieldConfig = c("Omega1"=1, "Epsilon1"=0, "Omega2"=1, "Epsilon2"=0)
- Single species occurrence with temporal interaction (1982 time series): FieldConfig = c("Omega1"=1, "Epsilon1"=1, "Omega2"=1, "Epsilon2"=1)
- Multi-species or multi-stage (1997 time series): FieldConfig = c("Omega1"=3, "Epsilon1"=0, "Omega2"=3, "Epsilon2"=0)

Structure on parameters among years:

The structure for intercepts or spatio-temporal variation across time was specified using input:

RhoConfig = c("Beta1"=0, "Beta2"=0, "Epsilon1"=0, "Epsilon2"=0)

By default (when RhoConfig[1]=0 and RhoConfig[2]=0), the model specifies that each intercept $\beta_1(t)$ and $\beta_2(t)$ is a fixed effect. By default (when RhoConfig[3]=0 and RhoConfig[4]=0), the model specifies that each spatio-temporal random effect $\varepsilon_1(s,f,t)$ and $\varepsilon_2(s,f,t)$ is independent among years. Here, the intercepts were defined as fixed effects and spatio-temporal random effects were independent among years.

Number of overdispersion factors

The number of catchability factors used for each component was defined via input:

OverdispersionConfig = c("Eta1"=0, "Eta2"=0)

where OverdispersionConfig[1] controls $n_{\delta 1}$, and OverdispersionConfig[2] controls $n_{\delta 2}$, and a value of zero again "turns off" that component of random covariation in catchability. Catchability factors remained "off".

Link functions and observation error distributions

The observation error distribution and the link-functions used to calculate expected encounter probabilities and positive catch rates were based on the two linear predictors via input:

ObsModel = c("PosDist"=0, "Link"=0)

The ObsModel vector has two components, where first column specifies the distribution for positive catch rates, and second element specifies the functional form for encounter probabilities. Here, the default configuration trialled was

$$\text{ObsModel} = c(1,0)$$

where ObsModel[1] indicates the distribution for the positive catch rates was lognormal and ObsModel[2] was the conventional delta-model using log-link for encounter probability. However, in most cases, it was found that species data had either 0% or 100% encounters in one or more years, and thus, the intercept for that year went to +/-Inf and the model would not converge. In this instance, the ObsModel vector was set to ObsModel=c(1,3), where ObsModel[2] indicated VAST should check for species-years combination with 100% encounter rates and when applicable, the intercept for encounter probability in that year was fixed to an extremely high value such that predicted encounter rates are near 100% for that year (Thorson & Barnett 2017).

Where ObsModel = c(1,0) did not converge and there was no indication of 0% or 100% encounters, a third variation of the ObsModel was trialled, and was often applicable to the multi-species analysis, ObsModel=c(2,1), fitting the positive catch rates to a gamma distribution and employing an alternative "Poisson-link delta-model" using log-link for numbers-density and log-link for biomass per number. Despite this, some models still did not converge. Model inputs and AIC values are shown in Table 11.

Table 11: Inputs for each VAST model run for each area (Economic Exclusive Zone, EEZ; Chatham Rise, CR; Sub-Antarctic, SUBA; North Island, NI), time series (19822018, 19972018), data series (research trawl survey, RT; observer data, OBS); population section (all sizes and sexes, ALL; by sex and maturity stage, MS; by sex and maturity stage and season, MSS)

Area	Date	Data	Temp-Int?	Pop	Model Specifications	*Dalatias licha*	*Centrophorus squamosus*	*Centroscymnus owstonii*	*Centroselachus crepidater*	*Etmopterus granulosus*	*Scymnodon plunketi*	*Deania calcea*
EEZ	1982	RT	N	All	AIC	17 205.2	NA	26 046.7	38 770.1	48 893.5	12 151.8	52 660.4
					ObsMod	1,3	NA	1,3	1,3	1,3	1,3	1,3
	1982	RT	Y	All	AIC	17 067.8	NA	25 839.0	38 451.9	48 152.7	NA	52 378.5
					ObsMod	1,3	NA	1,3	1,3	1,3	NA	1,3
CR	1982	RT	N	All	AIC	9 091.1	NA	13 159.6	22 688.0	30 241.9	6 398.7	31 937.2
					ObsMod	1,3	NA	1,3	1,3	1,3	1,3	1,3
	1982	RT	Y	All	AIC	8 979.3	NA	12 934.7	22 481.4	29 848.7	6 235.7	31 682.0
					ObsMod	2,1	NA	2,1	2,1	1,0	2,1	1,0
	1997	RT	N	All	AIC	5 208.0	5590.3	6 446.5	10 080.5	13 421.1	NA	15 407.0
					ObsMod	1,3	1,3	1,3	1,3	1,3	NA	1,3
	1997	RT	N	MS	AIC	1 986.5	NA	4 889.5	12 630.0	17 389.6	NA	18 751.4
					ObsMod	1,0	NA	1,3	2,1	2,1	NA	1,1
	1997	OBS	N	All	AIC	13 025.3	8 016.6	1 901.3	10 043.3	27 923.5	5 109.8	27 869.9
					ObsMod	1,3	2,1	1,3	2,1	1,3	2,1	2,1
SUBA	1982	RT	N	All	AIC	NA	5 454.7	NA	NA	9 900.0	NA	5 282.3
					ObsMod	NA	1,3	NA	NA	1,3	NA	1,3
	1982	RT	Y	All	AIC	NA	5 392.1	NA	NA	9 791.3	NA	5 286.9
					ObsMod	NA	1,3	NA	NA	1,0	NA	1,0
	1997	RT	N	All	AIC	NA	2 989.9	1 304.5	3 652.1	5 304.2	1273.2	2 885.8
					ObsMod	NA	1,3	1,3	1,3	1,0	1,0	1,3
	1997	RT	N	MS	AIC	NA	2 076.6	NA	3 867.3	6 845.1	NA	3 479.6
					ObsMod	NA	2,1	NA	2,1	2,1	NA	2,1
	1997	OBS	N	All	AIC	NA	3 872.3	NA	NA	4 357.1	NA	2 563.9
					ObsMod	NA	2,1	NA	NA	2,1	NA	1,,0
NI	All	RT	N	All	AIC	630.0	6 62.9	1 185.9	823.1	NA	NA	2 425.1
					ObsMod	1,3	1,1	1,3	1,3	NA	NA	1,3
	All	RT	Y	MS	AIC							3 591.9
					ObsMod							1,3
	All	RT	Y	MSS	AIC							2 445.5
					ObsMod							2,1
					All species combined							
MULTI	1982	RT	N	All	AIC	23 198.4						
					ObsMod	1,3						
	1982	RT	Y	All	AIC	23 318.4						
					ObsMod	2,1						

Appendix 3: Generalised Linear Model (GAM) outputs

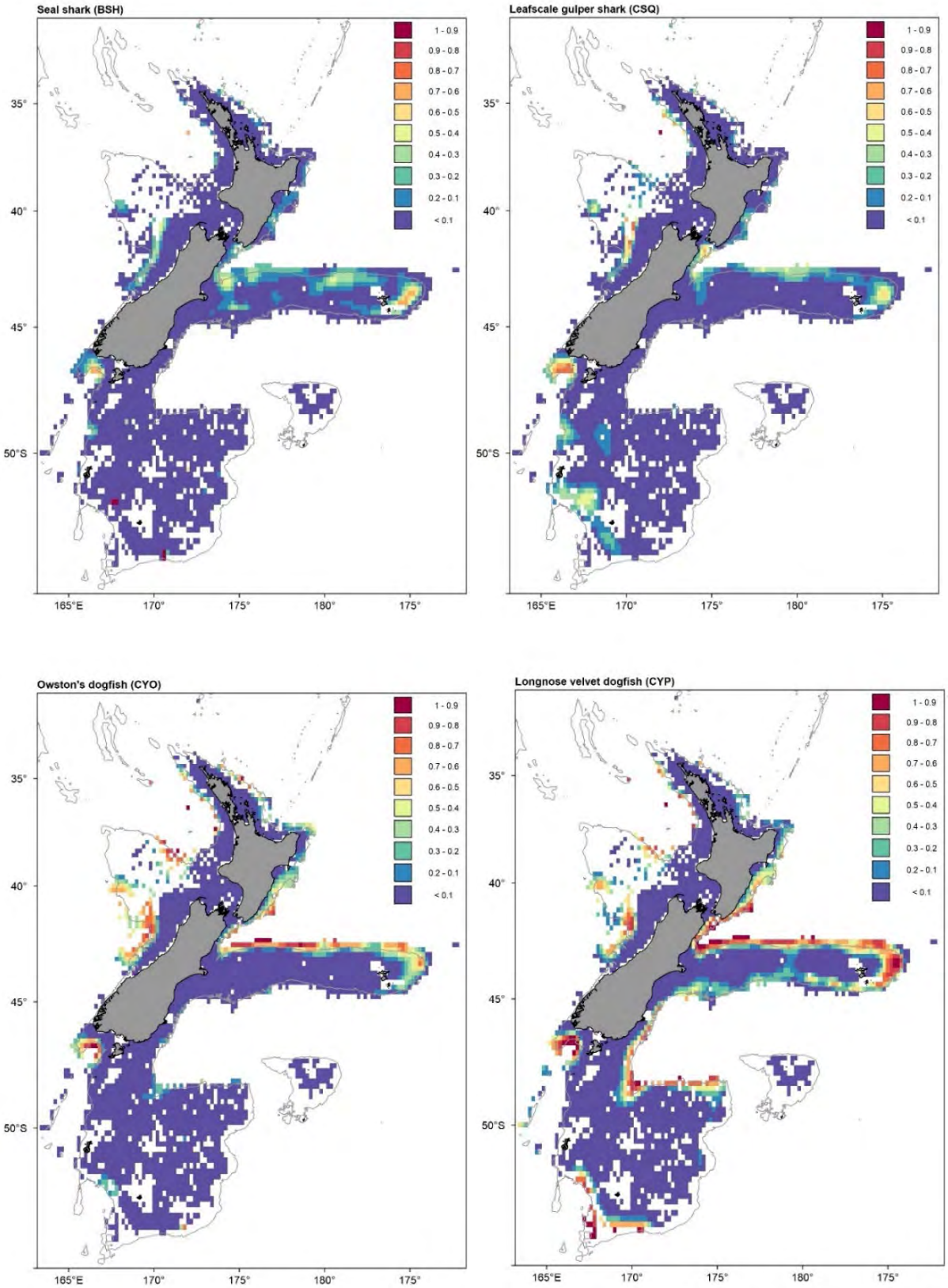

Figure 56: Map of the probability of occurrence for *Dalatias licha* (BSH), *Centrophorus squamosus* (CSQ), *Centroscymnus owstonii* (CYO), and *Centroselachus crepidater* (CYP) created by a Generalised Additive Model (GAM).

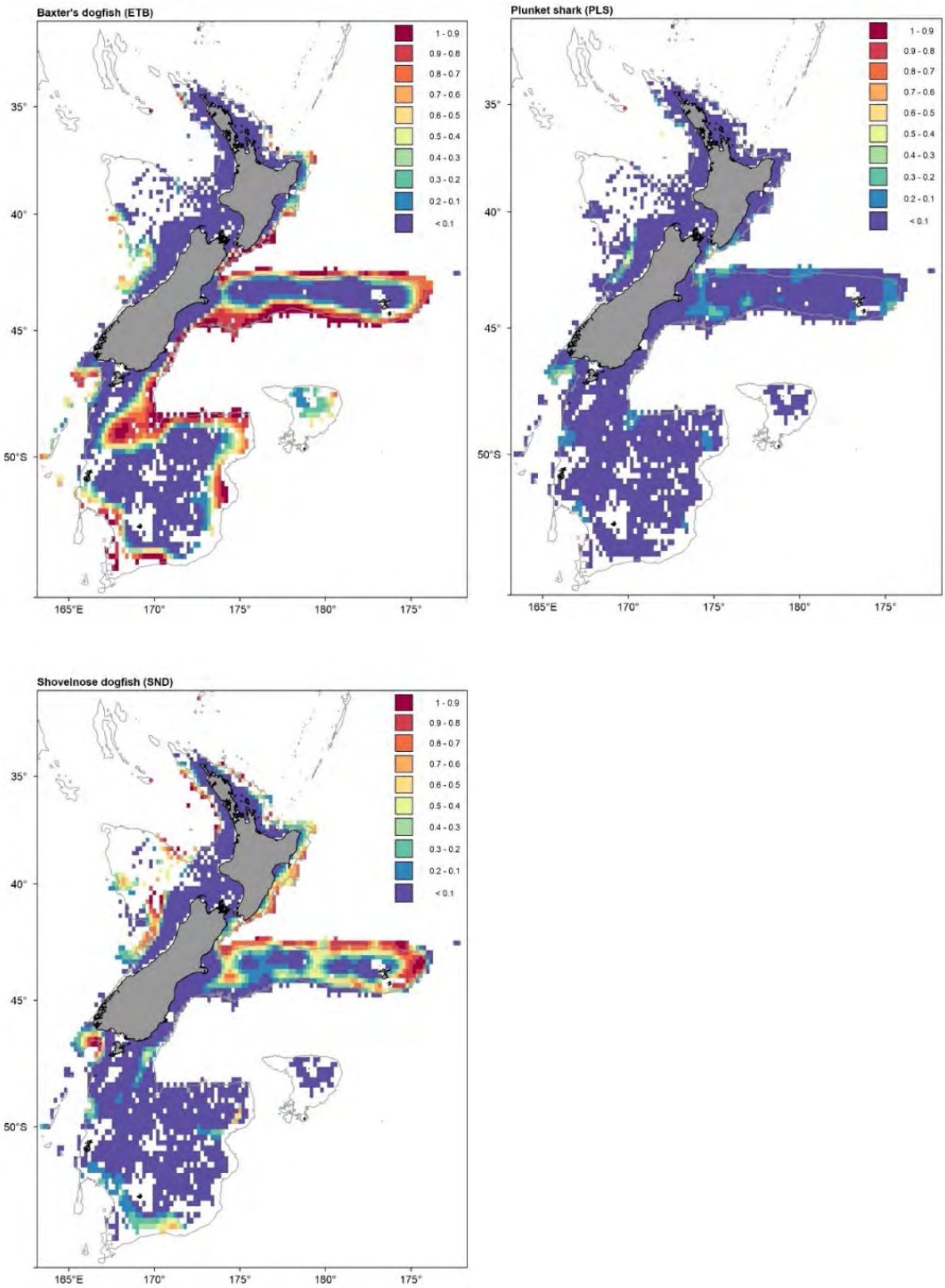

Figure 57: Map of the probability of occurrence for *Etmopterus granulosus* (ETB), *Scymnodon plunketi* (PLS), and *Deania calcea* (SND) created by a Generalised Additive Model (GAM).

Appendix 4: Multi-Species Analysis (2010–2018)

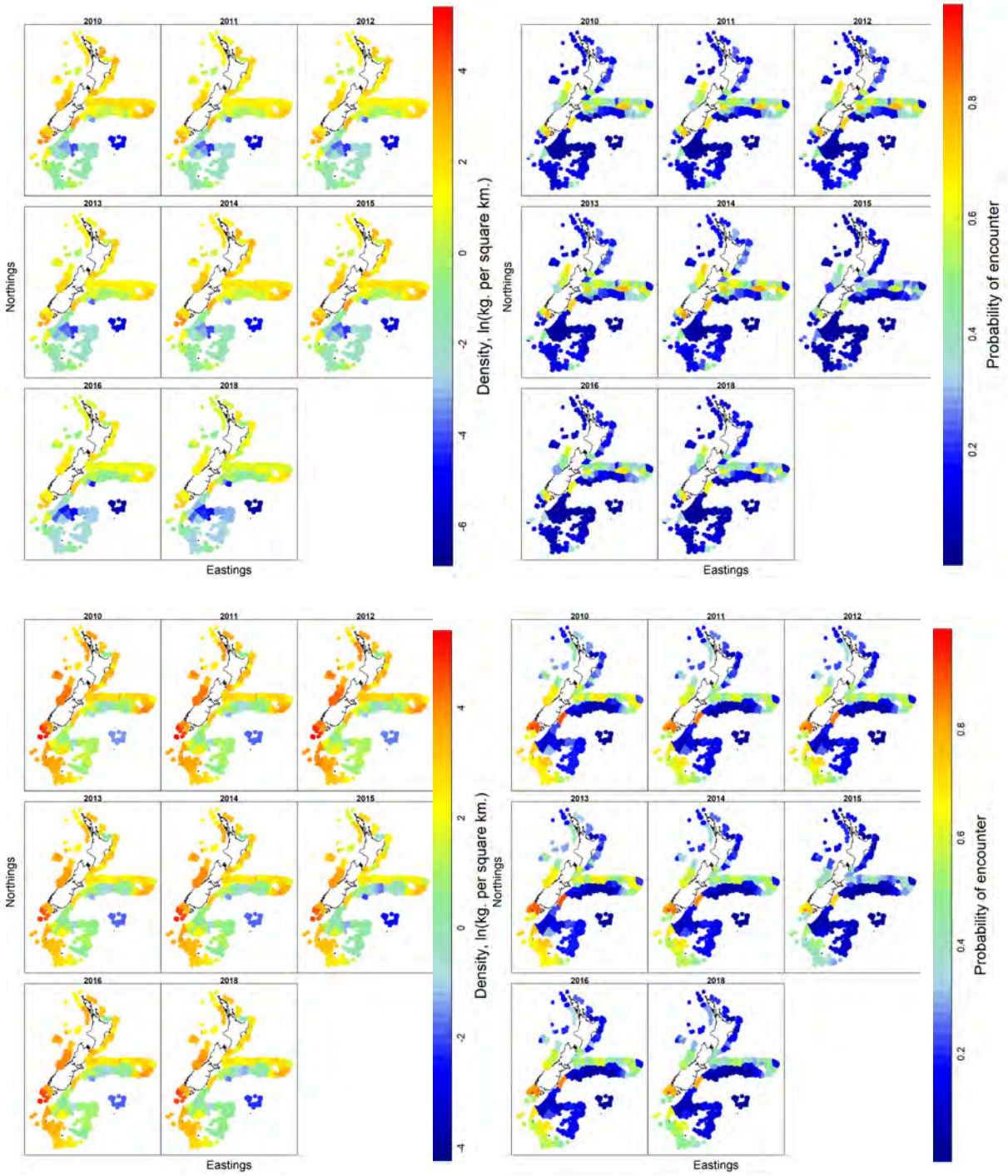

Figure 58: VAST multi-species outputs for relative density (kg km^{-2}) and probability of encounter for *Dalatias licha* (top) and *Centrophorus squamosus* (bottom) across the New Zealand Exclusive Economic Zone (EEZ).

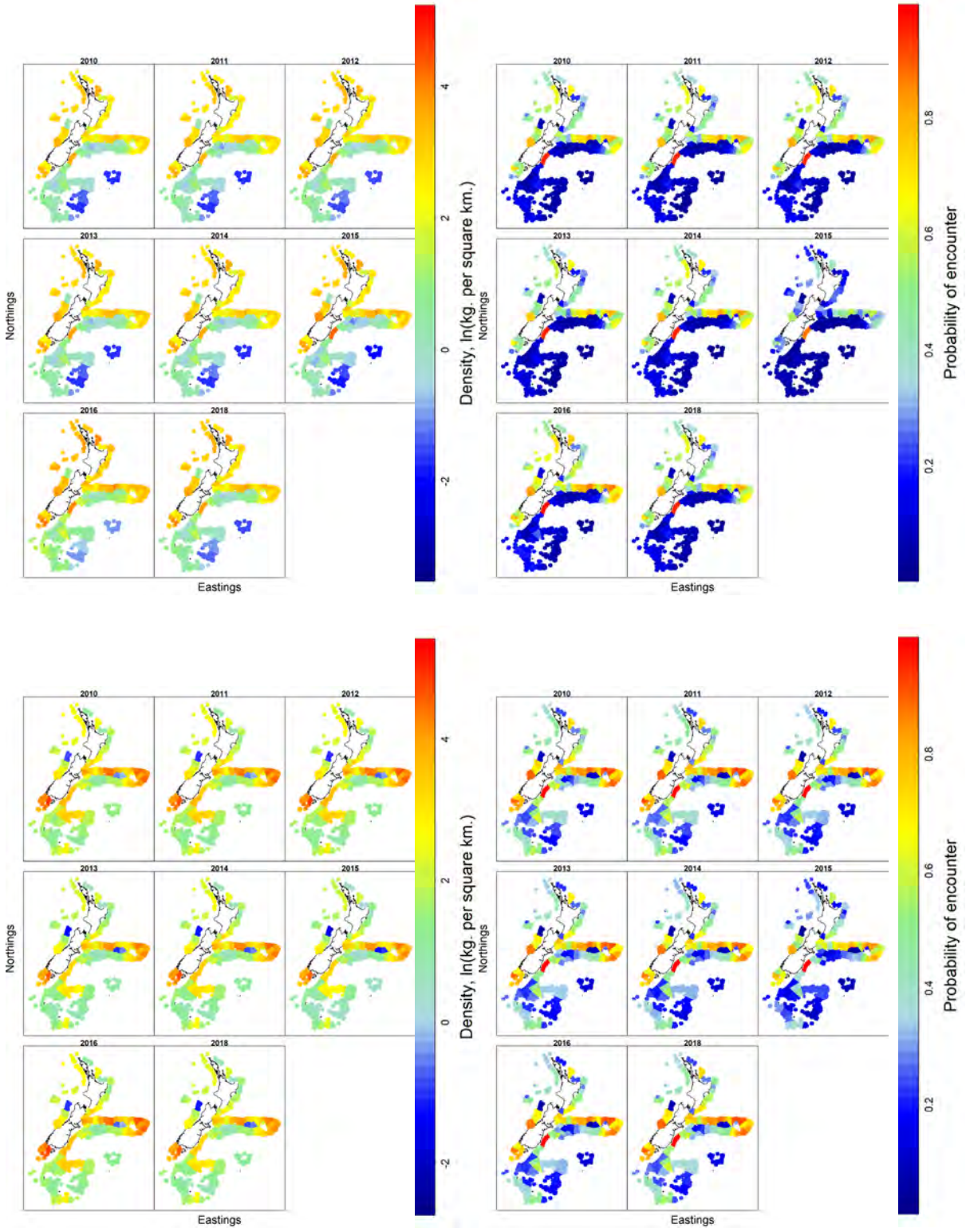

Figure 59: VAST multi-species outputs for relative density (kg km^{-2}) and probability of encounter for *Centroscymnus owstonii* (top) and *Centroselachus crepidater* (bottom) across the New Zealand Exclusive Economic Zone (EEZ).

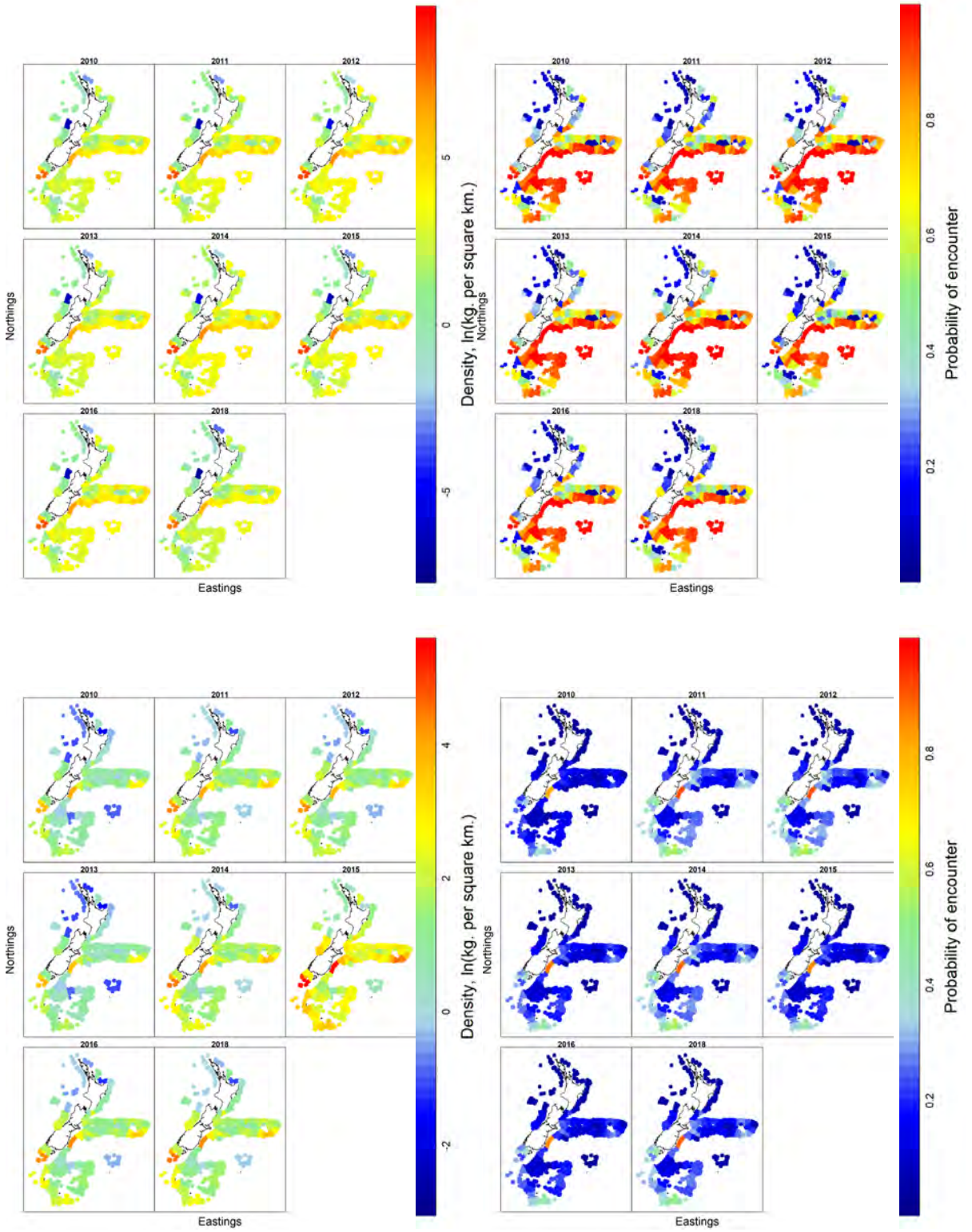

Figure 60: VAST multi-species outputs for relative density (kg km^{-2}) and probability of encounter for *Etmopterus granulosus* (top) and *Scymnodon plunketi* (bottom) across the New Zealand Exclusive Economic Zone (EEZ).

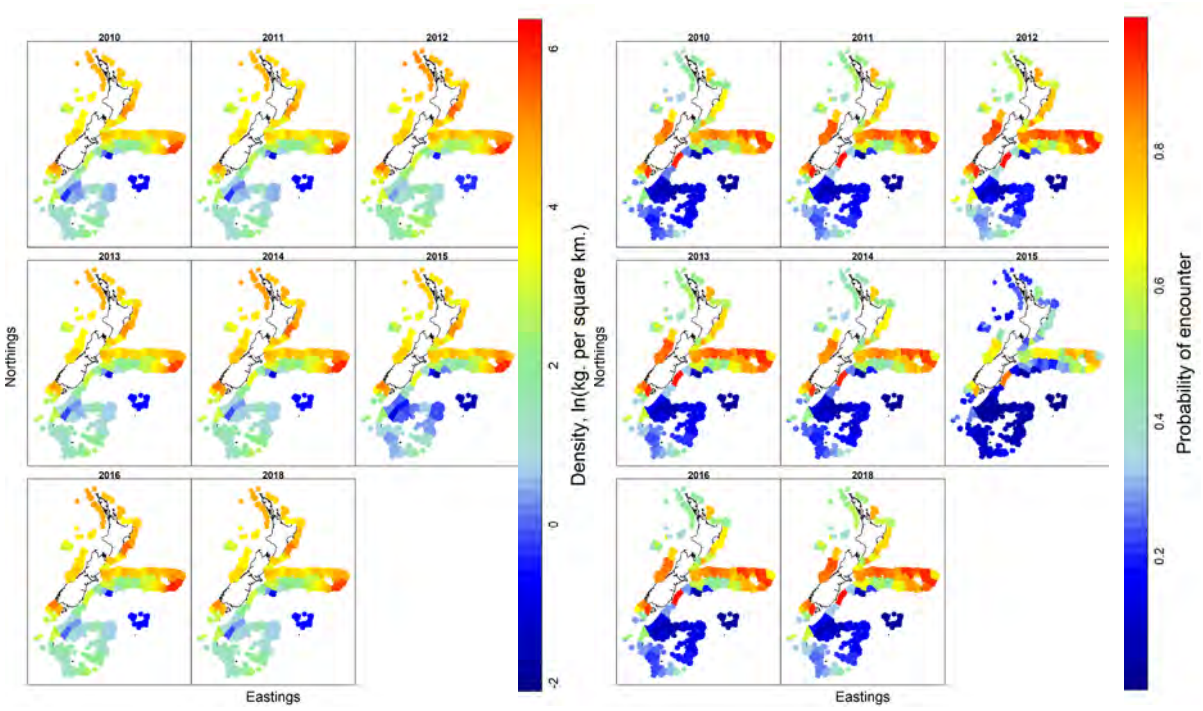

Figure 61: VAST multi-species outputs for relative density (kg km^{-2}) and probability of encounter for *Deania calcea* across the New Zealand Exclusive Economic Zone (EEZ).

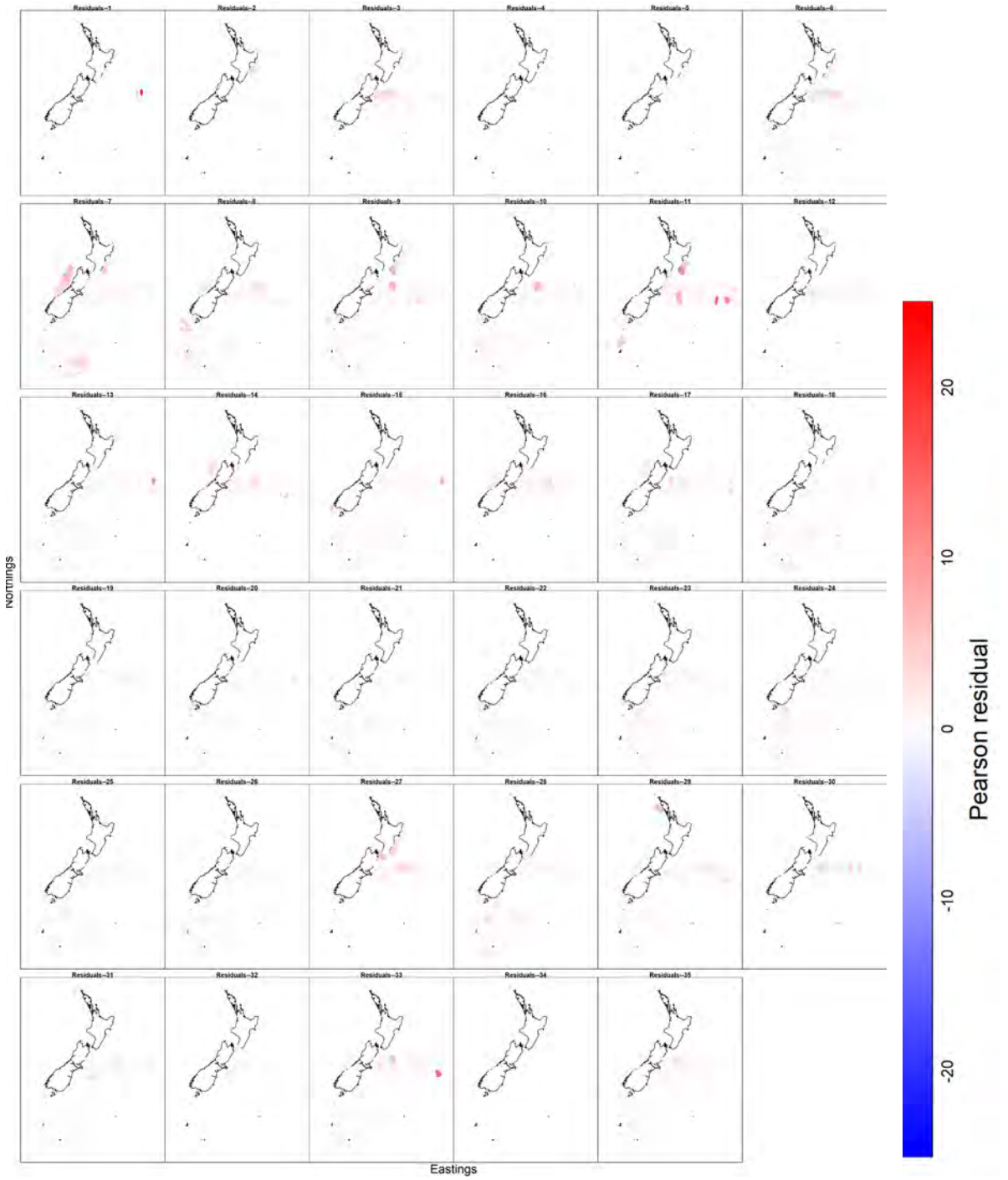

Figure 62: VAST outputs for Pearson residuals (goodness of fit) showing under or over fitting for catch rates of all species combined across the New Zealand Exclusive Economic Zone (EEZ).

Appendix 5: *Dalatias licha*

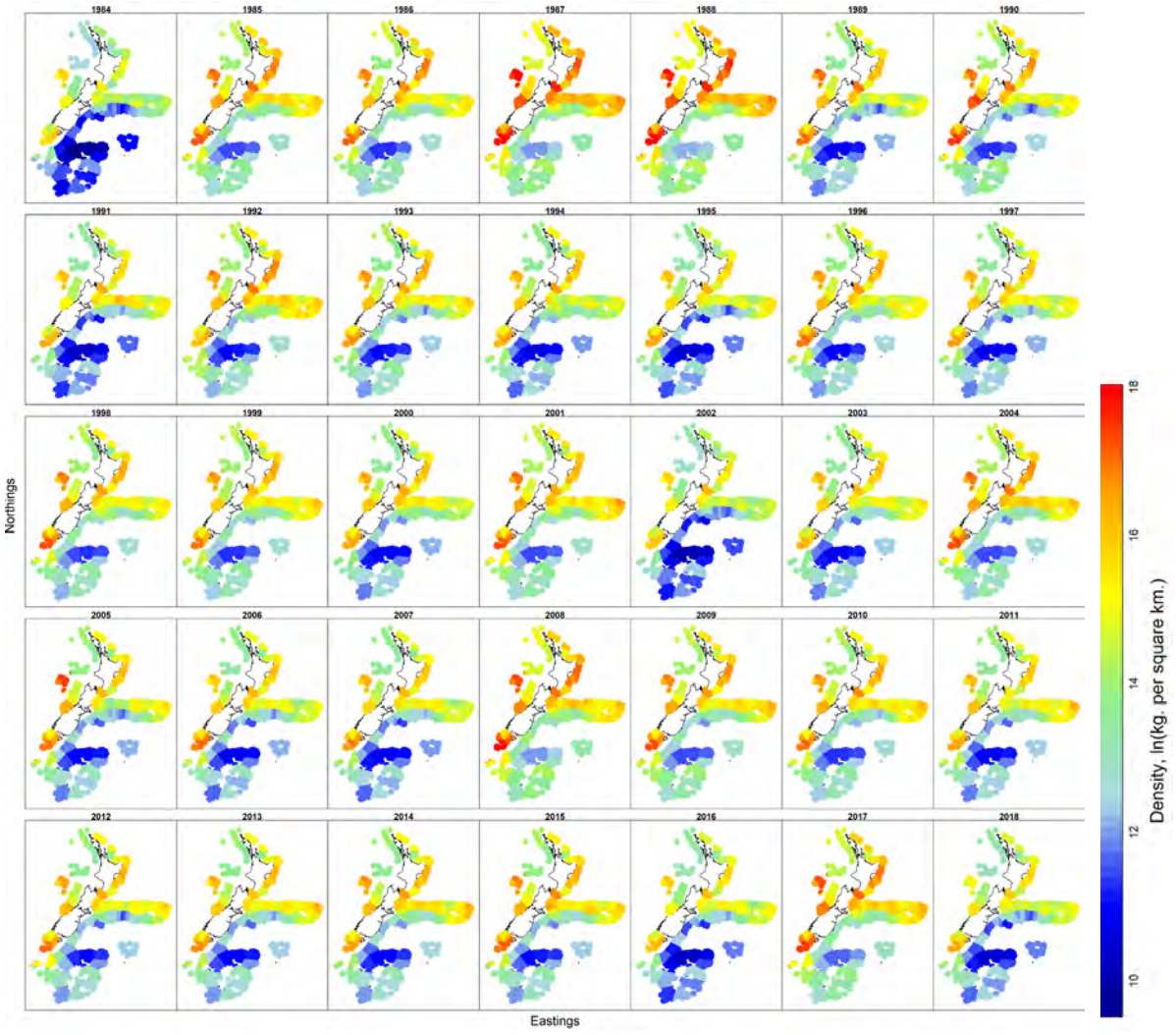

Figure 63: VAST outputs for relative density (kg km^{-2}) of *Dalatias licha* across the New Zealand Exclusive Economic Zone (EEZ) (1984–2018, from left to right for each panel).

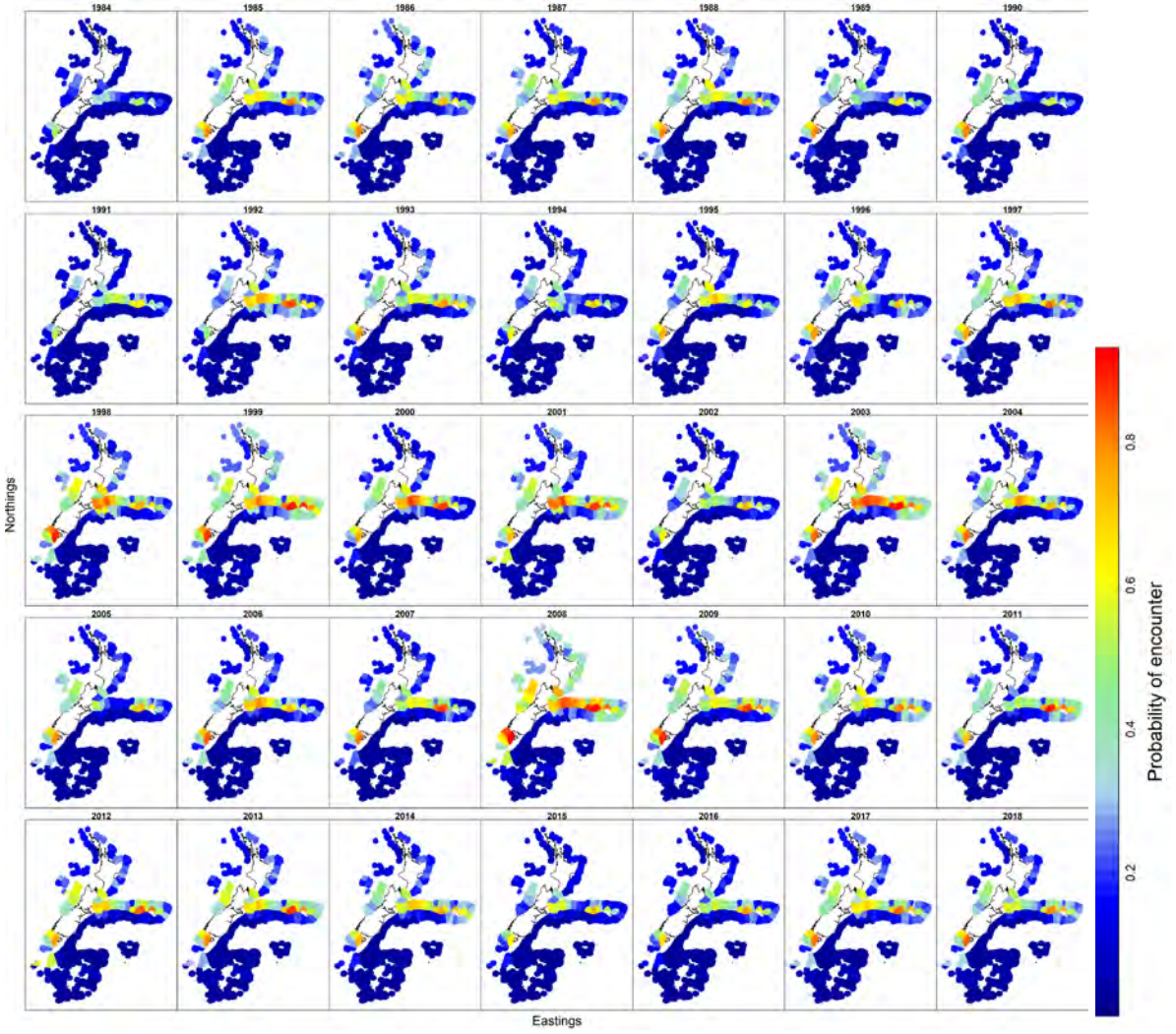

Figure 64: VAST outputs for probability of encounter of *Dalatias licha* across the New Zealand Exclusive Economic Zone (EEZ) (1984–2018, from left to right for each panel).

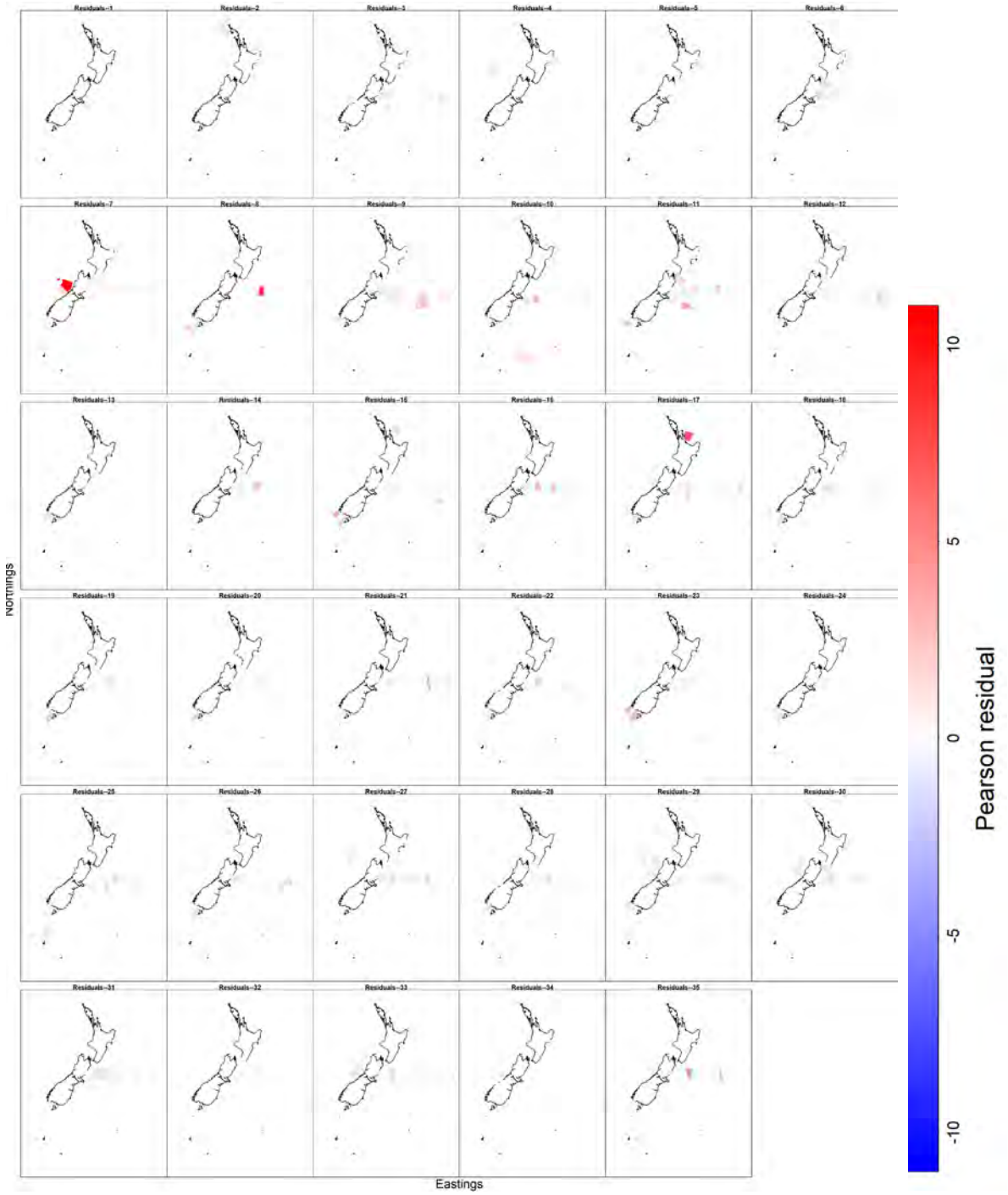

Figure 65: VAST outputs for Pearson residuals (goodness of fit) showing under or over fitting for catch rates of *Dalatias licha* across the New Zealand Exclusive Economic Zone (EEZ) (1984–2018, from left to right for each panel).

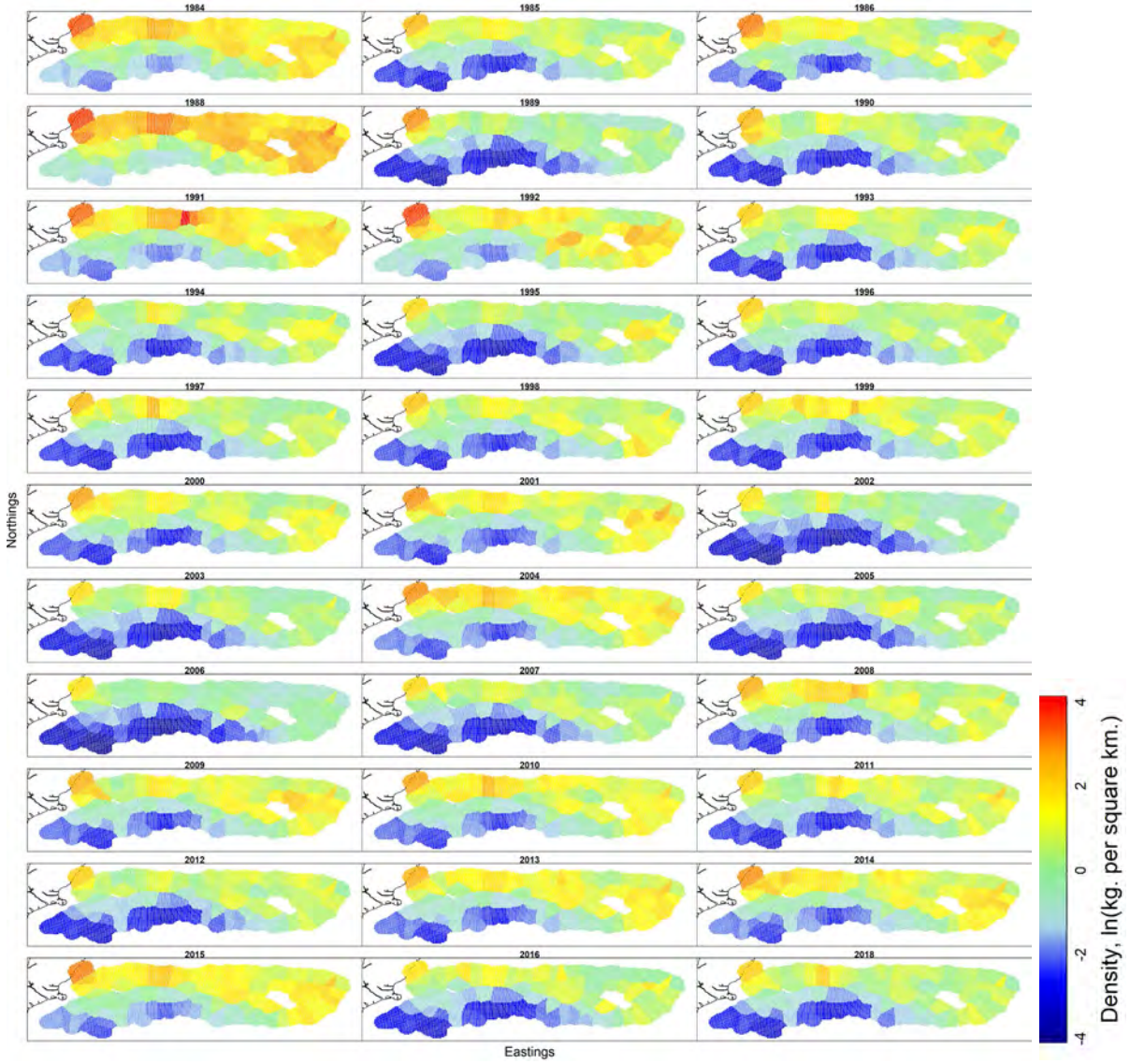

Figure 66: VAST outputs for relative density (kg km^{-2}) of *Dalatias licha* across Chatham Rise (1984–2018, from left to right for each panel).

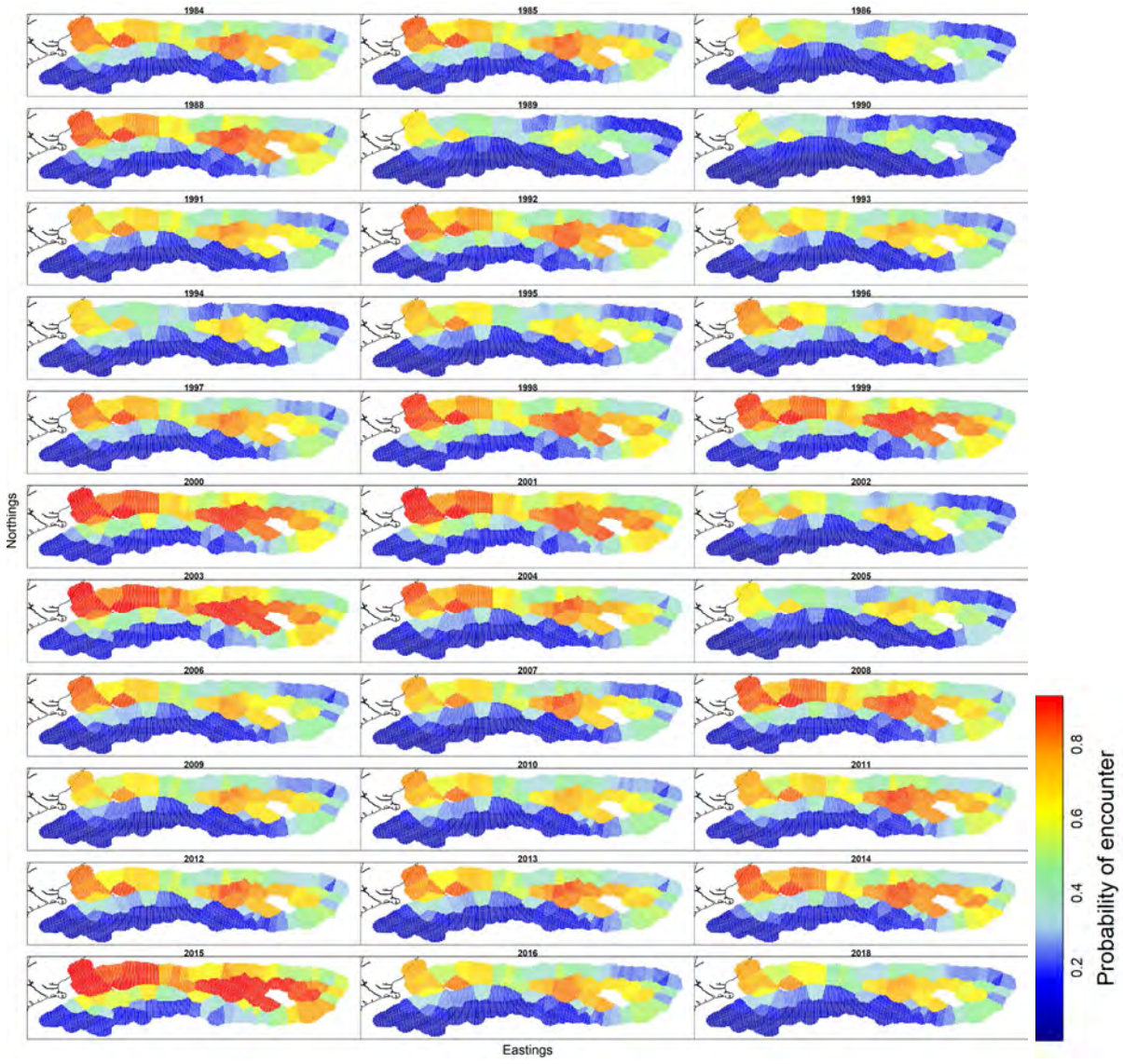

Figure 67: VAST outputs for probability of encounter of *Dalatias licha* across Chatham Rise (1984–2018, from left to right for each panel).

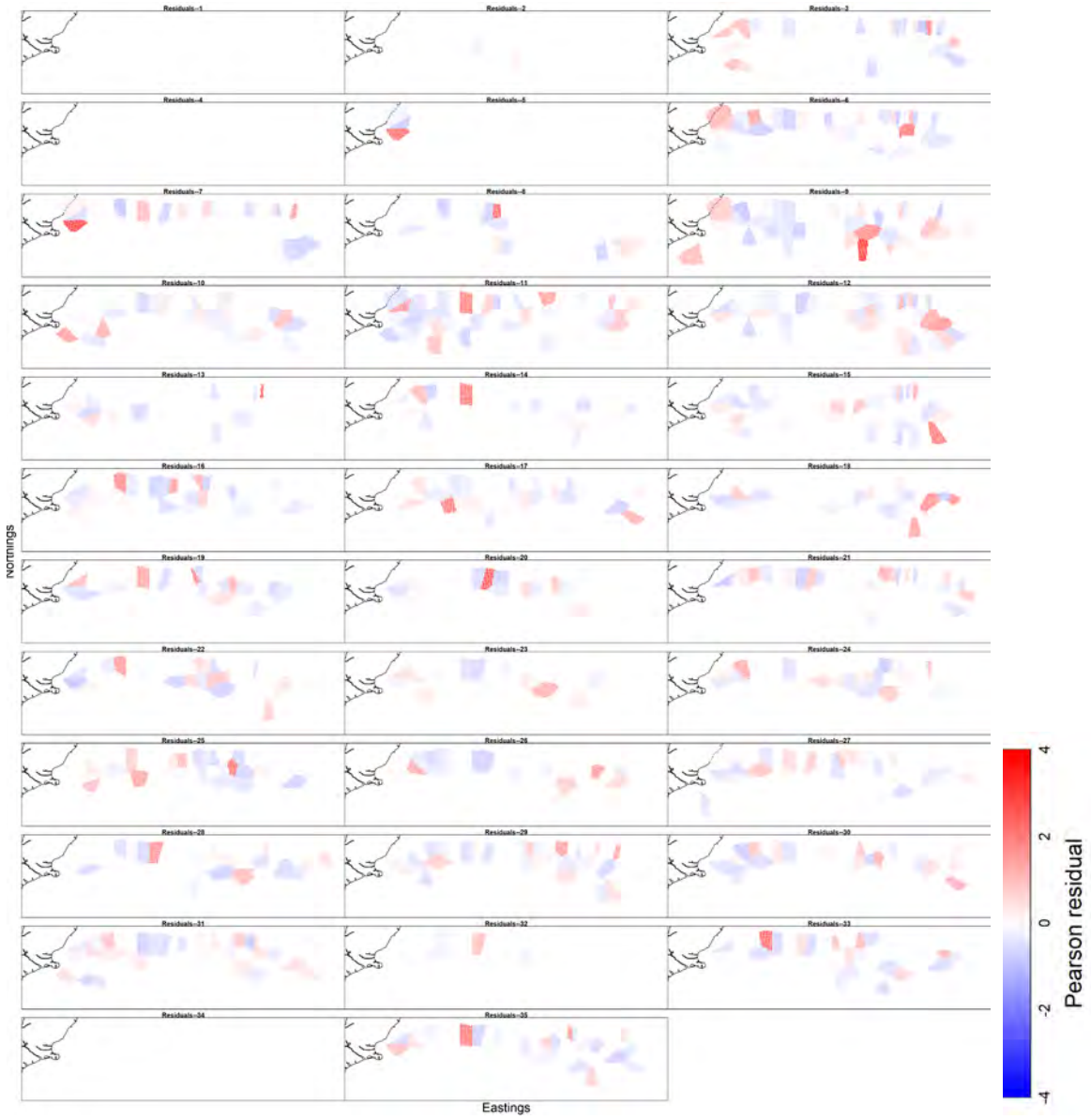

Figure 68: VAST outputs for Pearson residuals (goodness of fit) showing under or over fitting for catch rates of *Dalatias licha* across Chatham Rise (1984–2018, from left to right for each panel).

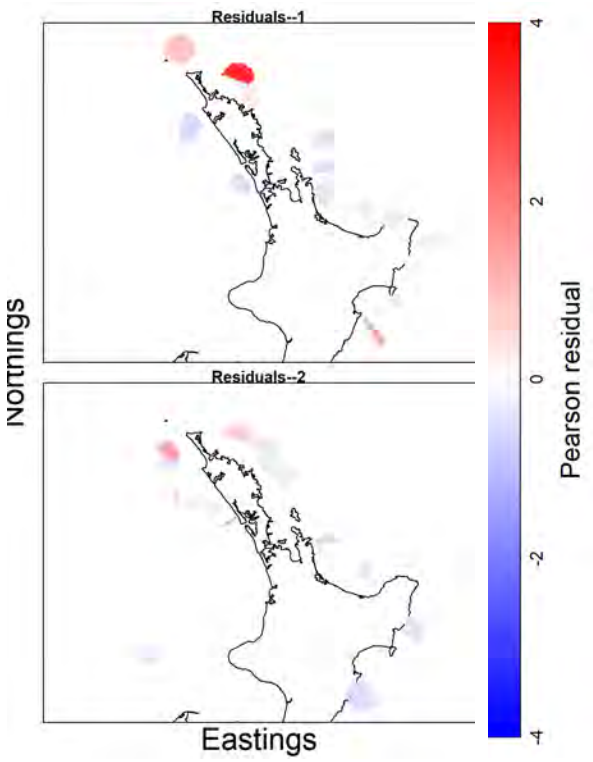

Figure 69: VAST outputs for Pearson residuals (goodness of fit) showing under or over fitting for catch rates of *Dalatias licha* around the North Island in 1985–1986.

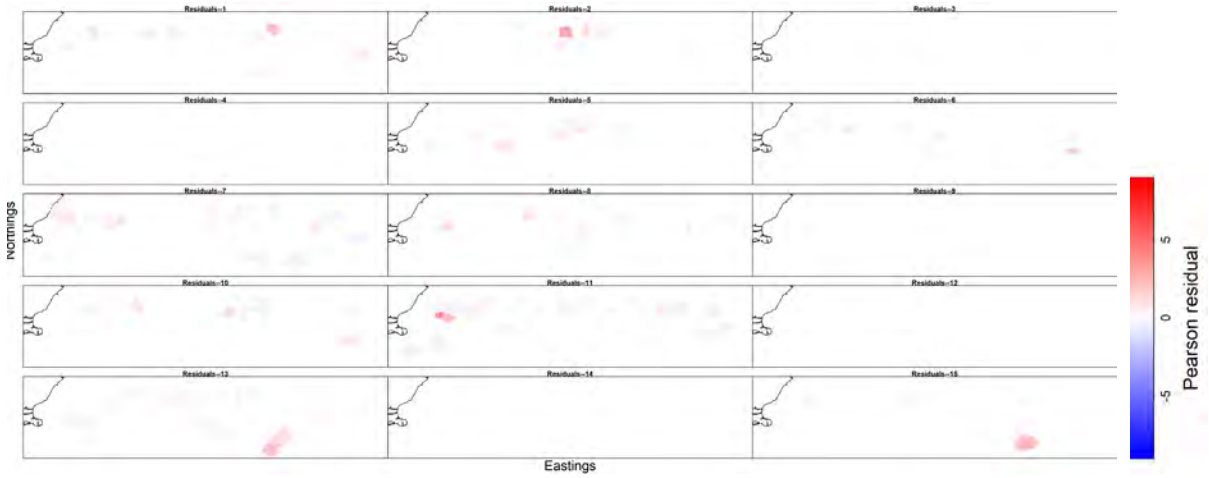

Figure 70: VAST outputs for Pearson residuals (goodness of fit) showing under or over fitting for catch rates of *Dalatias licha* by class across Chatham Rise (2004–2018, from left to right for each panel).

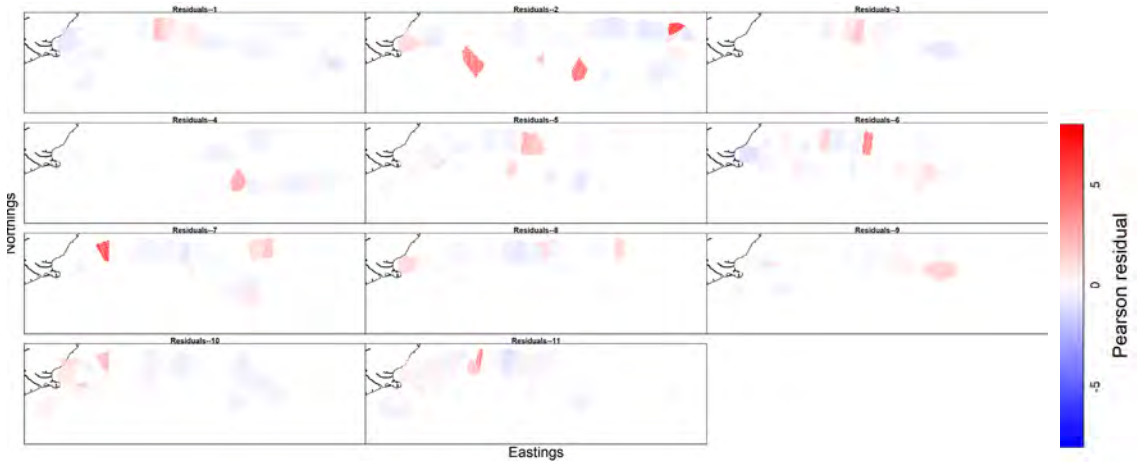

Figure 71: VAST outputs for Pearson residuals (goodness of fit) showing under or over fitting for observer catch rates of *Dalatias licha* across Chatham Rise (2008–2018, from left to right for each panel).

Appendix 6: *Centrophorus squamosus*

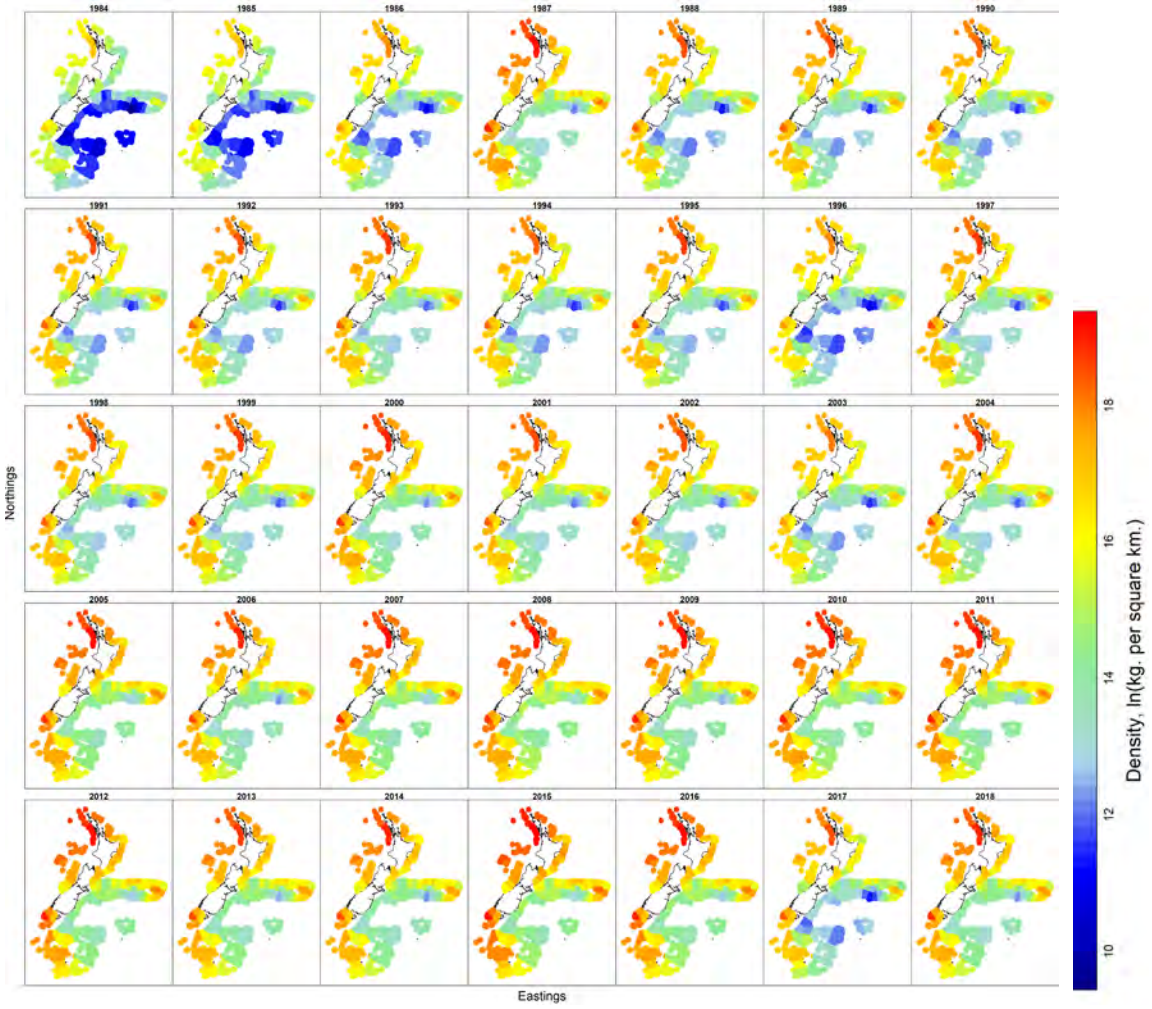

Figure 72: VAST outputs for relative density (kg km^{-2}) of *Centrophorus squamosus* across the New Zealand Exclusive Economic Zone (EEZ) (1984–2018, from left to right for each panel).

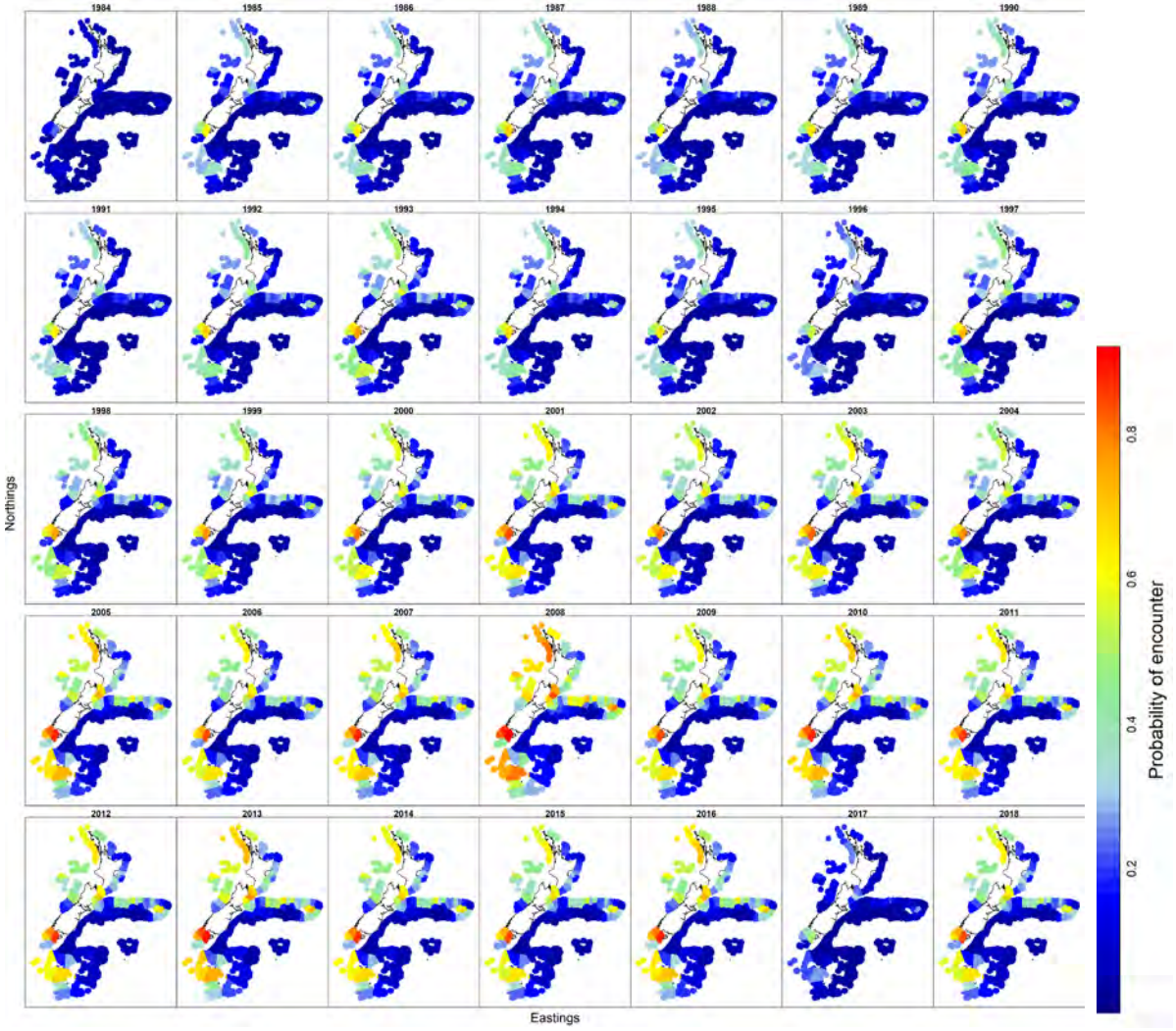

Figure 73: VAST outputs for probability of encounter of *Centrophorus squamosus* across the New Zealand Exclusive Economic Zone (EEZ) (1984–2018, from left to right for each panel).

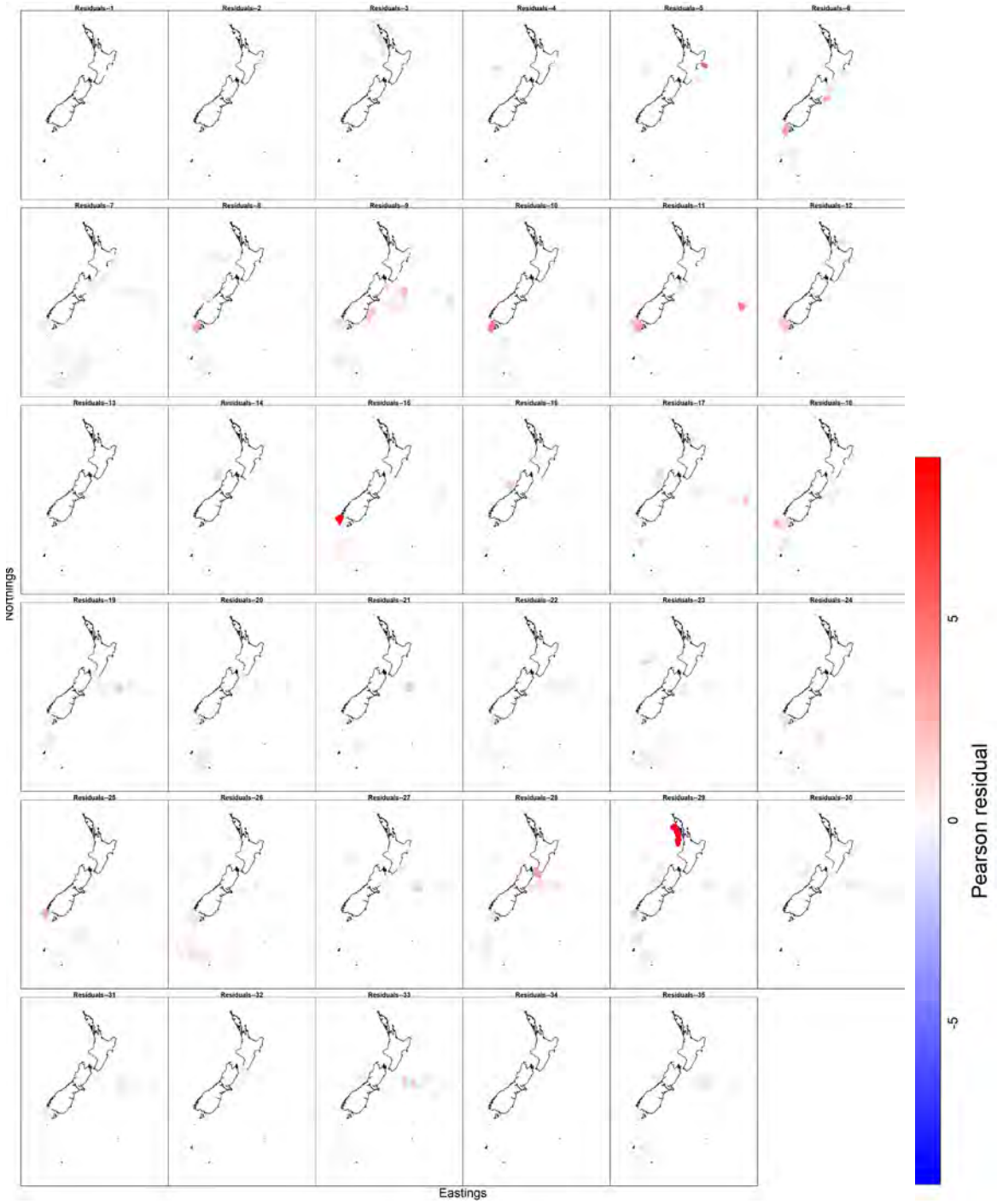

Figure 74: VAST outputs for Pearson residuals (goodness of fit) showing under or over fitting for catch rates of *Centrophorus squamosus* across the New Zealand Exclusive Economic Zone (EEZ) (1984–2018, from left to right for each panel).

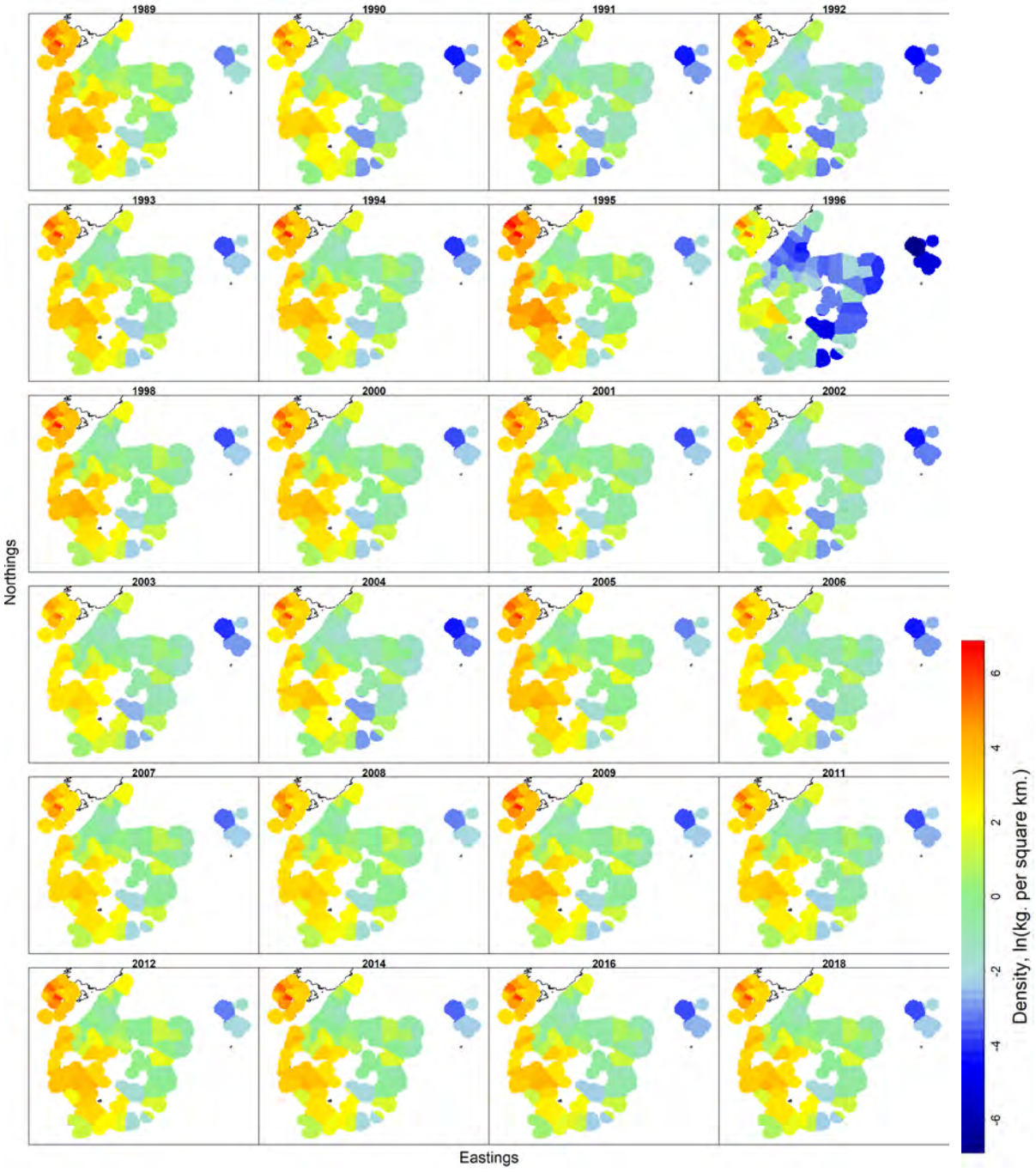

Figure 75: VAST outputs for relative density (kg km^{-2}) of *Centrophorus squamosus* across the Sub-Antarctic (1989–2018, from left to right for each panel).

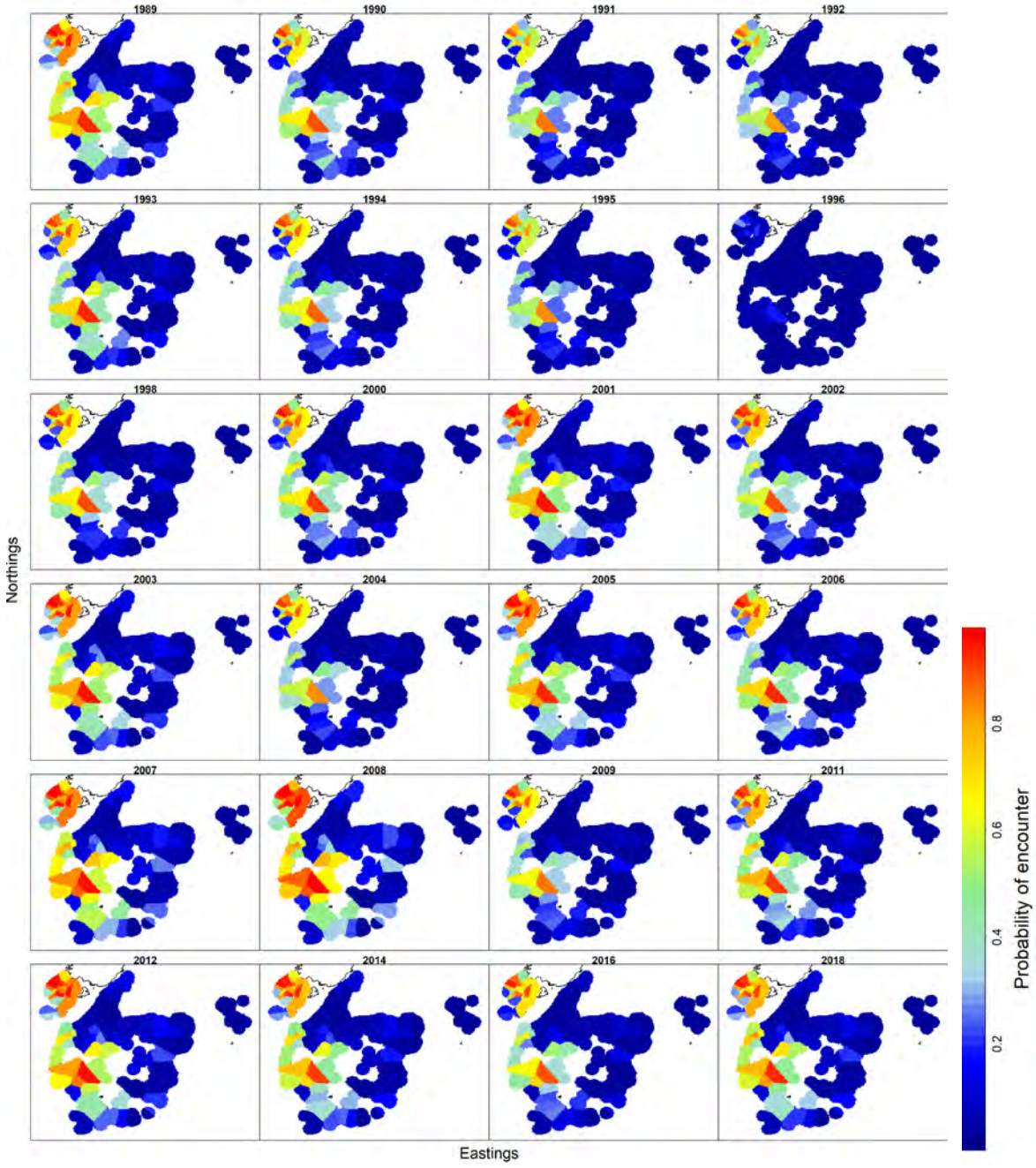

Figure 76: VAST outputs for probability of encounter of *Centrophorus squamosus* across the Sub-Antarctic (1989–2018, from left to right for each panel).

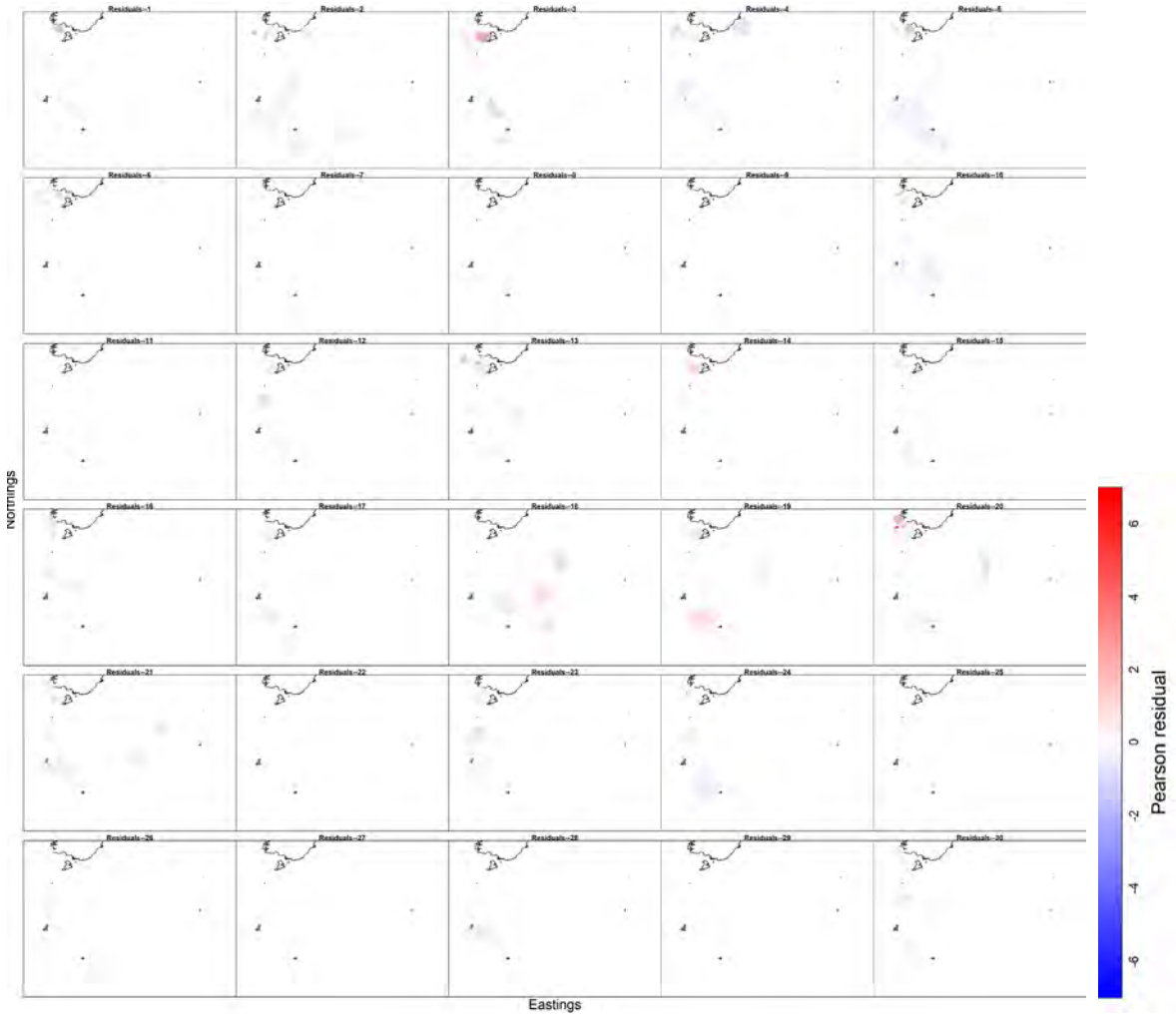

Figure 77: VAST outputs for Pearson residuals (goodness of fit) showing under or over fitting for catch rates of *Centrophorus squamosus* across the Sub-Antarctic (1989–2018, from left to right for each panel).

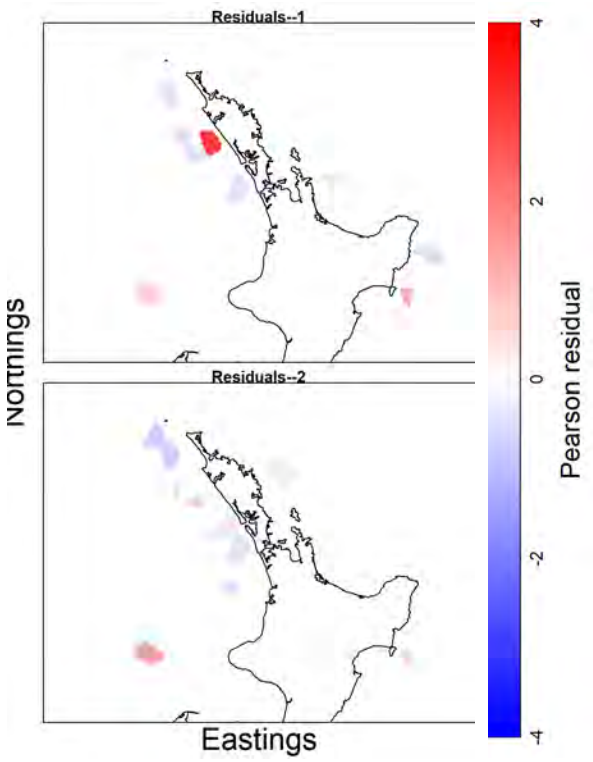

Figure 78: VAST outputs for Pearson residuals (goodness of fit) showing under or over fitting for catch rates of *Centrophorus squamosus* around the North Island in 1985–1986.

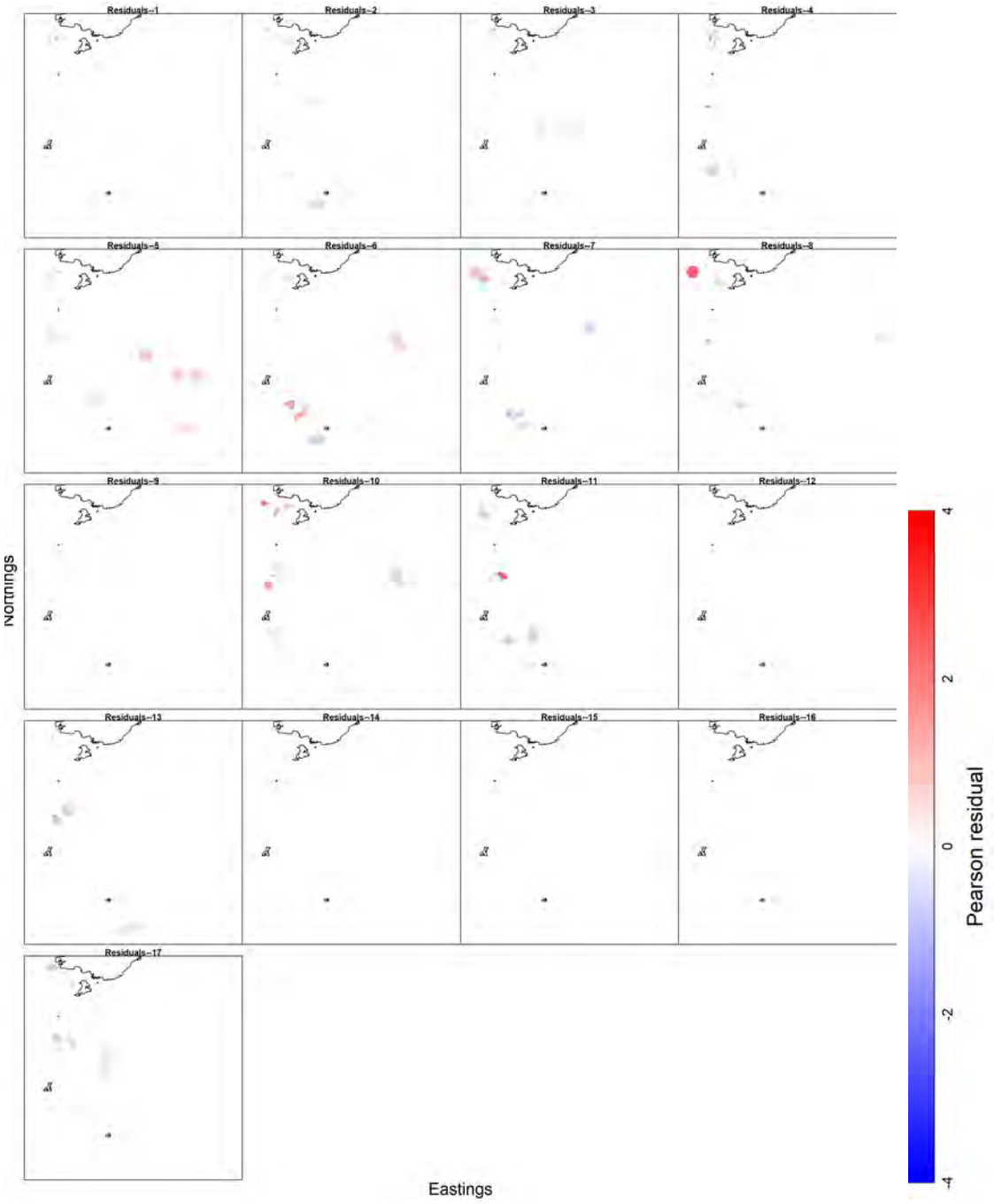

Figure 79: VAST outputs for Pearson residuals (goodness of fit) showing under or over fitting for catch rates of *Centrophorus squamosus* by class across the Sub-Antarctic (2002–2018, from left to right for each panel).

Figure 80: VAST outputs for Pearson residuals (goodness of fit) showing under or over fitting for observer catch rates of *Centrophorus squamosus* across Chatham Rise (2012–2018, from left to right for each panel).

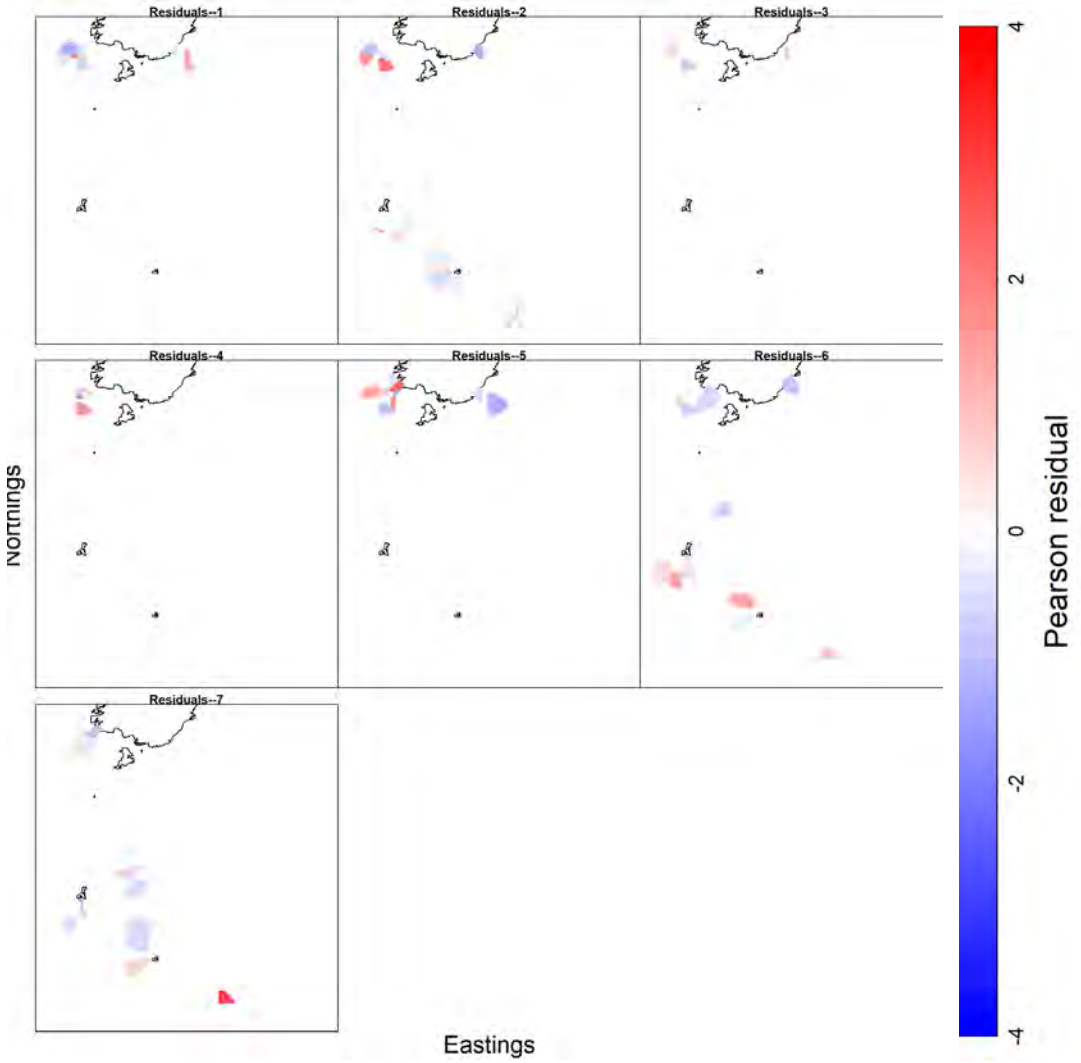

Figure 81: VAST outputs for Pearson residuals (goodness of fit) showing under or over fitting for observer catch rates of *Centrophorus squamosus* across the Sub-Antarctic (2012–2018, from left to right for each panel).

Appendix 7: *Centroscymnus owstonii*

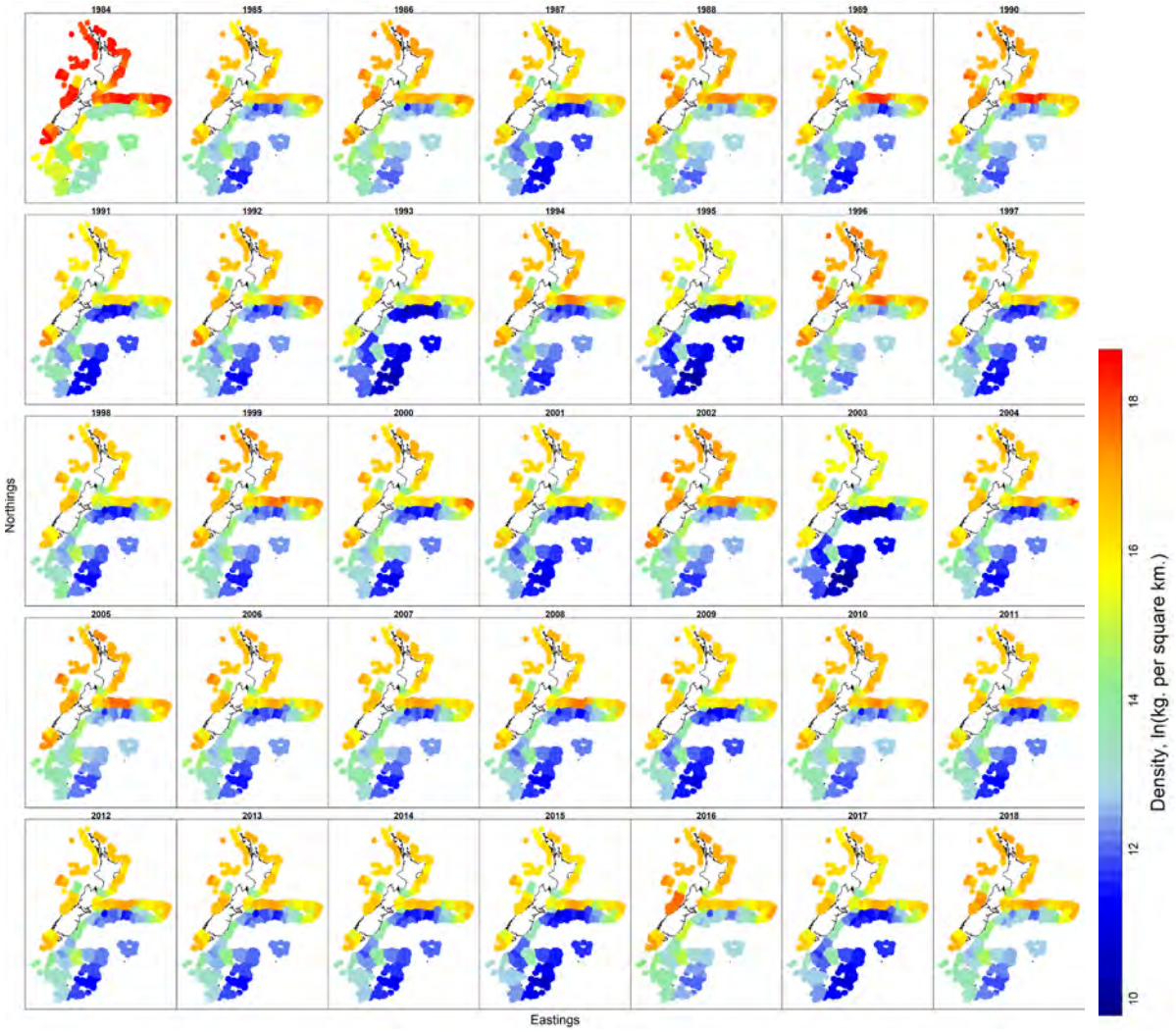

Figure 82: VAST outputs for relative density (kg km^{-2}) of *Centroscymnus owstonii* across the New Zealand Exclusive Economic Zone (EEZ) (1984–2018, from left to right for each panel).

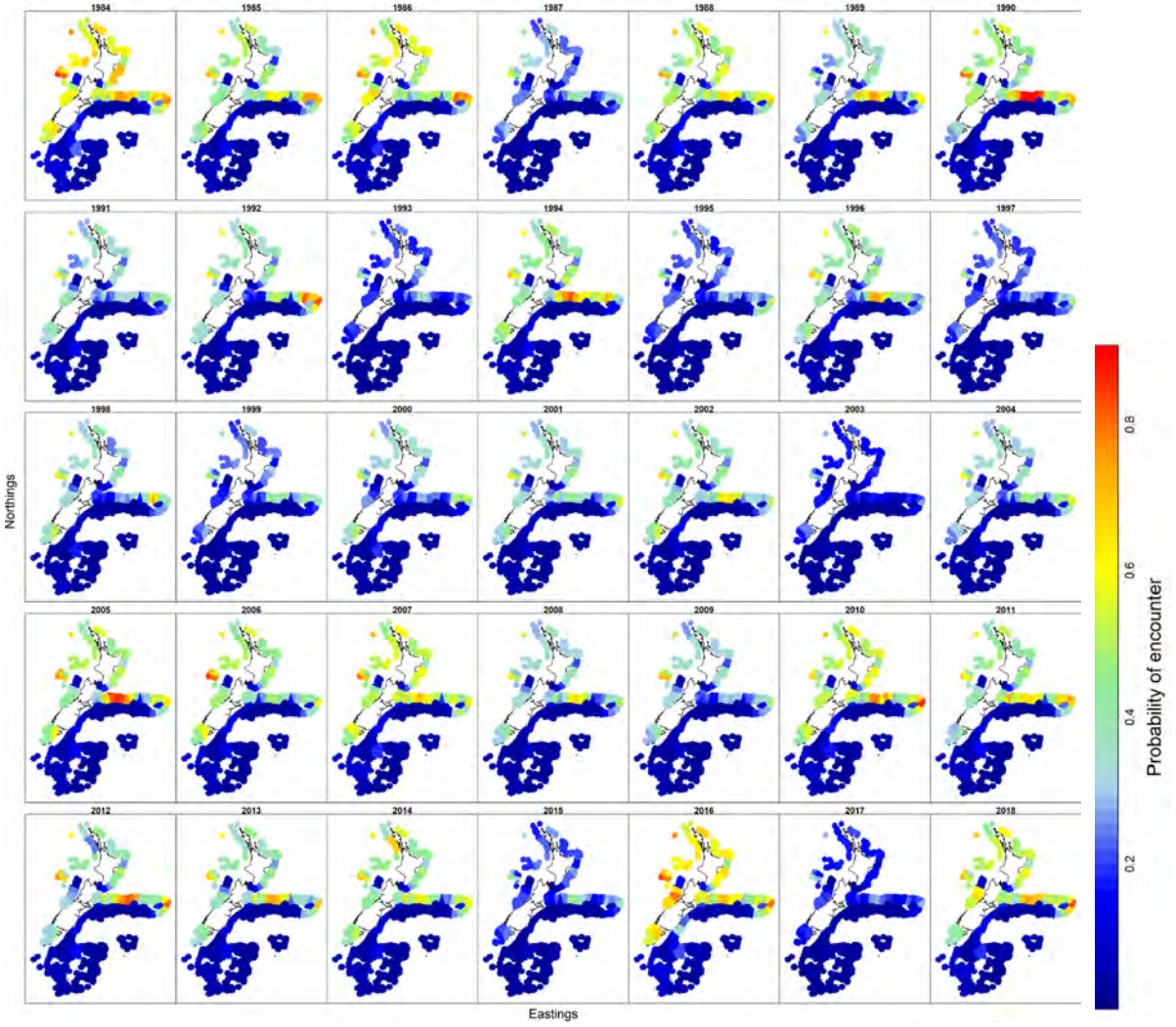

Figure 83: VAST outputs for probability of encounter of *Centroscymnus owstonii* across the New Zealand Exclusive Economic Zone (EEZ) (1984–2018, from left to right for each panel).

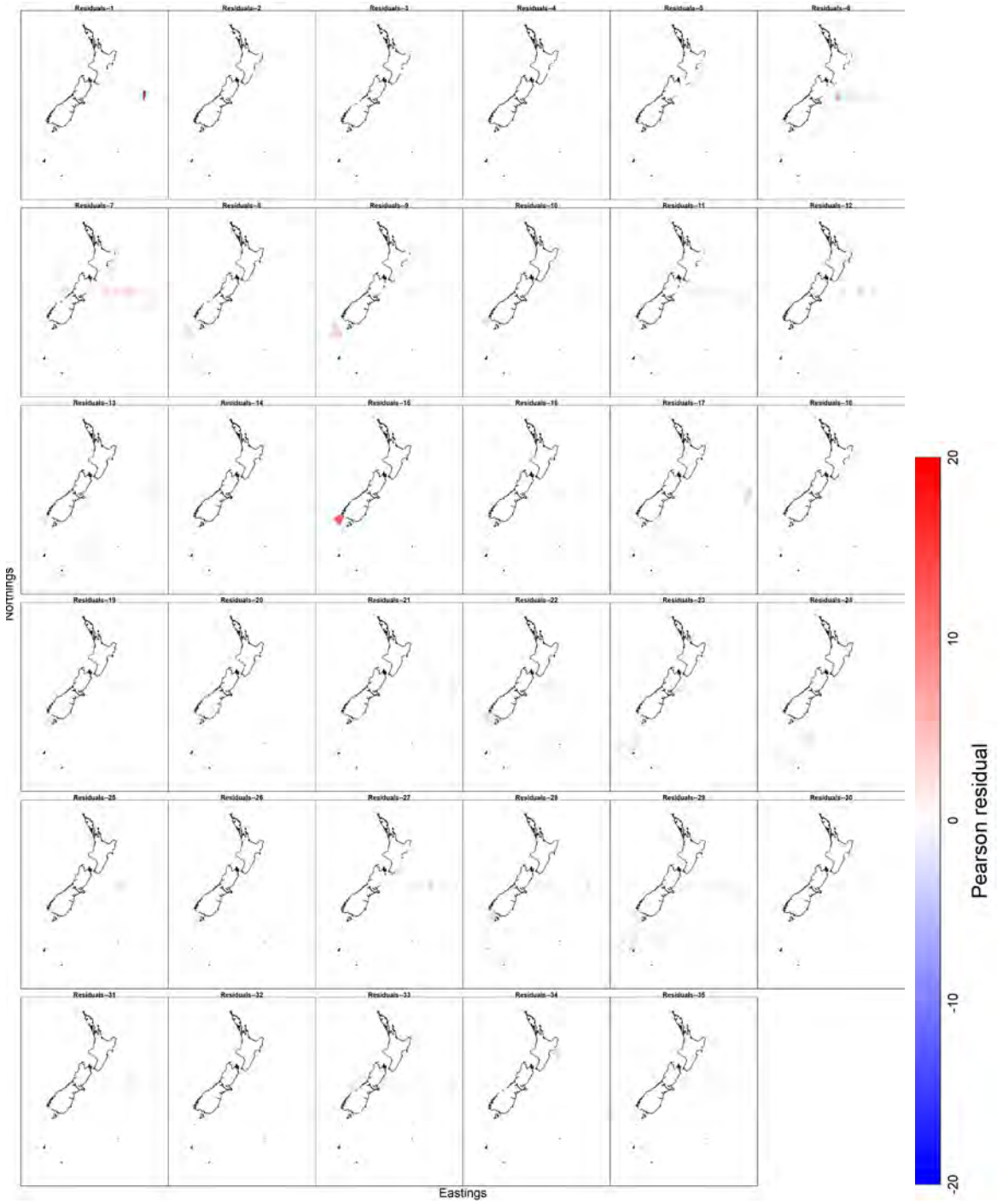

Figure 84: VAST outputs for Pearson residuals (goodness of fit) showing under or over fitting for catch rates of *Centroscymnus owstonii* across the New Zealand Exclusive Economic Zone (EEZ) (1984–2018, from left to right for each panel).

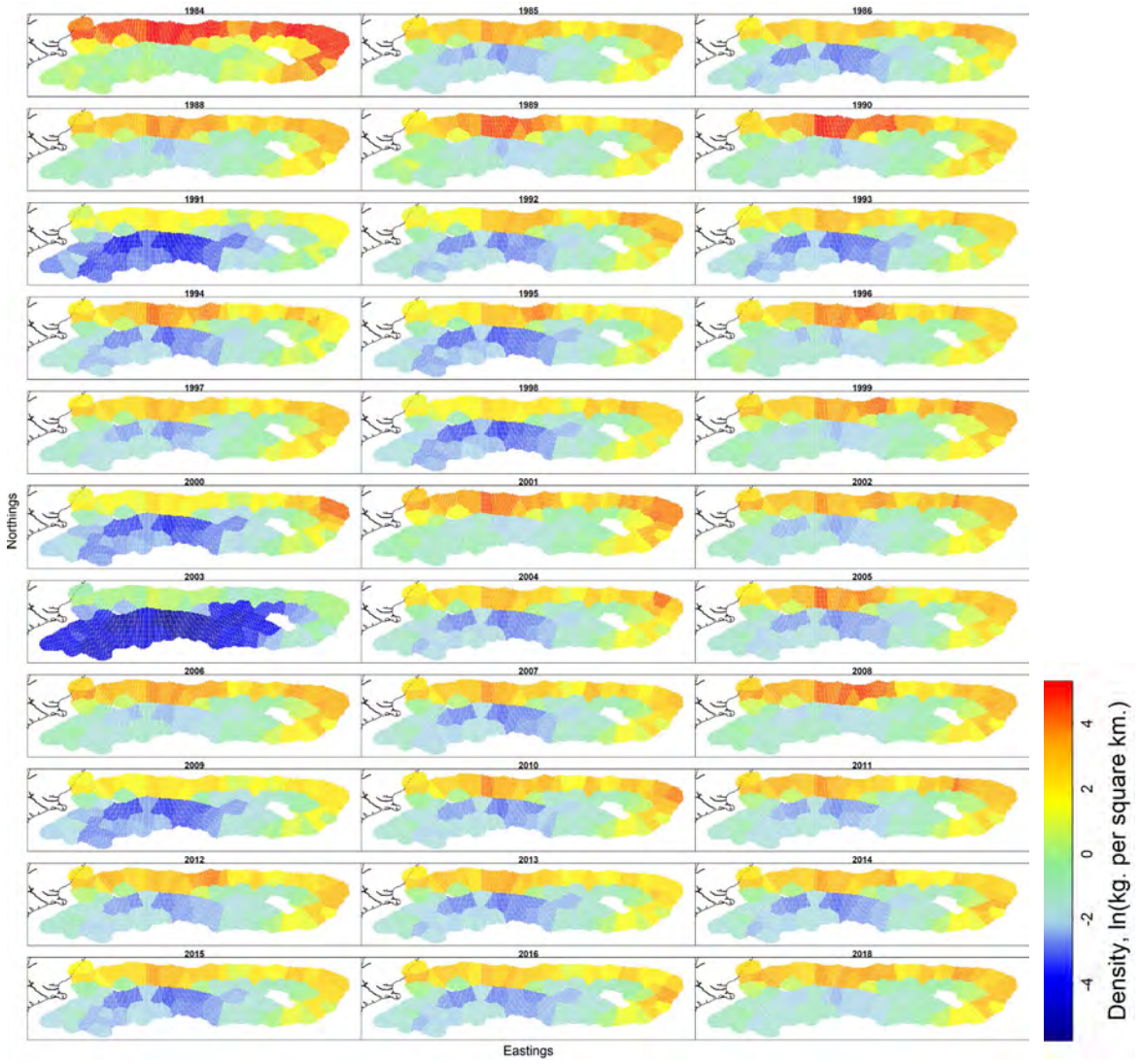

Figure 85: VAST outputs for relative density (kg km^{-2}) of *Centroscymnus owstonii* across Chatham Rise (1984–2018, from left to right for each panel).

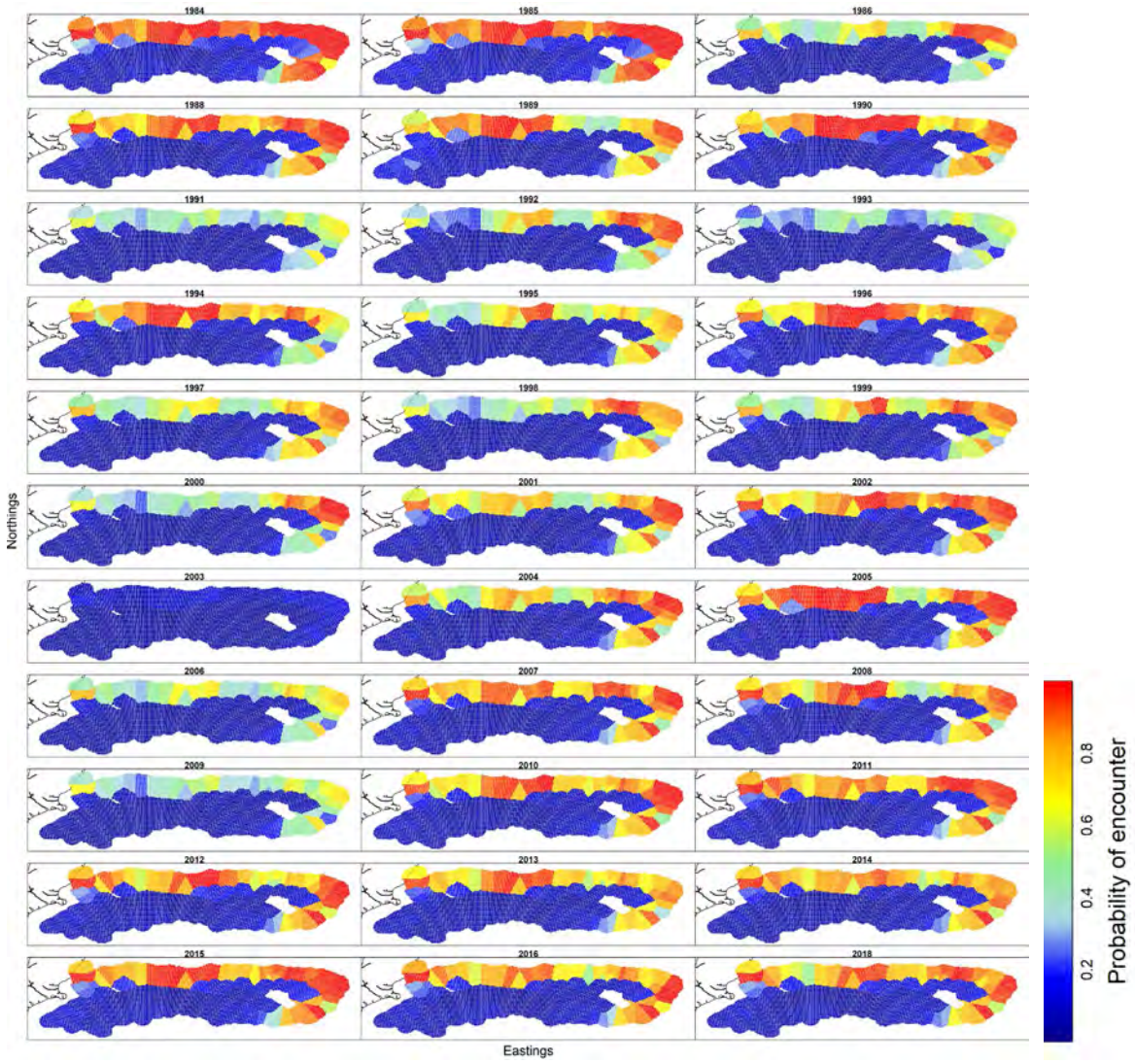

Figure 86: VAST outputs for probability of encounter of *Centroscymnus owstonii* across Chatham Rise (1984–2018, from left to right for each panel).

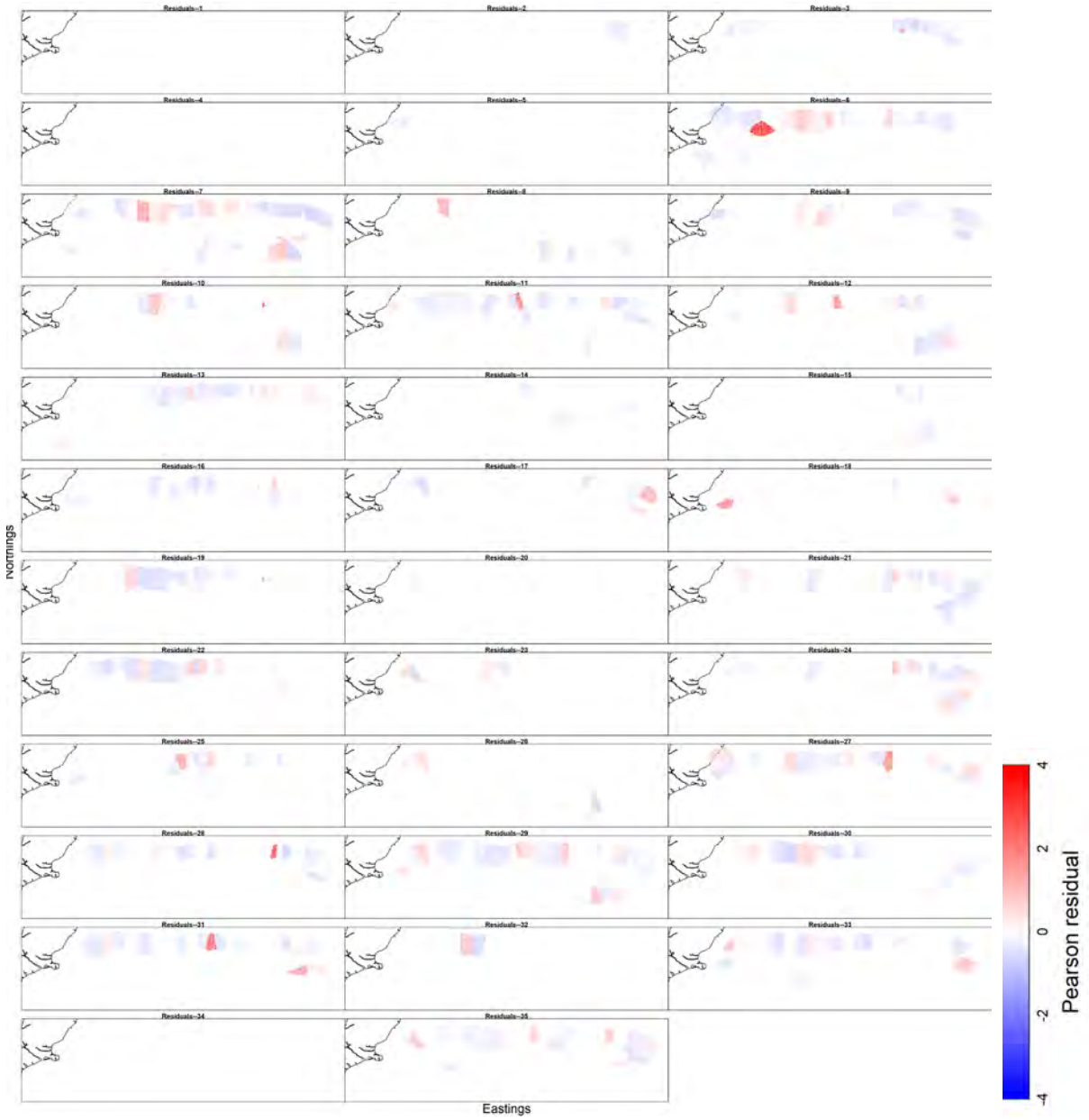

Figure 87: VAST outputs for Pearson residuals (goodness of fit) showing under or over fitting for catch rates of *Centroscymnus owstonii* across Chatham Rise (1984–2018, from left to right for each panel).

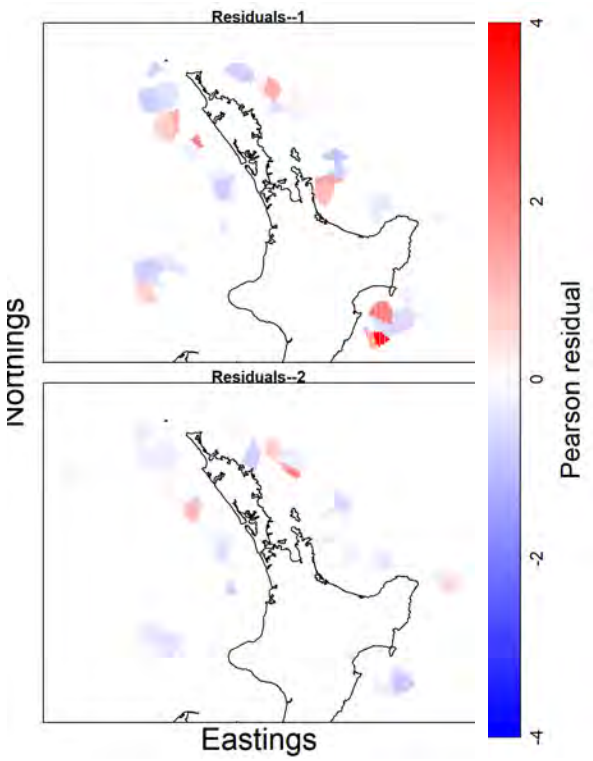

Figure 88: VAST outputs for Pearson residuals (goodness of fit) showing under or over fitting for observer catch rates of *Centroscymnus owstonii* around the North Island in 1985–1986.

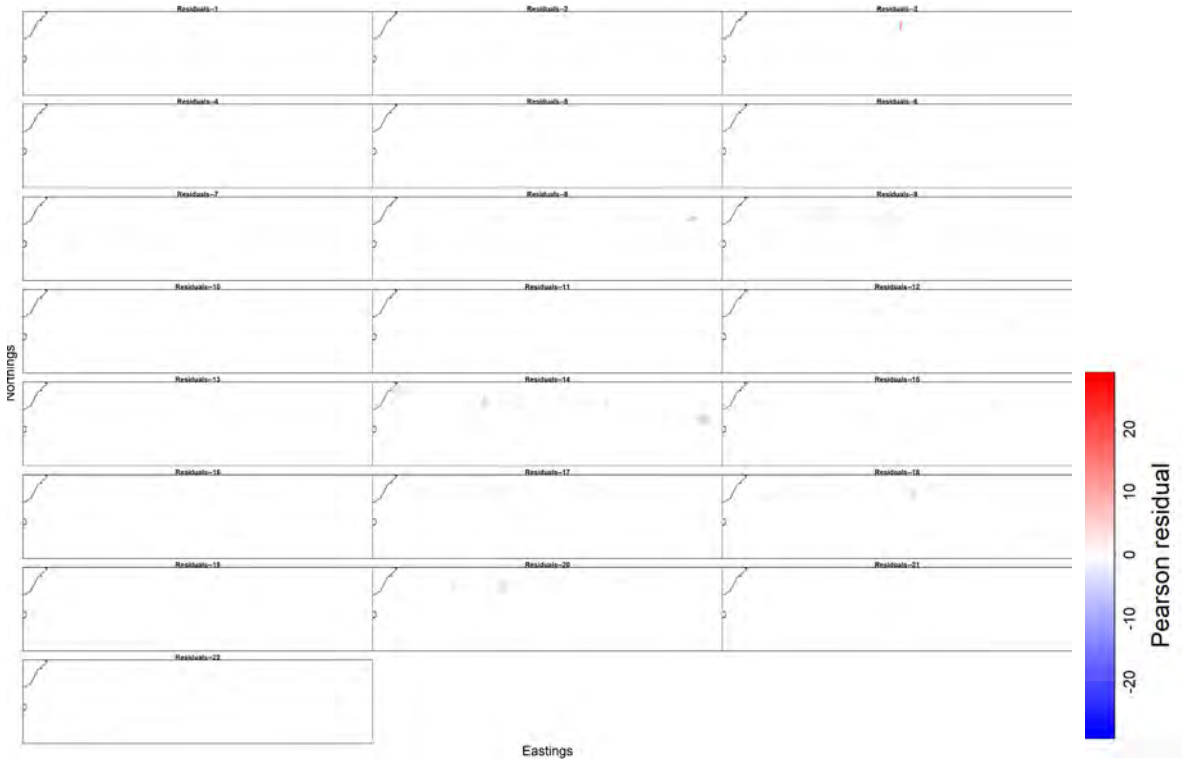

Figure 89: VAST outputs for Pearson residuals (goodness of fit) showing under or over fitting for catch rates of *Centroscymnus owstonii* by class across Chatham Rise (2002–2018, from left to right for each panel).

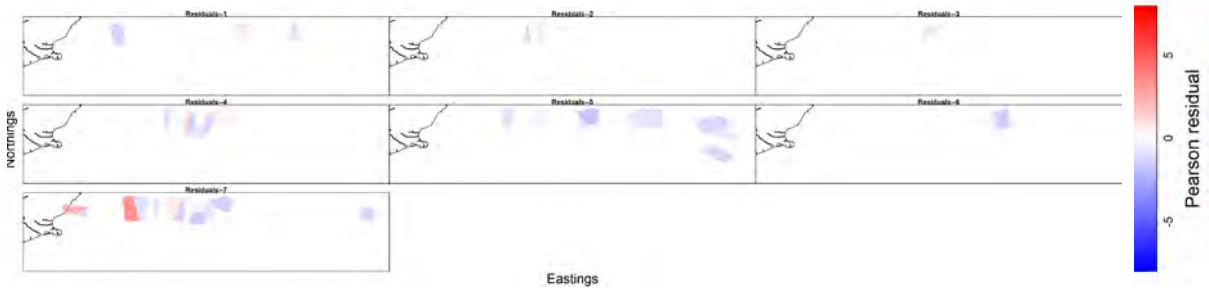

Figure 90: VAST outputs for Pearson residuals (goodness of fit) showing under or over fitting for observer catch rates of *Centroscymnus owstonii* across Chatham Rise (2012–2018, from left to right for each panel).

Appendix 8: *Centroselachus crepidater*

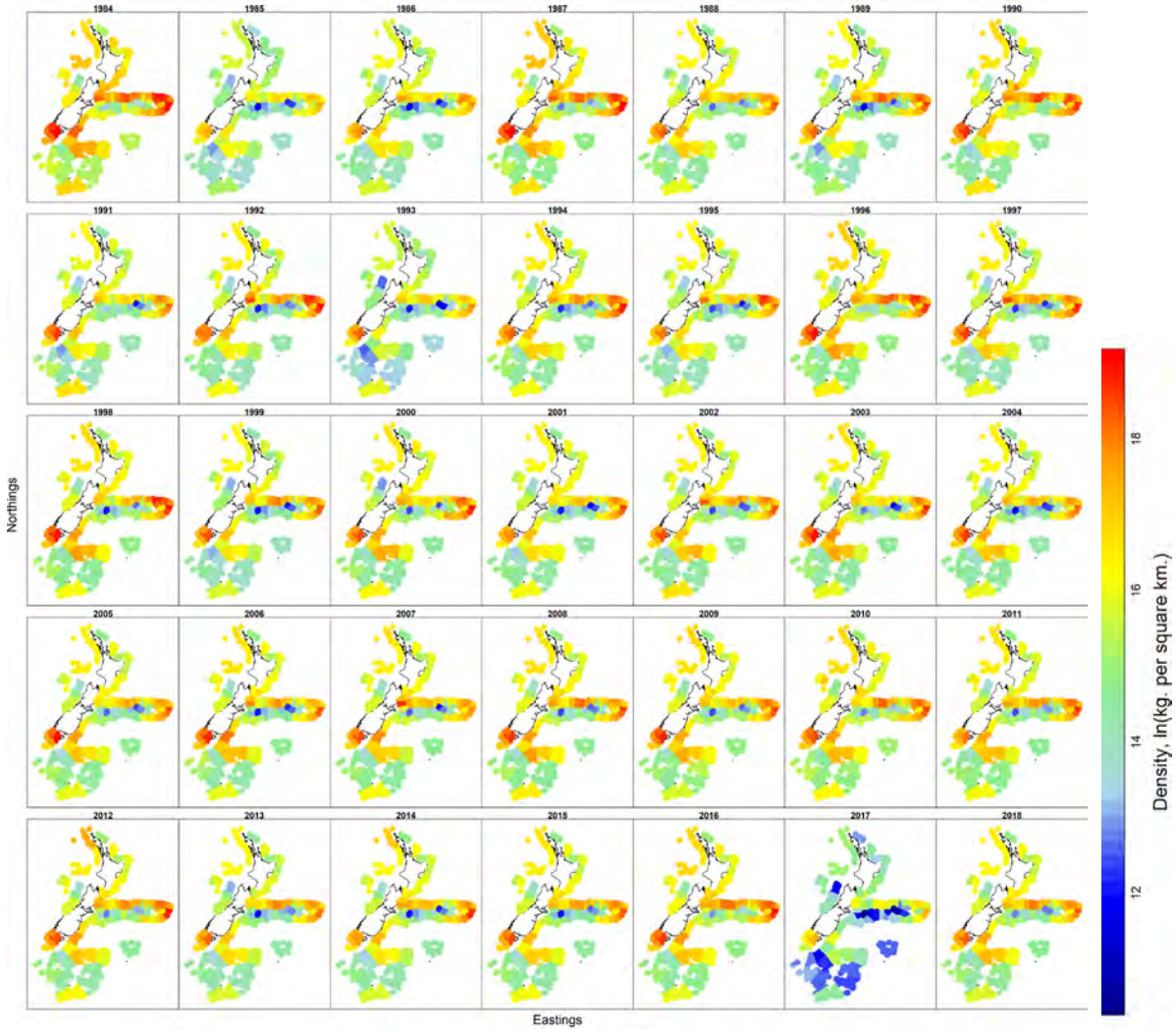

Figure 91: VAST outputs for relative density (kg km^{-2}) of *Centroselachus crepidater* across the New Zealand Exclusive Economic Zone (EEZ) (1984–2018, from left to right for each panel).

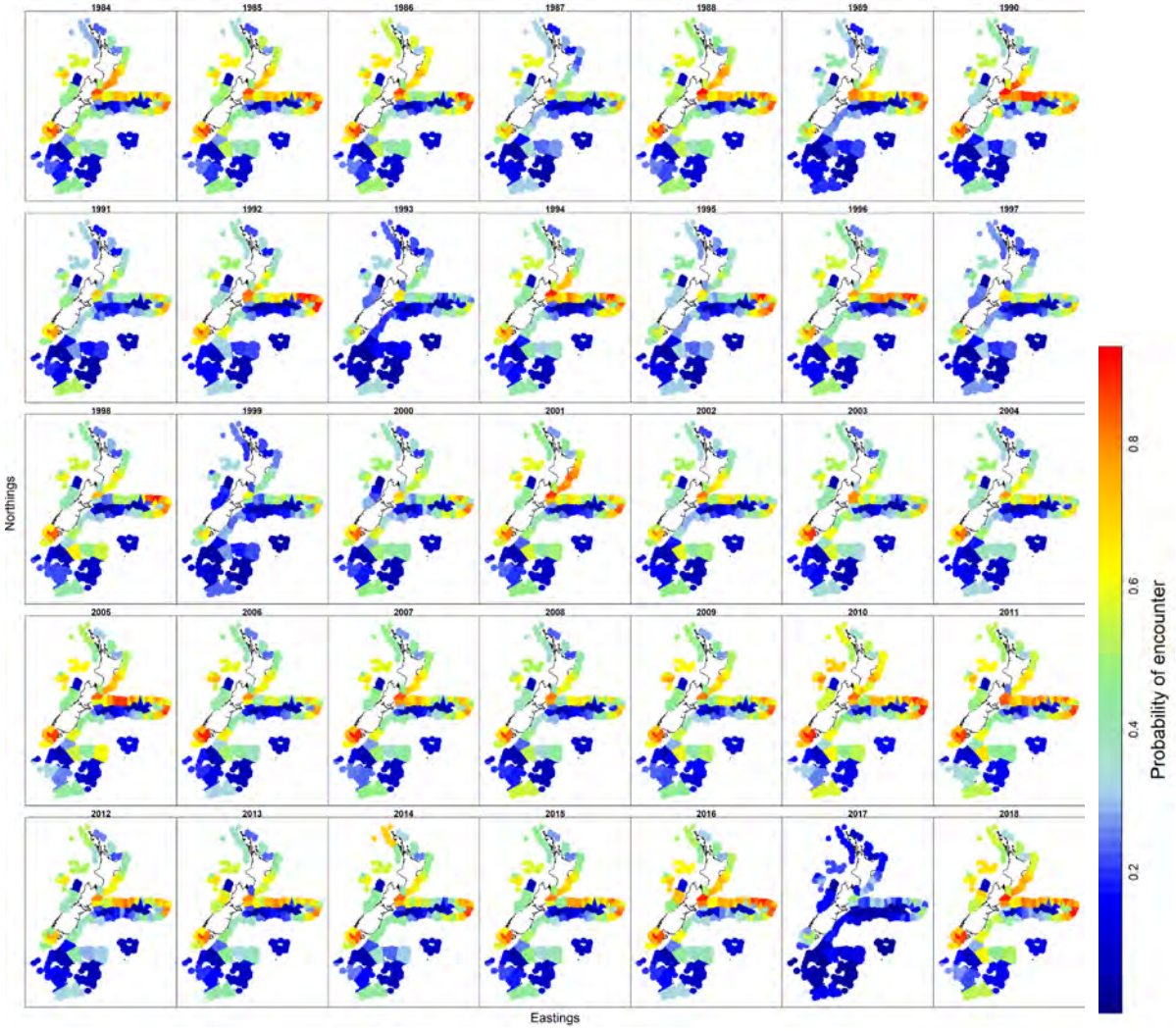

Figure 92: VAST outputs for probability of encounter of *Centroselachus crepidater* across the New Zealand Exclusive Economic Zone (EEZ) (1984–2018, from left to right for each panel).

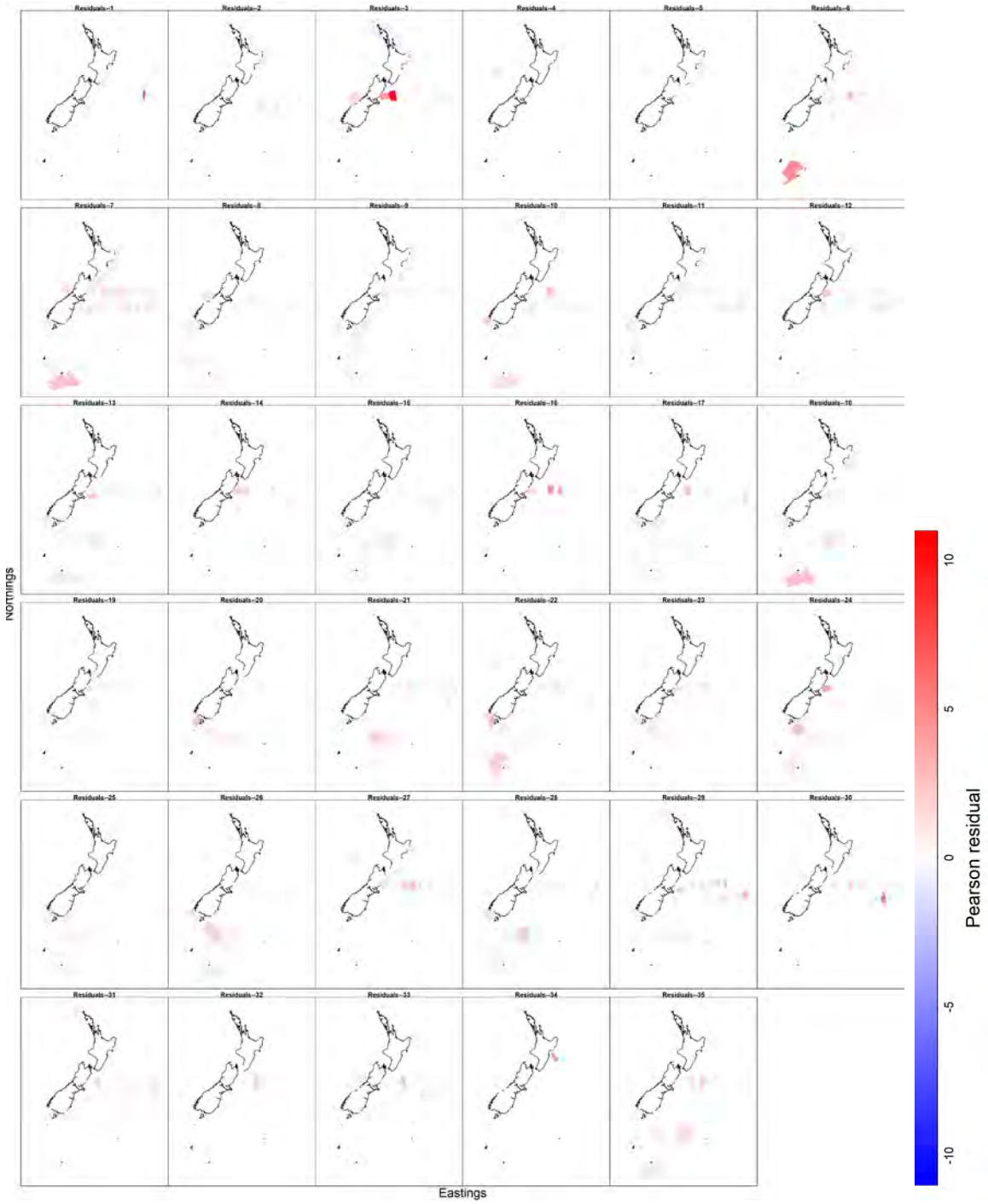

Figure 93: VAST outputs for Pearson residuals (goodness of fit) showing under or over fitting for catch rates of *Centroselachus crepidater* across the New Zealand Exclusive Economic Zone (EEZ) (1984–2018, from left to right for each panel).

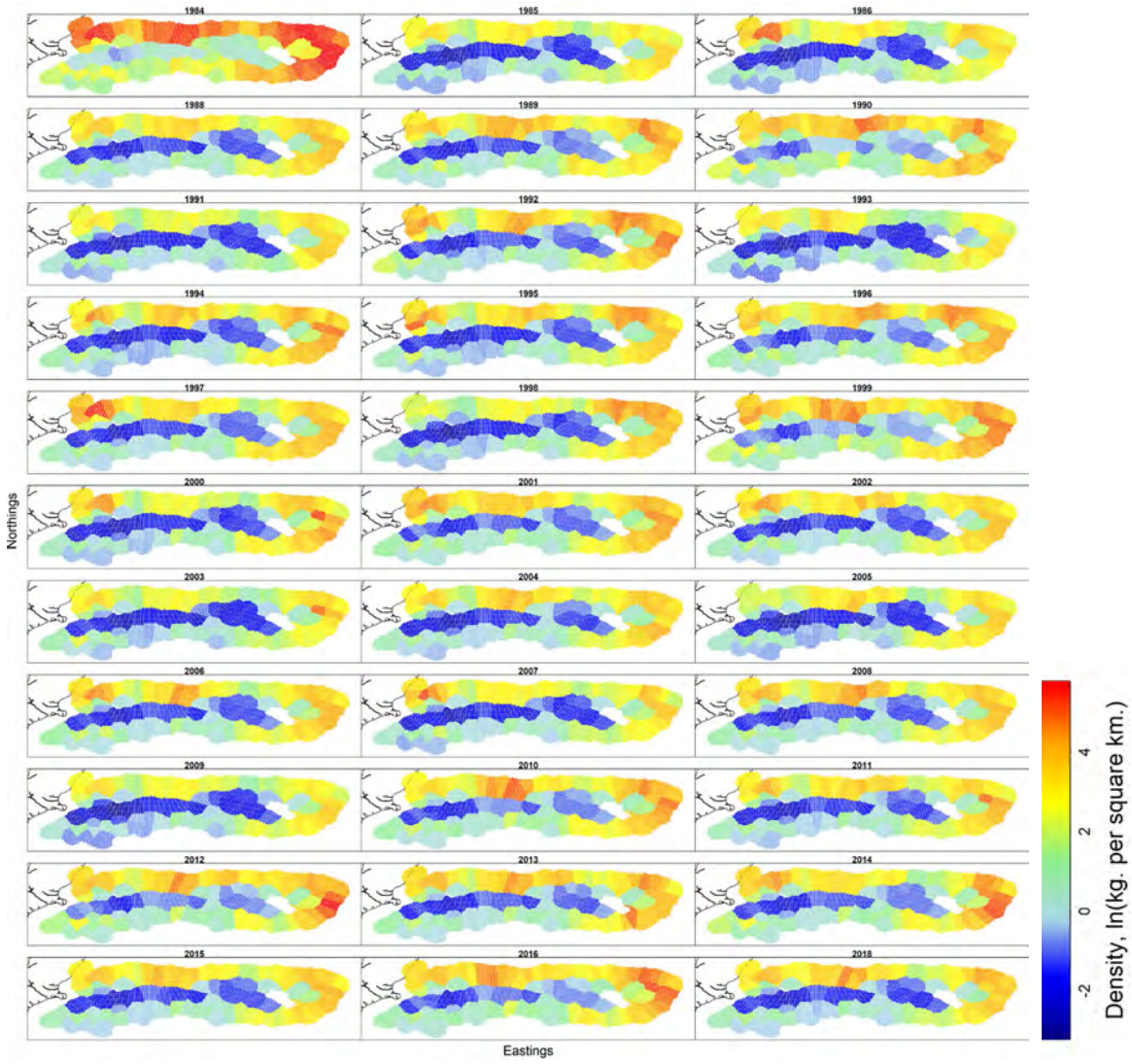

Figure 94: VAST outputs for relative density (kg km^{-2}) of *Centroselachus crepidater* across Chatham Rise (1984–2018, from left to right for each panel).

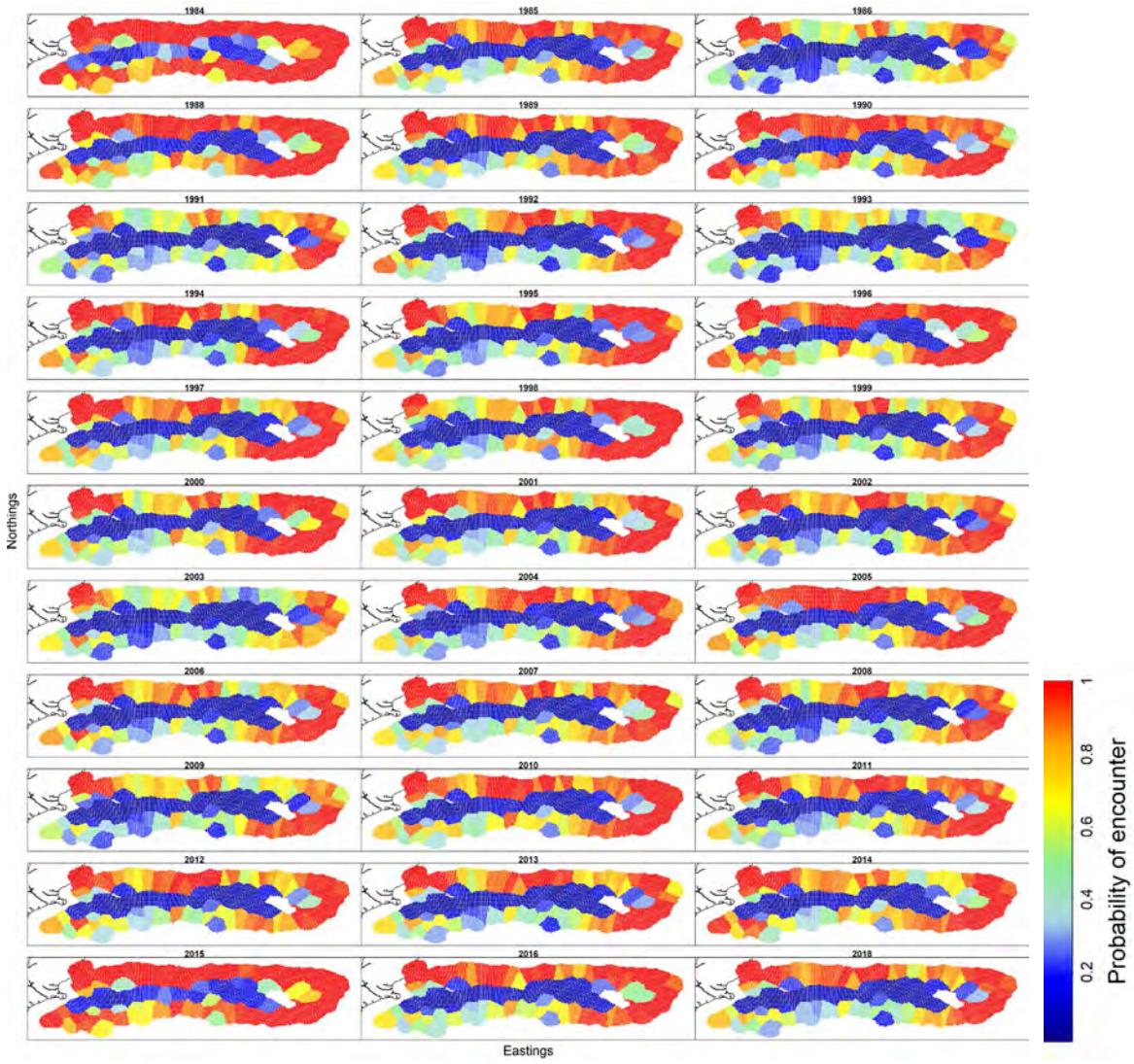

Figure 95: VAST outputs for probability of encounter of *Centroselachus crepidater* across Chatham Rise (1984–2018, from left to right for each panel).

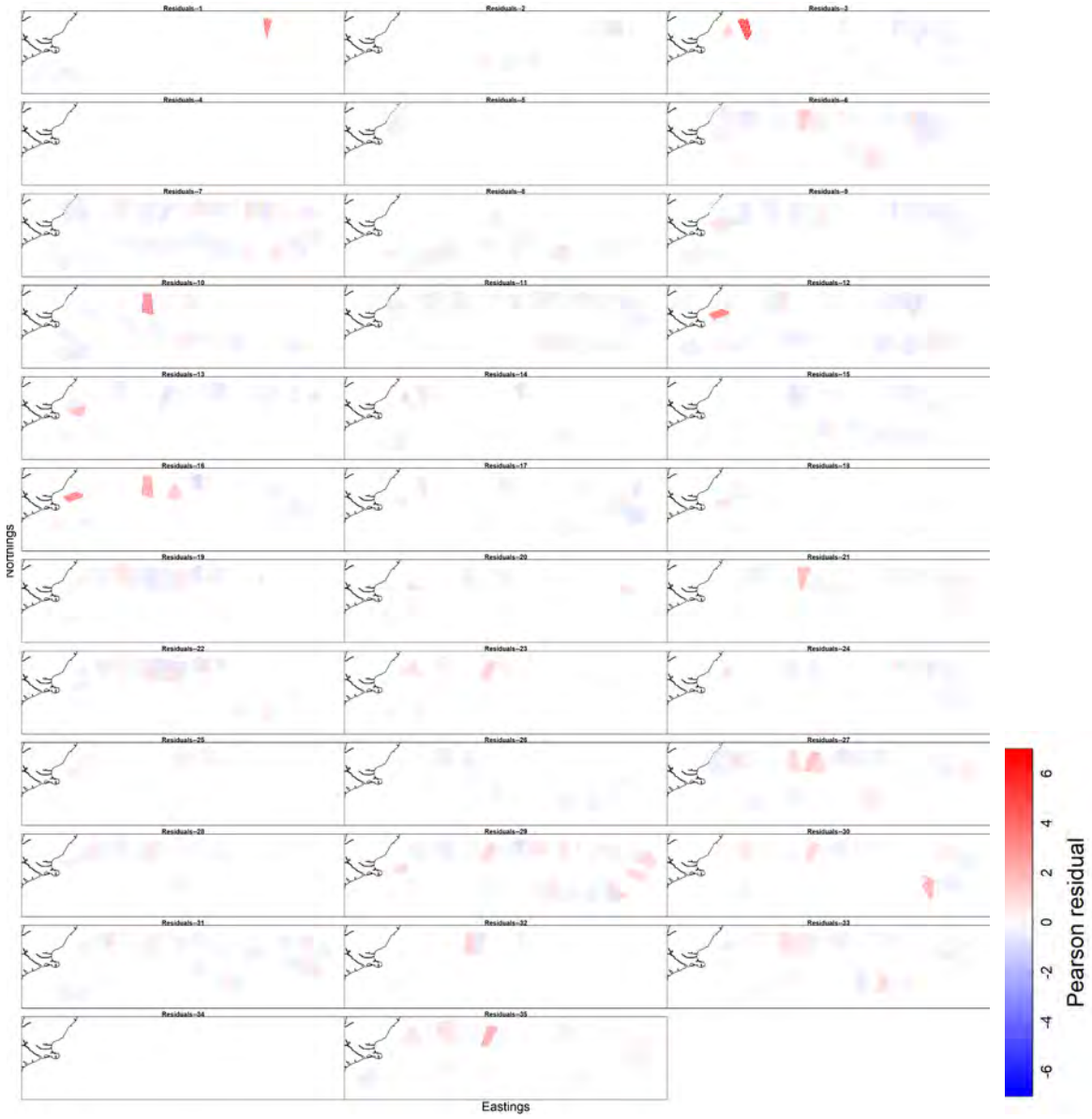

Figure 96: VAST outputs for Pearson residuals (goodness of fit) showing under or over fitting for catch rates of *Centroselachus crepidater* across Chatham Rise (1984–2018, from left to right for each panel).

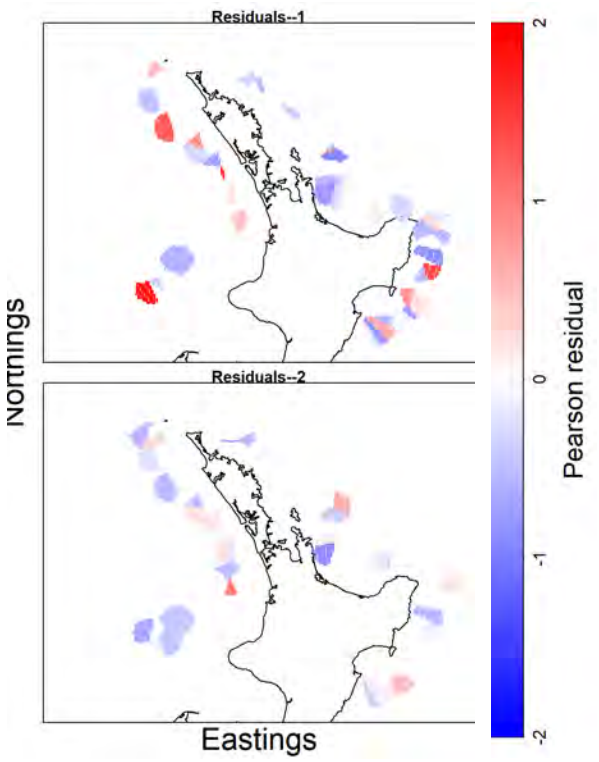

Figure 97: VAST outputs for Pearson residuals (goodness of fit) showing under or over fitting for observer catch rates of *Centroselachus crepidater* around the North Island in 1985–1986.

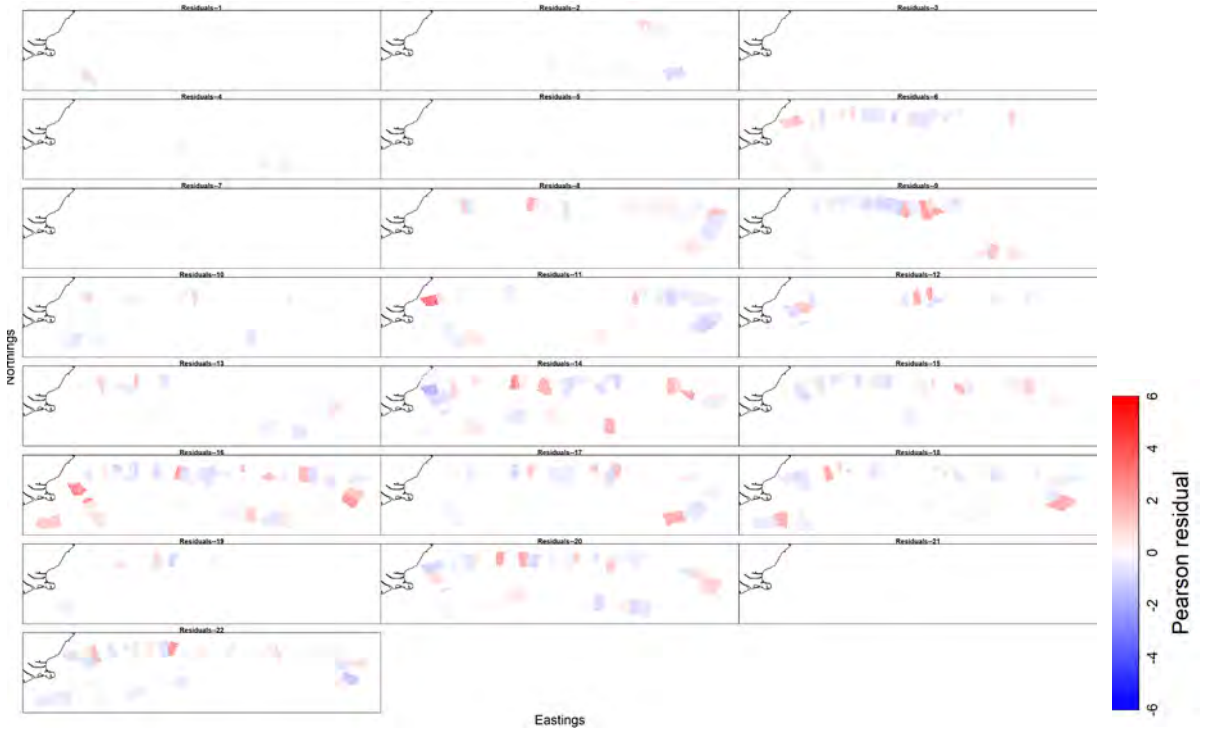

Figure 98: VAST outputs for Pearson residuals (goodness of fit) showing under or over fitting for catch rates of *Centroselachus crepidater* by class across Chatham Rise (1997–2018, from left to right for each panel).

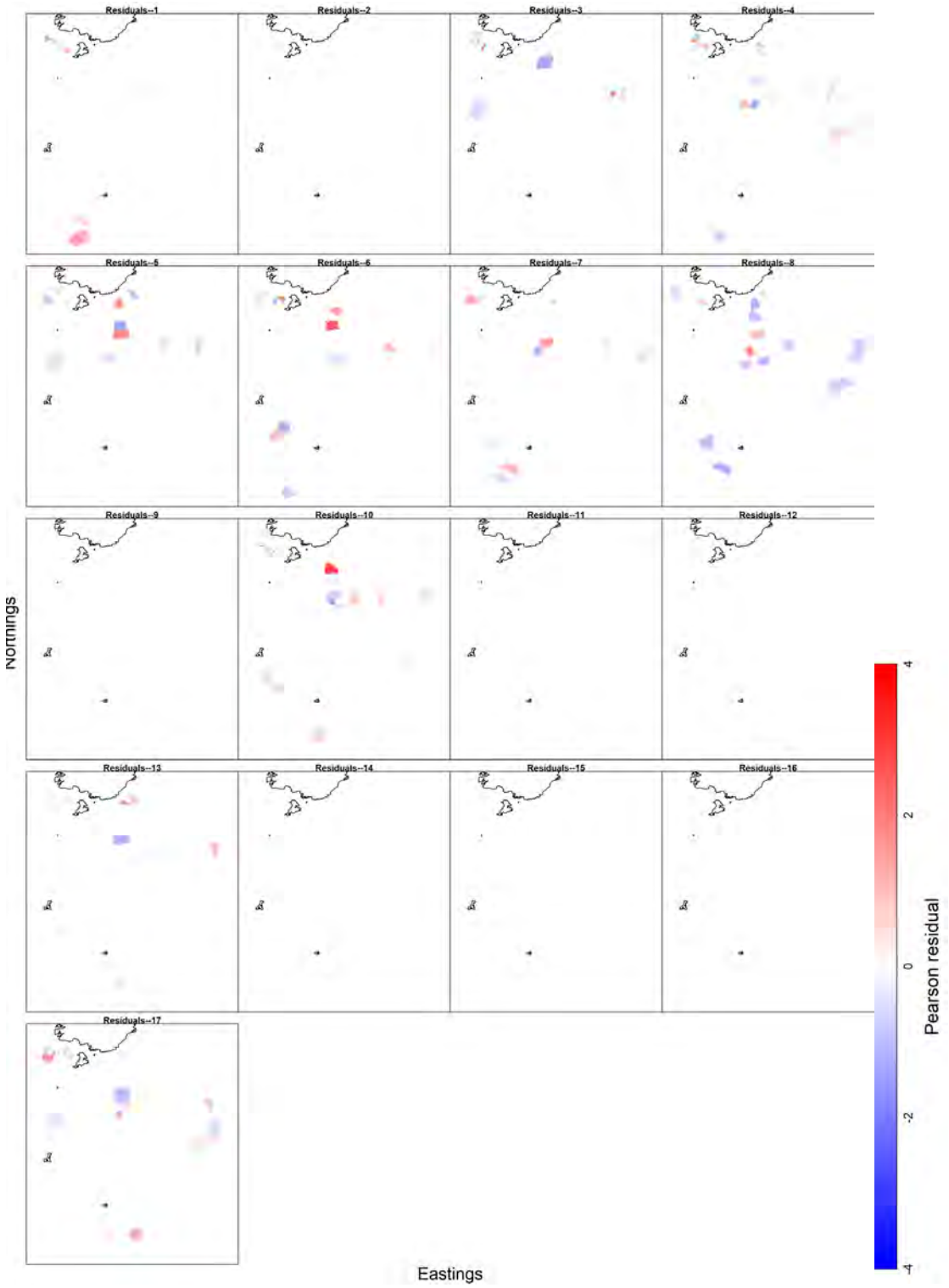

Figure 99: VAST outputs for Pearson residuals (goodness of fit) showing under or over fitting for catch rates of *Centroselachus crepidater* by class across the Sub-Antarctic (2002–2018, from left to right for each panel).

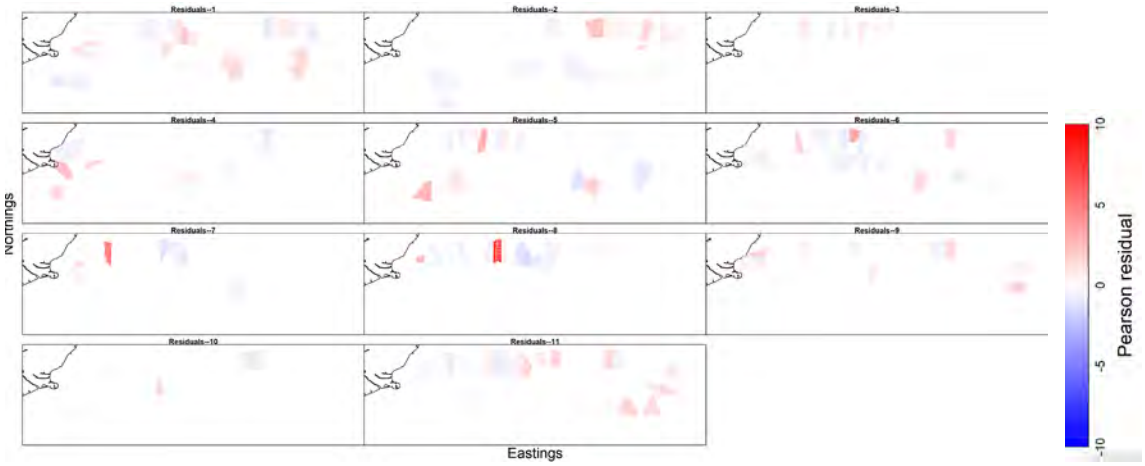

Figure 100: VAST outputs for Pearson residuals (goodness of fit) showing under or over fitting for observer catch rates of *Centroselachus crepidater* across Chatham Rise (2008–2018, from left to right for each panel).

Appendix 9: *Etmopterus granulosus*

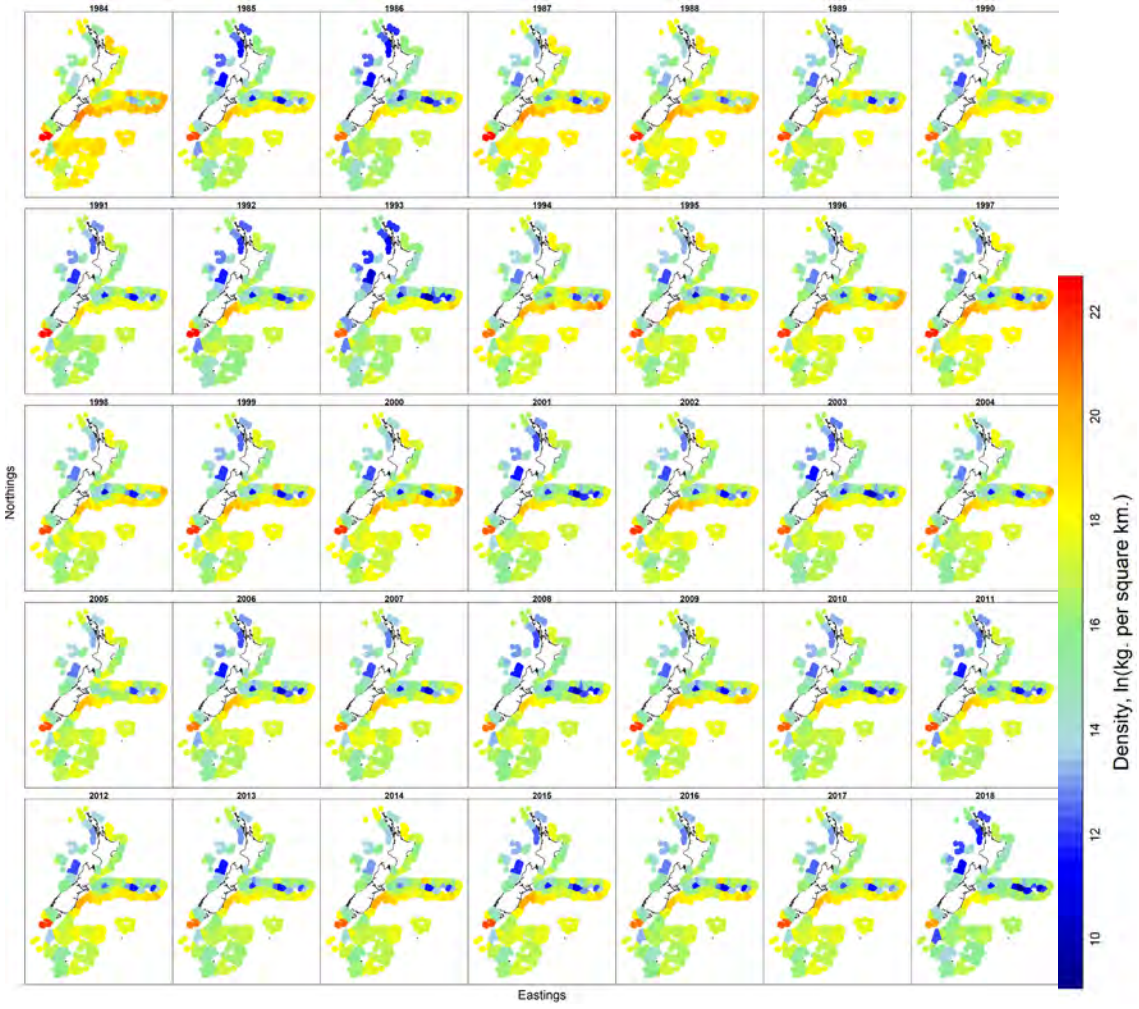

Figure 101:VAST outputs for relative density (kg km^{-2}) of *Etmopterus granulosus* across the New Zealand Exclusive Economic Zone (EEZ) (1984–2018, from left to right for each panel).

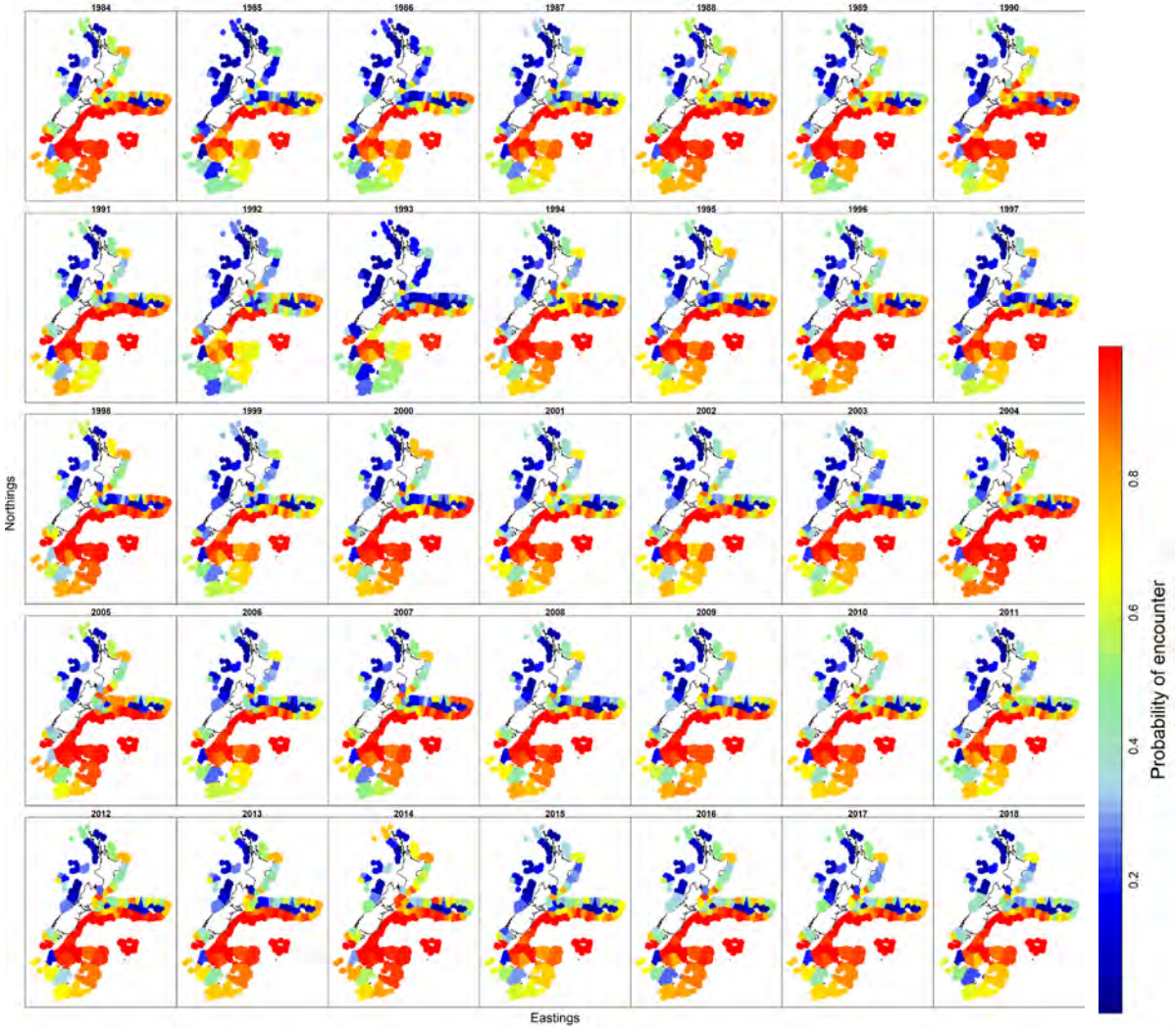

Figure 102:VAST outputs for probability of encounter of *Etmopterus granulosus* across the New Zealand Exclusive Economic Zone (EEZ) (1984–2018, from left to right for each panel).

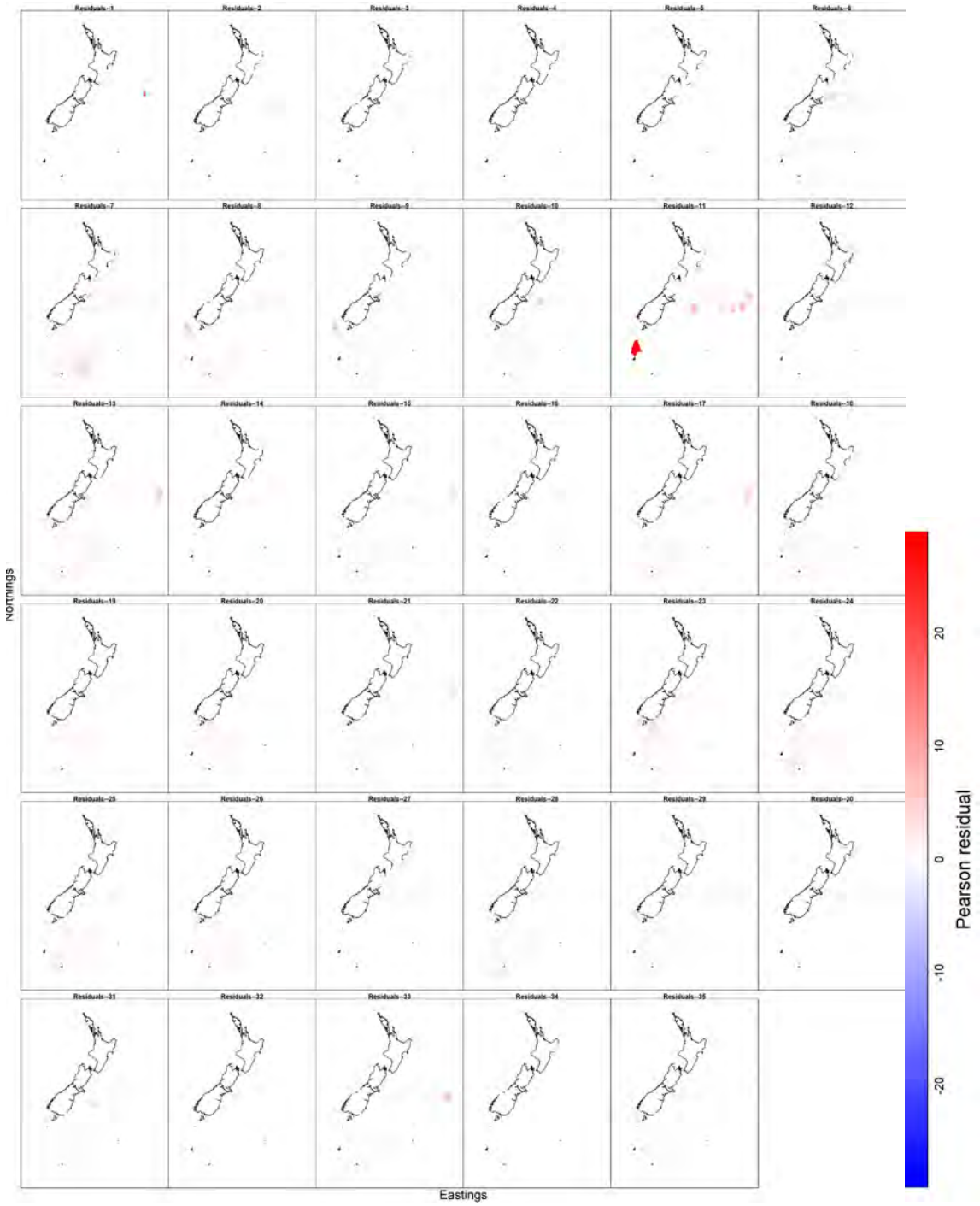

Figure 103: VAST outputs for Pearson residuals (goodness of fit) showing under or over fitting for catch rates of *Etmopterus granulosus* across the New Zealand Exclusive Economic Zone (EEZ) (1984–2018, from left to right for each panel).

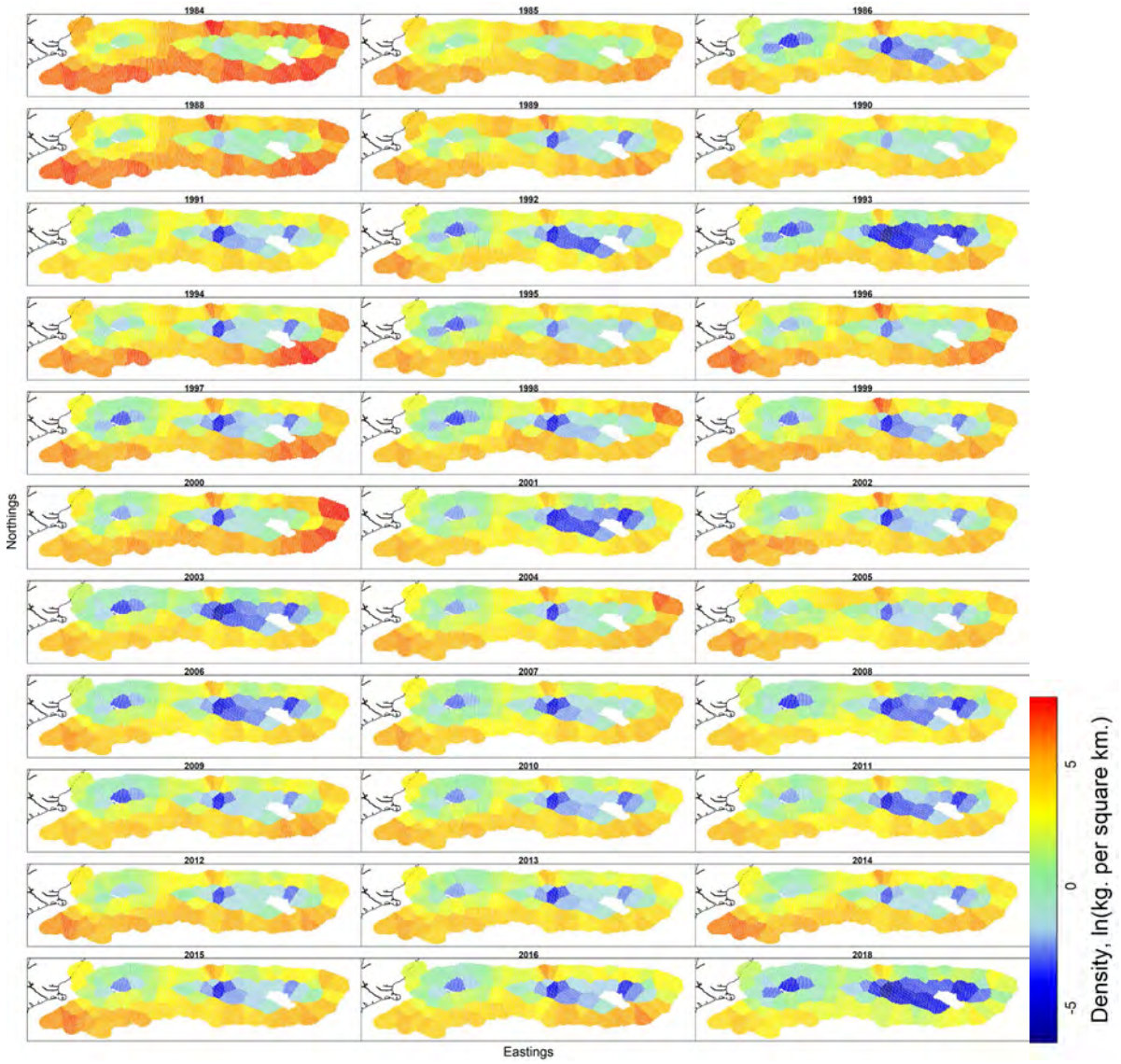

Figure 104:VAST outputs for relative density (kg km^{-2}) of *Etmopterus granulosus* across Chatham Rise (1984–2018, from left to right for each panel).

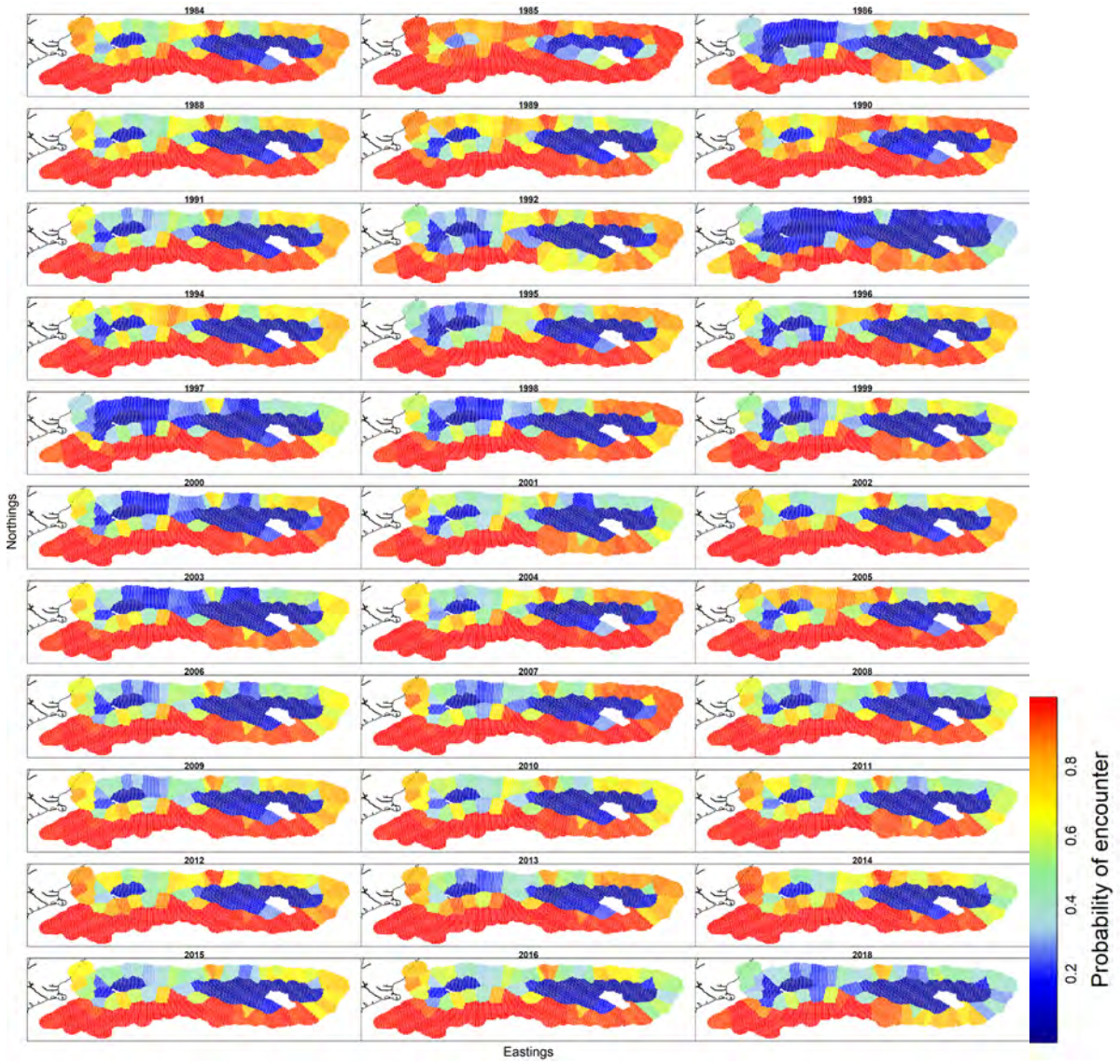

Figure 105:VAST outputs for probability of encounter of *Etmopterus granulosus* across Chatham Rise (1984–2018, from left to right for each panel).

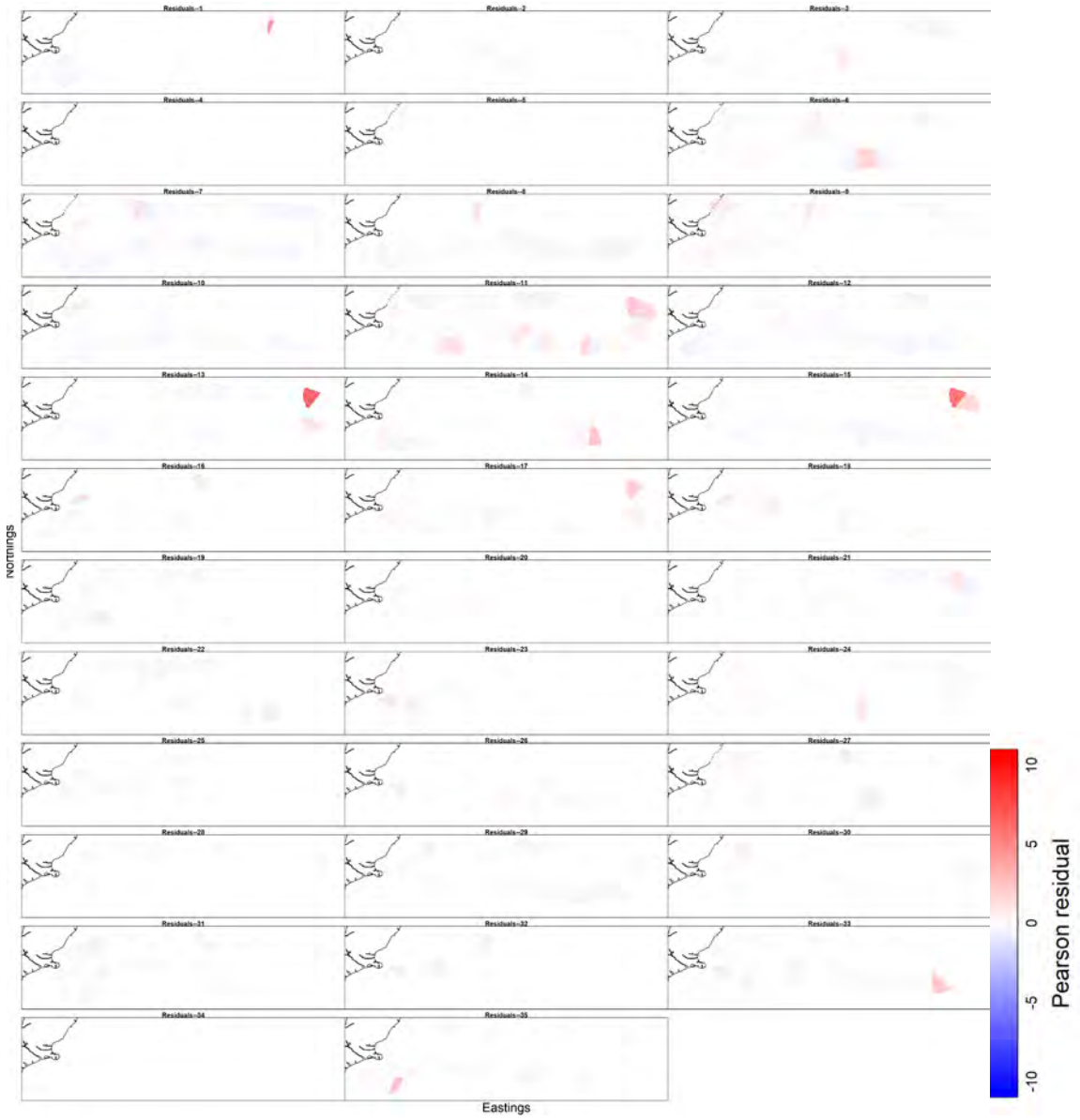

Figure 106: VAST outputs for Pearson residuals (goodness of fit) showing under or over fitting for catch rates of *Etmopterus granulosus* across Chatham Rise (1984–2018, from left to right for each panel).

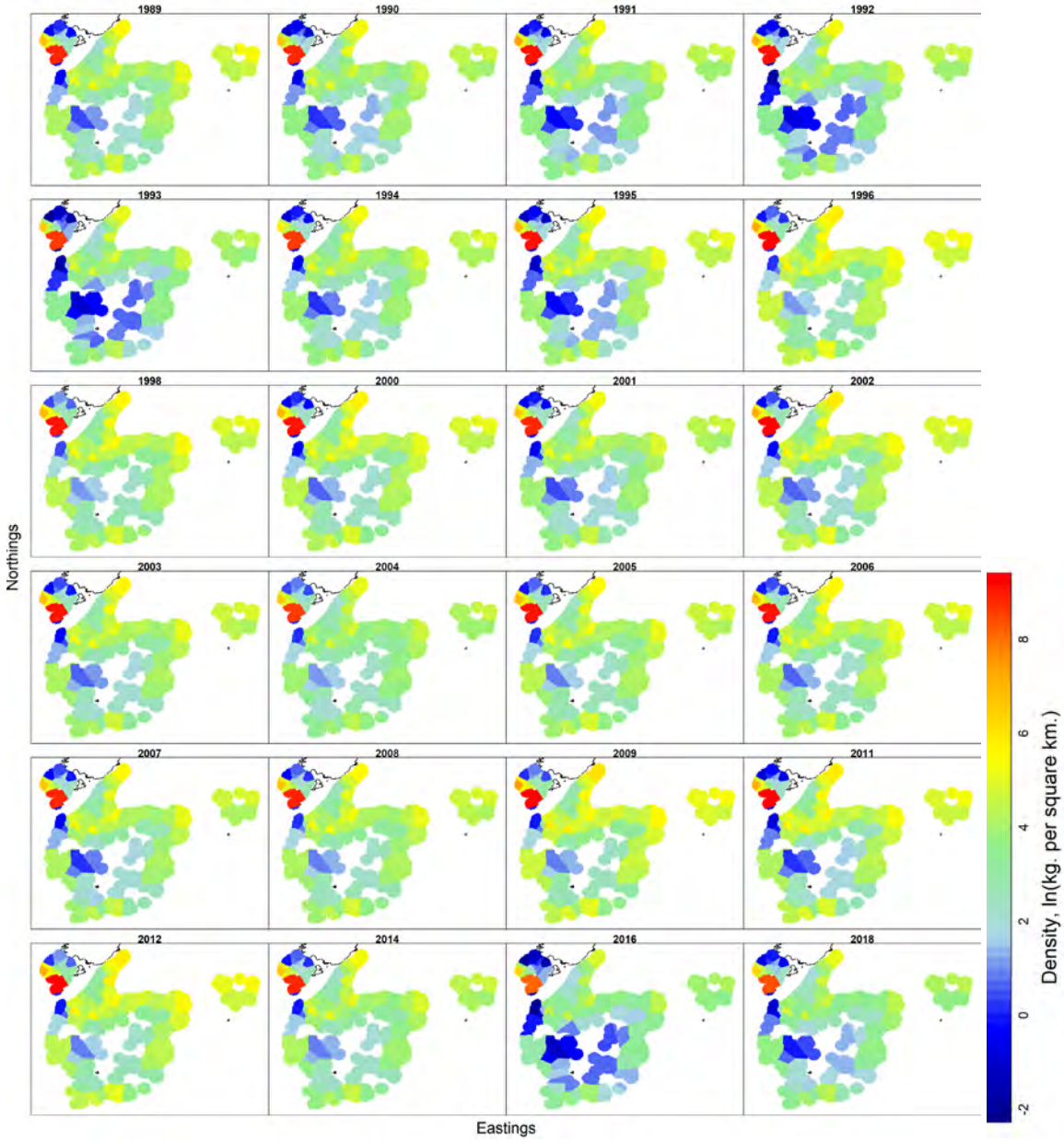

Figure 107: VAST outputs for relative density (kg km^{-2}) of *Etmopterus granulosus* across the Sub-Antarctic (1989–2018, from left to right for each panel).

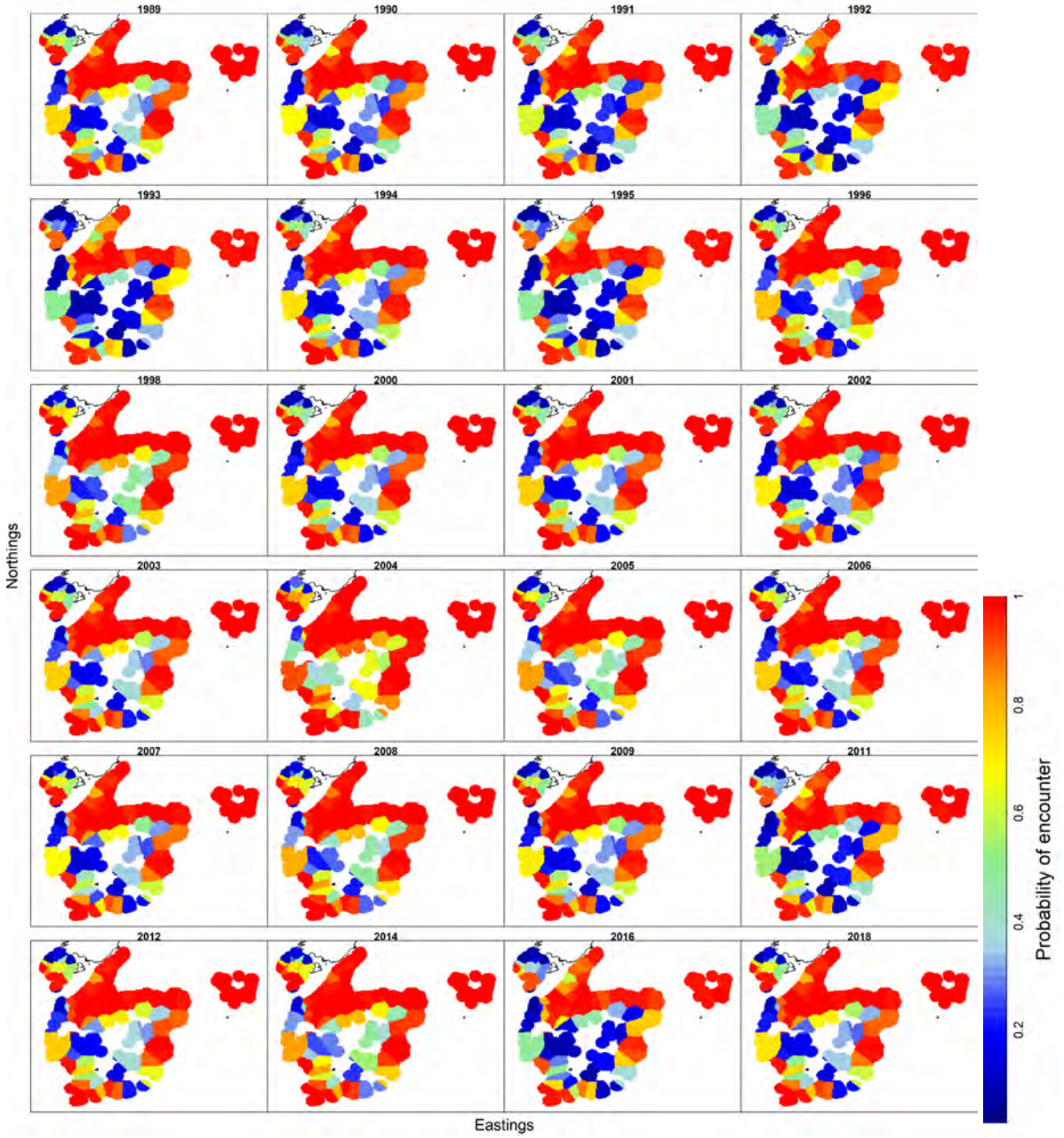

Figure 108: VAST outputs for probability of encounter of *Etmopterus granulosus* across the Sub-Antarctic (1989–2018, from left to right for each panel).

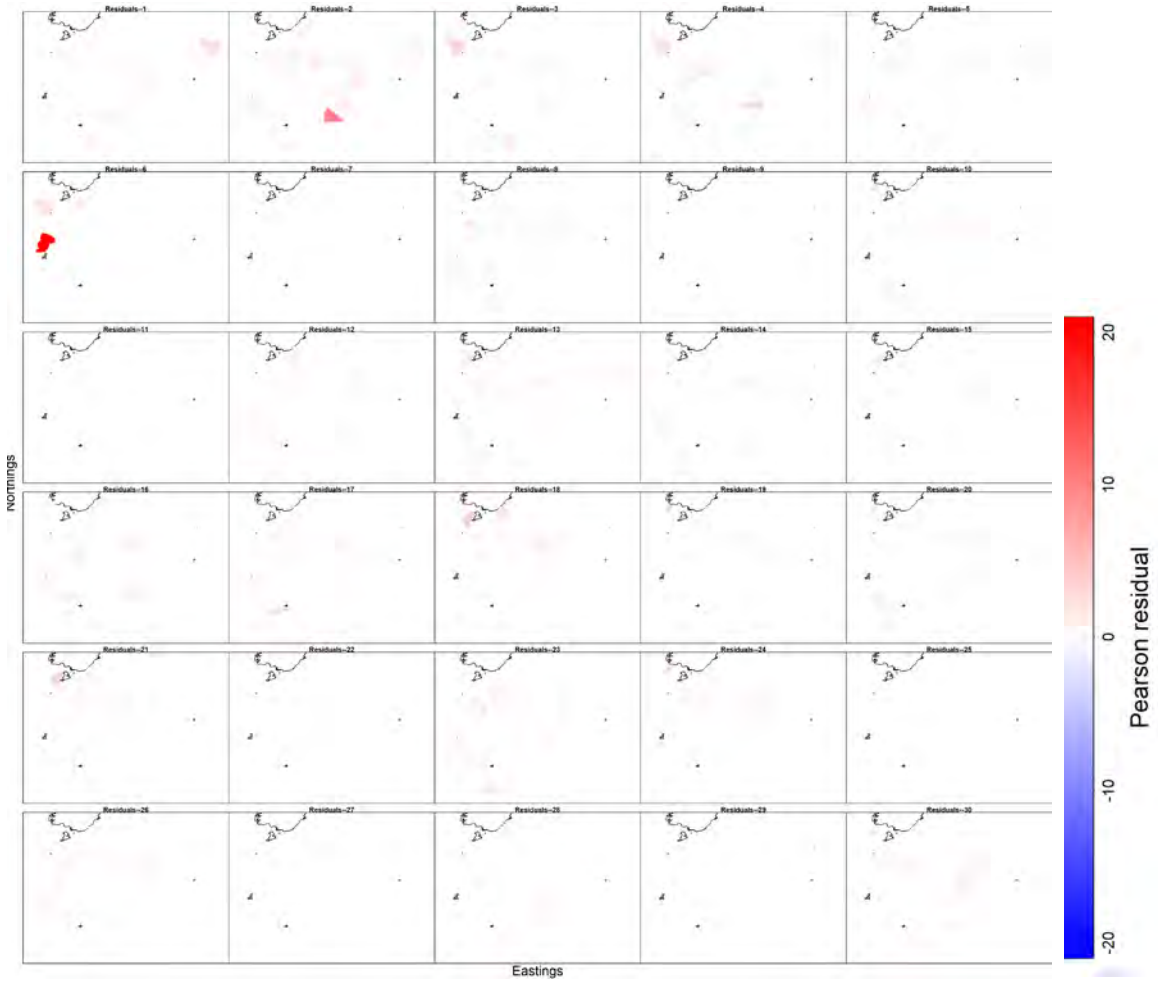

Figure 109: VAST outputs for Pearson residuals (goodness of fit) showing under or over fitting for catch rates of *Etmopterus granulosus* across the Sub-Antarctic (1989–2018, from left to right for each panel).

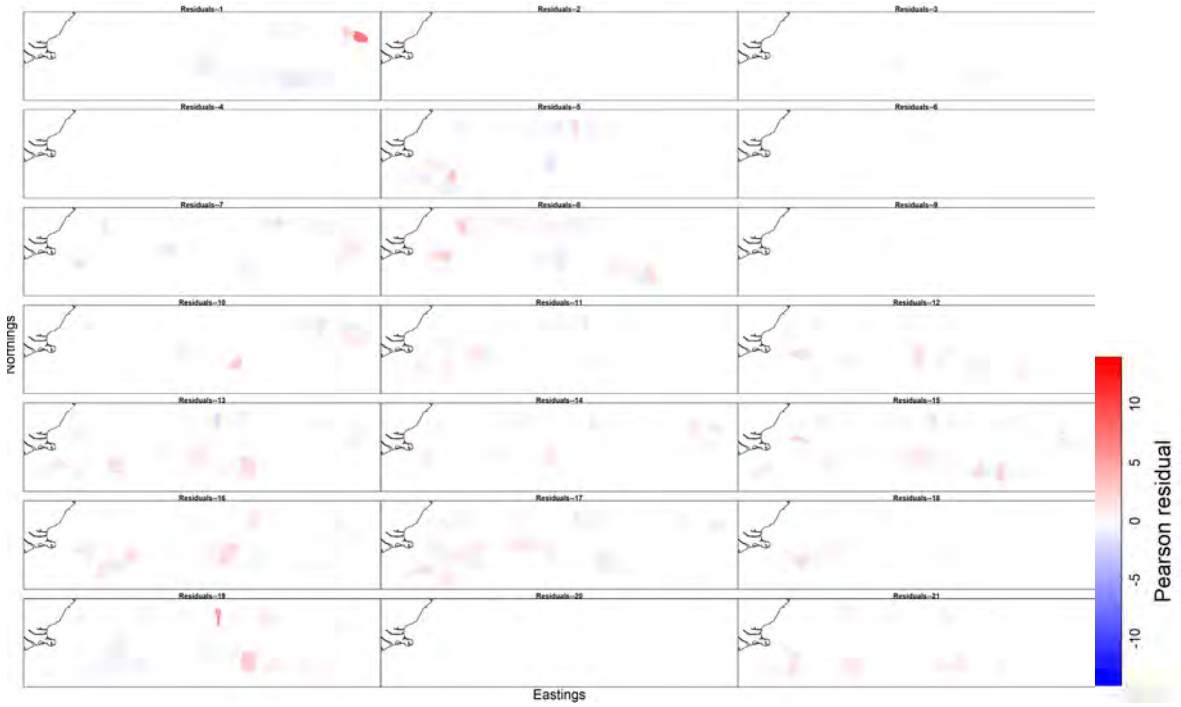

Figure 110: VAST outputs for Pearson residuals (goodness of fit) showing under or over fitting for catch rates of *Etmopterus granulosus* by class across Chatham Rise (1998–2018, from left to right for each panel).

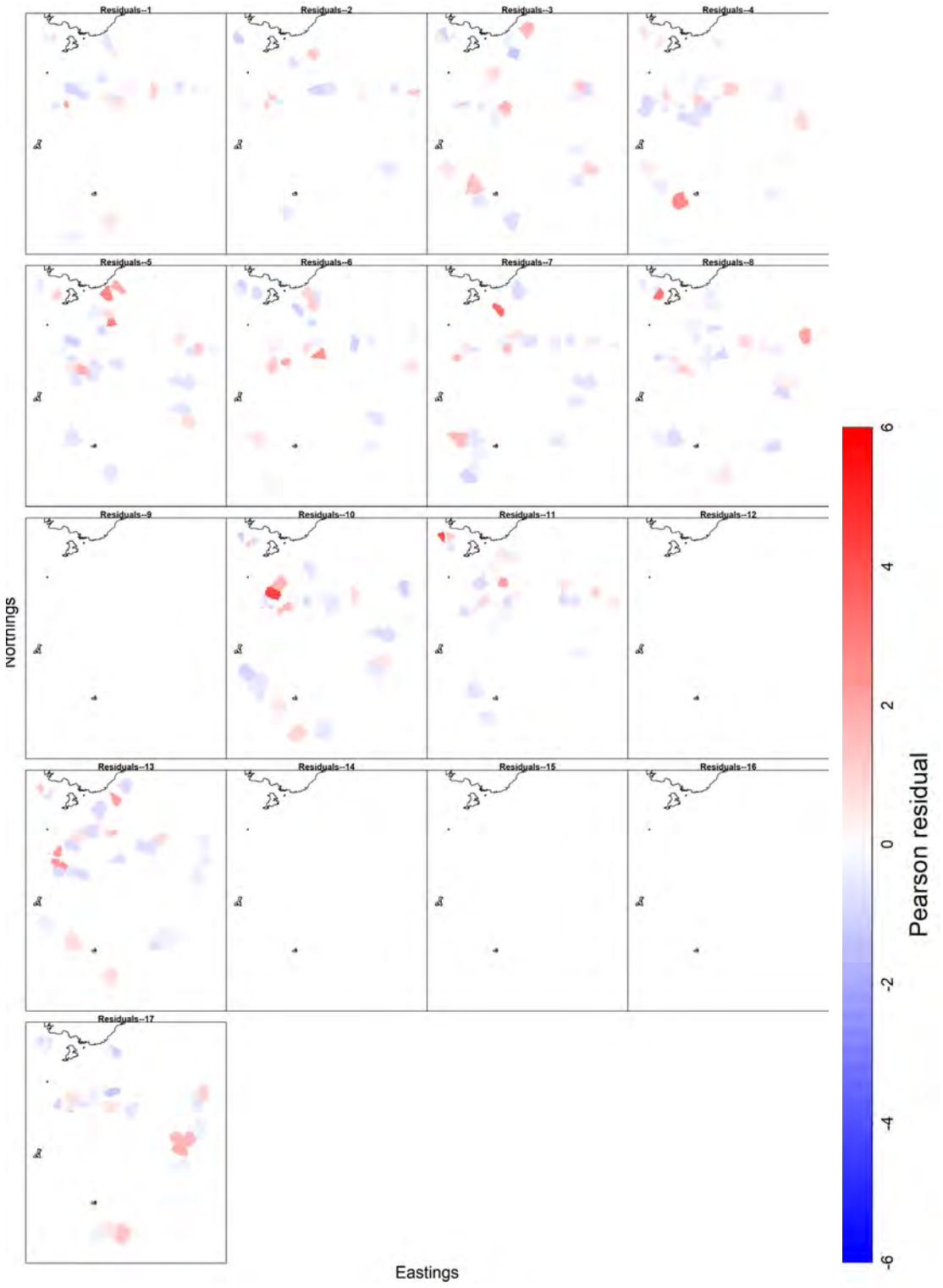

Figure 111: VAST outputs for Pearson residuals (goodness of fit) showing under or over fitting for catch rates of *Etmopterus granulosus* by class across the Sub-Antarctic (2002–2018, from left to right for each panel).

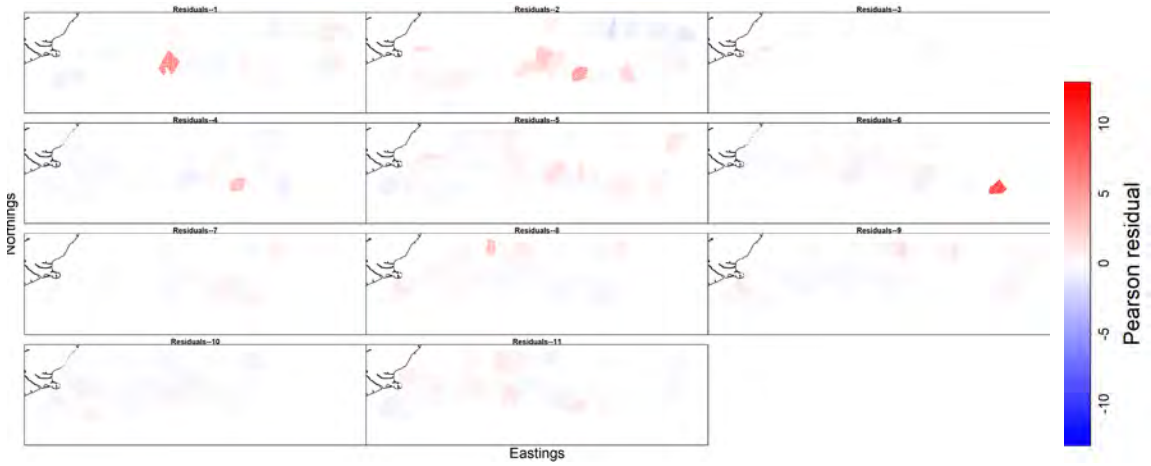

Figure 112: VAST outputs for Pearson residuals (goodness of fit) showing under or over fitting for observer catch rates of *Etmopterus granulosus* across Chatham Rise (2008–2018, from left to right for each panel).

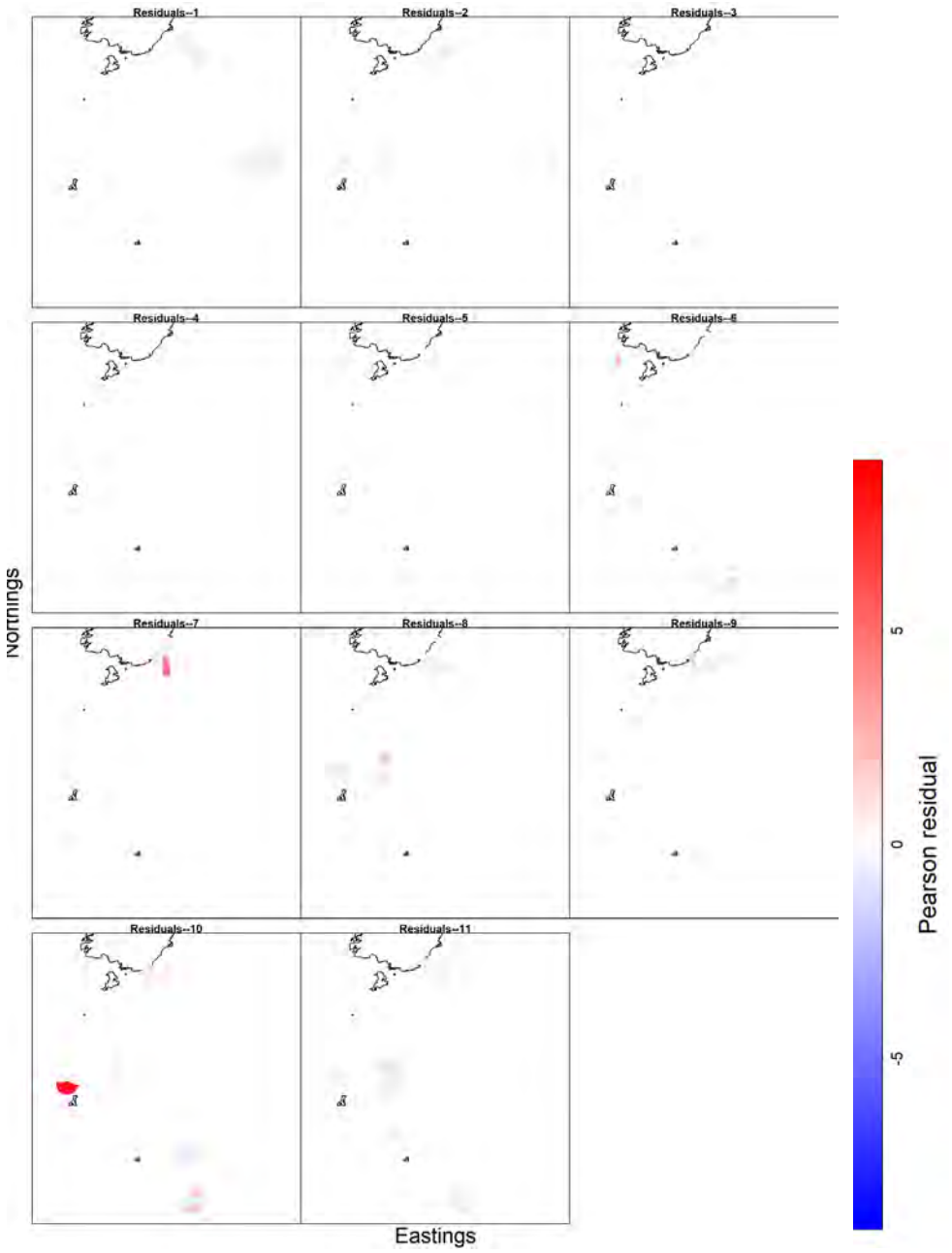

Figure 113: VAST outputs for Pearson residuals (goodness of fit) showing under or over fitting for observer catch rates of *Etmopterus granulosus* across the Sub-Antarctic (2008–2018, from left to right for each panel).

Appendix 10: *Scymnodon plunketi*

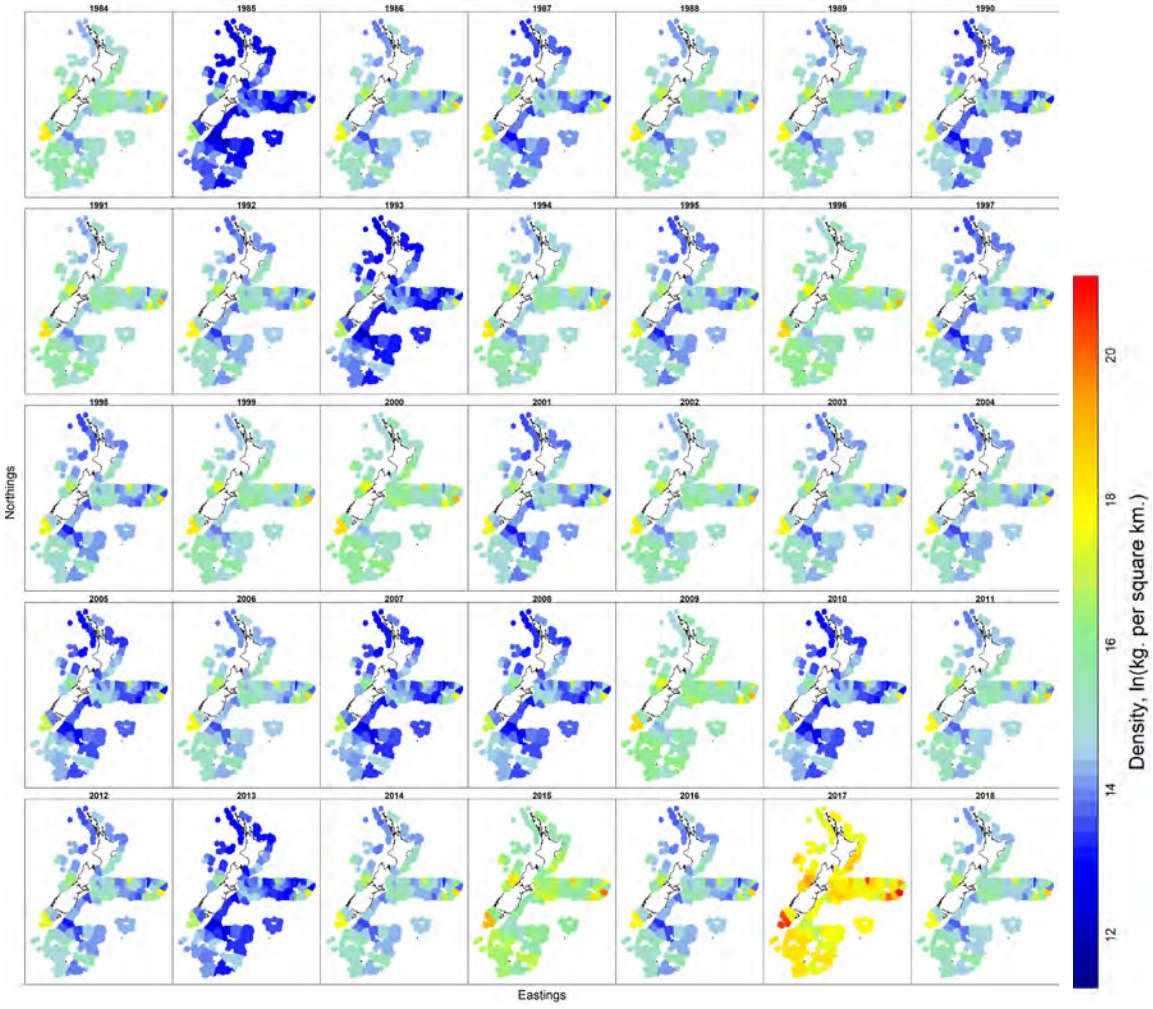

Figure 114:VAST outputs for relative density (kg km^{-2}) of *Scymnodon plunketi* across the New Zealand Exclusive Economic Zone (EEZ) (1984–2018, from left to right for each panel).

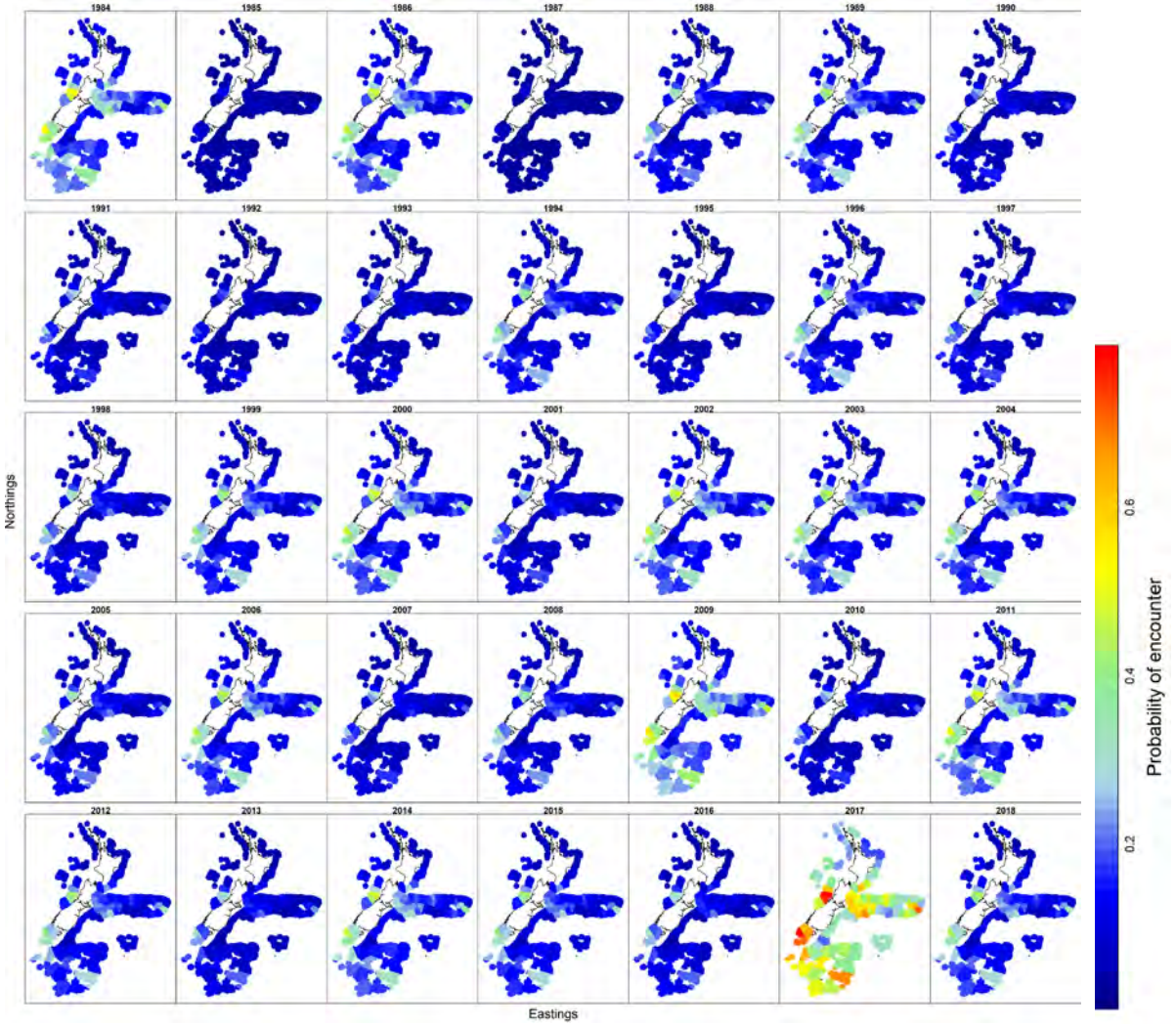

Figure 115:VAST outputs for probability of encounter of *Scymnodon plunketi* across the New Zealand Exclusive Economic Zone (EEZ) (1984–2018, from left to right for each panel).

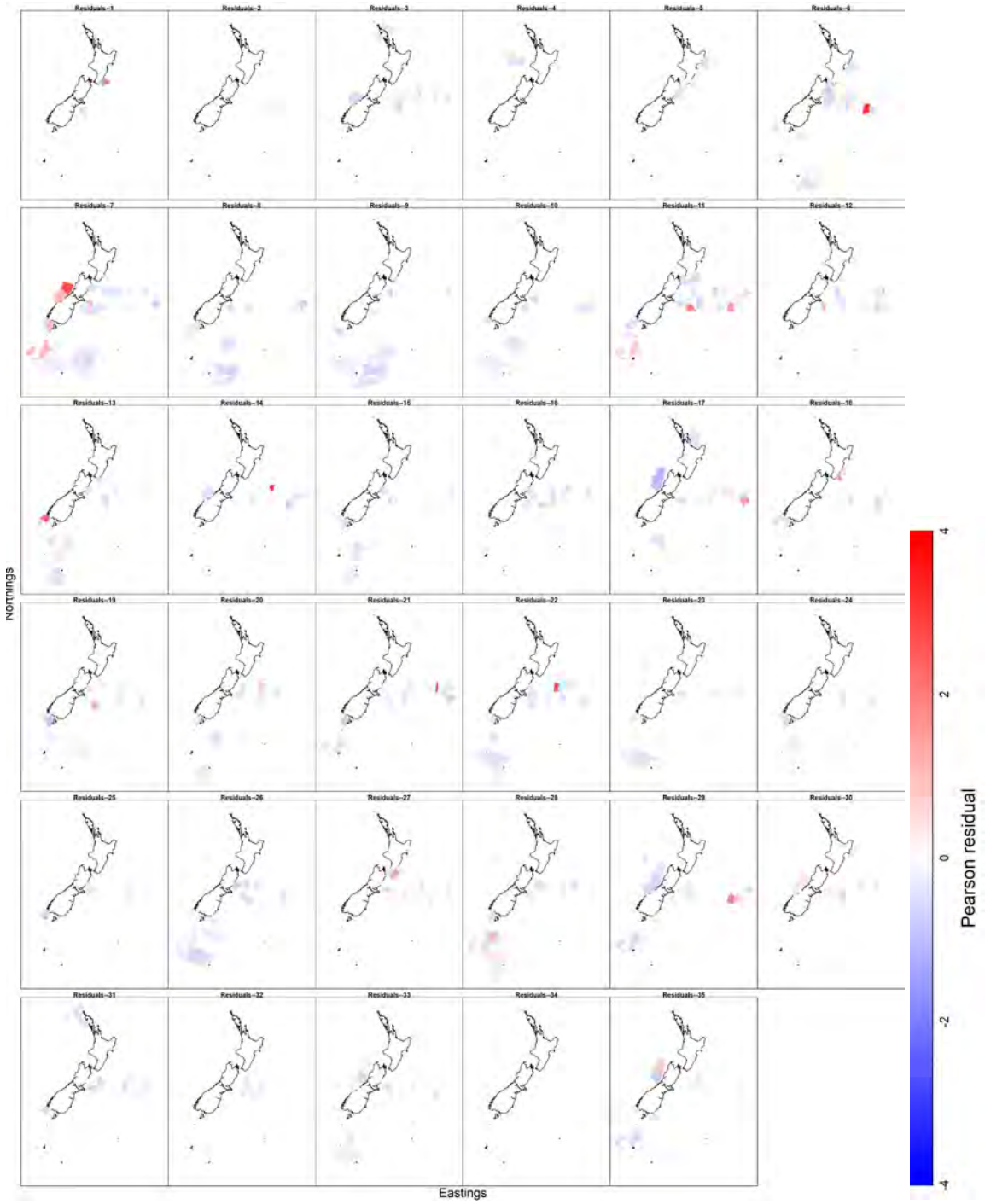

Figure 116: VAST outputs for Pearson residuals (goodness of fit) showing under or over fitting for catch rates of *Scymnodon plunketi* across the New Zealand Exclusive Economic Zone (EEZ) (1984–2018, from left to right for each panel).

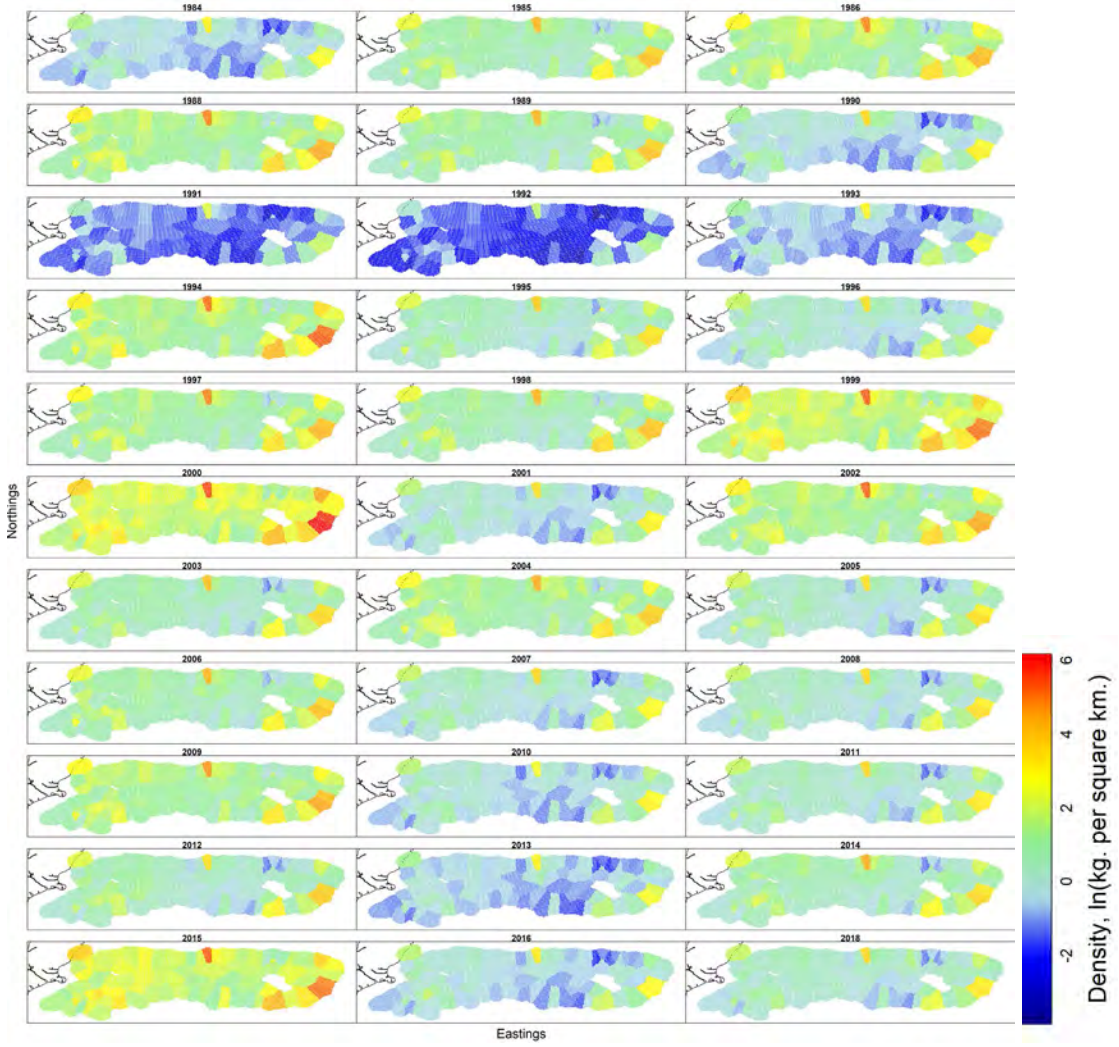

Figure 117:VAST outputs for relative density (kg km^{-2}) of *Scymnodon plunketi* across Chatham Rise (1984–2018, from left to right for each panel).

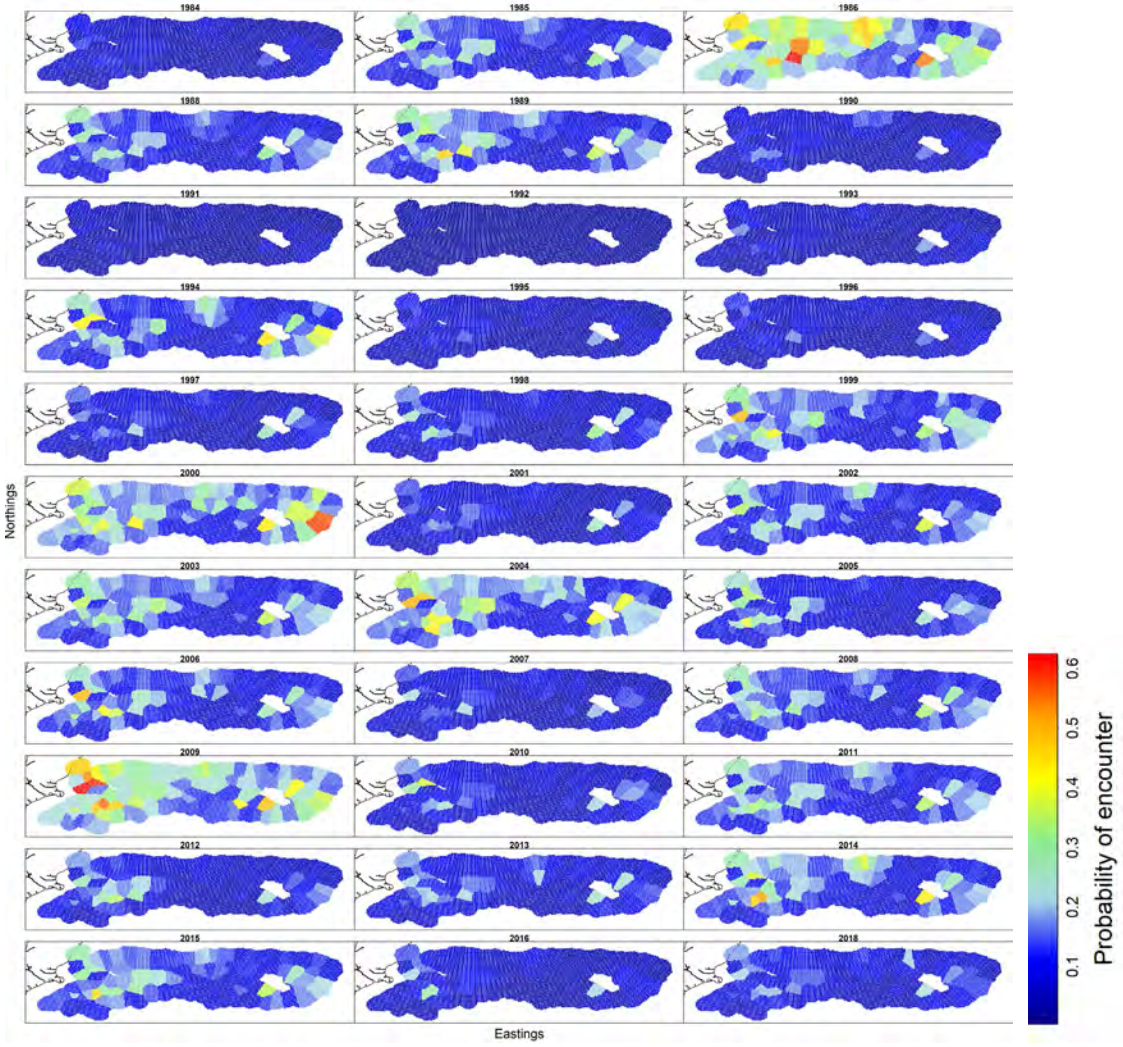

Figure 118:VAST outputs for probability of encounter of *Scymnodon plunketi* across Chatham Rise (1984–2018, from left to right for each panel).

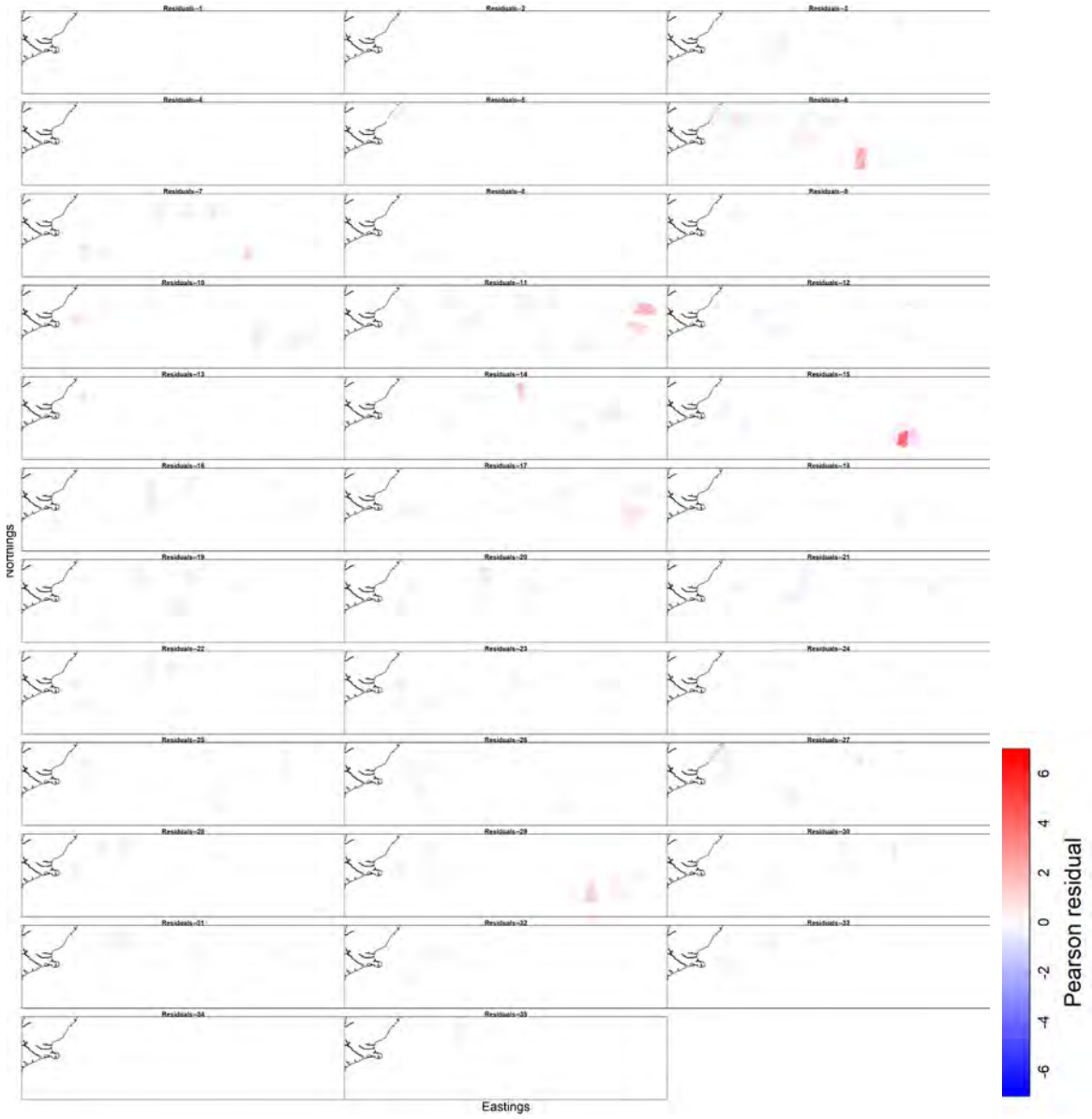

Figure 119:VAST outputs for Pearson residuals (goodness of fit) showing under or over fitting for catch rates of *Scymnodon plunketi* across Chatham Rise (1984–2018, from left to right for each panel).

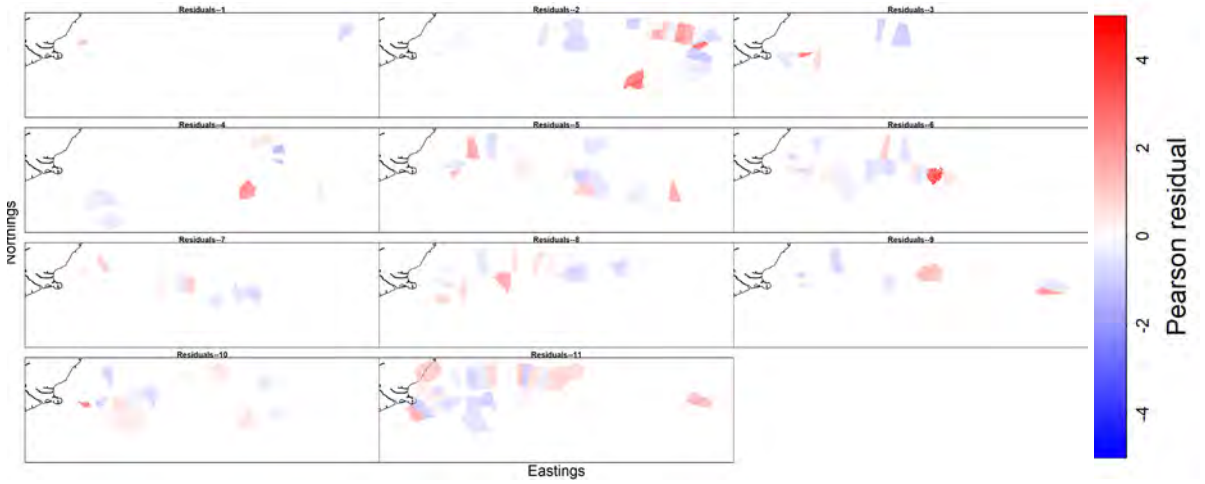

Figure 120: VAST outputs for Pearson residuals (goodness of fit) showing under or over fitting for observer catch rates of *Scymnodon plunketi* across Chatham Rise (2008–2018, from left to right for each panel).

Appendix 11: *Deania calcea*

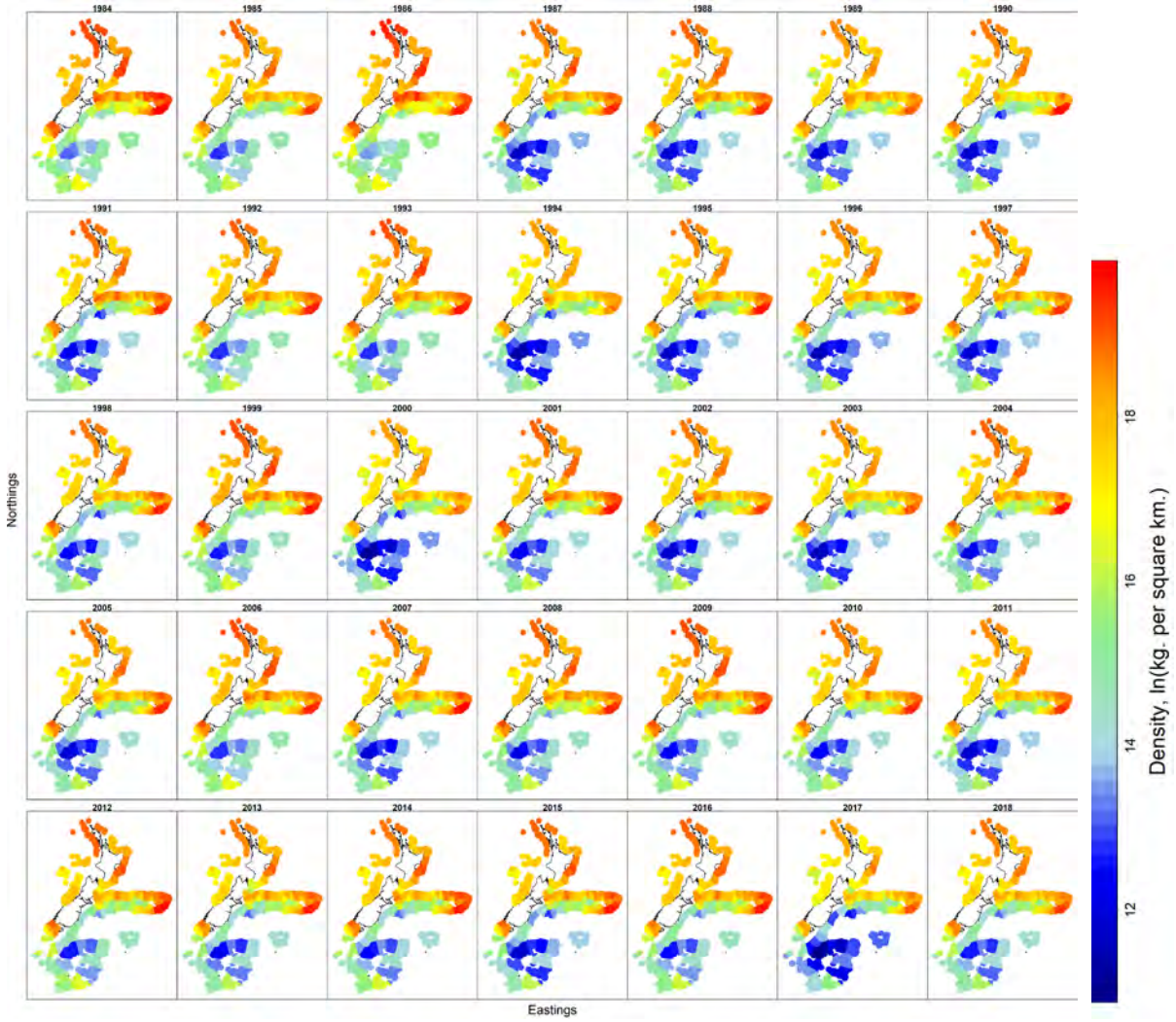

Figure 121:VAST outputs for relative density (kg km^{-2}) of *Deania calcea* across the New Zealand Exclusive Economic Zone (EEZ) (1984–2018, from left to right for each panel).

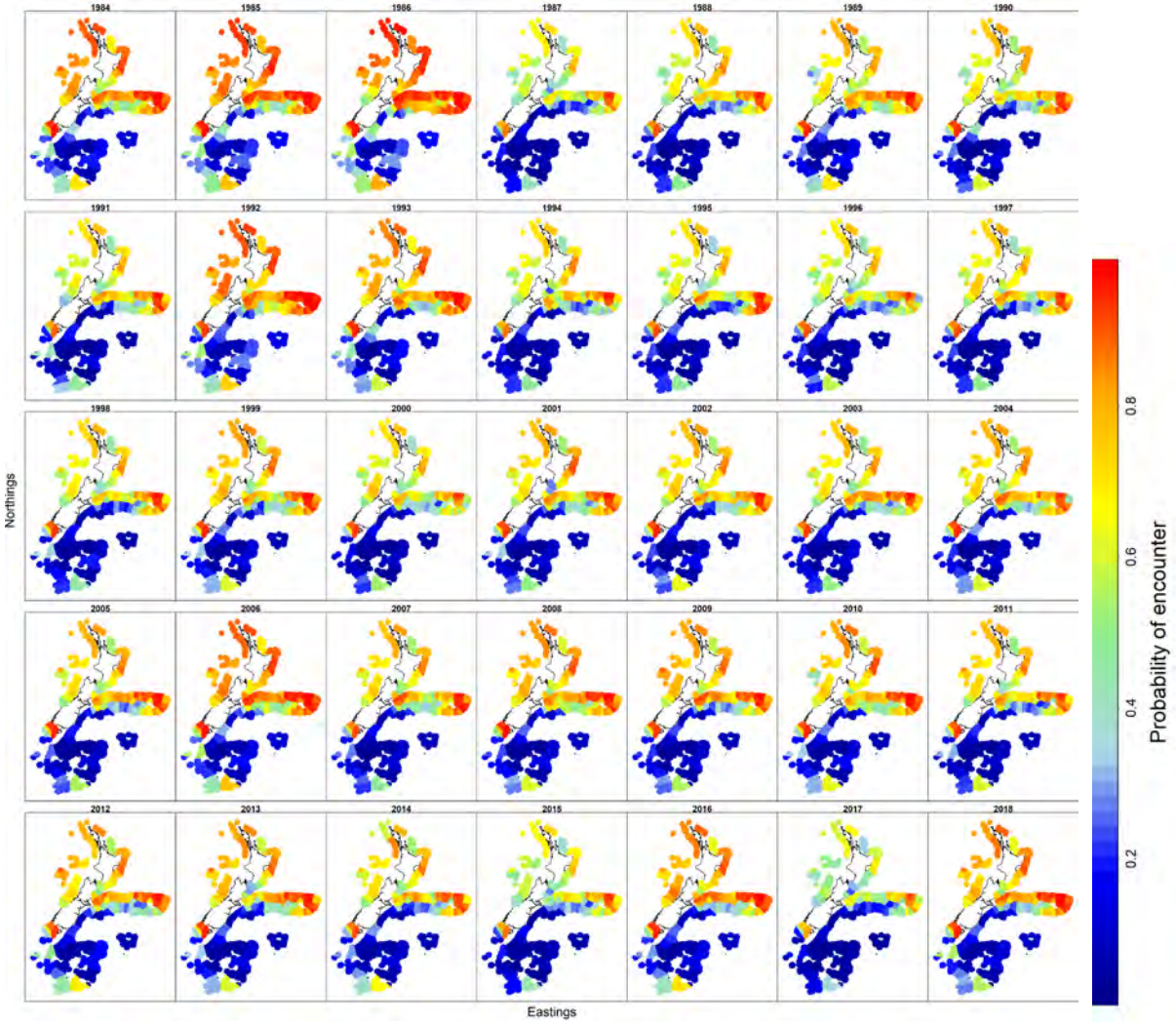

Figure 122: VAST outputs for probability of encounter of *Deania calcea* across the New Zealand Exclusive Economic Zone (EEZ) (1984–2018, from left to right for each panel).

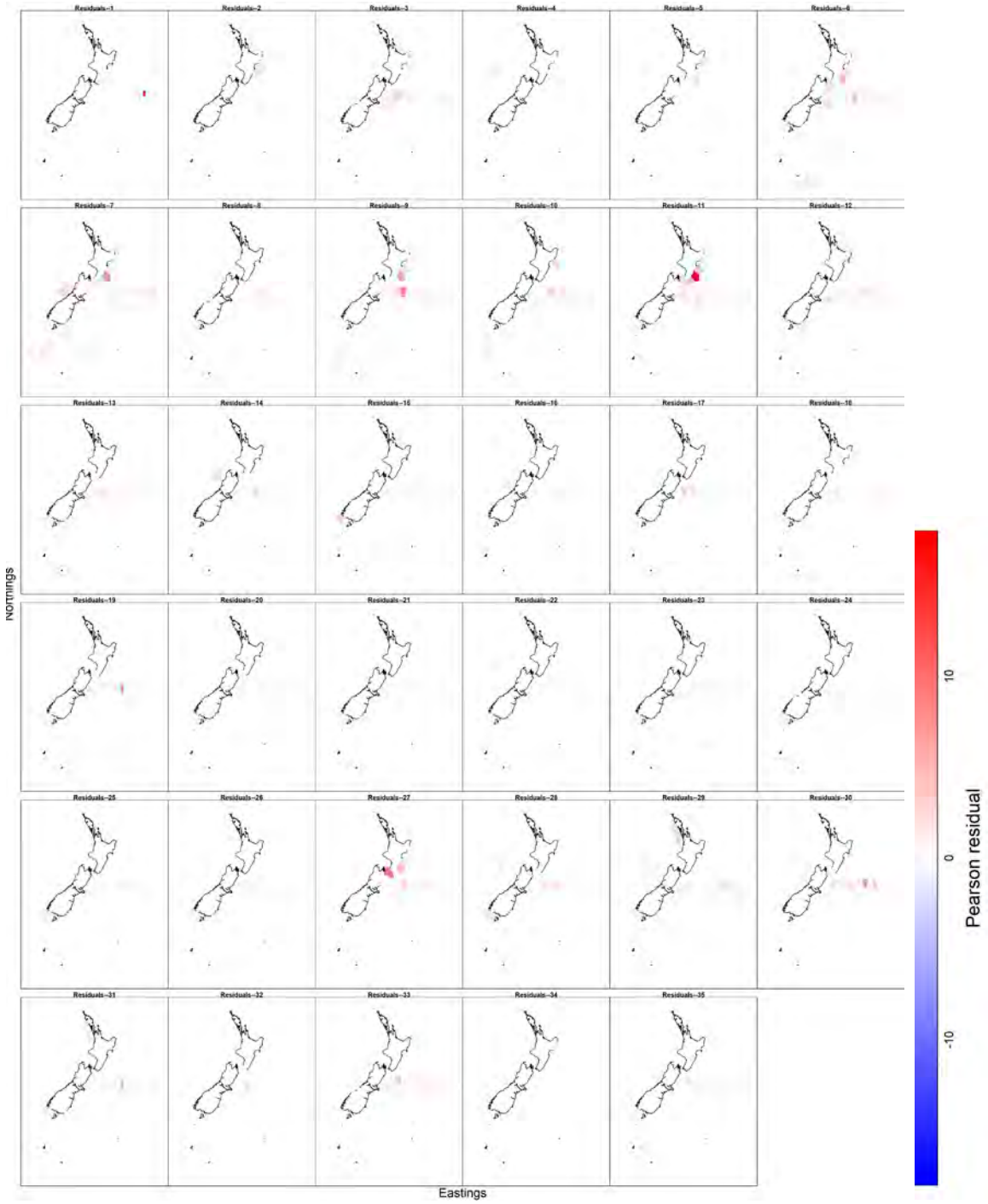

Figure 123: VAST outputs for Pearson residuals (goodness of fit) showing under or over fitting for catch rates of *Deania calcea* across the New Zealand Exclusive Economic Zone (EEZ) (1984–2018, from left to right for each panel).

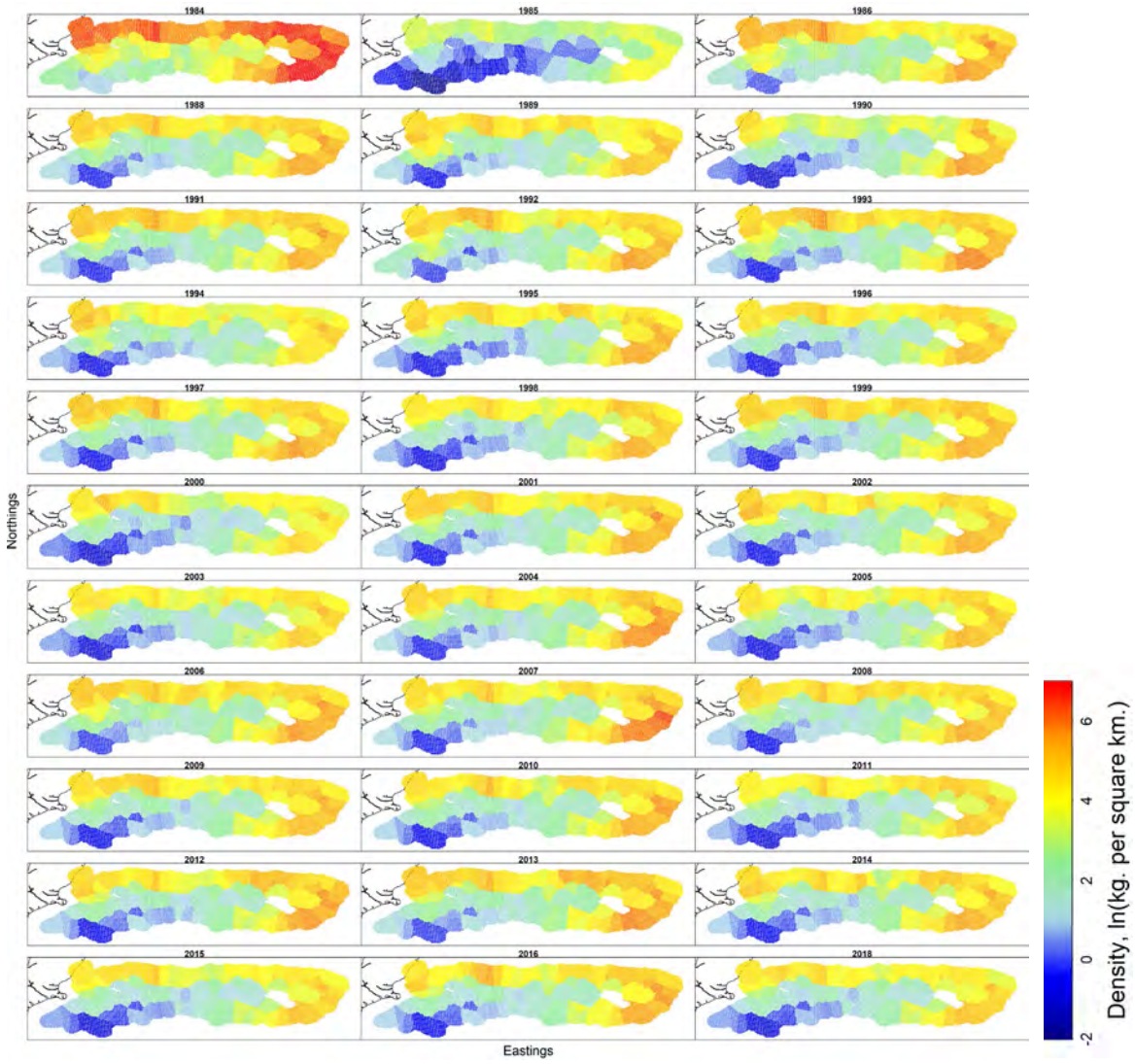

Figure 124: VAST outputs for relative density (kg km^{-2}) of *Deania calcea* across Chatham Rise (1984–2018, from left to right for each panel).

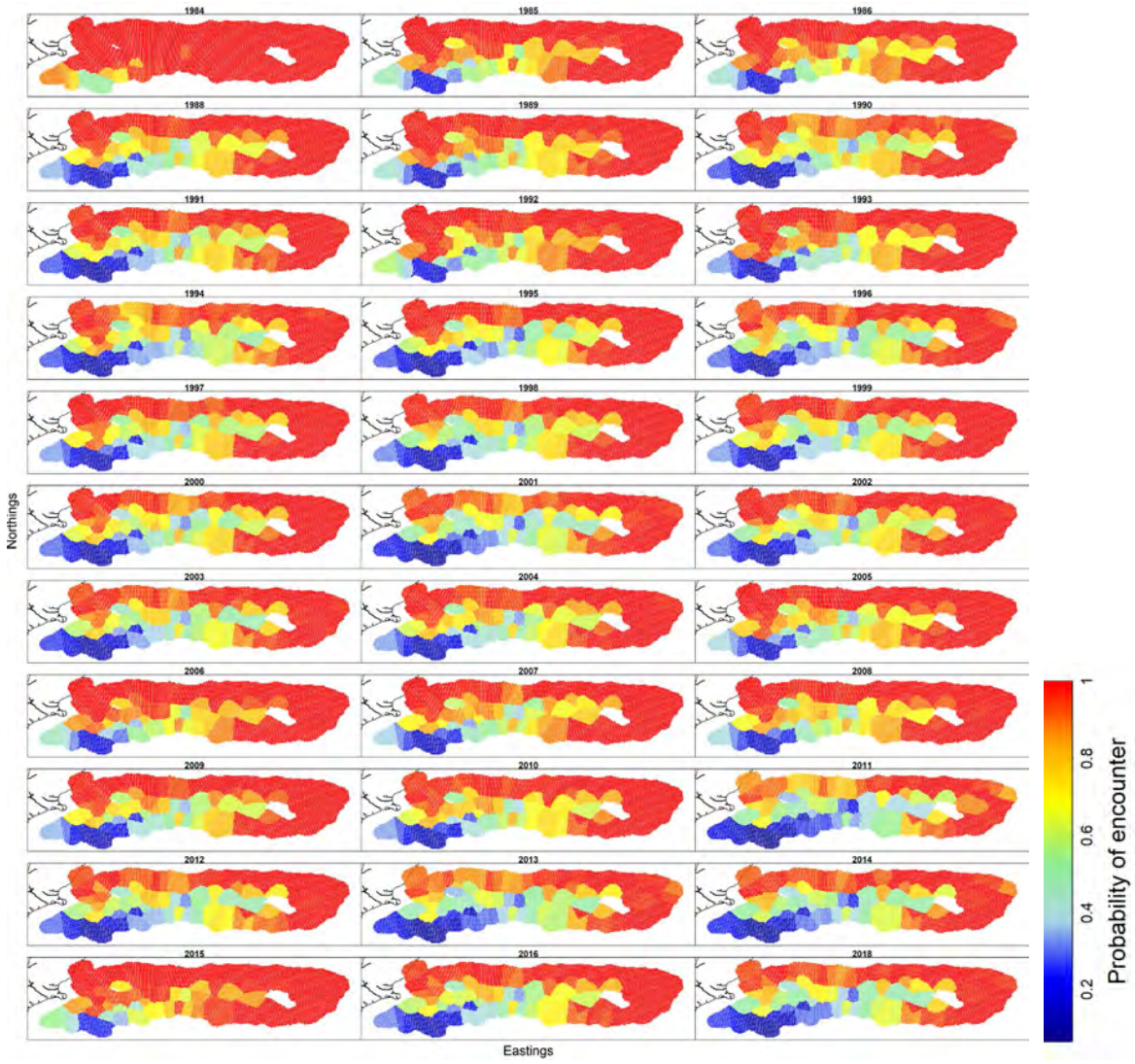

Figure 125: VAST outputs for probability of encounter of *Deania calcea* across Chatham Rise (1984–2018, from left to right for each panel).

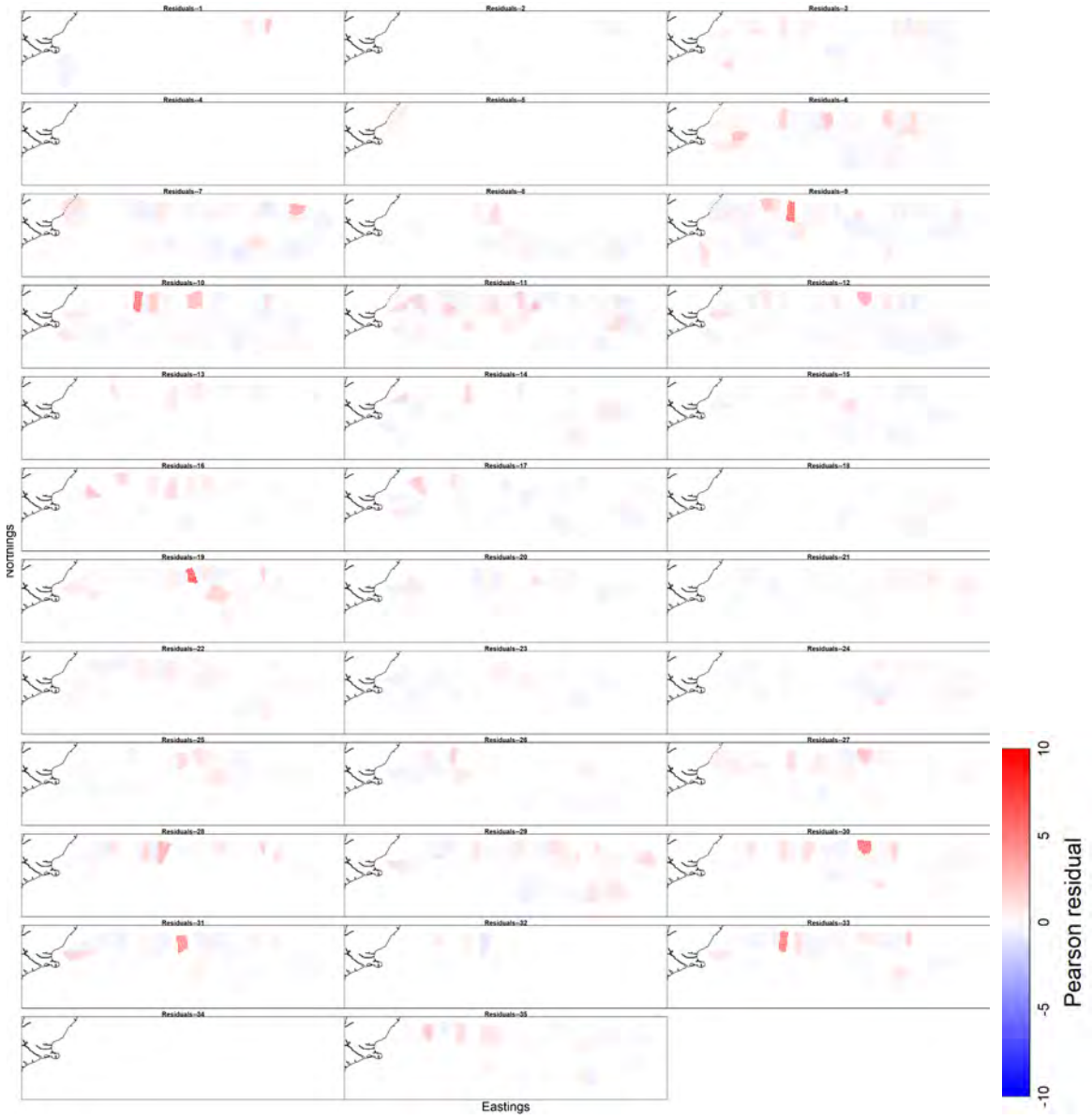

Figure 126: VAST outputs for Pearson residuals (goodness of fit) showing under or over fitting for catch rates of *Deania calcea* across Chatham Rise (1984–2018, from left to right for each panel).

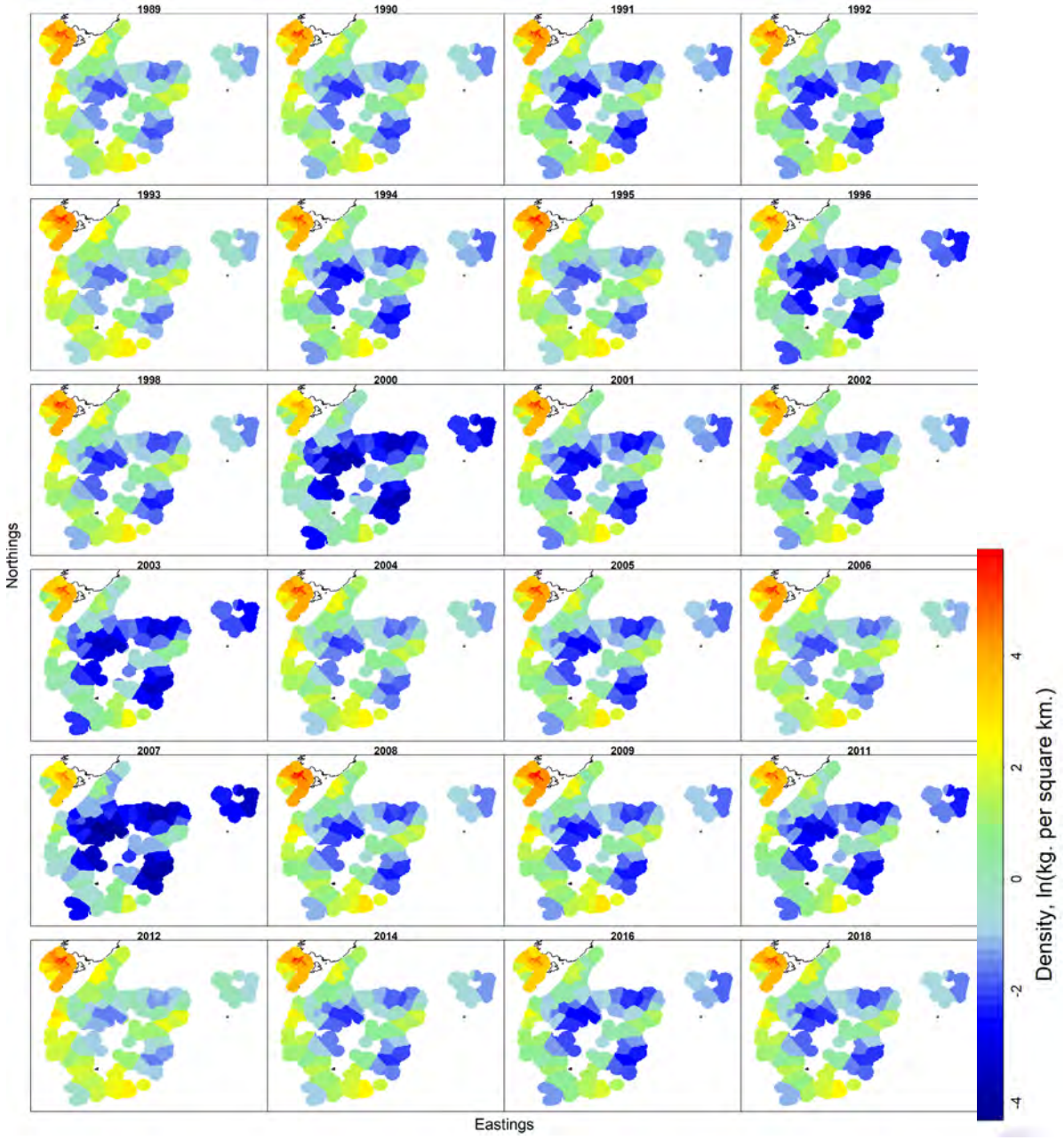

Figure 127:VAST outputs for relative density (kg km^{-2}) of *Deania calcea* across the Sub-Antarctic (1989–2018, from left to right for each panel).

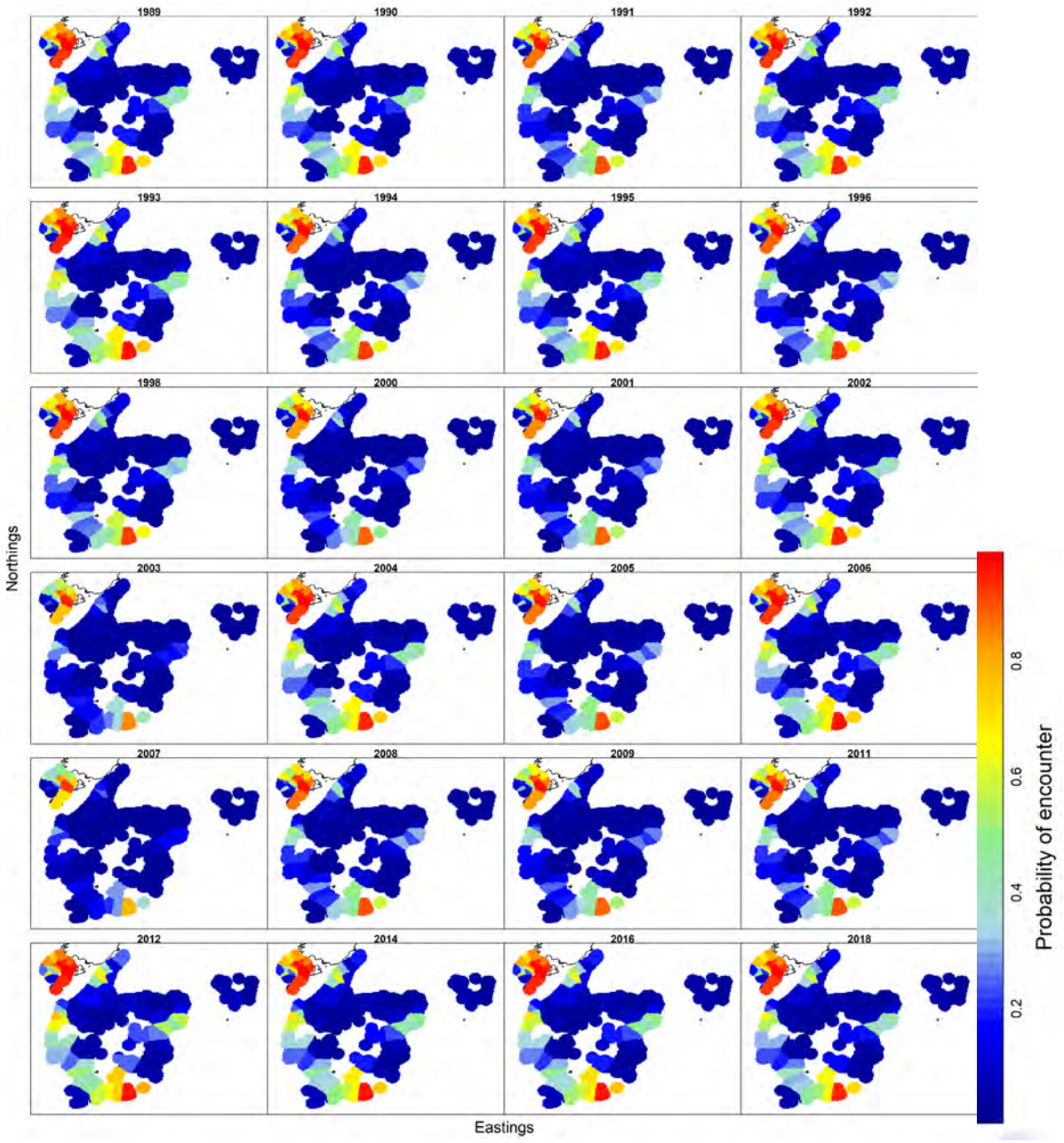

Figure 128:VAST outputs for probability of encounter of *Deania calcea* across the Sub-Antarctic (1989–2018, from left to right for each panel).

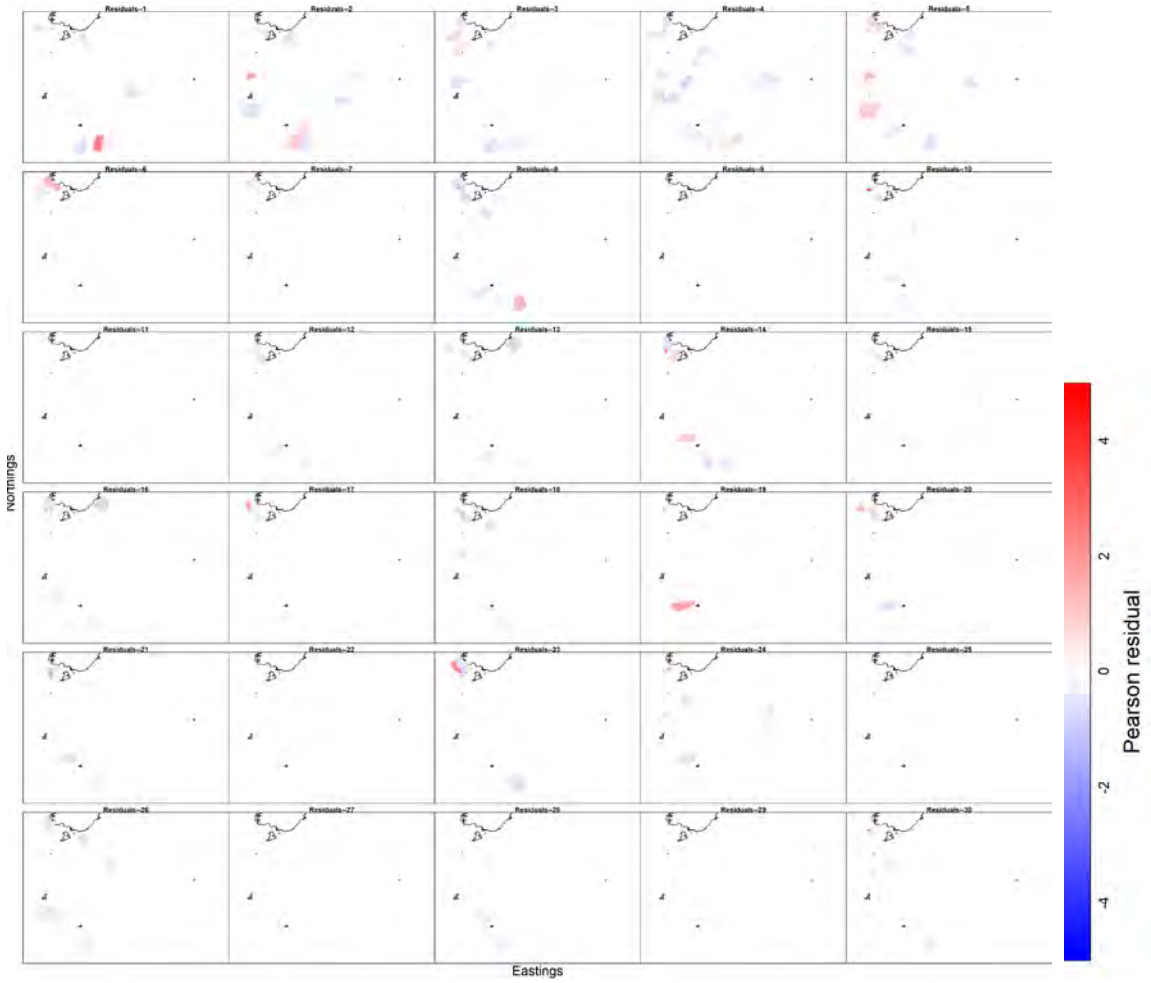

Figure 129:VAST outputs for Pearson residuals (goodness of fit) showing under or over fitting for catch rates of *Deania calcea* across the Sub-Antarctic (1989–2018, from left to right for each panel).

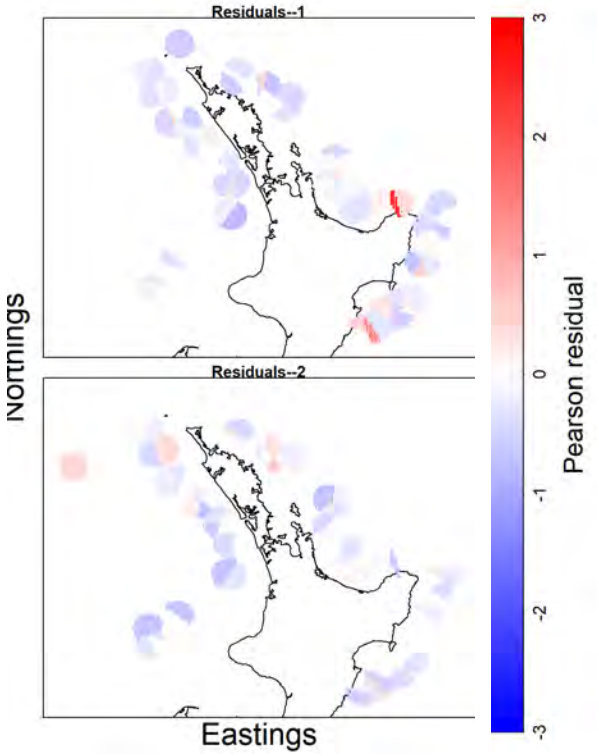

Figure 130: VAST outputs for Pearson residuals (goodness of fit) showing under or over fitting for catch rates of *Deania calcea* around the North Island in 1985–1986.

Figure 131: VAST outputs for Pearson residuals (goodness of fit) showing under or over fitting for catch rates of *Deania calcea* by class across Chatham Rise (1997–2018, from left to right for each panel).

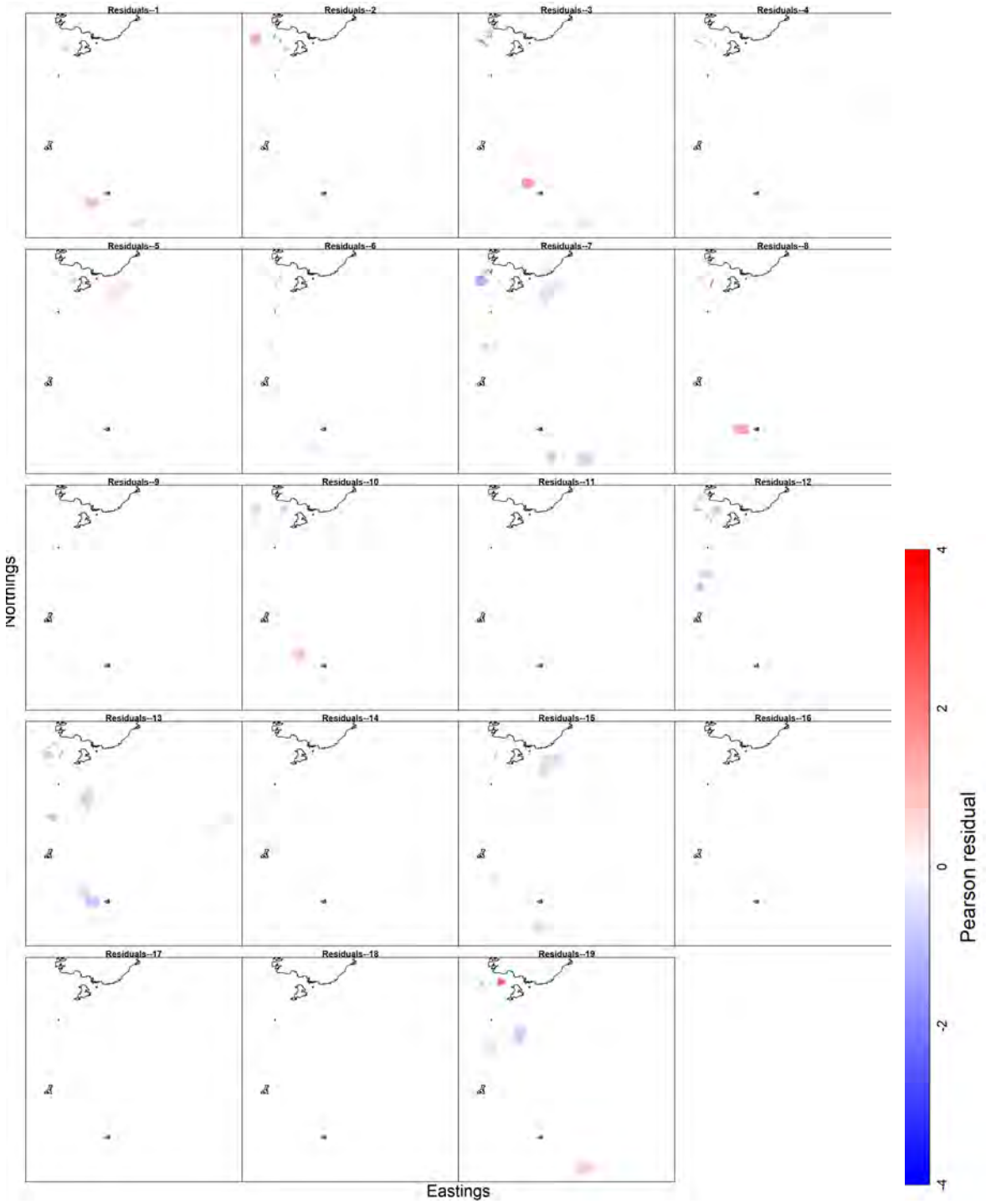

Figure 132: VAST outputs for Pearson residuals (goodness of fit) showing under or over fitting for catch rates of *Deania calcea* by class across the Sub-Antarctic (2000–2018, from left to right for each panel).

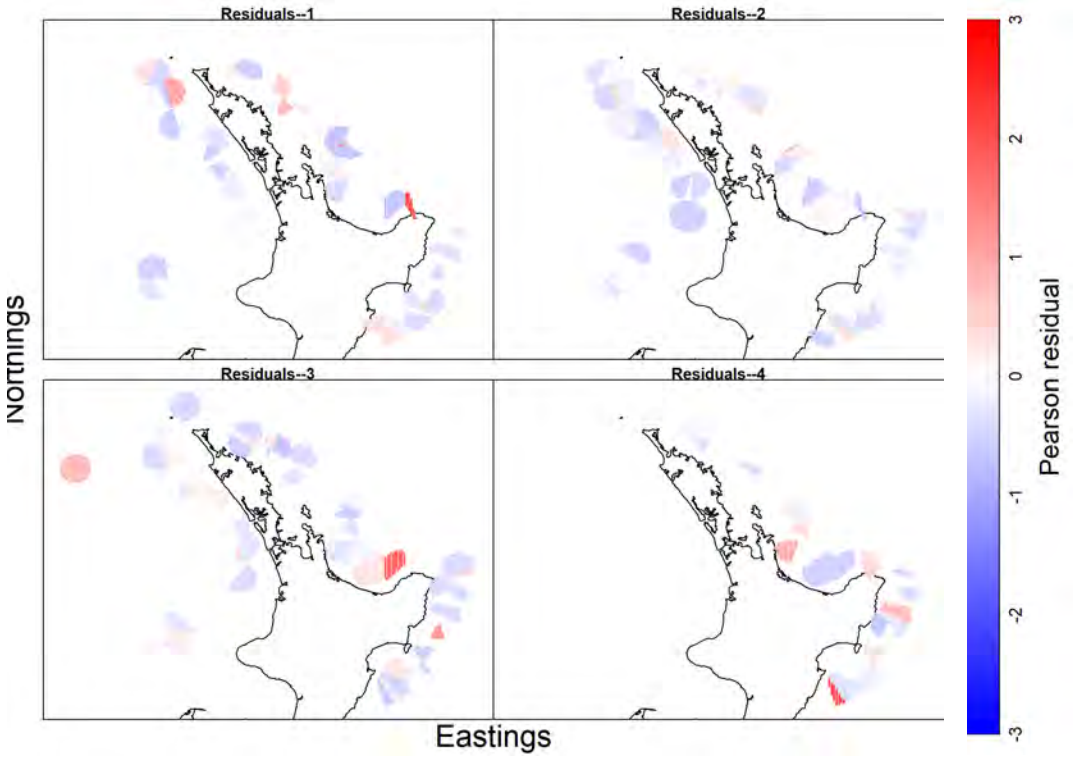

Figure 133: VAST outputs for Pearson residuals (goodness of fit) showing under or over fitting for catch rates of *Deania calcea* around the North Island of New Zealand (spring, 1; summer, 2; autumn, 3; winter, 4) in 1985–1986.

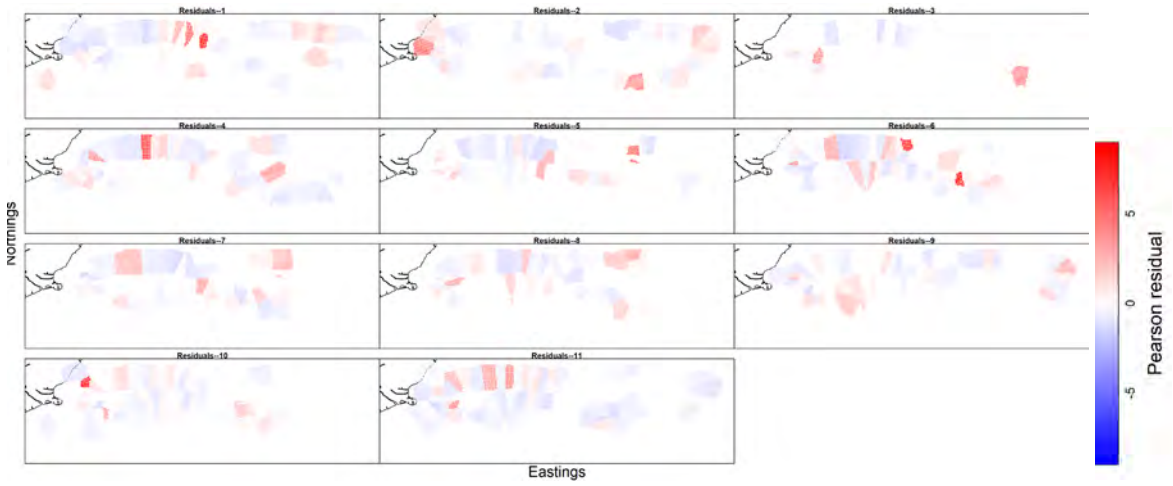

Figure 134: VAST outputs for Pearson residuals (goodness of fit) showing under or over fitting for observer catch rates of *Deania calcea* across Chatham Rise (2008–2018, from left to right for each panel).

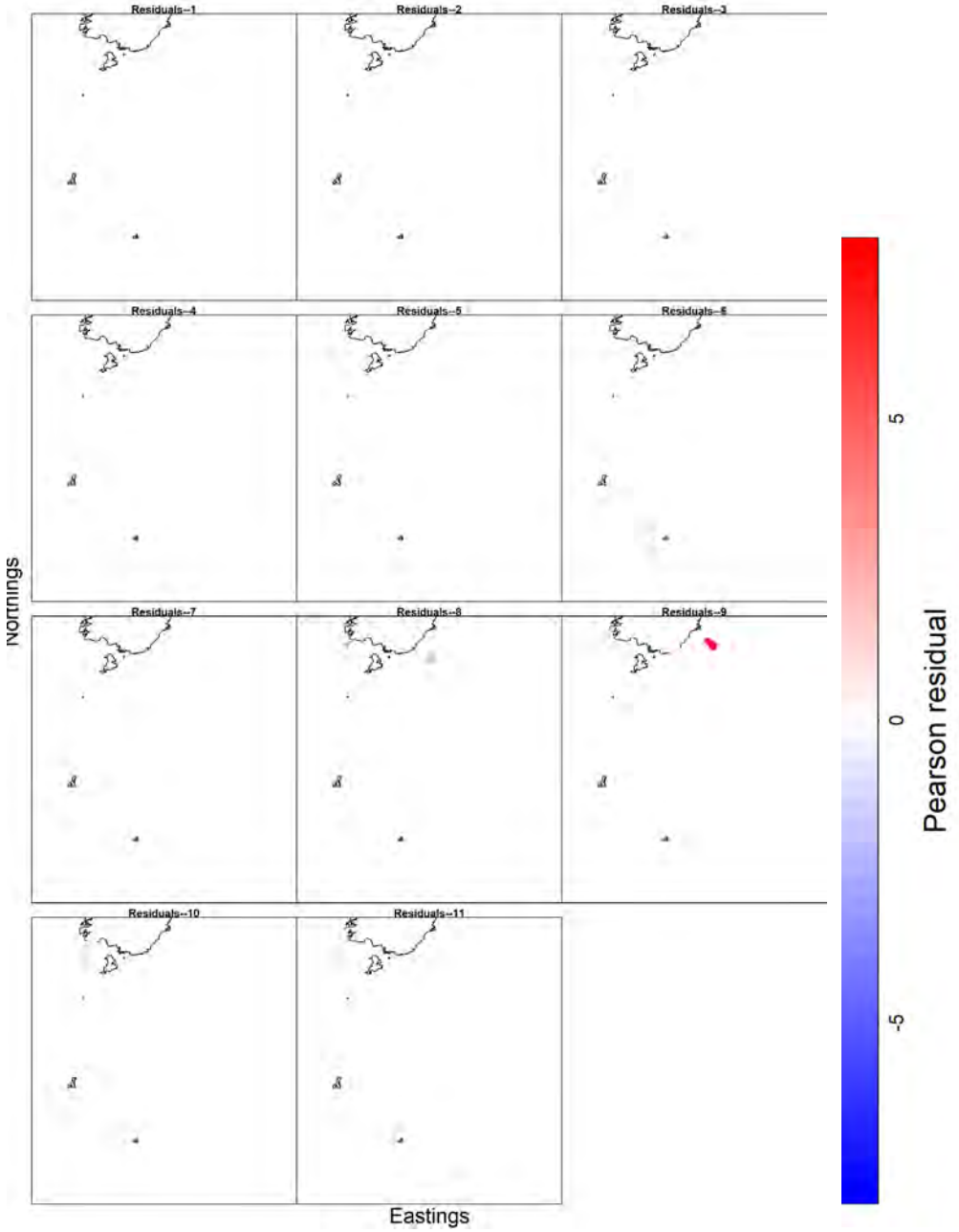

Figure 135: VAST outputs for Pearson residuals (goodness of fit) showing under or over fitting for observer catch rates of *Deania calcea* across the Sub-Antarctic (2008–2018, from left to right for each panel).